LBL-16998

Lawrence Berkeley Laboratory
UNIVERSITY OF CALIFORNIA

CHEMICAL BIODYNAMICS DIVISION

SOME NITROGEN-14 NMR STUDIES IN SOLIDS

T.K. Pratum
(Ph.D. Thesis)

November 1983

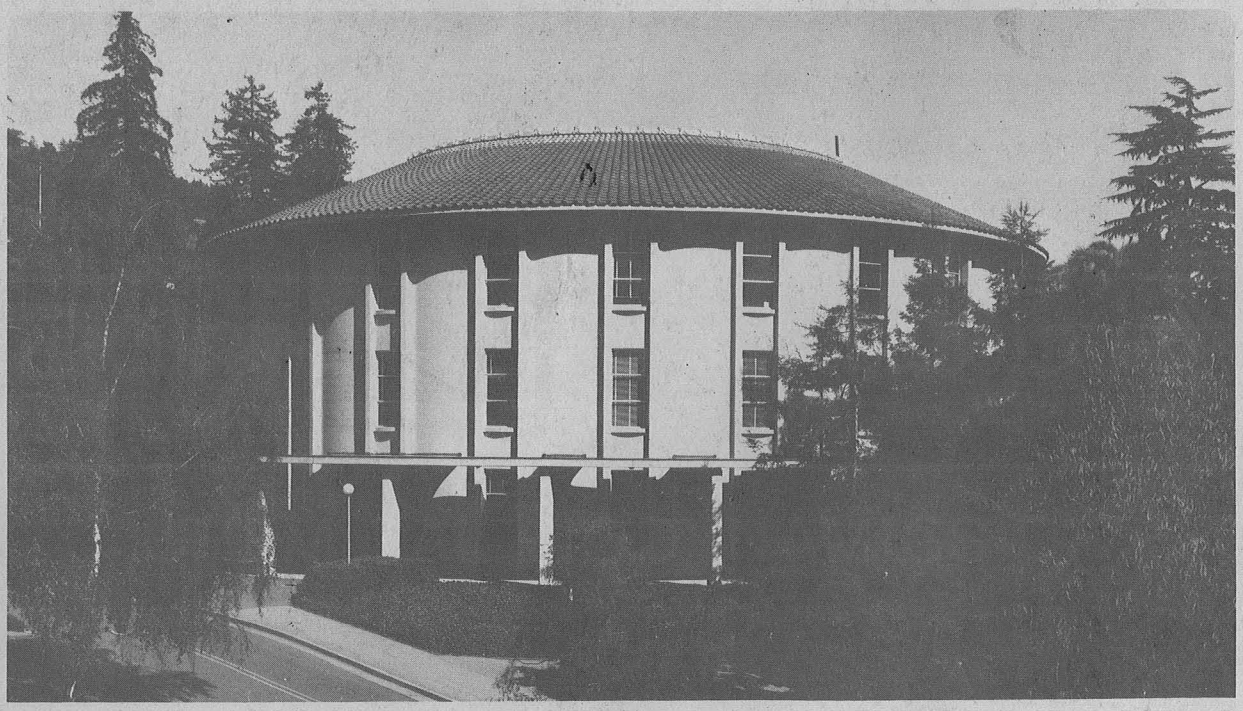

Prepared for the U.S. Department of Energy under Contract DE-AC03-76SF00098

LEGAL NOTICE

This book was prepared as an account of work sponsored by an agency of the United States Government. Neither the United States Government nor any agency thereof, nor any of their employees, makes any warranty, express or implied, or assumes any legal liability or responsibility for the accuracy, completeness, or usefulness of any information, apparatus, product, or process disclosed, or represents that its use would not infringe privately owned rights. Reference herein to any specific commercial product, process, or service by trade name, trademark, manufacturer, or otherwise, does not necessarily constitute or imply its endorsement, recommendation, or favoring by the United States Government or any agency thereof. The views and opinions of authors expressed herein do not necessarily state or reflect those of the United States Government or any agency thereof.

Lawrence Berkeley Laboratory is an equal opportunity employer.

LBL-16998

SOME NITROGEN-14 NMR STUDIES IN SOLIDS

Thomas Kingston Pratum
(Ph.D. Thesis)

Chemical Biodynamics
Lawrence Berkeley Laboratory
University of California
Berkeley, California 94720

November 1983

This work was supported by the Office of Energy Research, Office of Health and Environmental Research, Health Effects Research Division of the U.S. Department of Energy under Contract DE-AC03-76SF00098.

Some Nitrogen-14 NMR Studies in Solids

Thomas Kingston Pratum

Abstract

The nitrogen nucleus has the potential to be a valuable probe of electronic environment and molecular dynamics in chemical systems. This potential is investigated here via ^{14}N nuclear magnetic resonance (NMR) studies in high magnetic field. The first order quadrupolar perturbation of the ^{14}N NMR spectrum yields information regarding the static and dynamic properties of the surrounding electronic environment.

Observation of the ^{14}N NMR signal in solids is seldom an easy task, and the methods we have used for this purpose are discussed. Signal to noise problems caused by long ^{14}N longitudinal relaxation times (T_1) and small equilibrium polarizations are reduced by rotating frame cross polarization (CP) experiments betwen ^{14}N and ^{1}H. Here a simple theory is presented in which the three level spin-1 system of ^{14}N cross relaxes along two fictitious spin-1/2 two level systems; one of which is referred to as double quantum (DQ), and the other as zero quantum. Pure single quantum (SQ) cross relaxation occurs when these two systems are simultaneously Hartmann-Hahn matched to the protons, which is only possible for very small first order quadrupolar shifts (ω_Q). Large ω_Q's are most effectively matched by employing the DQ condition, where the ^{14}N radio frequency field (ω_1) is larger than the rotating frame effective field of the protons, but smaller than ω_Q. Broad quadrupolar powder patterns are most effectively matched when the protons are prepared via an adiabatic demagnetization in the rotating frame (ADRF) and ω_1 is adjusted so that the condition for DQ cross relaxation is satisfied across most of the spectrum. Conversion of the non-observable

DQ coherence to observable SQ coherence is accomplished via a large amplitude 90° pulse 45° out of phase relative to the mixing field.

Using quadrupolar echo and CP techniques, the ^{14}N quadrupolar coupling constants (e^2qQ/h) and asymmetry parameters (η) have been obtained for a variety of tetraalkylammonium compounds by observation of their quadrupolar powder patterns at various temperatures. For these compounds e^2qQ/h is found to range from 10-200 kHz, while η varies between 0 and 1.0. The inferred symmetry of the electronic environment is always found to exhibit a strong relationship to the crystallographic unit cell symmetry where this latter information is available. The temperature dependence of the ^{14}N T_1 in these compounds indicates that ^{14}N spin lattice relaxation occurs most effectively via dipolar interactions with rotating methyl groups.

For choline chloride and iodide the ^{14}N NMR powder patterns exhibit the effects of anisotropic molecular motion, while choline bromide spectra show no such effects. Spectral simulations indicate that the anisotropic motion in the chloride and iodide salts occurs about an axis passing through the nitrogen and oxygen atoms and, for the iodide salt, our results agree with a 180° flip-flop mechanism which has been previously proposed. At room temperature, the motion in the chloride salt occurs at a rate of about 10 kHz, while the iodide salt exhibits a flip-flop rate in excess of 250 kHz.

Acknowledgments

It is certainly impossible to acknowledge all who have contributed to this work, but I feel compelled to give it my best shot. Dr. Mel Klein is a tremendous individual, one who I will always remember with admiration. At times we've had our differences, but his concern has always been with me the individual, and he has really put up with a lot to make me happy. Mels' group has been a joy to work with. Greg (Karczmar) and Alan (Koretsky) have always provided stimulating discussion and absorbed large quantities of my verbal abuse. Although they will vehemently deny it, I consider them to be responsible for many of my research triumphs. Sun Un has given me confidence that our wonderful spectrometer will be in good hands for a few more years. Dave Britt, Dave Goodin, Vittal Yachandra, and Ron Guiles have all provided hours of spirited discussion, and have absorbed small, but important quantities of verbal abuse.

This work would have been impossible were it not for the contributions which have been made by Professor Alex Pines and his group. Alex has always managed to attract a great group of people. In particular, Jim Murdoch and Gary Drobny got me started in this field, and have provided hours of enlightening revelations. Dave Zax and Rob Tyco never cease to amaze me with their mastery of magnetic resonance, and the rest of the group are a fun bunch of people.

My cohorts on the second floor of the Melvin Calvin Lab have been responsible for my relative sanity (or insanity) to this very day. Marc "the Dinosaur" Donsky has provided spiritual inspiration. Mike Boska has kept me abreast of the latest Grateful Dead concerts, and

provided weekly (daily?) hangliding reports. Angelo "Moneybags" Castellino has kept me informed of the latest preaching of Dr. Gene Scott, and helped me escape the reality of the lab on several occasions. Steve Treon and John McCracken provided helpful suggestions. "Gypsy" Jim Cole, Dr. Ning Pon, Steve "Wasted" Worland, Ann McDermott, Dave Pearlman, Kerry Karukstis, Sara and Sarah have all done their part (however small). Last, but certainly not least, Ti-Sheng Young has unselfishly contributed many hours of his time attempting to explain x-ray crystallography, and helping to perform key experiments.

Other people in distant parts of the U.S. have helped to pull me through this with their timely letters and phone calls. In particular, my father Rolf is entirely responsible for my present status as a member of the scientific community by stimulating my scientific interests at a very early age. Barb, Mike, and Steve have all been essential in helping me through the crises which have beset our family in past years. Suzy, Mark, and Alice will probably never read this, but I have appreciated their friendship over the years. Dr. Ken Rousslang has served me well by showing me how much fun physical chemistry can be, and convincing me that a career at Albertson's would not be for the best.

Often forgotten are the laboratory staff members who carry out a lot of the "dirty work." Gary Smith is responsible for much advice and the proper functioning of the VAX; in my opinion he is clearly being paid less than 10% of his actual worth. Everett Harvey has also been very helpful with computer related problems. Mike Press was the source of useful advice regarding analog circuitry. Beth Klingel, Lois Soule, and Gloria Goldberg deserve a round of applause whenever another thesis rolls out of our laboratory. Carol Hacker has been responsible for

deciphering my handwritten draft of this thesis, and knowing when a w should be an omega (which she does very well). Dr. Richard Lemmon has been the source of much stimulating discussion regarding the choline halides, and Professor Melvin Calvin is, of course, responsible for our great laboratory which I was fortunate enough to be part of for the past several years.

This work was supported by the Office of Energy Research, Office of Health and Environmental Research, Health Effects Research Division of the U.S. Department of Energy under Contract DE-AC03-76SF00098.

Contents

Chapter Page

1. Introduction 1

1.1 Density Matrices 2

1.2 Nuclear Spin Interaction Hamiltonians 6

1.2.1 Zeeman 7

1.2.2 Radio Frequency 8

1.2.3 Quadrupolar 11

1.2.4 Magnetic Dipole-dipole 18

1.2.5 Chemical Shift 21

1.3 Powder Patterns 23

2. Techniques 30

2.1 Observation of FIDs 30

2.1.1 Quadrupolar Echoes 32

2.2.1 The Nature of Dipole Broadening 48

2.2.2 Decoupling 53

2.3 Cross Relaxation 60

2.3.1 Relaxation of Spins in High Field. 60

2.3.2 Nuclear Overhauser Enhancement 63

2.4 Rotating Frame Cross Relaxation 68

2.4.1 Rotating Frame Spin Thermodynamics 70

2.4.2 Rotating Frame Spin Dynamics 76

2.4.3 ^{14}N Cross Polarization 84

2.4.4 Rotating Frame Effective Fields 85

2.4.5 Hartmann-Hahn Conditions 90

2.4.6 Polarizations Produced 97

Chapter Page

2.4.7 Cross Polarized Echoes 98

2.4.8 Observed Echo Signals 104

2.4.9 Observed Frequency Response of the Cross Polarization 122

2.4.10 Some Quantitative Results from Simulations . . . 128

2.4.11 Large Off-Resonance Effects 139

2.4.12 Practical Considerations 143

3. ^{14}N Studies of Tetraalkylammonium Compounds 145

3.1 Experimental Procedures 146

3.2 Overview of Experimental Results 153

3.3 Discussion of Specific Compounds 163

3.3.1 Tetraalkylammonium Salts and Choline Salts 163

3.3.2 Amphiphiles 173

3.4 Concluding Remarks on EFGs 188

3.5 A Few Remarks on the ^{14}N T_1 189

4. Effects of Motion in the Choline Halides 194

4.0 Previous Work 194

4.1 Anisotropic Motion and Anisotropic Interactions in NMR 196

4.2 Experimental Results 206

4.2.1 Assumptions Made in the Analysis 209

4.2.2 Choline Bromide 210

4.2.3 Choline Chloride 211

4.2.4 Choline Iodide 231

Chapter Page

4.3 Conclusions 246

Appendix

A. Spherical Tensors 249

B. Fictitious Spin-1/2 Operators 254

C. Computer Programs 261

D. Spectrometer Modifications 290

References 300

1.0 Introduction.

Nuclear magnetic resonance (NMR) has been the topic of hundreds of theses in the past few decades. Some have dealt with the development of new techniques, while others with the application of the techniques to a variety of physical, chemical, and biological problems. Of course, some have handled both development and application, and this is the course I will follow here.

The utility of NMR lies in its ability to tell us something about molecular environment via small perturbations on the already tiny interaction between a nuclear spin and an enormous external magnetic field. The nucleus normally dealt with is the common proton, but here I will consider the slightly less common nitrogen 14(^{14}N). In the chemical world, the nitrogen atom is nearly ubiquitous. It frequently occupies key positions in organic, inorganic, and biological molecules; and, for this reason, its value as a spectroscopic probe is extremely high. Unfortunately, ^{14}N is difficult to observe because of its small Zeeman interaction with the external field (H_0) (the sensitivity of ^{14}N is about 10^{-3} that of protons). Another characteristic which is generally a great hinderance to NMR observation is the ^{14}N electric quadrupole moment. The electrostatic interaction between this moment and the surrounding electrons leads to homogeneously broadened lines in liquids and inhomogeneously broadened lines in solids; reducing the signal to noise ratio (S/N) even further. Fortunately, if S/N problems could be solved, the quadrupolar interaction would be an extremely sensitive probe of molecular environment and dynamics. With this in mind, I embark

upon my journey, which has involved many hours of machine shop time, spectrometer time, and cpu time.

Any discussion of technique and observation of nuclear spin interactions in solids must be preceeded by an introduction to the basic formalism involved. Prior to diving into this discussion, a few things should be kept in mind regarding my notation. The first concerns operators: in this first introductory chapter, the operator I will refer to the spins under observation (^{14}N), and the operator S will refer to the non-resonant spins (protons); in all of the following chapters this definition will be reversed (i.e., S will refer to ^{14}N, I to ^{1}H). This change helps me to feel a little more at home with the notation, I hope it doesn't confuse anyone else. Concerning units; ω will be used to denote angular frequency $2\pi\nu$, where ν signifies "normal" frequency (i.e., Hz, KHz, etc.). Interaction strengths are always given in frequency units. Theoretical calculations make use of angular frequency units, while experimental situations refer to normal frequency units.

1.1 Density Matrices

The results observed in any typical NMR experiment derive from a statistical mixture of quantum mechanical states and are best described in terms of a density matrix formalism [1]. A given quantum state ψ may be defined as a superposition of orthogonal basis states

$$\psi = \sum_i c_i u_i \quad , \tag{1.1}$$

where c_i is generally a complex number. The elements of a given density matrix ρ are essentially equal to the average of the statistical weights for the ensemble under consideration

$$\rho_{nm} = [c_n c_m^*] \quad . \tag{1.2}$$

The density matrix possesses the following properties [1]:

ρ is Hermitian,

$$\mathrm{Tr}(\rho) = 1, \text{ and} \tag{1.3a}$$

$$\mathrm{Tr}(A\rho) = \langle A \rangle: \tag{1.3b}$$

where Tr refers to the trace and $\langle A \rangle$ denotes the expected value of the operator A. The diagonal elements of ρ are known as populations, and Eq. (1.3a) states the fact that their sum must be conserved. The off diagonal elements are known as coherences, and given the property of one state evolving into another in a coherent manner (such that the ensemble average $\overline{\rho_n \rho_m^*} \neq 0$). Equation (1.3b) implies that ρ may be expanded in terms of N^2-1 orthogonal operators (where N is the dimensionality of the quantum system) as:

$$\rho = \sum_j \langle A_j \rangle A_j \quad . \tag{1.4}$$

From the Schrödinger equation

$$\frac{i}{\hbar} \mathcal{H}\psi = \frac{\partial}{\partial t} \psi \quad , \tag{1.5}$$

where $\mathcal{H}$ is the Hamiltonian or energy operator of the system, one may easily derive the time evolution of the density matrix as

$$\frac{\partial}{\partial t}\rho = -\frac{i}{\hbar}[\mathcal{H},\rho] \quad . \tag{1.6}$$

If $\mathcal{H}$ is time independent, this equation is easily integrated to:

$$\rho(t) = e^{-\frac{i}{\hbar}\mathcal{H}t}\,\rho(0)\,e^{\frac{i}{\hbar}\mathcal{H}t} \quad , \tag{1.7}$$

while if $\mathcal{H}$ is time dependent

$$\rho(t) = e^{-\frac{i}{\hbar}\int_0^{t'}\mathcal{H}(t)dt}\,\rho(0)\,e^{\frac{i}{\hbar}\int_0^{t'}\mathcal{H}(t)dt} \quad , \tag{1.8}$$

where the $\hbar$ is dropped in the case that $\mathcal{H}$ is expressed in angular frequency units. From the time evolution of ρ, all interesting properties of the system may be derived; hence Eqs. (1.7) and (1.8) are extremely important. For the purpose of computing $\rho(t)$ [2], $\mathcal{H}$ is diagonalized to find the eigenvalues E_j and matrix of eigenvectors U. The time evolution of ρ is then calculated via a series of matrix multiplications

$$\rho(t) = U\cdot e^{-\frac{i}{\hbar}E_j t}\cdot U^{\dagger}\rho(0)\cdot U\cdot e^{\frac{i}{\hbar}E_j t}\cdot U^{\dagger} \quad , \tag{1.9}$$

where $U^{\dagger}$ is the Hermitian adjoint of U. If $\mathcal{H}$ is time dependent and varying coherently, then it may be replaced by a time independent average Hamiltonian [38]. Whether $\mathcal{H}$ varys coherently or not, if

its time dependence is known Eq. (1.8) may be solved by breaking t' into a finite number of intervals Δt on which $\mathcal{H}$ is assumed to be time independent. The density matrix evolution is then calculated each step along the way to produce the final result.

Of course, an initial density matrix is needed, and this will most commonly result from thermodynamic equilibrium between the spins and their surroundings (the lattice). In analogy with classical statistical mechanics, it may be shown that the equilibrium density matrix is [1]:

$$\rho = Z^{-1} e^{-E/kT} \quad , \tag{1.10}$$

where Z is the partition function which satisfies Eq. (1.3a). At equilibrium, ρ must commute with the Hamiltonian of the system, and all off diagonal elements must be zero. The diagonal elements are given by

$$\rho_{nn} = \frac{e^{-E_n/kT}}{Z} \quad , \tag{1.11}$$

which, for a nuclear spin system, can be reduced to

$$\rho_{nn} = \frac{e^{-E_n/kT}}{2I+1} \quad . \tag{1.12}$$

Further, since the nuclear spin interaction energy E_n is very small compared to kT, the exponential may be expanded to linear terms:

$$\rho_{nn} = \frac{1 - {}^{E_n/kT}}{2I+1} \quad . \tag{1.13}$$

Removal of a unit matrix may be accomplished, without altering any observables, to yield

$$\rho_{nn_{eq}} = - \frac{E_n}{kT(2I+1)} \quad . \tag{1.14}$$

This is a convenient point to introduce the concept of temperature in NMR [3]. Temperature is a property which will be uniform over all parts of an isolated system at equilibrium. For a nuclear spin system at equilibrium with its surroundings, ρ will be described by Eq. (1.14) with T equal to the sample temperature (usually around 300°K). In order for the spins to reach equilibrium from a non-equilibrium state, it is necessary for them to exchange extremely tiny quanta. Because they can do this much more rapidly between themselves than with the lattice, it is possible for them to achieve an equilibrium situation described by a density matrix not corresponding to the lattice temperature. The temperature which would correspond to this density matrix is known as the "spin temperature", and can take on any value positive or negative [4]. When considering spin temperature, cool is better; cool spins exhibit large polarizations which can be observed, while hot spins exhibit no polarization (they are saturated).

1.2 Nuclear Spin Interaction Hamiltonians

One thing which I find appealing about NMR is that the nuclear spin Hamiltonian actually contains a finite number of terms and can be written down. I will consider a Hamiltonian consisting of Zeeman, radio frequency, chemical shift, quadrupole, and magnetic

dipole terms.

$$\mathcal{H} = \mathcal{H}_z + \mathcal{H}_{rf} + \mathcal{H}_Q + \mathcal{H}_{II} + \mathcal{H}_{IS} + \mathcal{H}_{cs} \tag{1.15}$$

In the following sections, these terms will be defined and elaborated upon somewhat.

1.2.1 Zeeman

The nuclear Zeeman term, $\mathcal{H}_z$, will always be the largest in any NMR experiment; in fact the size of this term defines whether we are performing a true NMR experiment, or some other type of experiment, such as nuclear quadrupole resonance (NQR) with a Zeeman perturbation. The Zeeman term describes the interaction of the nuclear magnetic moment μ with the large static magnetic field H_0 (usually produced within a superconducting solenoid):

$$\mathcal{H}_z = -\mu \cdot H_0 \tag{1.16}$$

The axis of H_0 is defined to be along the z-direction, hence

$$\mathcal{H}_z = \gamma\, I_z H_0 \quad , \tag{1.17}$$

where γ is the gyromagnetic ratio, and I_z is the z component of the angular momentum operator I. Since I_z obeys all of the standard rules for angular momenta:

$$I_z|\psi\rangle = m_z|\psi\rangle \; ; \; m = I, I-1, \ldots, -I \quad . \tag{1.18}$$

These levels of m define the possible energy levels between which we may induce transitions. The energy splitting for a single quantum ($\Delta m = 1$) transition will always equal

$$\Delta E = \gamma\hbar H_0$$

$$= \omega_0\hbar \quad . \tag{1.19}$$

The gyromagnetic ratio will vary from nucleus to nucleus, generally decreasing with increasing nuclear mass. For ^{14}N:

$$\gamma_N = 1.9323 \times 10^3 \text{ sec}^{-1} \text{ gauss}^{-1} \text{ rad} \quad ,$$

while for protons

$$\gamma_H = 2.6751 \times 10^4 \text{ sec}^{-1} \text{ gauss}^{-1} \text{ rad} \quad ,$$

The corresponding energy splittings in a 6.3×10^4 gauss field are 1.292×10^{-26} joules and 1.790×10^{-25} joules respectively. These energies would equal kT at about 10^{-2}°K, so the largest of the nuclear spin interactions is very small indeed.

1.2.2 Radio Frequency (r.f.)

Continuing with the external magnetic field interactions, the next largest, at appropriate times, will be that of the radio frequency field. This field will be transverse to the static field H_0, and its interaction is defined:

$$\mathcal{H}_{rf} = -2\gamma\, H_1 \cos\omega t\, I_x \quad ,$$

$$= -2\, \omega_1\, I_x \cos\omega t \quad , \tag{1.20}$$

where H_1 signifies the amplitude of the oscillating magnetic field at frequency ω. This linearly polarized field may be decomposed into two counter-rotating components:

$$\mathcal{H}_{rf} = -\omega_1\, (e^{-i\omega t I_z}\, I_x\, e^{i\omega t I_z} + e^{i\omega t I_z}\, I_x\, e^{-i\omega t I_z}) \tag{1.21}$$

It is now convenient to introduce the rotating frame transformation in order to remove the time dependence of $\mathcal{H}_{rf}$. Starting with the Schrödinger equation (Eq. 1.5), and using a Hamiltonian consisting of Zeeman and r.f. terms, the time dependence of $\mathcal{H}$ is removed by transferring it to ψ [5] through the definition

$$\psi = e^{i\omega t I_z}\psi' \quad . \tag{1.22}$$

With our Hamiltonian:

$$\mathcal{H} = -\omega_0 I_z - \omega_1 (e^{-i\omega t I_z}\, I_x\, e^{i\omega t I_z} + e^{i\omega t I_z}\, I_x\, e^{-i\omega t I_z}) \quad , \tag{1.23}$$

The Schrödinger equation in terms of the new ψ (Eq. 1.22) may be written:

$$-\omega\, I_z\, U\, \psi' + i\, U \frac{\partial \psi'}{\partial t} =$$

$$(-\omega_0\, I_z - \omega_1 (U I_x U^\dagger + U^\dagger I_x U)) U \psi' \quad , , \tag{1.24}$$

where I have set $U = e^{i\omega t I_z}$. Multiplication of Eq. (1.24) through on the left by $U^\dagger$, followed by a small amount of algebra, results in:

$$i \frac{\partial \psi}{\partial t} = [-(\omega_0 - \omega) I_z - \omega_1 (I_x + U^\dagger U^\dagger I_x U U)] \psi \quad . \tag{1.25}$$

Comparison of Eq. (1.25) and Eq. (1.5) shows that our rotating frame Hamiltonian is:

$$\mathcal{H} = -(\omega_0 - \omega) I_z - \omega_1 (I_x + U^\dagger U^\dagger I_x U U) \tag{1.26}$$

$$= -\Delta\omega I_z - \omega_1 (I_x + e^{-2i\omega t I_z}\, I_x\, e^{2i\omega t I_z}) \quad . \tag{1.27}$$

The term rotating at 2ω may be ignored so long as $\omega >> \omega_1$ (elsewise, it leads to a small offset term: the Bloch-Siegert shift [63]), yielding:

$$\mathcal{H} = -\Delta\omega Iz - \omega_1 I_x \tag{1.28}$$

as our final rotating frame Hamiltonian. Not only has the time dependence of the r.f. been removed, but along with it went the large and fairly uninteresting Zeeman term (if $\omega_0 = \omega$). Henceforth, all Hamiltonians will be presented in the rotating frame (unless

otherwise noted).

1.2.3 Quadrupolar

If our Hamiltonian were only made up of Zeeman and r.f. terms, NMR would be a very boring subject indeed. Fortunately, other magnetic and electrostatic perturbations yield a wealth of information. The most important of these for this thesis will be the electrostatic quadrupolar interaction.

The first observation of the nuclear quadrupolar interaction was made in connection with a molecular beam experiment in 1939 by Kusch, Millman and Rabi [6]. This observation of subsidiary minima in their magnetic resonance spectra was fully explained in terms of the electric quadrupolar interaction in 1945 by Feld and Lamb [7] .

Any charge distribution may be expanded in terms of its multipole moments, and, when this procedure is applied to a nucleus, one finds monopole, quadrupole, ... 2^{2I} pole moments which can interact electrostatically with the appropriate electronic distribution in the vicinity of the nucleus. The monopole moment obviously is responsible for the quantum energy levels of the atom, and corresponds to a very large energy of interaction which does not concern the NMR spectroscopist. The next non-vanishing term is the quadrupole (the odd power moments vanish by a parity argument [9]), and it will be important for any nucleus of spin $I \geq 1$. The hexadecapole interaction will exist for nuclei of spin $I \geq 1$, but has been too weak to observe thus far; and it would not exist for ^{14}N in any case.

Classically, a quadrupolar charge distribution is defined as one in which the quantity $\rho(r)\ (3z^2-r^2)$ (where $\rho(r)$ is the charge

density) integrated over all space is nonzero. It can easily be shown that such a distribution will have no energy of interaction in a uniform electric field $E = \nabla\phi$ (where ϕ is the scalar potential), but will interact with a gradient field $\nabla E = \nabla^2\phi$. This interaction between a quadrupolar nucleus and its surrounding electrons in zero magnetic field leads to NQR, which is not dealt with here. In high magnetic field, it leads to a perturbing energy best described by the interaction of a spin I with a coupling tensor $\underset{\sim}{V}$:

$$\mathcal{H}_Q = C(I \cdot \underset{\sim}{V} \cdot I) \quad , \tag{1.29}$$

where $C = \frac{eQ}{2I(2I-1)}$ is a constant dependent upon the nucleus in question. The quantity Q is known as the quadrupole moment of the nucleus. Quadrupole moments, in general, tend to be positive (indicating a cigar like charge distribution) and to increase with increasing nuclear mass. For ^{14}N, $Q = 1.6 \times 10^{-2}$ barns (1 barn = 10^{-24} cm^2); approximately a factor of six larger than the friendly deuterium atom. The Cartesian tensor $\underset{\sim}{V} = \{V_{ij}\}$ is composed of electric field gradient (efg) elements resulting from the surrounding electronic charge distribution, and will therefore be traceless by the Laplace equation: $\nabla^2\phi = 0$. The tensor can always be transformed to an axis system in which it is diagonal (the principle axis system or PAS) [8], and may accordingly be entirely defined by two parameters:

$$eq = V_{zz}, \quad \text{and}$$

$$\eta = \frac{V_{xx} - V_{yy}}{V_{zz}} \quad . \tag{1.30}$$

Derivation of the representation of $\mathcal{H}_Q$ with respect to H_0 is carried out in appendix A, resulting in Eq. (A.14):

$$\mathcal{H}_Q = \frac{e^2qQ}{8I(2I-1)\hbar}\,(3\cos^2\theta - 1+\eta\sin^2\theta\cos2\phi)(3I_z^{\,2}-I(I+1))$$

which, for spin I=1, becomes

$$\mathcal{H}_Q = \frac{e^2qQ}{8\hbar}\,(3\cos^2\theta - 1+\eta\sin^2\theta\cos2\phi)(3I_z^{\,2}-2) \quad . \qquad (1.31)$$

The quadrupolar frequency ω_Q (see figure 1) will be defined

$$\omega_Q = \frac{3e^2qQ}{8\hbar}\,(3\cos^2\theta - 1+\eta\sin^2\theta\cos2\phi) \quad . \qquad (1.32)$$

The truncated high field Hamiltonian (Eq. (1.31)) will remain valid so long as the high field Zeeman eigenstates hold true (i.e., $|\mathcal{H}_z| >> |\mathcal{H}_Q|$); when this is no longer the case, the second order correction term will be (for $\eta = 0$) [10]:

$$\mathcal{H}_Q^{(2)} = -\frac{9(e^2qQ)^2}{48\,\omega_0\hbar^2}\,I_z(\frac{3}{2}\cos^2\theta\,(1-\cos^2\theta)(8I_z^{\,2}-9)$$

$$+\frac{3}{8}\,(1-\cos^2\theta)^2\,(3-2I_z^{\,2})) \quad . \qquad (1.33)$$

A broad ^{14}N NMR line which is observable via the techniques I present here will be inhomogeneously broadened due to the orientation dependence of Eq. (1.32) to approximately 200 kHz. Using a Q for ^{14}N of 1.6×10^{-26} cm^2, the required field gradient eq would be approximately 3×10^{16} volts$\cdot cm^{-2}$. This seemingly enormous field

Figure 1. The Zeeman energy levels of a spin one nucleus in the absence and presence of a first order quadrupolar interaction; ω_Q is defined by Eq. (1.32).

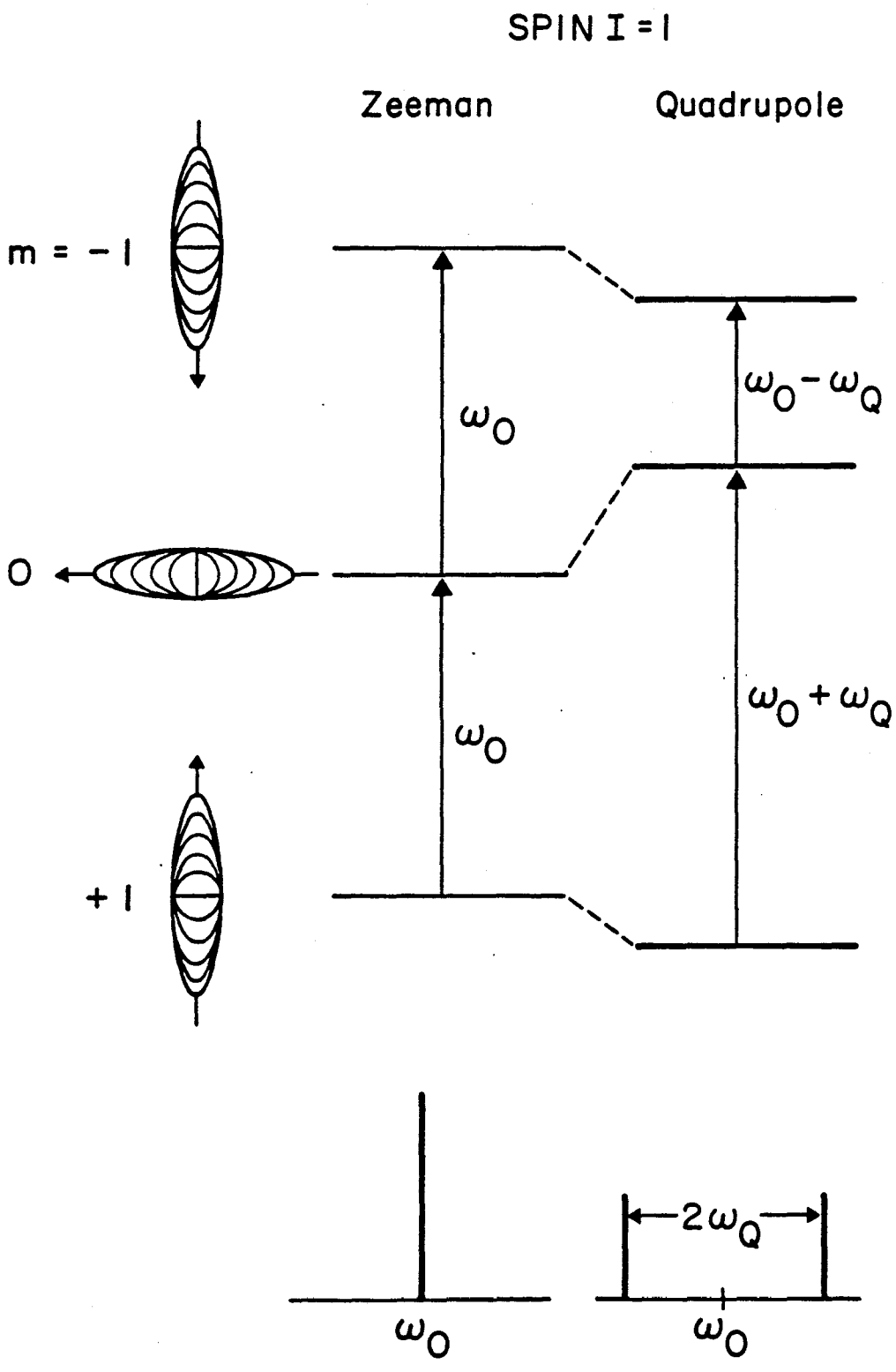

XBL 7610-4907

gradient is the result of many charges being confined to a very small volume around the nucleus. The maximum second order shift expected can be calculated with the help of Eq. (1.33). For the case just described, the shift will be $\frac{9}{64}\frac{(e^2qQ)^2}{\hbar^2\nu_0}$, or 127 Hz at ν_0 = 19.5 MHz (H_0 = 63.0 kGauss). For a spin one, this interaction will have the same effect as a chemical shift (it has a linear dependence on I_z), but it is small enough that it can be safely ignored in all that follows.

Our total Hamiltonian is now:

$$\mathcal{H} = -\Delta\omega I_z - \omega_1 I_x + \frac{\omega_Q}{3}(3\,I_z^{\,2}-2) \quad , \tag{1.34}$$

and this will be the form most commonly dealt with in this work. In order that I might carry out one more interesting transformation, and introduce a bit more formalism, I will convert (1.34) to fictitious spin 1/2 operators (described in appendix B):

$$\mathcal{H} = -2\Delta\omega\, I_z^{1-3} - \sqrt{2}\,\omega_1\,(I_x^{1-2}+I_x^{2-3}) + \frac{2\omega_Q}{3}(I_z^{1-2}-I_z^{2-3}) \quad . \tag{1.35}$$

This Hamiltonian is now conveniently rotated, as described in appendix B, by $\pi/2$ about I_y^{1-3} yielding:

$$\mathcal{H} = -2\Delta\omega\, I_x^{1-3} - 2\omega_1\, I_x^{2-3} + \frac{2\omega_Q}{3}(I_z^{1-2}-I_z^{2-3}) \quad , \tag{1.36}$$

which is a very desirable form when the irradiation is applied very near to resonance. Now, a modification of the quadrupolar term is accomplished by modulating the applied r.f. [11,19a]

$$\mathcal{H} = -2\omega_1 \; I_x^{2-3} \cos\omega_m t + \frac{2\omega_Q}{3}(I_z^{1-2} - I_z^{2-3}) \quad , \tag{1.37}$$

where I have set $\Delta\omega = 0$. The time dependence of this Hamiltonian is now removed in the same way as the transformation to the rotating frame. Redefining ψ in the Schrödinger equation (Eq. (1.5)) as

$$\begin{aligned} \psi' &= \exp\left(\frac{2\omega_m t}{3}\,(I_z^{1-2} + I_z^{2-3})\right)\cdot\psi \\ &= \exp\left(-\omega_m t \; I_z^{2-3} + \frac{\omega_m t}{3}(I_z^{1-2} + I_z^{2-3})\right)\cdot\psi \\ &= U\psi \quad , \end{aligned} \tag{1.38}$$

and decomposing the modulation into two counterrotating fields about I_z^{2-3}:

$$\mathcal{H} = -\omega_1(U^\dagger I_x^{2-3} U + U I_x^{2-3} U^\dagger) + \frac{2\omega_Q}{3}(I_z^{1-2} - I_z^{2-3}) \quad , \tag{1.39}$$

where this is possible because $[I_x^{2-3}, I_z^{1-2} + I_z^{1-3}] = 0$. Now we carry out steps analogous to Equations (1.24) through (1.27) and obtain

$$\mathcal{H} = -\omega_1 \; I_x^{2-3} - \omega_1 U U I_x^{2-3} U^\dagger U^\dagger + \frac{2\Delta\omega_Q}{3}\,(I_z^{1-2} - I_z^{2-3}) \quad . \tag{1.40}$$

The second term, which rotates at $2\omega_m$, may be neglected so long as $\omega_1 \ll \omega_m$, and Eq. (1.40) becomes

$$\mathcal{H} = -\omega_1 \; I_x^{2-3} + \frac{2\Delta\omega_Q}{3}\,(I_z^{1-2} - I_z^{2-3}) \quad , \tag{1.41}$$

with the reduced quadrupolar interaction $\Delta\omega_Q = \omega_Q - \omega_m$. Modulated r.f. has not been used in this study. As we will see later, its use would have led to terribly confusing results, not to mention the technical problems involved [11].

1.2.4 Magnetic Dipole-Dipole

Two nuclei of non-zero spin will interact when placed near each other due to their magnetic dipolar interaction. This interaction will take the form of:

$$\mathcal{H}_{I_i I_j} = \frac{\gamma_i \gamma_j \hbar}{r_{ij}^3} \left(I_i I_j - \frac{3(I_i \cdot r_{ij})(I_j \cdot r_{ij})}{r_{ij}^2}\right) \quad . \tag{1.42}$$

In the presence of an external magnetic field, we may define θ and ϕ as the polar angles describing the orientation of the internuclear vector r with respect to H_0, and express Eq. (1.42) as [12]:

$$\mathcal{H}_{I_i I_j} = \frac{\gamma_i \gamma_j \hbar}{r_{ij}^3} (A + B + C + D + E + F) \tag{1.43}$$

where

$$A = (1-3\cos^2\theta) I_{z_i} I_{z_j} \quad ,$$

$$B = -\frac{1}{4}(1-3\cos^2\theta)(I_i^+ I_j^- + I_i^- I_j^+) \quad ,$$

$$C = -\frac{3}{2}\sin\theta\cos\theta\, e^{-i\phi}(I_{z_i} I_j^+ + I_{z_j} I_i^+) \quad ,$$

$$D = -\frac{3}{2}\sin\theta\cos\theta\, e^{i\phi}(I_{z_i} I_j^- + I_{z_j} I_i^-) \quad ,$$

$$E = -\frac{3}{4}\sin^2\theta\, e^{-2i\phi}\, I_i^+ I_j^+,$$

and

$$F = -\frac{3}{4}\sin^2\theta\, e^{2i\phi}\, I_i^- I_j^- \quad . \tag{1.44}$$

For integral spin nuclei at low fields, where the Zeeman eigenstates are no longer necessarily valid, there exists the possibility that the dipolar interaction will be very much reduced, or vanish altogether [13]. With regard to the fields in which I work, this will never be true, and further, all non-secular terms in (1.44) will be ignored (since they mix the Zeeman eigenstates). The truncated dipolar Hamiltonian will contain only the secular terms A and B. Term A is responsible for a static energy shift and introduces an inhomogeneous linebroadening, while term B is the so called "flip-flop" term, inducing the simultaneous flipping of two spins in opposite directions, and a homogeneous linebroadening.

In order to obtain a rough idea of the order of magnitude of these dipolar terms for ^{14}N, consider the magnitude of the quantities $\frac{\gamma_I^2\hbar}{r_i^3}$ and $\frac{\gamma_I\gamma_s\hbar}{r_i^3}$ in the typical and well known compound $NH_4C\ell$. This substance crystallizes in a cubic $CsC\ell$ lattice with ammonium ions on each corner of the cube and a chloride ion inthe center; the quadrupole coupling for such an arrangement must vanish by symmetry arguments. The lattice constant, characterizing the distance between adjacent nitrogen atoms, is 3.8684 Å [14], yielding:

$$\frac{\gamma_I^2 \hbar}{r_i^3 \cdot 2\pi} = 10.8 \text{ Hz} \tag{1.45}$$

for the homonuclear interaction, and

$$\frac{4\gamma_I \gamma_S \hbar}{2\pi\ r_i^3} = 597.6 \text{ Hz} \tag{1.46}$$

for the heteronuclear interaction between neighboring pairs. The factor of 4 in the heteronuclear case takes into account the rapid tumbling of each ammonium ion which averages the intramolecular dipolar interactions to zero, making each lattice point appear as four protons. Of course, there are actually many more spins which contribute to each of these interactions, and their magnitude may become much larger.

The operator form of the homonuclear Hamiltonian will contain both static and flip-flop terms, and becomes:

$$\mathcal{H}_{II} = \frac{\gamma^2 \hbar}{r_{ij}^3} \left((1-3\cos^2\theta) I_{z_i} I_{z_j} - \frac{1}{4}(1-3\cos^2\theta)(I_i^+ I_j^- + I_i^- I_j^+)\right) \quad . \tag{1.47}$$

The flip-flop term will become non-secular and generally unimportant (except for certain relaxation effects) when the coupled spins have very dissimilar Zeeman energies. From this consideration our heteronuclear Hamiltonian becomes:

$$\mathcal{H}_{IS} = \frac{\gamma_I \gamma_S \hbar}{r_i^3} (1 - 3\cos^2\theta) I_z S_z \quad . \tag{1.48}$$

Modulation of this Hamiltonian in the rotating frame will give rise to decoupling and heteronuclear cross-relaxation effects to be discussed later.

1.2.5 Chemical Shift

Molecules are defined by their pattern of bonds, their electronic distribution. This electronic distribution, which is responsible for the quadrupolar coupling, will also react in various ways to shield the nucleus from the full effect of the static magnetic field. This interaction between the electronic distribution and H_0 is responsible for the chemical shift dispersion which makes NMR such a useful tool for chemical identification. It is easiest, once again, to express the chemical shift interaction in terms of a second rank tensor $\underset{\sim}{\sigma}$ as:

$$\mathcal{H}_{CS} = \gamma \cdot I \cdot \underset{\sim}{\sigma} \cdot H_0 \quad , \tag{1.49}$$

where the Cartesian tensor $\underset{\sim}{\sigma}$ is composed of chemical shielding elements in the reference frame of H_0. For my purposes, I will neglect any non-secular elements [15], leaving the tensor symmetric. It can therefore be decomposed into a scalar

$$\sigma_{ISO} = \frac{1}{3} \sum_i \sigma_{ii} \quad , \tag{1.50}$$

which is the isotropic chemical shift observed in liquids, and a traceless symmetric second rank tensor

$$\underset{\sim}{\sigma}' = \frac{1}{2}(\sigma_{ij}+\sigma_{ji}) - \sigma_{ISO} \quad . \tag{1.51}$$

This symmetric tensor may always be diagonalized in its own PAS, and thus be described completely by three parameters: σ_{xx}, σ_{yy}, and σ_{zz}, (or σ_{ISO} and any two of the others). Conversion to spherical tensors, and subsequent rotation about Euler angles θ and ϕ with respect to H_0, can be accomplished in a manner directly analogous to that used for the quadrupolar interaction (appendix A) to produce:

$$\mathcal{H}_{CS} = \sigma_{ISO} + \sigma_0[(3\cos^2\theta-1) + \eta\sin^2\theta\cos 2\phi]I_z \quad , \tag{1.52}$$

where

$$\sigma_0 = \sigma_{zz}-\sigma_{ISO}, \text{ and } \eta = \frac{\sigma_{xx}-\sigma_{yy}}{\sigma_{ISO}} \; .$$

The range of isotropic chemical shifts observed for nitrogen covers approximately 900 ppm [16], or about 18 kHz at a resonance frequency of 19.5 MHz. This implies the possibility of a fairly large anisotropic chemical shift interaction in solids. Fortunately (or, unfortunately, depending upon how one views it) the ^{14}N quadrupolar interaction has in all cases been observed to be orders of magnitude larger than the chemical shift. For example: in N_2 the ratio of chemical shift to quadrupole coupling (defined as $\gamma(\sigma_{ISO}-\sigma_{zz})H_0/(\frac{e^2qQ}{\hbar}))$ is approximately 2.5×10^{-3} [17], while for L-histidine it is approximately 2×10^{-4} for the ammonium nitrogen

and 2×10^{-3} for each of the heterocyclic nitrogens [18]. From this it follows that I will almost always be able to entirely neglect the effect of anisotropic chemical shifts.

1.3 Powder Patterns

Orientation dependent interactions, such as the quadrupole or chemical shift, produce, in solids, sharp resonance lines representing each inequivalent nuclear site exhibited. In a powder, where all orientations are represented with equal probability, these lines merge together to form a lineshape commonly referred to as a powder pattern. Powder patterns would be useless were it not for the fact that they can yield information characteristic of the tensor they represent.

To derive the characteristic powder pattern lineshape, we need only determine the number of orientations which correspond to each frequency of our spectrum. As an example, take the quadrupolar interaction (Eq. (1.31)), where the first order quadrupolar shift is defined by Eq. (1.32) as

$$\omega_Q = \frac{3\ e^2qQ}{8\ \hbar}\ (3\ \cos^2\theta - 1 + \eta \sin^2\theta\ \cos 2\phi) \quad .$$

The powder pattern intensity is given by $d\Omega/d\omega_Q = \sin\theta\ d\theta d\phi/d\omega_Q$. For the axial case ($\eta$=0), we only need to deal with θ dependence, givng

$$I(\omega) \sim \sin\theta(\sin 2\theta)^{-1} \quad , \qquad (1.53)$$

This spectrum consists of shoulders at $\pm \frac{3\ e^2qQ}{4\ \hbar}$ and spikes at $\pm \frac{3\ e^2qQ}{8\ \hbar}$ (see Figure 2). Analytic expressions for the general case ($\eta \neq 0$) have been known for many years, and are given by [19]:

$$I(\omega) \sim \frac{V_{zz}-V_{xx}}{\omega-V_{xx}} \int_0^{\pi/2} \{1 - \frac{(V_{yy}-V_{xx})}{(V_{zz}-V_{yy})} \cdot \frac{(V_{zz}-\omega)}{(\omega-V_{xx})} \sin^2\gamma\}^{-1/2} d\gamma \tag{1.54}$$

where $V_{yy} < \omega < V_{zz}$, and

$$I(\omega) \sim \frac{(V_{zz}-V_{xx})(V_{zz}-V_{yy})}{(V_{zz}-\omega)(V_{yy}-V_{xx})} \int_0^{\pi/2} \{1 - \frac{(\omega-V_{xx})(V_{zz}-V_{yy})}{(V_{zz}-\omega)(V_{yy}-V_{xx})} \sin^2\gamma\}^{-1/2} d\gamma \tag{1.55}$$

where $V_{xx} < \omega < V_{yy}$; and

$$V_{xx} = (1-\eta)\ \frac{3}{8}\ \frac{e^2qQ}{\hbar} \tag{1.56a}$$

$$V_{yy} = (1+\eta)\ \frac{3}{8}\ \frac{e^2qQ}{\hbar} \tag{1.56b}$$

$$V_{zz} = -\ \frac{3}{4}\ \frac{e^2qQ}{\hbar} \tag{1.56c}$$

are the points which define the principle values of the quadrupole coupling tensor. The integrals in Eqs. (1.54) and (1.55) are commonly known as elliptical integrals, for which polynomial

Figure 2. NMR powder spectra for various values of the asymmetry parameter $\eta = \frac{V_{xx}-V_{yy}}{V_{zz}}$.

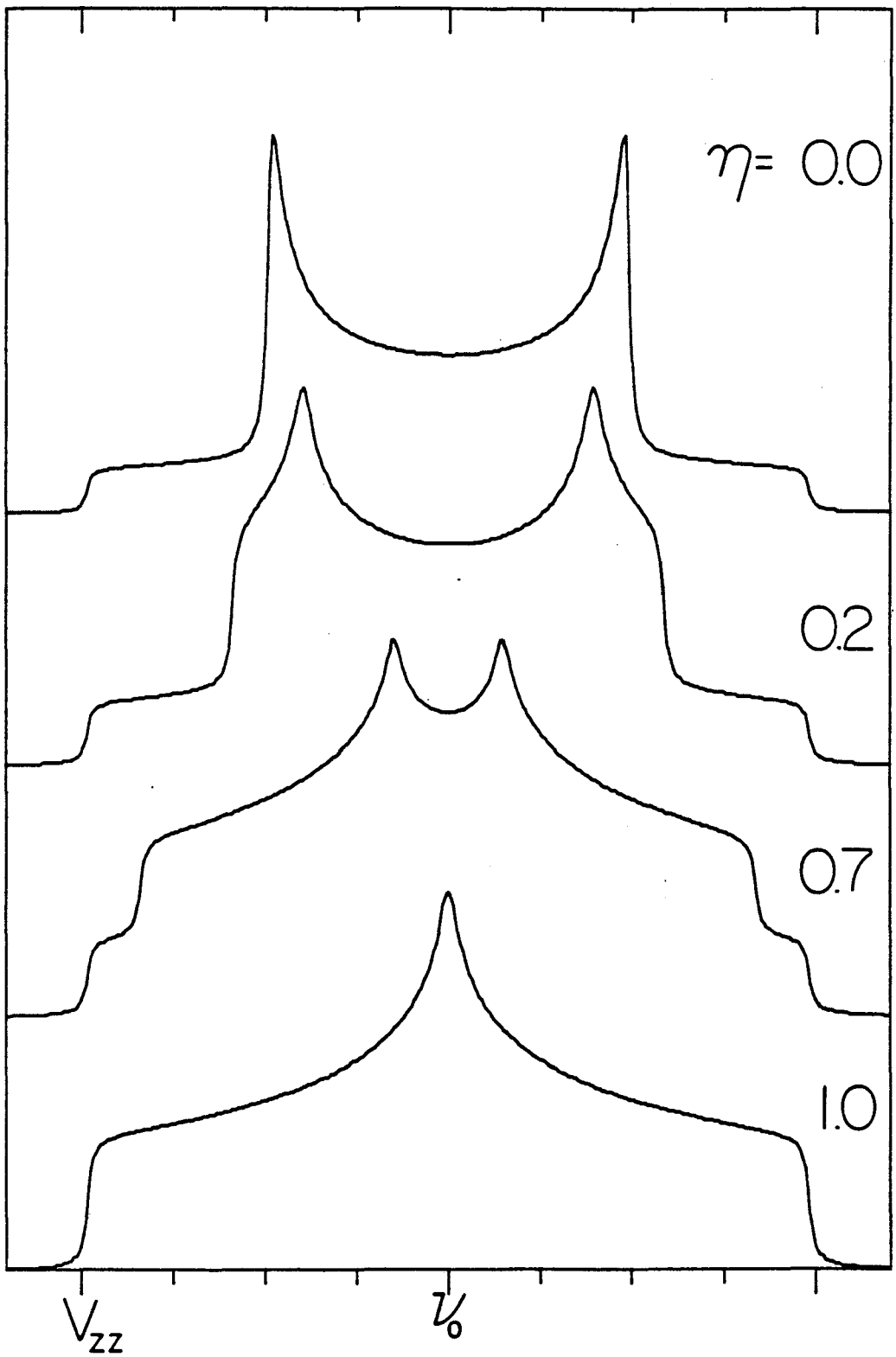

XBL 839-11509

Figure 3. NMR powder spectra resulting from a combination of chemical shift and first order quadrupolar interactions. The two tensors are assumed to be aligned parallel to one another, and % CS is defined:

$$\% \text{ CS} = 100 \cdot \left(\frac{\gamma(\sigma_{ISO}-\sigma_{ZZ})H_0}{\left(\frac{e^2qQ}{\hbar}\right)}\right) .$$

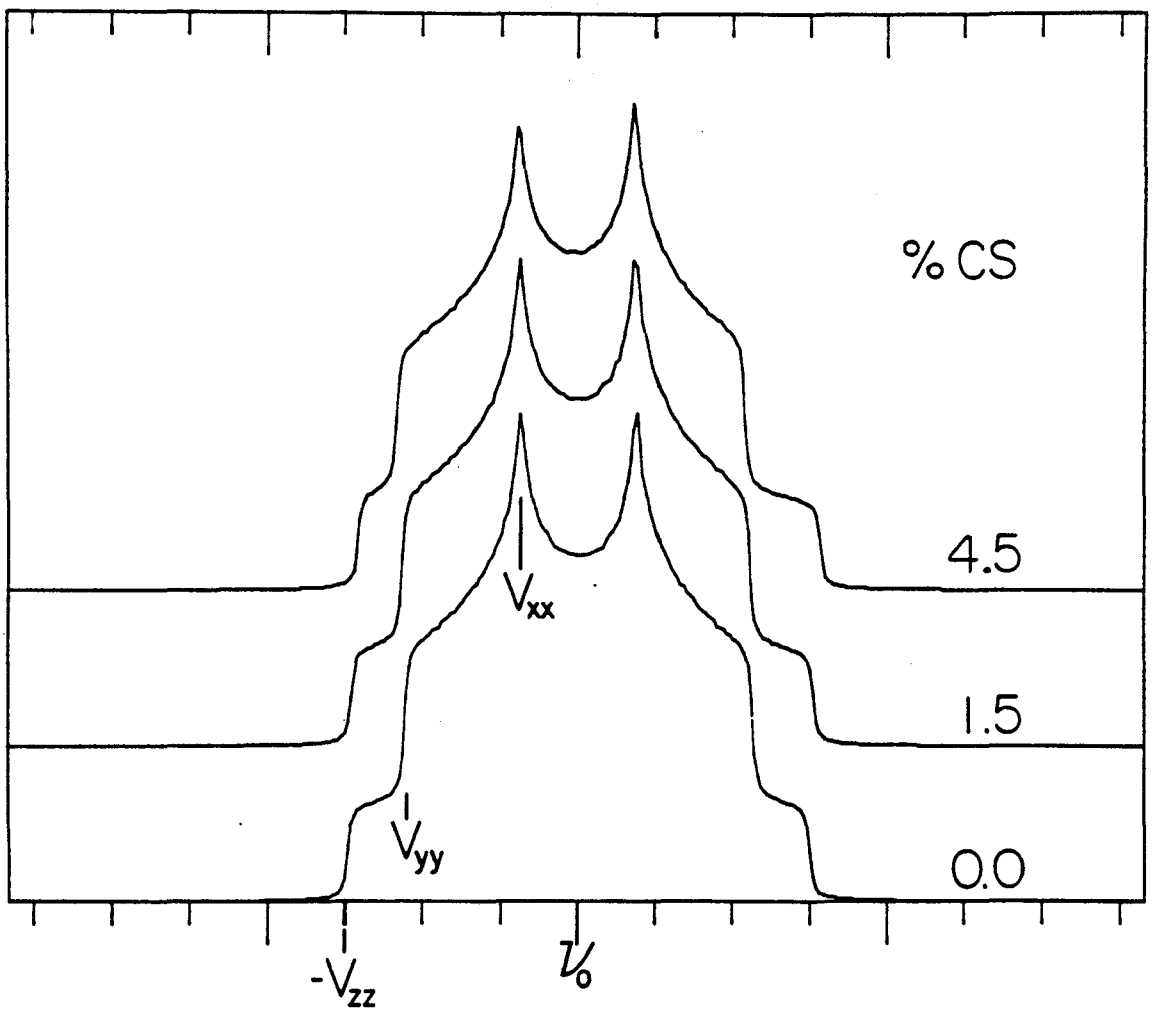

XBL 839-11511

approximations are available [20]. With sufficient S/N the principle values are fairly easily gleaned from such a spectrum. Problems are encountered with broad spectra since, as the breadth of the spectrum increases, the S/N (in the absence of instrumental demands to be discussed later) decreases in approximate proportion.

If the powder pattern is not the result of one interaction, or if it is perturbed by motion, then the lineshape $d\Omega/d\omega$ must be numerically calculated on a computer. This approach has been taken in order to generate many theoretical spectra presented here, such as the combination chemical shift-quadrupole powder patterns of Figure 3 where we see that the anisotropic chemical shift interaction would have to be far larger than anyone would ever imagine in order to noticeably perturb the powder pattern.

In this work, I deal almost entirely with powdered samples, and hence powder patterns. The primary reasons for this are crystallization difficulties, and experimental simplicity. Of course, by following this path I have lost all information regarding the relationship between the coupling tensor and the crystalline reference frame. In forthcoming pages I will describe the methods which have been used to obtain NMR powder spectra of ammonium and tetraalkylammonium compounds.

Chapter 2: Techniques

2.1 Observation of FID's

The quadrupolar powder pattern will be quite broad, covering a frequency range of $\pm \frac{3}{4} \frac{e^2qQ}{h}$. Observation of such broad lineshapes has been achieved for many years via continuous wave (c.w.) NMR techniques, however, the time required to obtain adequate c.w. S/N can sometimes be excessive. Considering the fact that the frequency response, or spectral density, and the impulse response, or autocorrelation of a linear system are fourier transform pairs, it should, at least in principle, be possible to obtain all frequency domain information by recording the time domain autocorrelation, or free induction decay (fid) [24,25,26]. This is the basis of the fourier transform (f.t.) NMR technique, which has come to dominate the field in the past two decades. The obvious advantage of the technique is that the entire spectrum may be "swept" in the time required to record the fid; usually on the order of milliseconds.

The equation describing the time evolution of the observable fid following a pulse along y will be:

$$G(t) = \mathrm{Tr}(S_+ \, e^{-i\mathcal{H}t} \, S_x \, e^{i\mathcal{H}t}) \quad , \tag{2.1}$$

where $\mathcal{H}$ will typically contain every term in Eq. (1.13), with the exception of the r.f. term; for my purposes $\mathcal{H}_Q$ will dominate. In order to successfully apply the f.t. technique, it is necessary to digitally sample G(t) undistorted at a rate at least twice its bandwidth; or, at a rate equal to its bandwidth if quadrature detection is employed. The sampling process itself is not

difficult using digital circuits presently available, but the actual observation of the signal presents some difficulty. The most commonly used method of detecting an fid is via the voltage produced by its time dependent flux within a tuned r.f. coil. A conventional LC coil circuit tuned to ω_0 will have a bandwidth $\Delta\omega$ defined by its $Q = \omega_0/\Delta\omega$. For simple circuit configurations, the Q is determined by losses in the circuit (resistive) and its value will determine both the output voltage available for a given flux, and the noise voltage produced within the circuit. The implication here is that the S/N is very dependent upon the Q, and in fact, it is commonly thought to vary as $Q^{1/2}$ [27]. Unfortunately, a tuned circuit, once excited with an r.f. voltage on the order of one or two hundred volts, will require a time of approximately $20\ Q/\omega_0$ to ring down before the very small nuclear resonance signal, on the order of tenths to hundreds of microvolts, may be observed. At a frequency of 20 MHz and a Q of 100, this corresponds to approximately 30 μsec of "dead time". Because information regarding the broadest part of the lineshape is contained in the initial part of the fid, loss of the first 30 μsec of the fid is almost always intolerable. Various methods of reducing the ringdown time without reducing the effective Q of the circuit have been introduced [28,29], but even with these, a few μsec of deadtime must be tolerated. Additionally, I will demonstrate later that, even in the total absence of any ringdown, there exists a dead time for the quadrupolar fid becuase it begins before the pulse ends.

2.1.1 Quadrupolar Echoes

Fortunately, a very nice solution to the problem has existed for quite some time. It has long been known that the evolution of a system governed by inhomogeneous interactions can be reversed by the appropriate pulse, or sequence of pulses. This reversal at a time τ leads to the formation of an echo at 2τ, and was first observed by Hahn for the inhomogeneous Zeeman interaction in 1950 [30]. The first order quadrupolar interaction is also inhomogeneous and reversible, and the use of quadrupolar echoes [31,32] permits the observation of an undistorted fid, so long as τ may be extended beyond the probe ringdown time. The major limitation of quadrupolar echoes derives from irreversible T_2 processes, which will be discussed in a later chapter.

The classic quadrupolar echo sequence consists of two pulses of 90° rotation, differing in phase by 90°, and separated by a delay τ. In order to demonstrate the mechanics of this sequence, it is most convenient to utilize the fictitious spin 1/2 operator formalism (Appendix B). Initially consider an isolated spin 1 irradiated on resonance; Eq. (1.36) will become:

$$\mathcal{H} = -\,2\omega_1\, S_x^{2-3} + \frac{2\omega_Q}{3}\,(S_z^{1-2} - S_z^{2-3}) \tag{2.2}$$

describing x irradiation, and

$$\mathcal{H} = -\,2\omega_1\, S_y^{1-2} + \frac{2\omega_Q}{3}\,(S_z^{1-2} - S_z^{2-3}) \tag{2.3}$$

describing y irradiation. It will be assumed here that $\omega_1 >> \omega_Q$, so that the Hamiltonian during irradiation will consist of only an r.f. term. The equilibrium density matrix (Eq. (1.14)) will be proportional to S_z^{1-3}, which, in this reference frame, becomes S_x^{1-3}, and we can employ Eq. (17) and B.6 to determine its evolution. Following the first pulse:

$$e^{2i\omega_1 t_p S_x^{2-3}} \; S_x^{1-3} \; e^{-2i\omega_1 t_p S_x^{2-3}} =$$

$$S_x^{1-3} \cos\omega_1 t_p + S_y^{1-2} \sin\omega_1 t_p \quad , \tag{2.4}$$

and, for $\omega_1 t_p = \pi/2$, this reduces to S_y^{1-2}. Before considering the first delay period, the following useful relations should be kept in mind:

$$\frac{2\omega_Q}{3} (S_z^{1-2} - S_z^{2-3}) = \omega_Q S_z^{1-2} - \frac{\omega_Q}{3} (S_z^{1-3} + S_z^{2-3}) \tag{2.5a}$$

$$= -\omega_Q S_z^{2-3} + \frac{\omega_Q}{3} (S_z^{1-2} + S_z^{1-3}) \quad , \tag{2.5b}$$

and

$$[S_y^{1-2} \; , \; S_z^{1-3} + S_z^{2-3}] = 0 \tag{2.6a}$$

$$[S_x^{2-3} ,, \; S_z^{1-3} + S_z^{1-2}] = 0 \quad . \tag{2.6b}$$

Evolution under the first order quadrupolar interaction during τ_1 reduces to:

$$e^{-i\omega_Q\tau_1 S_z^{1-2}} S_y^{1-2} e^{i\omega_Q\tau_1 S_z^{1-2}} =$$

$$S_y^{1-2} \cos\omega_Q\tau_1 - S_x^{1-2} \sin\omega_Q\tau_1 \tag{2.7}$$

The second pulse along y results in:

$$e^{2i\omega_1 t_p S_y^{1-2}} (S_y^{1-2} \cos\omega_Q\tau_1 - S_x^{1-2} \sin\omega_Q\tau_1)\, e^{-2i\omega_1 t_p S_y^{1-2}} =$$

$$S_y^{1-2} \cos\omega_Q\tau_1 + S_x^{1-2} \sin\omega_Q\tau_1 \quad , \tag{2.8}$$

where $\omega_1 t_{p_2} = \pi/2$. The second delay period evolution is easily calculated as:

$$e^{-i\omega_Q\tau_2 S_z^{1-2}} (S_y^{1-2} \cos\omega_Q\tau_1 + S_x^{1-2} \sin\omega_Q\tau_1)\, e^{i\omega_Q\tau_2 S_z^{1-2}} =$$

$$\cos\omega_Q\tau_1 (S_y^{1-2} \cos\omega_Q\tau_2 - S_x^{1-2} \sin\omega_Q\tau_2)$$

$$- \sin\omega_Q\tau_1 (S_x^{1-2} \cos\omega_Q\tau_2 + S_y^{1-2} \sin\omega_Q\tau_2) \quad . \tag{2.9}$$

Equation (2.9) becomes independent of ω_Q when the first delay τ_1 equals the second delay τ_2; this is the quadrupolar echo we have been seeking. Certain very useful properties should be noticed at this time: (1) essentially zero time resolution is obtained for the quadrupolar fid, and (2) from Eq. (2.7), the phase of the echo will be invariant to a 180° phase shift of the second pulse. This second property has been very important in my work, allowing suppression of ringing and other spurious transients (e.g., magneto-

acoustic ringing [33]) coherent with the phase of the second pulse.

In nearly all of the experiments I present here, observation of the fid was accomplished with a quadrupolar echo, making this an extremely important topic worthy of further discussion. The preceeding deliberation on the quadrupolar echo, which makes it appear as a perfect pulse sequence, is not an accurate description of the actual experimental situation. First and foremost, ω_1 is seldom much larger than the largest ω_Q present; and often is considerably smaller. This effect may be calculated analytically by retaining the quadrupolar portion of the Hamiltonian during r.f. irradiation. We proceed by diagonalizing Eq. (2.2) written as

$$\mathcal{H} = -2\omega_1 S_x^{2-3} - \omega_Q S_z^{2-3} + \frac{\omega_Q}{3}\left(S_z^{1-2}+S_z^{1-3}\right) \tag{2.10}$$

for the first pulse via a rotation of $-\theta$ about S_y^{2-3}, where $\theta = \mathrm{atan}(2\omega_1/\omega_Q)$, and

$$\mathcal{H} = -2\omega_1 S_y^{1-2} + \omega_Q S_z^{1-2} - \frac{\omega_Q}{3}\left(S_z^{1-3}+S_z^{2-3}\right) \tag{2.11}$$

for the second pulse via a rotation about S_x^{1-2} to obtain

$$\mathcal{H}^T = -\omega_e S_z^{2-3} + \frac{\omega_Q}{3}\left(S_z^{1-2}+S_z^{1-3}\right) \tag{2.12}$$

for the x pulse, and

$$\mathcal{H}^T = -\omega_e S_z^{1-2} - \frac{\omega_Q}{3}\left(S_z^{1-3}+S_z^{2-3}\right) \tag{2.13}$$

for the y pulse, where

$$\omega_e = (4\omega_1^2+\omega_Q^2)^{1/2} \quad . \tag{2.14}$$

I remark here that Eq. (1.35) can always be converted to diagonal form via a tilt so long as $\Delta\omega$ can be neglected in relation to ω_1; which is almost always the case. In order to obtain an exact analytical expression for the effect of the on resonance quadrupolar echo sequence upon the equilibrium density matrix ρ_0, it is necessary to carry out the following steps:

1) tilt ρ_0 into the frame in which $\mathcal{H}$ is diagonal
2) calculate the evolution of ρ_0 to $\rho(t_1)$ via Eqns. (1.7) and (2.10)
3) tilt $\rho(t_1)$ back to the original reference frame
4) calculate the evolution of $\rho(t_1)$ to $\rho(t_1+\tau_1)$ in the original reference frame
5) repeat steps 1, 2, and 3 using the Hamiltonian Eq. (2.11) in order that $\rho(t_1+\tau_1+t_2)$ may be obtained
6) the evolution of $\rho(t_1+\tau_1+t_2)$ to $\rho(t_1+\tau_1+t_2+\tau_2)$ is accomplished to obtain the observed signal as a function of τ_2.

Fortunately, the tedious operator algebra has already been carried out (2, 23, 40), and the resulting expression of the observable coefficient of S_y^{1-2} as a function of the various times involved may be easily calculated. After some manipulation, it is possible to obtain:

$$\rho(t_1+\tau_1+t_2+\tau_2) = \sin\theta \sin\frac{\omega_e t_2}{2} \cos\omega_Q(\tau_1+t_1/2)\cdot$$

$$\{(\cos^2\theta \cos\omega_{e}t_2+\sin^2\theta)(\cos\omega_Q\tau_2\ S_y^{1-2}-\sin\omega_Q\tau_2 S_x^{1-2}) +$$

$$\cos\theta \sin\omega_e t_2(\cos\omega_Q\tau_2\ S_x^{1-2}+\sin\omega_Q\tau_2 S_y^{1-2})\}$$

$$- \sin\theta \sin\frac{\omega_e t_1}{2} \sin\omega_Q(\tau_1+t_1/2)\cdot$$

$$\{\cos\omega_e t_2(\cos\omega_Q\tau_2\ S_x^{1-2}+\sin\omega_Q\tau_2 S_y^{1-2}) +$$

$$\sin\omega_e t_2 \cos\theta\ (\cos\omega_Q\tau_2 S_y^{1-2}-\sin\omega_Q\tau_2 S_x^{1-2})\} \quad , \qquad (2.15)$$

where I have neglected all density matrix elements which are uninteresting, and will not lead to an observable signal (such as S_z^{1-2}). The operator S_y^{1-2} in this reference frame corresponds to observable y magnetisation in the laboratory frame ($\frac{\sqrt{2}}{2}(S_y^{1-2}+S_y^{2-3})$), while S_x^{1-2} corresponds to a non-observable antiphase single quantum coherence ($\frac{\sqrt{2}}{2}(S_y^{1-2}-S_y^{2-3})$). The observable may be extracted from (2.15) as

$$\langle S_y^{1-2}\rangle = \sin\theta \sin\frac{\omega_e t_1}{2} \cos\omega_Q(\tau_1+t_1/2)\cdot$$

$$\{(\cos^2\theta \cos\omega_e t_2+\sin^2\theta) \cos\omega_Q\tau_2+\cos\omega \sin\omega_e t_2 \sin\omega_Q\tau_2\}$$

$$- \sin\theta \sin\frac{\omega_e t_1}{2} \sin\omega_Q(\tau_1+t_1/2)\cdot$$

$$\{\cos\omega_e t_2 \sin\omega_Q\tau_2 + \sin\omega_e t_2 \cos\theta \cos\omega_Q\tau_2\} \quad . \qquad (2.16)$$

Figure 4. The magnitude of the observable coefficient S_y following a pulse along S_x for several values of pulse rise time.

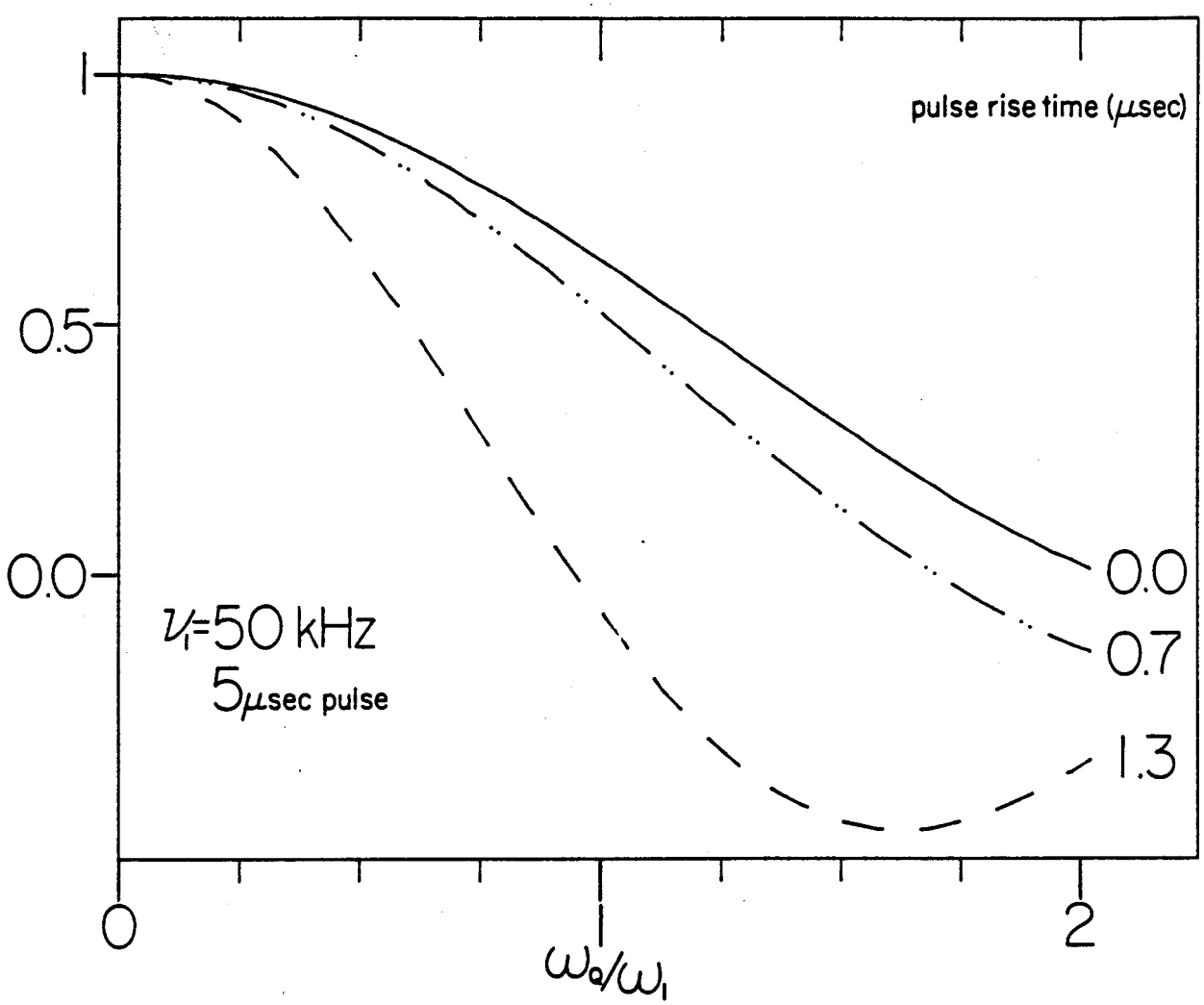

XBL 839-11504

A few things should be noticed about this equation. Firstly, the initial pulse gives the fid what is essentially a phase shift of half the pulse length. The fid appears to begin halfway through the pulse and it is impossible to attain absolute zero time resolution from one pulse no matter how short the ringdown time. This shift will result in echo formation when τ_2 equals $\tau_1+t_1/2$ instead of when τ_2 equals τ_1; the truth of this prediction has been demonstrated experimentally without exception. Secondly, Eq. (2.16) possesses an oscillatory behavior (Figures 5 and 6) which has the approximate functional form of $\sin^2\omega_Q(\tau_1+t_1/2)$ [2]. These oscillations are due to the differing effect of the second pulse depending upon whether $\rho(\tau_1+t_1/2)$ contains more S_x^{1-2} or S_y^{1-2}; for very hard (large ω_1) pulses, the effect will vanish. These undulations are never observed experimentally. What we will observe is given by the solid line in Figure 5, which is well described by the echo sequence distortion function of Bloom et al., [34]. It is possible to see exactly how this comes about by a re-examination of Eq. (2.16). From this equation it is necessary to extract the portion corresponding to a time dependence of $\cos\omega_Q(\tau_1+t_1/2-\tau_2)$, which will become independent of ω_Q when τ_2 equals $\tau_1+t_1/2$. Using the identity

$$\cos\omega_Q(\tau_1+t_1/2-\tau_2) = \cos\omega_Q(\tau_1+t_1/2)\cos\omega_Q\tau_2 + \sin\omega_Q(\tau_1+t_1/2)\sin\omega_Q\tau_2$$

we first extract from (2.16)

$$\sin\theta \sin\frac{\omega_e t_1}{2} \{(\cos^2\theta \cos\omega_e t_2 + \sin^2\theta)\cos\omega_Q \tau_2 \cos\omega_Q(\tau_1 + t_1/2)$$

$$- \cos\omega_e t_2 \sin\omega_Q \tau_2 \sin\omega_Q(\omega_1 + t_1/2)\} \tag{2.17}$$

and make use of the identity:

$$\cos\omega_e t_2 = 1-2\sin^2\frac{\omega_e t_2}{2} = \cos^2\frac{\omega_e t_2}{2} - \sin^2\frac{\omega_e t_2}{2}$$

to yield the desired extrication as:

$$\sin^3\theta \sin\frac{\omega_e t_1}{2} \sin^2\frac{\omega_e t_2}{2} (\cos\omega_Q \tau_2 \cos\omega_Q(\tau_1 + t_1/2)$$

$$+ \sin\omega_Q t_2 \sin\omega_Q(\tau_1 + t_1/2)) \quad ; \tag{2.18}$$

which becomes:

$$D(\omega_1,\omega_Q) = \sin^3\theta \sin\frac{\omega_e t_1}{2} \sin^2\frac{\omega_e t_2}{2} \tag{2.19}$$

at the echo maximum. This is the function of Bloom et al., and I have used it to correct computer generated powder patterns for the effect of finite pulse lengths.

Of course, as I mentioned before, the pulse lengths are not only finite, but so are the rise and fall times (i.e., the pulses are not square). The effect of this on density matrix evolution may be calculated as described in Section 1.1, by breaking the time dependent pulse amplitude into a finite number of sub-pulses, each of which has a time independent amplitude so as to describe the

Figure 5. The magnitude of the observable coefficient S_y following the quadrupolar echo sequence: $90^\circ_x-\tau-90^\circ_y-\tau$. The dotted line is obtained by computing $Tr(\rho(t_1+\tau+t_2+\tau)S_y^{1-2})$, the solid line is the fourier transform of the calculated fid starting at the echo maximum, and the crosses represent values computed from the echo sequence distortion function of Bloom et al. [34] (Eq. (2.19)).

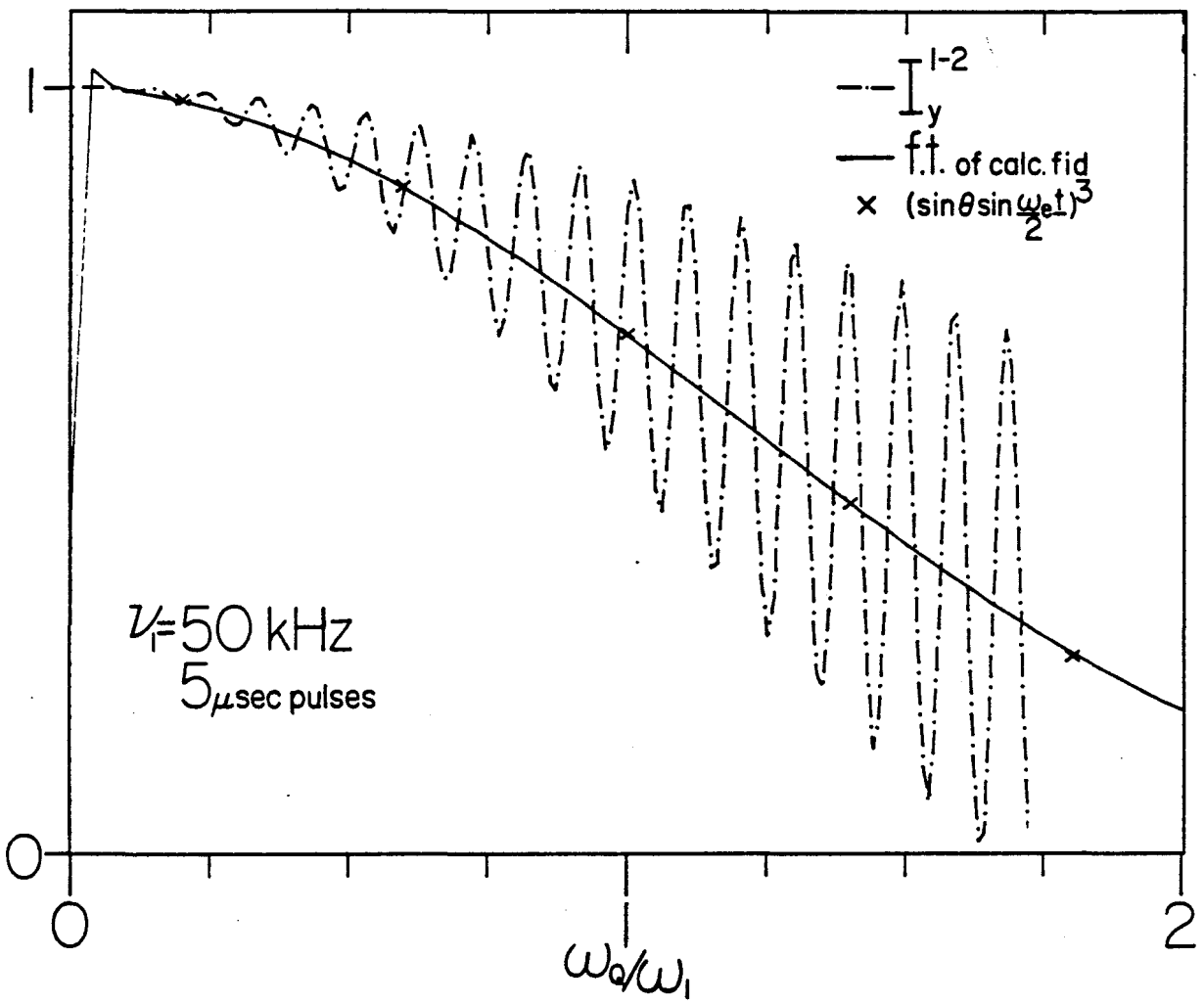

XBL 839-11505

Figure 6. The magnitude of the observable coefficient S_y following the quadrupolar echo sequence for infinitesimal and finite pulse rise time. Both lines were obtained by computing $Tr(\rho(t_1+\tau+t_2+\tau)S_y^{1-2})$.

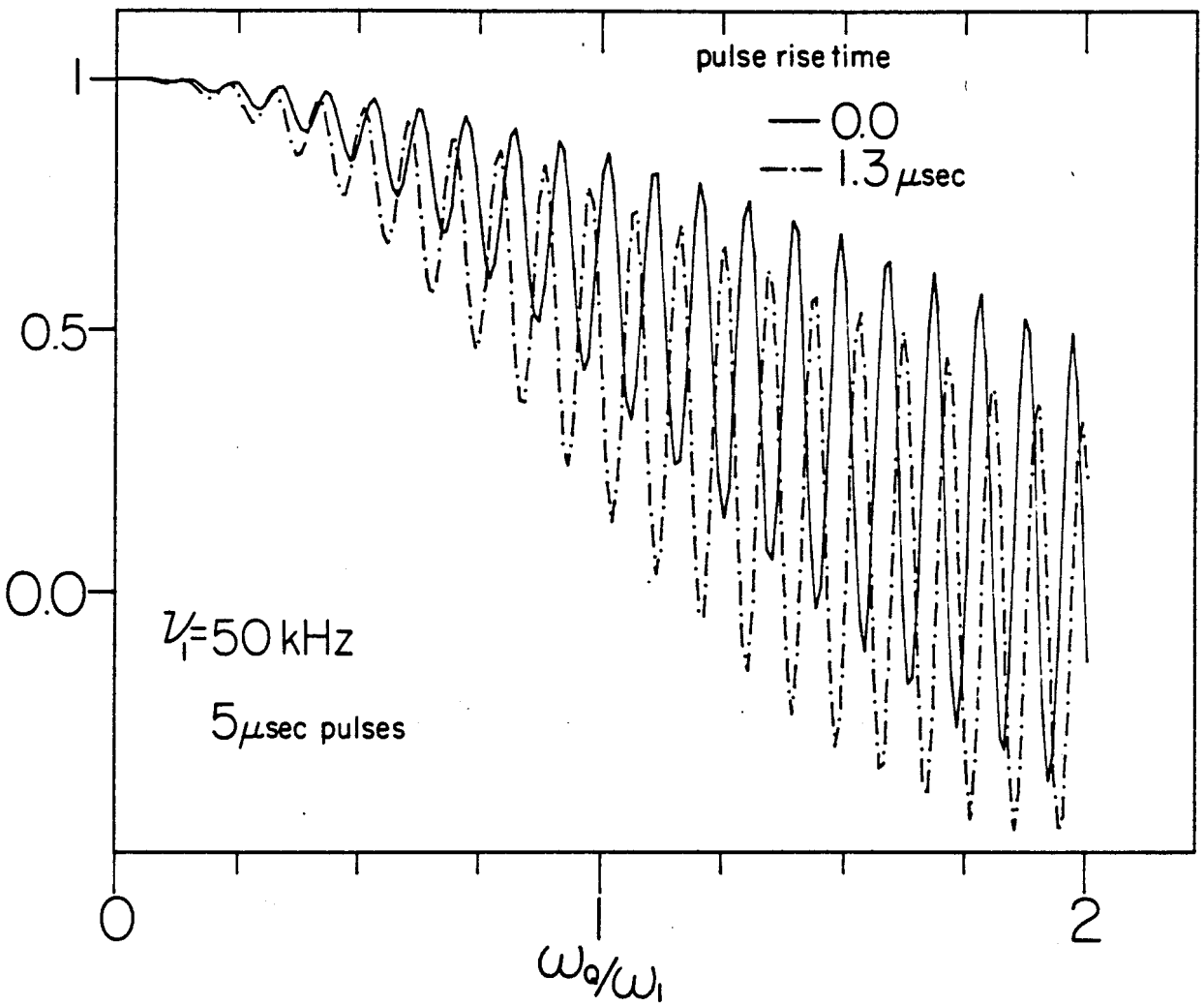

XBL 839-11506

envelope of the pulse:

$$H_1(t) = H_{1_{max}}(1-e^{-t/Tr}) \quad 0 \leq t \leq t_p \tag{2.20a}$$

$$= H_{1_{max}} e^{-t/Tr} \quad t_p \leq t \quad , \tag{2.20b}$$

and satisfy

$$\int_0^{t' \leq t_p} H_1(t)dt = H_{1_{max}} t_p \tag{2.21}$$

where

$$Tr = 2Q/\omega_0 \tag{2.22}$$

is the characteristic ringdown time of the tuned circuit. The result of this calculation for a single pulse (see Figure 4) is a significant degradation of the observable response following the pulse as the risetime increases. This is primarily because the fid begins halfway through the pulse, and the longer in time the pulse persists, the greater is the evolution at large ω_Q; in other words, this is almost entirely a deadtime problem. As Figure 6 demonstrates, this problem is much alleviated in the echo, where the dead time is removed. I have corrected none of my spectra for the effects of finite rise and fall times, primarily because I don't believe it is necessary.

The effect of the probe time constant (Eq. (2.20)) will also result in the so-called "phase glitch" [35]; in which a pulse is

produced of time dependent phase during its rising and falling periods. This results in a small off-axis rotation during each pulse, whose cumulative effects may be large for many pulses [36], but for the simple two pulse sequence it is not likely significant.

I feel that there is one more characteristic of this quadrupolar echo sequence which is worthy of discussion. Starting with Eq. (2.4), and assuming the conditions $\omega_1 >> \omega_Q$ and $\omega_1 t_1 = \pi/2$ are satisfied, the first pulse creates only a coefficient of S_y^{1-2}. Now, consider the effect of a resonance offset during the first delay period. The Hamiltonian during this period becomes:

$$\mathcal{H} = -2\Delta\omega\ S_x^{1-3} + \frac{2\omega_Q}{3}\ (S_z^{1-2} - S_z^{2-3}) \tag{2.23}$$

The evolution of S_y^{1-2} due to (2.23) is easily calculated:

$$\rho(t_1+\tau_1) = \cos\Delta\omega\tau_1(S_y^{1-2}\ \cos\omega_Q\tau_1 - S_x^{1-2}\ \sin\omega_Q\tau_1)$$

$$+ \sin\Delta\omega\tau_1(S_x^{2-3}\ \cos\omega_Q\tau_1 + S_y^{2-3}\ \sin\omega_Q\tau_1) \quad . \tag{2.24}$$

The desired echoing effect of the second pulse depends upon there being S_y^{1-2} and S_x^{1-2} in the density matrix, for the effect of this pulse on S_x^{2-3} and S_y^{2-3} is to create z magnetization and double quantum-coherence; not desirable from an observables point of view at all. Therefore, when the $\cos\Delta\omega\tau_1$ term goes to zero, the echo vanishes. There does exist some utility in this measurement, for it allows one to determine, with very good accuracy (< 100 Hz) the off-resonance condition when echoing a broad powder pattern (where an

accurate frequency domain measurement is all but impossible). So long as the echo isn't disappearing due to irreversible T_2 processes, one can use the relationship

$$\Delta\nu = (4\ \tau_{vanish})^{-1} \tag{2.25}$$

to determine the off-resonance condition. If we are in the unfortunate situation of having a large anisotropic chemical shift along with our quadrupolar coupling, then the quadrupolar echo spectrum may become horribly distorted (Figure 7). I do not expect to encounter large anisotropic chemical shifts, so this is not likely to happen.

To close out this section, I should point out that the frequency response of the echo sequence may be varied through the use of a composite pulse sequence [71]. In particular, the sequence [72] 45_x-$135_{\bar{x}}$-135_y-$45_{\bar{y}}$ acts as a compensated 90° pulse on a spin 1 system, increasing the frequency response near the center of the spectrum, but causing it to fall off more rapidly in the wings.

2.2.1 The Nature of Dipolar Broadening

I have demonstrated that the first order quadrupolar interaction may be refocused fairly easily, giving essentially zero time resolution with respect to this interaction. The question now arises as to the other coupling mechanisms in Equation 1.15; in particular, the dipolar interactions, both homo and heteronuclear. These, being perturbations involving many spins, will not typically add any structure to our powder pattern,

Figure 7. The consequences of chemical shift evolution during the quadrupolar echo sequence for a powder spectrum broadened by both first order quadrupole and anisotropic chemical shift interactions.

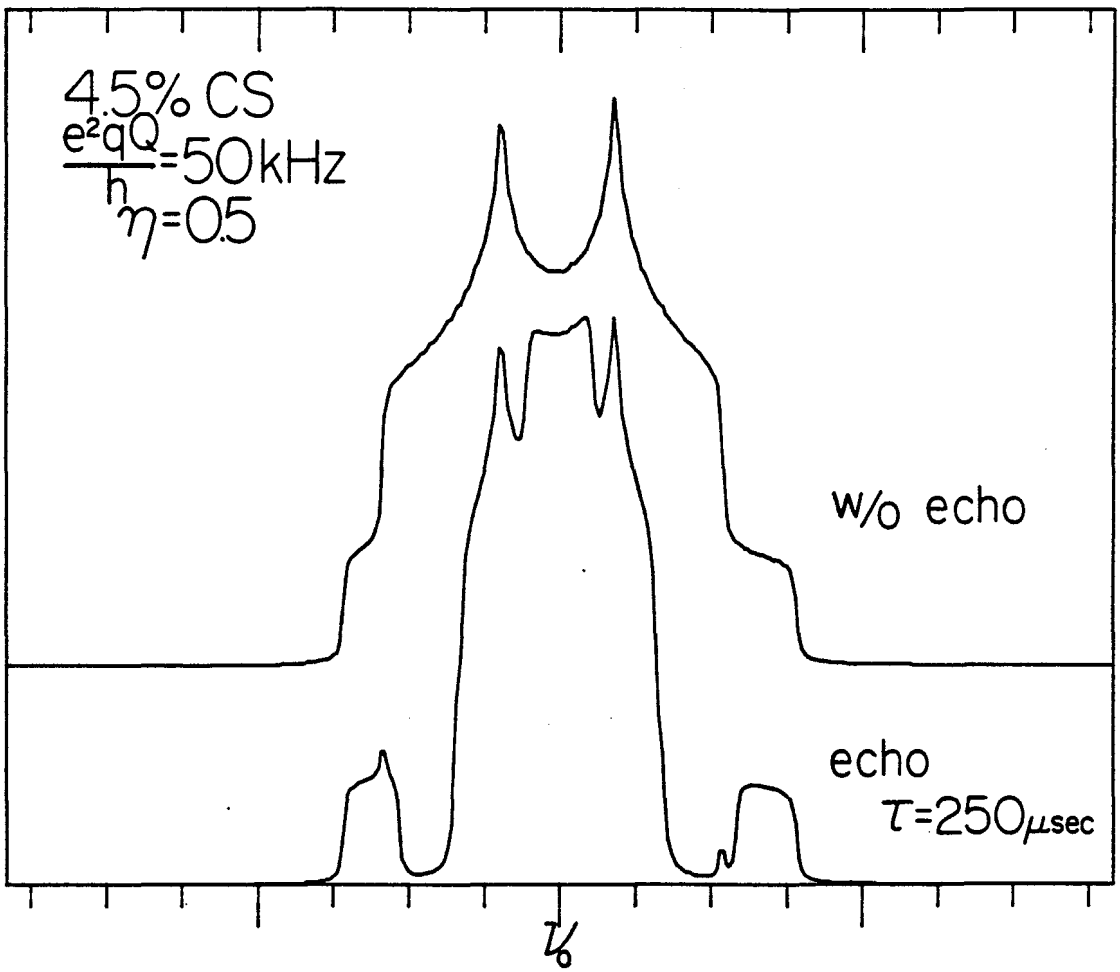

XBL 839-11508

but will merely broaden it. The broadening function is most suitably described in terms of its moments:

$$M_n = \frac{\int \omega^n \, I(\omega)\, d\omega}{\int I(\omega)\, d\omega} \quad , \tag{2.26}$$

where the zeroth moment (M_0) will be equal to one, the first moment will be the average frequency, the second moment will be the average squared frequency, etc. These moments may, at least in principle, be explicitly calculated, and, with a sufficient number of moments, a faithful representation of the broadening function may be obtained. In particular, the second moment may be calculated, with the aid of Eq. (2.1), as [37]:

$$M_2 = - \frac{\mathrm{Tr}[\mathcal{H}, S_x]^2}{\mathrm{Tr}[S_x]^2} \quad , \tag{2.27}$$

where I will consider $\mathcal{H}$ to contain only the dipolar terms $\mathcal{H}_{SS}$ and $\mathcal{H}_{IS}$. If the broadening takes on a gaussian form, then the relationship between the full width at half maximum (fwhm) and M_2 is [38]:

$$\Delta\omega = 2.36 \, M_2^{1/2} \quad . \tag{2.28}$$

If the broadening takes a lorentzian form, then M_2 will exceed $\Delta\omega_{fwhm}$ by a large amount, because a considerable portion of the intensity lies in the outer wings.

This broadening, in whatever form it takes, will tend to wash out spectral features and is highly undesirable. To get an idea of its magnitude, it is possible to calculate $M_2^{1/2}$ for $NH_4C\ell$ (see Section 1.2.4) via [38]:

$$M_2^{1/2} = (\frac{3}{5} \cdot 8.5 \cdot S(S+1))^{1/2} \frac{\gamma^2\hbar}{2\pi a^3} \quad , \tag{2.29}$$

where a is the lattice constant 3.3684 Å. Plugging in all of the values from Section 1.2.4, I obtain:

$$M_{2SS} = 34.5 \text{ Hz} \tag{2.30}$$

for the homonuclear interaction, and

$$M_{2IS}^{1/2} = 1.91 \text{ KHz} \tag{2.31}$$

for the heteronuclear interaction. Homonuclear flip-flops among the I spins will tend to reduce the fwhm of the heteronuclear broadening by increasing the fourth moment, giving the lineshape more lorentzian character. The maximum linewidth reduction we could expect from this mechanism would be a factor of the ratio of the gyromagnetic ratios; which, in the case of ^{14}N and ^{1}H is 13.8. Experimentally, I observe a ^{14}N NMR signal in $NH_4C\ell$ at room temperature which fits well to a lrentzian curve of fwhm equal to 550 Hz (the quadrupolar coupling should vanish for $NH_4C\ell$ due to lattice symmetry).

2.2.2 Decoupling

The homonuclear interaction between two ^{14}N nuclei seems very small, and its consideration will lead to a complicated quadrupolar echo situation (39), so I will presently ignore it. The heteronuclear term, by contrast, will be at least an order of magnitude larger and may be very troublesome. Spectra will not only be broadened, but the interaction is not refocused by the quadrupolar echo and so will lead to lower S/N in any echo experiment.

The most common and convenient method of reduction of $\mathcal{H}_{IS}$ is the application of a large r.f. decoupling field to the I spins. Consider a Hamiltonian consisting of this field plus $\mathcal{H}_{IS}$:

$$\mathcal{H} = -\omega_1 I_x - \Delta\omega I_z + 2\sum_i b_i \; I_{z_i} \; S_z^{1-3} \quad , \tag{2.32}$$

where

$$b_i = \frac{\gamma_I \gamma_S \hbar}{r_i^3} (3 \cos^2\theta_i - 1) \quad , \tag{2.33}$$

and fictitious spin 1/2 operators are used for the S spins. The first two terms in (2.32) are consolidated via a tilt about I_y of θ = atan $(\frac{\omega_1}{\Delta\omega})$ to yield:

$$\mathcal{H}^T = -\omega_e I_z + 2\sum_i b_i \; S_z^{1-3} \; (I_{z_i} \cos\theta + I_{x_i} \sin\theta) \quad , \tag{2.34}$$

where $\omega_e = (\omega_1^2 + \Delta\omega^2)^{1/2}$. Since the first term in (2.34) does not commute with the tilted dipolar coupling, the coupling will become time dependent as:

$$\mathcal{H}^T_{IS}(t) = e^{i\omega_e t I_z}\, \mathcal{H}^T_{IS}\, e^{-i\omega_e t I_z}$$

$$= 2\cos\theta \sum_i b_i\, I_{z_i}\, S_z^{1-3}$$

$$+ 2\sin\theta \sum_i b_i\, S_z^{1-3}\, (I_{x_i}\cos\omega_e t - I_{y_i}\sin\omega_e t) \quad . \qquad (2.35)$$

It is now right and proper to replace (2.35) by its average over one cycle of ω_e. The time independent coherently averaged Hamiltonian is obtained via average Hamiltonian theory [43], and is given by [44]:

$$\overline{\mathcal{H}_{IS}(t)} = \overline{\mathcal{H}^0_{IS}} + \overline{\mathcal{H}^1_{IS}} + \overline{\mathcal{H}^2_{is}} \quad \ldots \qquad (2.36)$$

where

$$\overline{\mathcal{H}^0_{IS}} = 2\cos\theta \sum_i b_i\, S_z^{1-3}\, I_{z_i} \quad , \qquad (2.37)$$

$$\overline{\mathcal{H}^1_{IS}} = \frac{4\sin\theta}{\omega_e} \sum_i S_z^{1-3^2}\, b_i^{\,2}\, (\cos\theta\, I_{x_i} - \frac{\sin\theta}{2} I_{z_i}) \quad , \qquad (2.38)$$

$$\overline{\mathcal{H}^2_{is}} = \frac{8\sin\theta}{\omega_e^{\,2}} \sum_i S_z^{1-3^3}\, b_i^{\,3}\, (P_2(\cos\theta)\, I_{x_i} - \frac{\sin 2\theta}{2} I_{z_i}) \; . \qquad (2.39)$$

We now wish to eliminate, or discard these terms one by one. The zeroth order term (Eq. (2.37)) vanishes when the I spin irradiation is applied on resonance. The first order term (Eq. (2.38)) will not contribute to the second moment of a spin 1/2 nucleus because $[S_z^{\,2}, S_x] = 0$, but for a spin 1 nucleus this is no longer true, and this will be the most important term to eliminate. The contribution of (2.38) to the second

moment (Eq. (2.27) will be reduced so long as the I spin irradiation is applied on resonance, and

$$\omega_{1I} > \left(\frac{\mathrm{Tr}[S_z^{\,2} \sum_i b_i^{\,2} I_{z_i}, S_x]^2}{4(\mathrm{Tr}[S_x]^2)} \right)^{1/2} . \qquad (2.40)$$

The reasonable implication here is that the I spin r.f. field amplitude must be much larger than the rms linewidth ($M_{2IS}^{1/2}$) due to the heteronuclear term in order to eliminate the effect of this term on the evolution of the system. The second order term (Eq. (2.39)) would be the most important term if I were dealing with spin 1/2 nuclei, and this term is slightly easier to eliminate through decoupling (because of ω_e and b_i dependence).

The experimental results of decoupling are shown in Figures 8 and 9. Decoupling really is necessary because some of these compounds are literally loaded with protons, rendering an M_{2IS} which is much larger than my simple minded estimates would indicate. I note parenthetically that the decoupled lorentzian linewidth for $NH_4C\ell$ decreases to 370 Hz (from 550 Hz), and I can excite a $90_x - 90_y$ echo while decoupling. The residual linewidth may be caused by incomplete elimination of $\mathcal{H}_{IS}$, homonuclear spin interactions, or residual quadrupolar couplings resulting from small crystal defects. Because of the estimated extremely tiny size of the ^{14}N-^{14}N homonuclear coupling, and because of the presence of the echo, the most likely residual broadening mechanism is quadrupolar coupling due to lattice defects.

Figure 8. The effect of decoupling on the corss-polarized ^{14}N NMR powder spectrum of tetrabutylammonium bromide at -60°C. Each spectrum is the result of 200 transients using a mixing field of 50 kHz for both ^{14}N and ^{1}H, and a 5 μsec echo pulse.

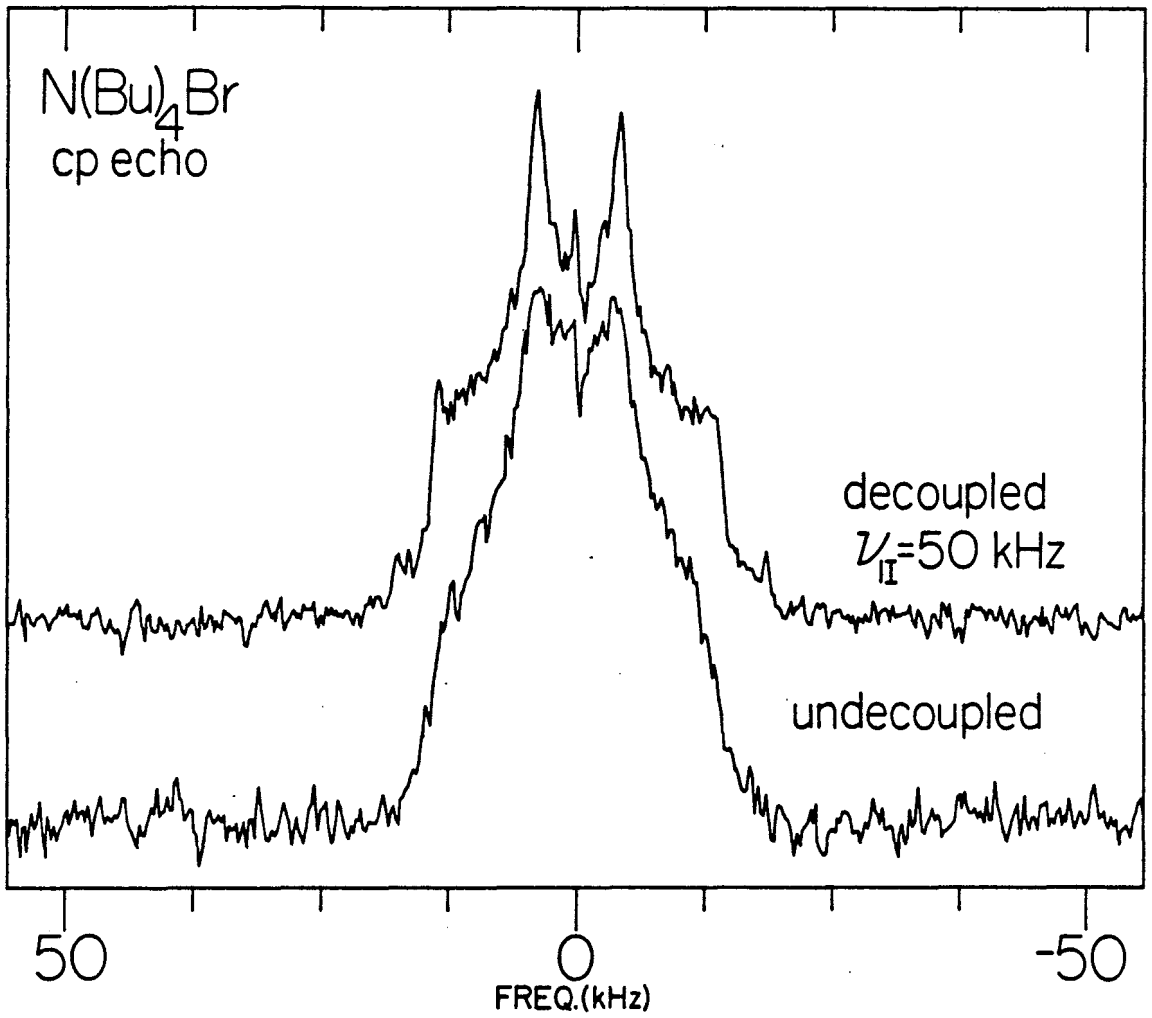

XBL 839-11507

Figure 9. Decay of the single (S.Q.) and double (D.Q.) quantum echo as a function of the echo delay time τ for ammonium sulfate powder at room temperature. The single quantum echoes were the result of quadrupolar echo sequences on Zeeman polarization, while the double quantum echoes were obtained by an ADRF cross-polarization experiment (section 2.4) using a 5 msec mixing period and a ^{14}N r.f. field amplitude of 8.3 kHz.

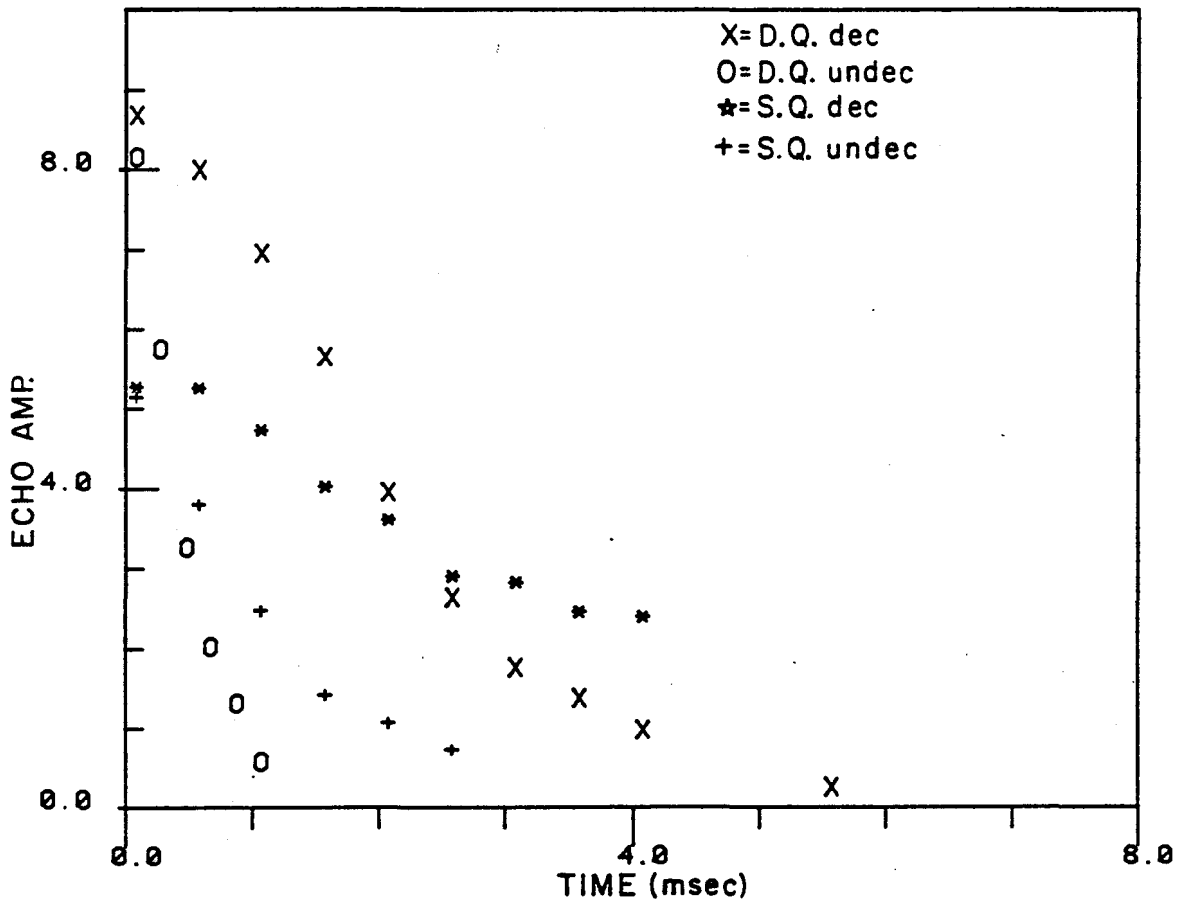
X= D.Q. dec
O= D.Q. undec
✱= S.Q. dec
+= S.Q. undec
8.0
4.0
0.0
ECHO AMP.
0.0
4.0
8.0
TIME (msec)

XBL 834-9380

2.3 Cross-relaxation

Hopefully, the reader is now convinced that the proton decoupled quadrupolar echo is the method of choice for observing ^{14}N powder lineshapes in a relatively undistorted manner. However, one is left wondering if it is possible to increase the sensitivity of the experiment over that which is available from a puny Zeeman polarization. Put in simple terms, the signal available from an ensemble of nuclei, neglecting the noise, will be primarily dependent upon the equilibrium Zeeman polarization and the frequency of observation (because of Faradays law of induction). Both of these factors may be increased by increasing H_0, but this is not often feasible from an economic standpoint. If one cannot change H_0, then the frequency being observed (ω_0) is fixed. This leaves us with attempting to increase the available polarization above that due to the Zeeman interaction. We have this option at our disposal because of the potential of the spin system for attaining a temperature (the spin temperature) far different from that of the lattice.

2.3.1 Relaxation of Spins in High Field

I have, until now, assumed that the spins interact only with well defined Hamiltonians, resulting in coherent density matrix evolution. In the real world, there will always be thermal noise present, and this thermal motion will add a small time dependent portion to the Hamiltonian of Eq. (1.6). The inclusion of this small perturbation is most easily accounted for by the incorporation of the phenomenological relaxation times T_1 and T_2 [45] into Eq. (1.6) as:

$$\frac{\delta\rho}{\delta t} = -\frac{i}{\hbar}[\mathcal{H},\rho] - \frac{\rho_{diag}-\rho_0}{T_1} - \frac{\rho_{off}}{T_2} \quad , \tag{2.41}$$

where ρ_0 refers to the density matrix at thermal equilibrium, ρ_{diag} to the diagonal elements of ρ, and ρ_{off} to the off diagonal elements. The longitudinal relaxation time T_1 is thought of as the inverse rate of energy exchange along the high field axis of quantization, while the transverse relaxation time T_2 is related to the inverse rate of exchange along the perpendicular axis, and is responsible for equilibrium among the spins. For the simplest case, in which $\mathcal{H}$ in Eq. (2.41) is nonexistent, the diagonal elements approach equilibrium as:

$$\rho_{diag} \sim 1 - e^{-t/T_1} \quad , \tag{2.42}$$

and the off-diagonal elements decay as:

$$\rho_{off} \sim e^{-t/T_2} \quad . \tag{2.43}$$

Calculation of T_1 and T_2, and comparison with experiment, may yield a wealth of information (an example is given in the last chapter), but the most qualitative terms are sufficient for this discussion, and they were set forth many years ago by Bloembergen, Purcell, and Pound [46]. Fluctuating local magnetic interactions of the form

$$\mathcal{H}(t) = \gamma\hbar(H_x(t)I_x + H_y(t)I_y + H_z(t)I_z) \quad , \tag{2.44}$$

or electric field gradients (for $I \geq 1$)

$$\mathcal{H}(t) = \frac{eQ}{4\hbar} \left(V_{zz}(t)(3\ I_z^{\ 2}-2)+(V_{xx}(t)-V_{yy}(t))(I_x^{\ 2}-I_y^{\ 2})\right) \qquad (2.45)$$

will induce transitions between the nuclear spin energy levels. Consider, for the moment, Eq. (2.44). If $H_x(t)$ and $H_y(t)$ have a considerable density of fluctuations (spectral density J) in the neighborhood of ω_0, then transitions will be induced along I_z and thermal relaxation will result. Additionally, fluctuations at 2 ω_0 will induce transitions because of the rotating frame argument used in section 1.2.2 (Eq. (2.44) will contain a counter-rotating component). Therefore, the longitudinal relaxation time will be related to the spectral density of the fluctuation at the frequencies ω_0 and 2 ω_0:

$$1/T_1 = k_1 J(\omega_0) + k_2 J(2\ \omega_0) \quad . \qquad (2.46)$$

The values of k_1 and k_2 will depend upon the relaxation mechanism, and will contain a factor of the squared coupling operator. Because the electrostatic quadrupolar coupling has the potential to be much larger than the magnetic dipolar coupling, T_1's due to quadrupolar coupling could potentially be much shorter.

Similarly, an equation relating T_2 to a fluctuating perturbation may be derived. In this case we wish to relax along x or y, so the important fluctuations occur along z, and either y or x. Fluctuations along z involve operators which are diagonal in the Zeeman eigenstates, and so cannot exchange energy between spins. These will contribute to T_2 through a static (zero frequency) term. Fluctuations along x or y involve operators which connect states of differing m_z, so the

dependence on spectral densities at ω_0 and $2\ \omega_0$. The overall result is

$$1/T_2 = C_0 J(0) + C_1 J(\omega_0) + C_2 J(2\ \omega_0) \quad , \tag{2.47}$$

with C_1, C_2, and C_3 depending upon the mechanism of relaxation. If the variation of the perturbation is described by a stationary Markov process, which seems most reasonable, then J(0) must always be greater than or equal to $J(\omega > 0)$. For this reason, T_2 is always less than or equal to T_1; T_2 commonly being on the order of milliseconds, and T_1 on the order of seconds.

Of course, Equations (2.46) and (2.47) are valid only for liquids and gases, where the motions are isotropic. In solids we must deal with anisotropic motion and anisotropic couplings, leading to anisotropic relaxation. To a first approximation, this merely involves an orientation dependence of the constants in Eqs. (2.46) and (2.47) [48]. I should also mention that these equations neglect some other contributions to relaxation, such as chemical exchange, but they do give us a feeling for what the world of relaxation is all about.

2.3.2 Nuclear Overhauser Enhancement (NOE)

The NOE derives from the supposition that coupled spin systems will likely have coupled relaxation parameters, and thus by perturbing one spin species, we may be able to polarize the other. The longitudinal relaxation of two coupled spins will obey the following set of coupled equations [47]:

$$\frac{d\langle I_z\rangle}{dt} = -\frac{1}{T_{II}}\left(\langle I_z\rangle - I_0\right) - \frac{1}{T_{IS}}\left(\langle S_z\rangle - S_0\right) \tag{2.48a}$$

$$\frac{d\langle S_z\rangle}{dt} = -\frac{1}{T_{SI}}\left(\langle I_z\rangle - I_0\right) - \frac{1}{T_{SS}}\left(\langle S_z\rangle - S_0\right) \quad , \tag{2.48b}$$

where I_0 and S_0 are the equilibrium values of I_z and S_z respectively. Prior to defining the various relaxation times involved, let us see what happens when a resonant r.f. field is applied to the I spins such that $\langle I_z\rangle$ vanishes (i.e., the I spin temperature goes to infinity). Under this condition, Eq. (2.48b) becomes:

$$\frac{d\langle S_z\rangle}{dt} = \frac{I_0}{T_{SI}} - \frac{1}{T_{SS}}\left(\langle S_z\rangle - S_0\right) \quad . \tag{2.49}$$

To obtain the equilibrium S spin magnetization, we set Eq. (2.49) equal to zero and obtain:

$$\langle S_z\rangle = S_0 + I_0 \frac{T_{SS}}{T_{SI}} \quad , \tag{2.50}$$

or, the relative enhancement

$$\frac{\langle S_z\rangle}{S_0} = 1 + \frac{I_0}{S_0}\,\frac{T_{SS}}{T_{SI}}$$

$$= 1 + \frac{\gamma_I I(I+1)}{\gamma_S S(S+1)}\,\frac{T_{SS}}{T_{SI}} \quad . \tag{2.51}$$

Now we see that the relaxation times T_{SS} and T_{SI} are all important in

determining whether this experiment yields any enhancement. Qualitatively, the longitudinal relaxation time T_{SS} will depend upon the coupling between the S spins and the lattice, and between the S and I spins; while T_{SI} is only dependent upon the coupling between the S and I spins, and gives the contribution of T_{1I} to T_{1S}. So, in order to obtain a large S spin NOE, the I and S spins must be tightly coupled, while the S spins should be well insulated from the lattice.

Now, I wish to obtain a ^{14}N NOE from protons, and the implication for this is primarily that the ^{14}N quadrupolar spin lattice interaction must be small in order to allow significant relaxation through the ^{14}N-^{1}H dipolar mechanism. I have experimentally investigated the utility of this signal enhancement method, with disappointing results. The experiment is performed in two steps: (a) the protons are irradiated on resonance for a time on the order of ^{14}N T_1, (b) either a single pulse, or a quadrupolar echo sequence is given, and the resulting fid is recorded. A typical result for a single crystal of $(NH_4)_2HPO_4$ is shown in Figure 10. The NOE is large, approximately a factor of 7, but anisotropic (as significant enhancement occurs for only one quadrupolar splitting). The anisotropic effect is not unexpected, since the heteronuclear dipolar coupling will be anisotropic. Unfortunately, the only compounds which exhibited a significant NOE were the ammonium salts; a few tetraalkylammonium compounds yielded a small NOE (on the order of 1.5), but this is hardly worth mentioning. Failure of this experiment is most likely due to a strong coupling between the ^{14}N quadrupole moment and the lattice.

Figure 10. The result of the nuclear overhauser experiment on a particular orientation of a diammonium hydrogen phosphate single crystal for various proton saturation times. The solid line follows an exponential relaxation of time constant 670 msec.

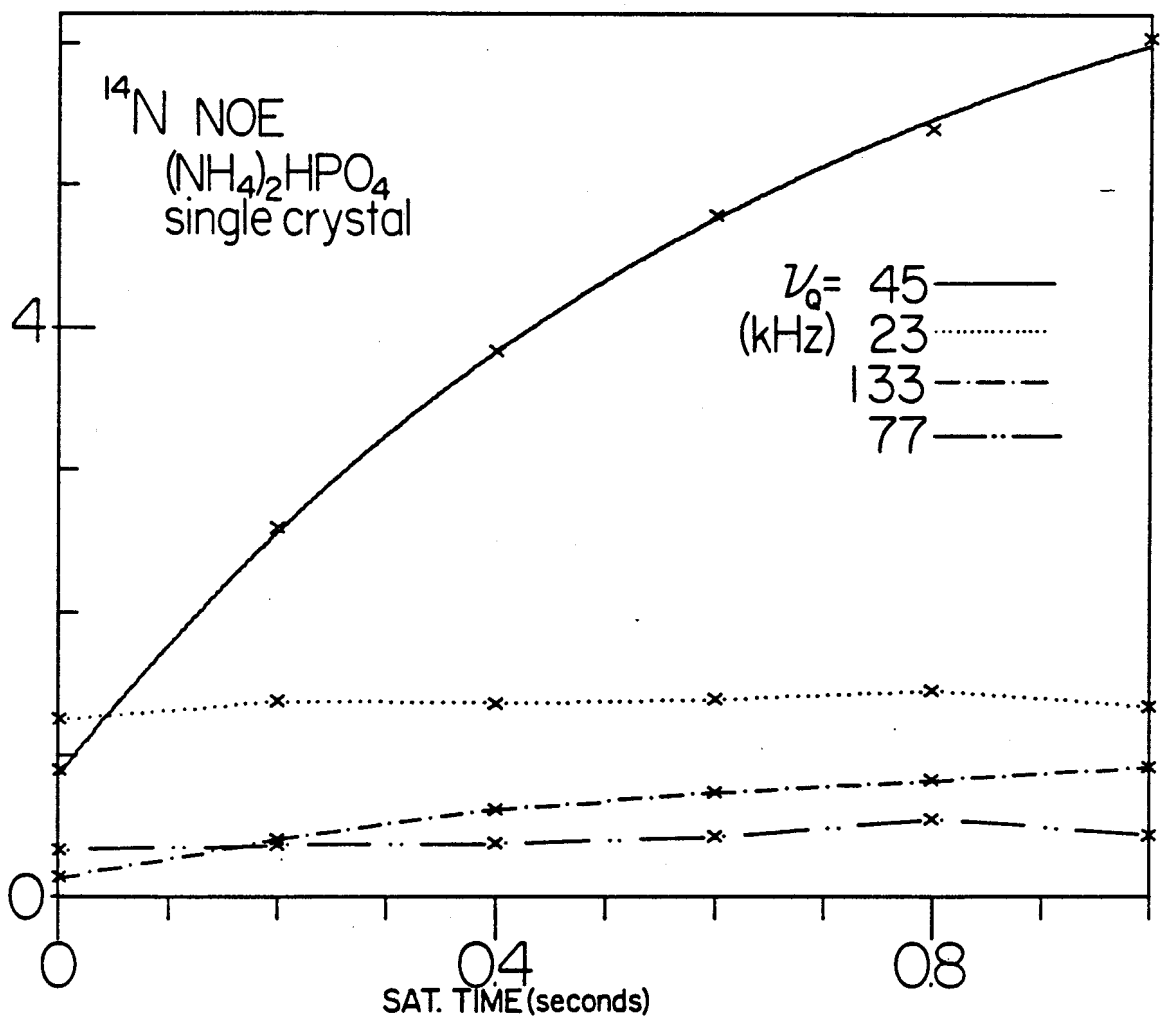

XBL 839-11510

Any cross-relaxation experiment performed in high field is expected to yield somewhat anisotropic results because of the truncated nature of the Hamiltonians involved. What is most objectionable about the NOE, if it works at all, is that it is very slow. This inefficiency leads to significant sample heating during the experiment. The NOE is sluggish because it is dependent upon dipolar fluctuation spectral densities at the sum and difference frequencies of the two nuclear species [47]. These spectral densities are likely to be tiny (in the absence of further external perturbation), so the NOE is a slow process. Fortunately, it is possible to obtain a cross-relaxaton which occurs more on the order of T_2 via rotating frame experiments to be described in the next section.

2.4 Rotating Frame Cross-relaxation

If it were only possible to have a different static field felt by each nuclear species in a heteronuclear coupled pair, then these fields could be adjusted such that $\omega_{0I} = \omega_{0S}$, and the cross-relaxation would occur very rapidly for it would depend upon a spectral density at zero frequency. That this is substantially possible was proven by Hartmann and Hahn [52]. Their method is to apply resonant r.f. fields to both the I and S spins, thereby transforming the important properties of the system out of the laboratory frame, and into the rotating frame; where the "effective field" will be the r.f. field (so long as the r.f. field interaction strength exceeds that of other rotating frame interactions, such as homonuclear dipole).

A typical rotating frame cross-relaxation experiment will consist of the following steps; (1) the strongly resonating I spins are transferred from high field to a much smaller effective field via a spin lock (SL), or adiabatic demagnetization in the rotating frame

(ADRF) [51], (2) a resonant r.f. field is applied to the S spins in order that they may have an effective field on which to polarize (I will refer to this as the mixing period), and (3) after a period of time (on the order of T_2) the S spin r.f. field is suddenly removed, and the S spin fid is observed directly (direct detection cross-polarization), or the I spin fid is observed (either by sudden removal of the spin locking field, or via a 45° pulse on the ADRF state [53]) and compared with the equilibrium I spin fid in order to obtain the relative I-S magnetization transfer (indirect detection). The rate of cross-relaxation, (T_{IS}^{-1}) is very dependent upon the manner in which step (2) is performed. In particular, when the respective r.f. field strengths $\gamma_I H_{1I}$ and $\gamma_S H_{1S}$ are adjusted to equality, which is only possible for SL and known as Hartmann-Hahn matching, cross-relaxation becomes extremely rapid because equal quanta are exchanged among the spins.

The most widely used and successful form of this experiment is known as proton enhanced nuclear induction spectroscopy (PENIS) [54], and takes advantage of the ever present proton as the I spin, while observing the S spins directly. The primary virtues of direct detection are highest available resolution, and simplicity of spectral interpretation. Spin decoupling during S spin observation is easily accomplished via the common everyday technique outlined in section 2.2.2. By contrast, in the indirect detection experiment, the S spin frequency domain must be mapped point by point by varying the S irradiation frequency during the mixing period. One can only hope that the double resonance lineshape at each frequency takes on a simple form so as not to grossly distort the desired spectrum

beyond recognition. Additonally, decoupling the I spins in the indirect detection experiment is difficult, although it may be accomplished [55]. The only advantage of indirect detection is an additional increase in sensitivity which comes from detecting a higher frequency spin (once again, Faradays law is brought into play). If the lineshape is amenable to ft NMR at all, then direct detection is the way to go.

2.4.1 Rotating Frame Spin Thermodynamics

The NOE is not conveniently analyzed in terms of equilibrium thermodynamics because the I spins are always displaced from equilibrium by the application of an r.f. field, and the thermal contact between the two systems is very feeble, being of the same order as the contact between each individual system and its surroundings. By contrast, rotating frame cross-relaxation experiments are most conveniently described in thermodynamic terms. To a first approximation, spin-lattice relaxation may be ignored, and the entire process is analogous to two bodies of different temperature coming to equilibrium by thermal contact.

To begin, assume the existence of two spin systems describable by the total Hamiltonian:

$$\mathcal{H} = -\omega_{0I} I_z - \omega_{0S} S_z - 2\,\omega_{1I} I_x \cos\omega_I t - 2\,\omega_{1S} \cos\omega_S t$$

$$+ \mathcal{H}_{II} + \mathcal{H}_{IS} \quad , \qquad (2.52)$$

where I ignore quadrupolar interactions (which are conveniently added later), S spin homonuclear interactions (which are likely to be

extremely feeble); the dipolar interactions $\mathcal{H}_{II}$ and $\mathcal{H}_{IS}$ are given by Eqs. (1.47) and (1.48) respectively. Equation (2.52) may be transformed easily to a doubly rotating frame representation, using a method like that of section 1.2.2, to yield:

$$\mathcal{H} = -\Delta\omega_I I_z - \omega_{1I} I_x - \Delta\omega_S S_z - \omega_{1S} S_x + \mathcal{H}_{II} + \mathcal{H}_{IS} \quad . \tag{2.53}$$

I now drop the offset terms for they, like the quadrupolar interaction, are conveniently added later. I will also assume that $\mathcal{H}_{IS}$ corresponds to a very small energy not important in a thermodynamic sense. Our reduced Hamiltonian becomes:

$$\begin{aligned} \mathcal{H} &= -\omega_{1I} I_x - \omega_{1S} S_x + \mathcal{H}_{II} \\ &= \mathcal{H}_I + \mathcal{H}_S + \mathcal{H}_D \quad , \end{aligned} \tag{2.54}$$

defining the three thermodynamic reservoirs with which we are most concerned; the I spin, the S spin, and the I spin dipolar. In a spin lock experiment, $\mathcal{H}_I >> \mathcal{H}_D$, and the I and S spin reservoirs are brought into thermal contact; while the ADRF experiment equilibrates the S spin and I spin dipolar reservoirs. Since the system is assumed to be isolated from the outside world, the energy provided by the terms in Eq. (2.54) must be conserved. We may invoke this energy conservation in order to determine the state of the system following equilibration. The energy is given by:

$$E = \mathrm{Tr}(\rho_{eq}\, \mathcal{H}) \quad , \tag{2.55}$$

where the equilibrium rotating frame density matrix

$$\rho_{eq} = \frac{1}{2I+1} (\beta_I E_I + \beta_D E_D) + \frac{1}{2S+1} \beta_S E_S \tag{2.56}$$

is related to the laboratory frame density matrix by

$$\rho_{eq} = e^{-i(\omega_{0I} I_z + \omega_{0S} S_z)} \rho_L e^{i(\omega_{0I} I_z + \omega_{0S} S_z)} \quad . \tag{2.57}$$

In equation (2.56), $\beta = (kT)^{-1}$, and I implicitly assume the existence of a spin temperature in the rotating frame [49] for each reservoir. Plugging Eqs. (2.54) and (2.56) into (2.55), one obtains:

$$E = \frac{\gamma_I^2 \hbar^2 I(I+1)}{3} (\beta_I H_{1I}^2 + \beta_D \frac{Tr[\mathcal{H}_D^2]}{Tr[I_x^2]})$$

$$+ \frac{\gamma_S^2 \hbar^2 S(S+1)}{3} \beta_S H_{1S}^2 \quad , \tag{2.58}$$

where I have made use of the relation [37]:

$$Tr[I_x^2] = \frac{1}{3} I(I+1)(2I+1) \quad . \tag{2.59}$$

Equation (2.58) is now simplified, by extracting the Curie constants, to yield

$$E = \beta_I C_I H_{1I}^2 + \beta_D C_I H_L^2 + \beta_S C_S H_{1S}^2 \quad , \tag{2.60}$$

where the local field is defined [50]:

$$H_L^2 = \frac{\mathrm{Tr}[\mathcal{H}_D^{\,2}]}{\gamma_I^2\,\hbar^2\,\mathrm{Tr}[I_x^2]} \quad , \tag{2.61}$$

and factors of N_I and N_S have been incorporated into the Curie constants to account for the many spin macroscopic observables. Equation (2.60) will essentially be valid for all time in the absence of spin-lattice or heteronuclear coupling. However, when we invoke this latter mechanism, the I and S spin temperatures approach equilibrium leaving the total energy unchanged. Prior to contact, it is not unreasonable to assume that β_S=0, so that the state of the system following equilibration must satisfy:

$$\beta_0 C_I H_{1I}^2 + \beta_0 C_I H_L^2 = \beta_f (C_I H_{1I}^2 + C_I H_L^2 + C_S H_{1S}^2) \quad , \tag{2.62}$$

where β_0 has replaced β_I, and β_f is the final equilibrium spin temperature. In the ADRF experiment, H_{1I}=0, so

$$\beta_0 C_I H_L^2 = \beta_f (C_I H_L^2 + C_S H_{1S}^2) \quad , \tag{2.63}$$

or

$$\frac{\beta_0}{\beta_f} = 1 + \frac{C_S}{C_I}\frac{H_{1S}^2}{H_L^2}$$

$$= 1 + \varepsilon\eta^2 \quad , \tag{2.64}$$

where

$$\varepsilon = \frac{N_S\ S(S+1)}{N_I\ I(I+1)} \quad ,$$

and

$$\eta = \frac{\gamma_S\ H_{1S}}{\gamma_I\ H_L} \quad . \tag{2.65}$$

The SL experiment is analyzed in a similar manner, with H_{1I} replacing H_L. We would like to see how this rotating frame equilibrium relates to the "normal" lattice equilibrium; so β_0 must be related to β_L (the inverse lattice temperature). Both the ADRF and spin lock should ideally be isentropic processes. This implies that [50]:

$$\beta_0 = B_L \cdot H_0 \left(\left(\frac{\Delta\omega}{\gamma}\right)^2 + H_1^2 + H_L^2\right)^{-1/2} \quad , \tag{2.66a}$$

which, for $\Delta\omega = 0$, becomes

$$\beta_0 = \beta_L\ H_0/H_L \qquad \text{(ADRF)} \quad , \tag{2.66b}$$

$$\beta_0 = \beta_L\ H_0/H_{1I} \qquad \text{(SL)} \quad . \tag{2.66c}$$

We may now express Equation (2.64) as

$$\frac{\beta_L}{\beta_f} = \frac{H_L}{H_0}\ (1 + \varepsilon\eta^2) \quad , \tag{2.67}$$

where, once again, H_L is merely replaced with H_{1I} for SL. The observable magnetization following an ideal 90° pulse on an equilibrium density matrix will be:

$$M_0 = Tr(\rho_{eq}\mathcal{H}_z) = \beta_L\ C_S\ H_0 \quad , \tag{2.68}$$

so the relative signal enhancement becomes

$$\frac{M_F}{M_0} = \frac{\beta_F\ C_S\ H_{1S}}{\beta_L\ C_S\ H_0} = \frac{H_{1S}}{H_L}\ (1 + \varepsilon\eta^2)^{-1} \tag{2.69}$$

or, using Eq. (2.65)

$$\frac{M_F}{M_0} = \frac{\gamma_I}{\gamma_S}\ \eta(1 + \varepsilon\eta^2)^{-1} \quad . \tag{2.70}$$

This equation indicates the kind of enhancements we might obtain assuming the equilibration between the two systems is 100% efficient. The only parameter in Equation (2.70) at the disposal of the experimentor for adjustment is η; maximizing the enhancement with respect to η yields:

$$\eta_{max} = (\varepsilon)^{-1/2} \quad , \tag{2.71}$$

at which point

$$\frac{M_F}{M_0} = \frac{\gamma_I}{\gamma_S}\ \frac{1}{2\sqrt{\varepsilon}} \quad . \tag{2,72}$$

This corresponds to equalizing the heat capacities of the I and S spins by increasing the S spin r.f. field (because ε is almost always less than one). Unfortunately, this tends to violate the matching of energy splittings in the rotating frame, resulting in an inefficient energy transfer which depends upon spectral densities away from zero. I should note here that this process is not limited to a single contact, but may be repeated many times (until the rotating frame proton spin temperature becomes excessive), and the signals added to give an overall enhancement, for n contacts, of (η=1) [54]:

$$\frac{M_F}{M_0} = \frac{\gamma_I}{\gamma_S} (1 - \varepsilon)^n \quad . \tag{2.73}$$

2.4.2 Rotating Frame Spin Dynamics

Obviously, this experiment will yield a large signal enhancement so long as adequate thermal contact exists between the two systems. Assuming the absence of spin-lattice couplings, the spin temperatures of the I and S reservoirs will follow a set of coupled equations of the form [56]:

$$\frac{d\beta_S}{dt} = - \frac{(\beta_S - \beta_I)}{T_{IS}} \tag{2.74a}$$

$$\frac{d\beta_I}{dt} = - \varepsilon\eta^2 \frac{(\beta_I - \beta_S)}{T_{IS}} \quad , \tag{2.74b}$$

where $\varepsilon\eta^2$, the ratio of S to I spin heat capacities, takes into account the fact that the spin temperatures will only change at the same rate if the heat capacities of the two reservoirs are equal. These equations have the solution:

$$\beta_S = \beta_F(1 - e^{-(1+\varepsilon\eta^2)t/T_{IS}}) \tag{2.75a}$$

$$\beta_I = \beta_F + (\beta_0-\beta_F)\ e^{-(1+\varepsilon\eta^2)t/T_{IS}} \quad , \tag{2.75b}$$

where β_F and β_0 are defined in Eq. (2.64). Since the observable magnetization is linearly related to the inverse temperature β, Eqs. (2.75) predict an exponential growth of the magnetization during the mixing period. That this is indeed observed experimentally is shown in Figure 11.

Unfortunately, we cannot always neglect rotating frame spin-lattice couplings, and I must take a little time now for a brief examination of these. For the purposes of this discussion, we may use the same arguments presented in section 2.3.1 to describe laboratory frame spin-lattice interactions (this is a "weak collision" argument, which is not always valid in the rotating frame [66]). First we define the phenomenological relaxation times $T_{1\rho}$ and T_{1D} through the equation:

$$\frac{dM_x}{dt} = -\frac{M_x-M_0}{T_{1x}} \quad ; \quad x = \rho \text{ or } D \quad , \tag{2.76}$$

where ρ refers to relaxation along the r.f. field H_1 and D refers

Figure 11. The heteronuclear cross-relaxation of NH_4Cl (20°C) and $N(Bu)_4Br$ (-60°C) for spin lock (SL) and ADRF experiments. The points for $N(Bu)_4Br$ represent echo amplitudes, while those for NH_4Cl represent amplitudes of frequency domain spectra. The lines through the points represent the best exponential fits to the data, and yield the following cross-relaxation times (T_{IS}): NH_4Cl ADRF = 4.1 msec, NH_4Cl SL = 2.1 msec, $N(Bu)_4Br$ SL = 1.1 msec, $N(Bu)_4Br$ ADRF = 8.5 msec.

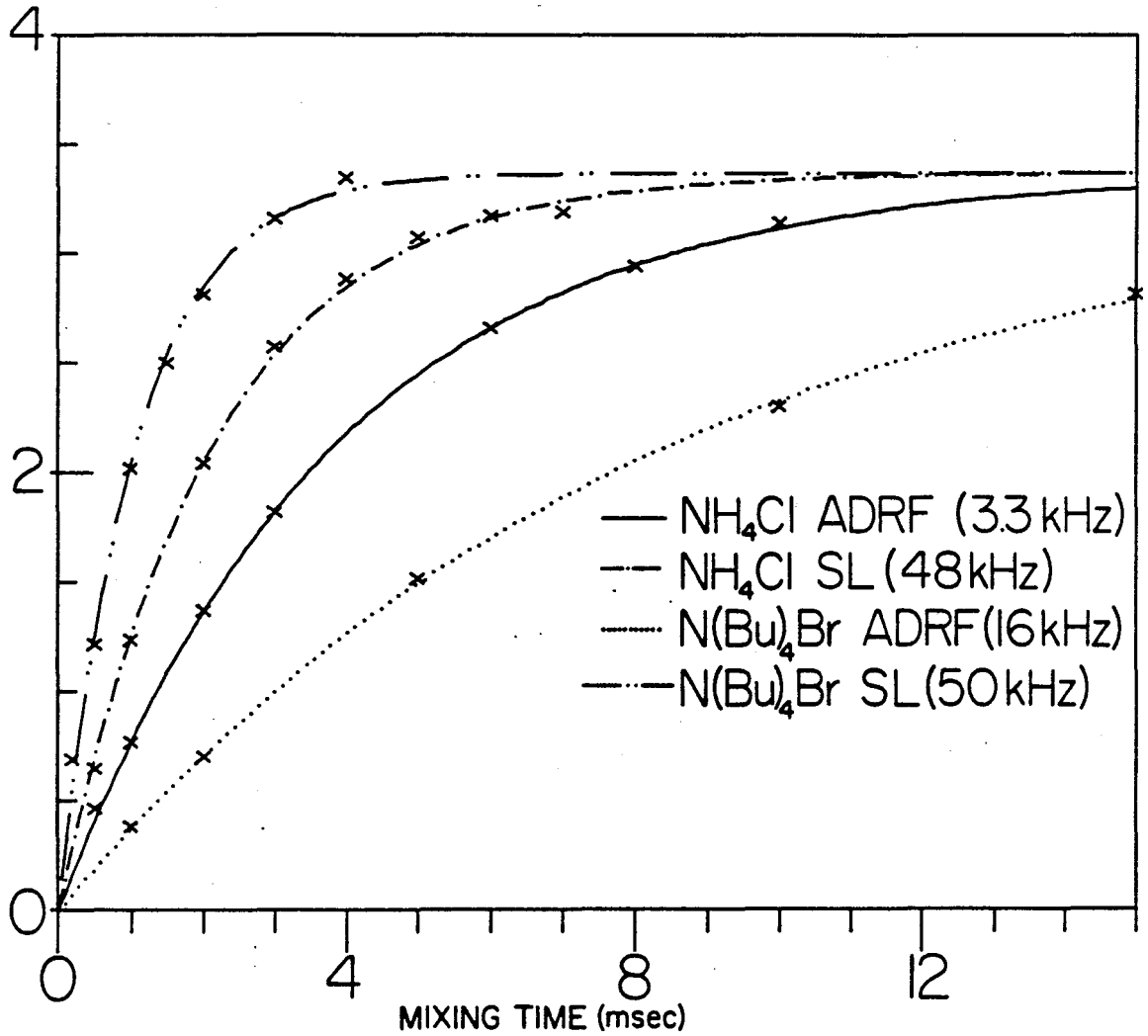

XBL 839-11499

to relaxation along the local field H_L due to fluctuating magnetic dipoles, an equation analogous to Eqs. (2.46) may be derived. However, we are in the rotating frame, where H_1 is that "static" field, and the dipolar interaction (Eq. (1.43)) takes on a time dependence at ω_0 and $2\omega_0$. These considerations yield [66,69]:

$$\frac{1}{T_{1\rho}} = k_1 J(\omega_0) + k_2 J(2\omega_0) + k_3 J(2\omega_1) \quad , \tag{2.77}$$

where k_1, k_2 and k_3 are constants containing a factor of $\gamma^4\hbar^2$. An analogous equation could also be derived for relaxation of a quadrupolar nucleus due to fluctuating field gradients, but suffice it to say that $T_{1\rho}$'s owing to quadrupolar interactions could be much shorter (because $(\frac{e^2qQ}{\hbar})^2$ is possibly much larger than $\gamma^4\hbar^2$). Similar arguments will apply to T_{1D}. Because ω_1 will almost always be much smaller than ω_0, T_{1x} will be sensitive to slow motions. The effect of T_{1x} is, obviously, a "heat leak" for both the I and S spins which will compete with cross-relaxation for magnetization. The inclusion of this spin-lattice relaxation modifies Eq. (2.74) to:

$$\frac{d\beta_S}{dt} = -\frac{(\beta_S-\beta_I)}{T_{1S}} - \frac{(\beta_S-\beta_L)}{T_{1\rho}} \tag{2.78a}$$

$$\frac{d\beta_I}{dt} = -\frac{\varepsilon\eta^2(\beta_I-\beta_S)}{T_{IS}} - \frac{(\beta_I-\beta_L)}{T_{1X}} \quad . \tag{2.78b}$$

where $x = \rho$ or D (the S spins have only the possibility of relaxation along their r.f. field). Equations (2.78) may be solved to yield

a very complicated expression which I will not reproduce here, but may be found in Appendix B of [59]. I have always tried to neglect T_{1X} effects; if we are lucky, T_{1X} will be orders of magnitude longer than T_{IS}. However, this type of relaxation is an excellent indication of slow motional effects, and also the most common reason for failure of a cross-polarization experiment. I will defer any further discussion of this phenomenon until the next chapter.

Returning to Eqs. (2.75), we notice that the all important parameter here is the cross-relaxation time T_{IS}, whose derivation has been the subject of several studies [56,57]. Because of the importance of this parameter, I will devote considerable space to its discussion. An expression for T_{IS} may be derivdd using the master equation for the rate of change of the density matrix in the presence of a perturbing coupling [47] as [57]:

$$T_{IS}^{-1} = \mathrm{Tr}[\mathcal{H}_S]^{-1} \int dt\ \mathrm{Tr}([\mathcal{H}_{IS},\mathcal{H}_S]\ e^{-i(\mathcal{H}_S+\mathcal{H}_I)t}$$

$$\times\ [\mathcal{H}_{IS},\mathcal{H}_S]\ e^{i(\mathcal{H}_S+\mathcal{H}_I)t}\ ) \quad , \tag{2.79}$$

where $\mathcal{H}_{IS}$ is the perturbing coupling (defined in Eq. (1.48)), and $\mathcal{H}_I$ and $\mathcal{H}_S$ are the rotating frame Hamiltonians of the I and S spins respectively (here, $\mathcal{H}_I$ will generally contain both r.f. and homonuclear dipole terms). In the case of on resonance irradiation, Eq. (2.79) may be explicitly evaluated, and reduced to the following [59]:

$$T_{IS}^{-1} = \frac{1}{2} M_{2IS} J_X(\omega_{es}-\omega_{ei}) \tag{2.80a}$$

for the SL case, and

$$T_{IS}^{-1} = M_{2IS} J_Z(\omega_{es}) \tag{2.80b}$$

for the ADRF case. In these expressions, ω_{ei} and ω_{es} are the rotating frame effective fields of the I and S spins respectively, and use has been made of the relationship between rotating and laboratory frame homonuclear interactions;

$$\mathcal{H}_{II}^{rot} = \frac{1}{2} (3 \cos^2\theta-1)\mathcal{H}_{II} \quad , \tag{2.81}$$

where $\theta = \text{atan}(\omega_{1I}/\Delta\omega_I)$. M_{2IS} is the dipolar second moment of the S spins due to the I spins, and is defined

$$M_{2IS} = \frac{\text{Tr}[\mathcal{H}_{IS},\mathcal{H}_S]^2}{\text{Tr}[\mathcal{H}_S]^2} \quad . \tag{2.82}$$

The spectral density $Jp(\omega)$ is defined

$$J_p(\omega) = \int \cos\omega t \; C_p(t)dt; \quad p = x \text{ or } z \tag{2.83}$$

where $C_p(t)$ is the autocorrelation function of the I spins due to homonuclear flip-flop processes; and may be expressed as [68]:

$$C_p(t) = \frac{\text{Tr}_I(\mathcal{H}_{IS}(t)\mathcal{H}_{IS})}{\text{Tr}_I(\mathcal{H}_{IS})^2} \quad , \quad \text{where}$$

$\mathcal{H}_{IS}(t)$ represents the heteronuclear Hamiltonian which has become time dependent owing to dipolar flip-flops. Evaluation of the traces (over the I spins) yields

$$C_p(t) = \frac{\mathrm{Tr}(\sum_i b_i\, I_{p_i}\, e^{-im\mathcal{H}_{II}t} \sum_i b_i\, I_{p_i}\, e^{im\mathcal{H}_{II}t})}{\mathrm{Tr}(\sum_i b_i\, I_{p_i})^2} \quad , \quad (2.84)$$

where, for ADRF p=z, m=1; while for SL p=x, m=-1/2. It is not often convenient to evaluate Eq. (2.84), so it is commonly replaced with a simple analytic function such as a lorentzian or gaussian. I feel compelled here to point out that this "random" flip-flop process may be reversed [70], leading to a seemingly forbidden growth of the correlation from zero; this is in sharp contrast to the correlation of a thermally fluctuating dipole (for which there is no known reversal mechanism).

We are now in a position to make some rather general statements regarding the cross-relaxation rate T_{IS}^{-1}. Note that Eqs. (2.80) consist of two terms: a coupling term which registers the coupling between the I and S spins in the rotating frame, and a spectral density function whose purpose is similar to that of section 2.3.1. Neglecting spin-lattice relaxation, the cross-relaxation rate will be large so long as the coupling between the two spin species is strong, and the spectral density samples frequencies near zero. For the spin lock experiment, the I and S spin effective fields may always be adjusted so that (somewhere in the spectrum) the spectral density attains its maximum value. For the ADRF state, the homonuclear flip-flops are ineffective at modulating $\mathcal{H}_{IS}$ in a coherent manner, hence the spectral density is sampled at the S spin effective

field; and this may be reduced to zero only with disasterous results (i.e., η in Eq. (2.70) becomes zero, and the enhancement vanishes). So, in general, the SL cross-relaxation rate will be larger than that due to the ADRF process. Even so, the ADRF experiment is often preferable because η is usually large (leading to a large equilibrium magnetization), and only one r.f. field is required during the mixing period.

2.4.3 ^{14}N Cross-Polarization

Prior to my arrival on the scene, two limiting cases applicable to ^{14}N-^{1}H cross-polarization had been treated in the literature. When the r.f. field is very much larger than ω_Q, we may ignore the latter, and ^{14}N behaves very much like a spin 1/2 nucleus. When the r.f. field is much smaller than ω_Q, we find ourselves in the situation of double quantum cross-polarization [59,60]. The much more common intermediate $\omega_1 \approx \omega_Q$ situation had never been investigated. Further, a quadrupolar broadened powder pattern had not been cross-polarized (although, an indirect detection dynamic polarization experiment had been achieved [61]). Because of the tremendous advantages of this experiment, and because it is not always possible to find oneself in a purely single or purely double quantum regime, I took it upon myself to investigate this intermediate process. The results are not at all disappointing.

Considering the nature of powder patterns (section 1.3) it is not in the least bit surprising to realize the existence of problems inherent in their cross-polarization. The powder pattern is orientationally inhomogeneous, and so are the homo and heteronuclear dipolar interactions, which are ever so important in the

cross-relaxation. This results in a T_{IS}^{-1} which varies across the powder pattern. If it were possible to carry out the contact for infinite time, this would make no difference. For a realistic experiment however, powder pattern distortion is the likely result. This distortion has been previously observed for the cross-polarization of a chemical shift powder pattern [54], and has been attributed to the orientation dependence of M_{2IS}. In principle, the correlation function may also possess an orientation dependence, and this too has indeed been observed [40,57,58]. These orientation dependencies may be theoretically unravelled only in fairly simple spin systems for which detailed structural data are available. In my formulation of this problem I choose, as a first approximation, to ignore the orientation dependence of M_{2IS} and $J(\omega)$. All that is left is the orientation dependence of the ^{14}N rotating frame effective field(s) which enter into Eqs. (2.70) and (2.80). Justification for this simple approach is provided by its sufficiency in explaining our results.

2.4.4 Rotating Frame Effective Fields

Derivation of the rotating frame effective field(s) for a spin one nucleus is fairly easily accomplished starting with Eq. (1.36):

$$\mathcal{H} = -\ 2\Delta\omega\ S_x^{1-3} - 2\ \omega_1\ S_x^{2-3} + \frac{2\omega_Q}{3}\ (S_z^{1-2} - S_z^{2-3}) \quad .$$

Generally, I will be interested in the case where $\Delta\omega$ is small, but for now I include it in order to obtain an estimate for when it may be neglected. Consider:

$$\mathcal{H} = -2\Delta\omega\ S_x^{1-3} - 2\omega_{1S}\ S_x^{2-3} + \omega_Q\ S_z^{1-2} - \frac{\omega_Q}{3}\ (S_z^{1-3}+S_z^{2-3}) \quad , \tag{2.85}$$

and consolidate the first two terms via a tilt about S_y^{1-2} of 2ϕ, where $\phi = \mathrm{atan}(\Delta\omega/\omega_{1S})$. The last term emerges from this transformation unscathed, and we find

$$\begin{aligned}\mathcal{H}^T &= -\ 2\omega_{ez}\ S_x^{2-3} + \omega_Q\ e^{-i2\phi S_y^{1-2}}\ S_z^{1-2}\ e^{i2\phi S_y^{1-2}} \\ &\qquad - \frac{\omega_Q}{3}\ (S_z^{1-3} + S_z^{2-3}) \\ &= -\ 2\omega_{ez}\ S_x^{2-3} + \omega_Q\ (S_z^{1-2}\ \cos 2\phi - S_x^{1-2}\ \sin 2\phi) \\ &\qquad - \frac{\omega_Q}{3}\ (S_z^{1-3} + S_z^{2-3}) \quad ,\end{aligned} \tag{2.86}$$

where

$$\omega_{ez} = (\omega_{1S}^2 + \Delta\omega^2)^{1/2} \quad . \tag{2.87}$$

It is necessary at this point to neglect the term in Eq. (2.82) corresponding to S_x^{1-2}, because its inclusion results in a Hamiltonian which cannot be diagonalized by simple tilts. The coefficient of this term

$$\sin 2\phi = \frac{2\Delta\omega\ \omega_{1S}}{\Delta\omega^2+\omega_{1s}^2} \tag{2.88}$$

will be small only if $\Delta\omega << \omega_{1s}$, so for the present, I will assume Eq. (2.88) vanishes entirely and I have

$$\mathcal{H}^T = -\ 2\omega_{ez}\ S_x^{2-3} + \frac{2\omega_Q}{3}\ (S_z^{1-2} - S_z^{2-3}) \quad , \tag{2.89}$$

where $\omega_{ez} \sim \omega_{1S}$ (I will return to the case where $\omega_{ez} \neq \omega_{1S}$ later). Equation (2.89) may now be put in diagonal form via a tilt of $-\theta$ about S_y^{2-3}, where $\theta = \mathrm{atan}(2\omega_1/\omega_Q)$, to yield an expression exactly like Eq. (2.12)

$$\mathcal{H}^T = -\ \omega_e\ S_z^{2-3} + \frac{\omega_Q}{3}\ (S_z^{1-2} + S_z^{1-3}) \quad . \tag{2.90a}$$

The effective field along S_z^{2-3} is defined by Eq. (2.14) as

$$\omega_e = (4\ \omega_1^2 + \omega_Q^2)^{1/2} \quad .$$

Taking advantage of the linear dependence of the z operators (Eq. (B.1)), Eq. (2.90a) may be rearranged to yield two degenerate expressions:

$$\mathcal{H}^T = -\ (\frac{\omega_e - \omega_Q}{2})\ S_z^{1-3} - (\frac{2\omega_Q}{3} + (\frac{\omega_e - \omega_Q}{2}))(S_z^{2-3} - S_z^{1-2}) \quad , \tag{2.90b}$$

and

$$\mathcal{H}^T = (\frac{\omega_e + \omega_Q}{2})\ S_z^{1-2} + (\frac{2\omega_Q}{3} + (\frac{\omega_e + \omega_Q}{2}))(S_z^{1-3} + S_z^{2-3}) \quad . \tag{2.90c}$$

Figure 12. The rotating frame energy levels of a spin one nucleus experiencing r.f. irradiation as a function of its first order quadrupolar interaction (ω_Q).

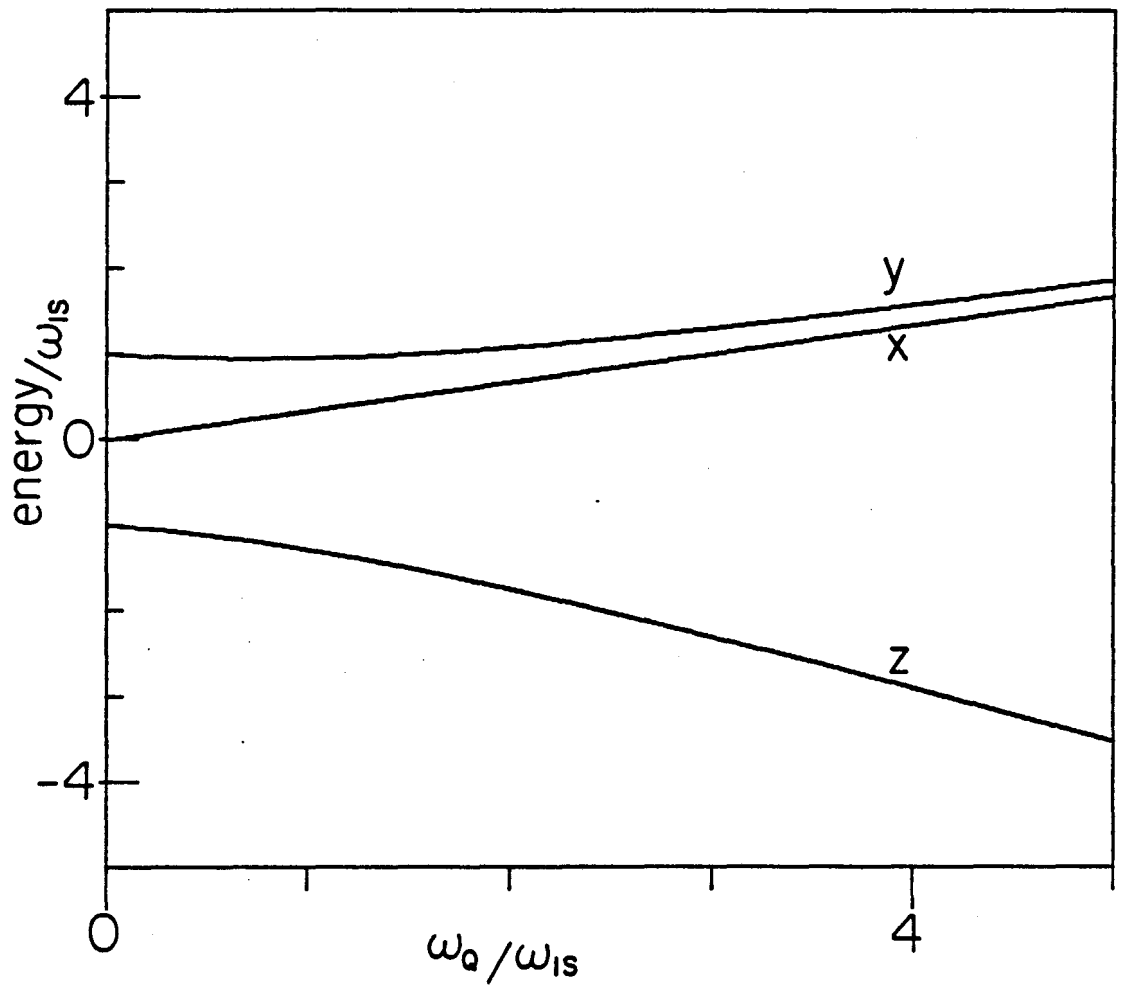

XBL 834-9383

The eigenvalues of this Hamiltonian are plotted in Figure 12 as a function of ω_Q. The eigenstates x, y, and z are defined:

$$|x\rangle = \frac{\sqrt{2}}{2}\left(|+1\rangle - |-1\rangle\right) \quad ,$$

$$|y\rangle = \frac{\sqrt{2}}{2}\cos\frac{\theta}{2}\,|+1\rangle - \sin\frac{\theta}{2}\,|0\rangle + \frac{\sqrt{2}}{2}\cos\frac{\theta}{2}\,|-1\rangle \quad ,$$

and

$$|z\rangle = \frac{\sqrt{2}}{2}\sin\frac{\theta}{2}\,|+1\rangle + \cos\frac{\theta}{2}\,|0\rangle + \frac{\sqrt{2}}{2}\sin\frac{\theta}{2}\,|-1\rangle \quad .$$

The three rotating frame energy splittings (effective fields) are:

$$\omega_e^{(2-3)} \quad , \quad \frac{\omega_e - \omega_Q}{2}\,(1-3) \quad , \quad \text{and } \frac{\omega_e + \omega_Q}{2}\,(1-2) \quad .$$

Naively, one might think that, during the mixing period, magnetization grows along the three diagonal operators in the tilted frame in accordance with their effective fields. That this is not the case will be shown in the next section.

2.4.5 Hartmann-Hahn Conditions

Modulation of the heteronuclear dipolar interaction by the rotating frame I and S spin Hamiltonians will induce time dependent flip-flop terms in the rotating frame whose effect will be rapidly averaged (i.e., decoupled) unless the I and S spin parts of $\mathcal{H}_{IS}$ are modulated at the same frequency. This, we must remember, is the basis for the Hartmann-Hahn condition [63]. At the Hartmann-Hahn match, time dependent flip-flop terms become time independent

(like term B of Eq. (1.44)), and the cross-relaxation process is completely analogous to a group of homonuclei coming to "equilibrium" via their mutual dipolar coupling.

The starting point must, of course, be the heteronuclear Hamiltonian (in terms of fictitious spin 1/2 operators):

$$\mathcal{H}_{IS} = 2 \sum_i b_i \, S_z^{1-3} \, I_{zi} \quad , \tag{2.91}$$

where b_i is defined in Eq. (2.33). Straightforward transformation of this into the tilted frame via $U^+ \mathcal{H}_{IS} U$, where $U = e^{i\frac{\pi}{2} I_y} e^{i\frac{\pi}{2} S_y^{1-3}} \cdot e^{-i\theta S_y^{2-3}}$, yields

$$\mathcal{H}_{IS}^T = 2 \sum_i b_i \, I_{x_i} \, (\cos \frac{\theta}{2} \, S_x^{1-3} + \sin \frac{\theta}{2} \, S_x^{1-2}) \quad , \tag{2.92}$$

where it is impliclty assumed that the I spin irradiation is applied on resonance. We now wish to find the effect of the Hamiltonian:

$$\mathcal{H}_I + \mathcal{H}_S = -\omega_{1I} I_z - \omega_e S_z^{2-3} + \frac{\omega_Q}{3} (S_z^{1-3} + S_z^{1-2}) \tag{2.93}$$

on $\mathcal{H}_{IS}^T$. The I spin term in Eq. (2.92) will become

$$\mathcal{H}_{IS}^{IT}(t) = e^{-i\mathcal{H}^T t} \, I_{x_i} \, e^{i\mathcal{H}^T t}$$

$$= I_{x_i} \cos\omega_I t - I_{y_i} \sin\omega_I t \quad , \tag{2.94}$$

while the S spin term will become

$$\mathcal{H}_{IS}^{ST}(t) = e^{-i\mathcal{H}^T t}\, \mathcal{H}_{IS}^{ST}\, e^{i\mathcal{H}^T t}$$

$$= e^{-i\mathcal{H}^T t}\, (\cos\frac{\theta}{2}\, S_x^{1-3} + \sin\frac{\theta}{2}\, S_x^{1-2}) e^{i\mathcal{H}^T t} \quad . \quad (2.95)$$

After performing the operator algebra and a bit more manipulation, Eq. (2.95) becomes:

$$\mathcal{H}_{IS}^{ST}(t) = \cos\frac{\theta}{2}\, (\cos(\frac{\omega_e-\omega_Q}{2})t\; S_x^{1-3} - \sin(\frac{\omega_e-\omega_Q}{2})t\; S_y^{1-3})$$

$$+ \sin\frac{\theta}{2}\, (\cos(\frac{\omega_e+\omega_Q}{2})t\; S_x^{1-2} + \sin(\frac{\omega_e+\omega_Q}{2})t\; S_y^{1-2}) \quad (2.96)$$

in which it is clear, from Eqs. (2.90), that only the fields $-(\frac{\omega_e-\omega_Q}{2})$ along S_z^{1-3} and $\frac{\omega_e+\omega_Q}{2}$ along S_z^{1-2} are effective in cross-relaxation. The Hartmann-Hahn matching conditions, obtained by multiplying Eq. (2.96) by Eq. (2.94) are

$$1. \quad \omega_{1I} = \frac{\omega_e-\omega_Q}{2} \quad (2.97a)$$

$$2. \quad \omega_{1I} = \frac{\omega_e+\omega_Q}{2} \quad . \quad (2.97b)$$

When $\omega_Q = 0$, both reduce to $\omega_{1I} = \omega_{1S}$ (as they must), and when ω_Q is much larger than ω_{1S}, condition 1 becomes $\omega_{1I} = \omega_{1S}^2/\omega_Q$ (the double quantum matching condition [59]). Conditions 1 and 2 are plotted as a function of ω_Q in Figure 13.

Through Eqs. (2.76), (2.90), (2.92), and (2.96), we can calculate the relaxation rates in analogy with Eqs. (2.80). Relaxation due to condition 1 occurs along S_z^{1-3} in the tilted frame, and will have a

Figure 13. Hartmann-Hahn matching conditions 1 and 2 as a function of ω_Q (Eq. (2.97)).

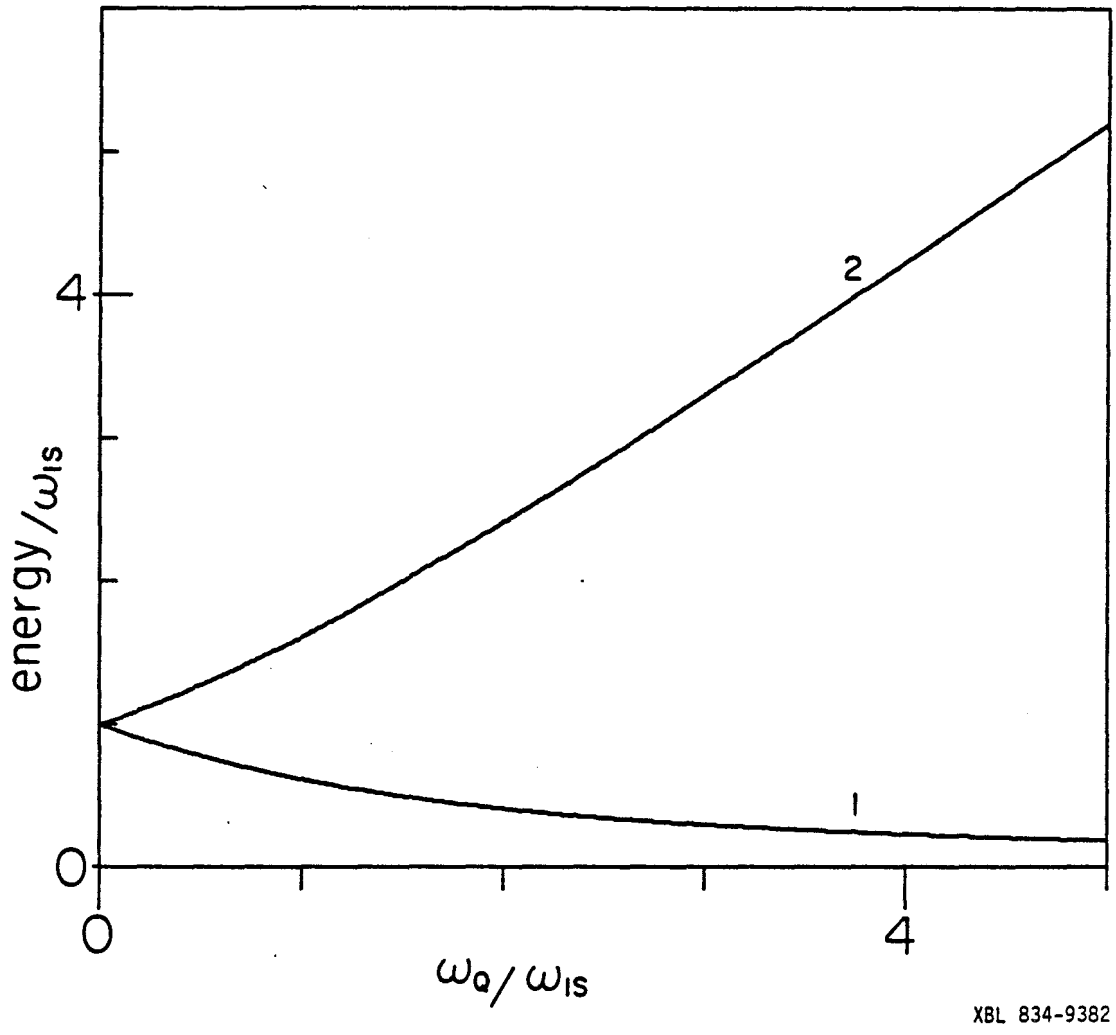
4
0
energy/ω_{IS}
2
1
0
4
ω_Q/ω_{IS}
XBL 834-9382

relaxation rate, for the ADRF case:

$$T_{IS}^{-1} = \cos^2 \frac{\theta}{2} M_{2IS}^{1-3} J_z \left(\frac{\omega_e - \omega_Q}{2}\right) \quad , \tag{2.98}$$

while that due to condition 2 occurs along S_z^{1-2}, and is characterized by

$$T_{IS}^{-1} = \sin^2 \frac{\theta}{2} M_{2IS}^{1-2} J_z \left(\frac{\omega_e + \omega_Q}{2}\right) \quad . \tag{2.99}$$

It is to be noted that the second moments

$$M_{2IS}^{1-3} = \frac{Tr[2 \sum_i b_i I_{x_i} S_x^{1-3}, S_z^{1-3}]^2}{Tr[S_z^{1-3}]^2}$$

and

$$M_{2IS}^{1-2} = \frac{Tr[2 \sum_i b_i I_{x_i} S_x^{1-2}, S_z^{1-2}]^2}{Tr[S_z^{1-2}]^2}$$

will be equal. Therefore, the ratio of the two relaxation rates will be:

$$\frac{T_{IS}^{-1}(S_z^{1-3})}{T_{IS}^{-1}(S_z^{1-2})} = \frac{\cos^2 \frac{\theta}{2}}{\sin^2 \frac{\theta}{2}} \frac{J_z\left(\frac{\omega_e - \omega_Q}{2}\right)}{J_z\left(\frac{\omega_e + \omega_Q}{2}\right)}$$

$$= \left(\frac{\omega_e + \omega_Q}{\omega_e - \omega_Q}\right) \frac{J_z\left(\frac{\omega_e - \omega_Q}{2}\right)}{J_z\left(\frac{\omega_e + \omega_Q}{2}\right)} \quad . \tag{2.100}$$

Incidentally, the $\cos^2$ and $\sin^2$ factors are commonly referred to as efficiency factors [63]. Since the two effective fields are opposite in sign, and because the relaxation rates become equal when $\omega_{1S} >> \omega_Q$, full overlap of conditions 1 and 2 results in a polarization along S_z^{2-3} in the tilted frame which is characterized by

$$T_{IS}^{-1} = M_{2IS}^{2-3} J_z \left(\frac{\omega_e}{2}\right) \quad . \tag{2.101}$$

Whenever ω_Q is small relative to ω_{1S}, but not extremely small, the two matching conditions will overlap partially. In this situation, my preceeding treatment is not quite correct, since it corresponds to a neglect of cross terms (between the 1-2 and 1-3 transitions) which become important in this region. These cross terms will be multiplied by efficiency factors of $\sin\theta$, and will have a tendency to bolster the cross-relaxation rate (i.e., make it larger than we might expect) in this region. This situation of overlap is very difficult to deal with, and I shall not consider it in detail.

2.4.6 Polarizations Produced

The rotating frame cross-polarization experiment yields a coherence in the x-y frame which may or may not be observed; depending upon which operator has been polarized under what conditions. In order to determine which operator(s) in the laboratory frame result from this rotating frame experience, it is necessary to return to the laboratory frame. S_z^{1-3} returns as an observable coefficient S_x of $\sin\theta = 2\omega_{1S}/\omega_e$ (which will appear as an fid immediately following

Table 2.I

Polarizations Resulting from Cross-Polarization Process

Laboratory Frame Polarization	Operator Polarized (tilted frame) S_z^{2-3}	S_z^{1-3}	S_z^{1-2}
Z.Q.	$-\frac{\cos\theta}{2}$	$\frac{3}{2}\sin^2\frac{\theta}{2}$	$\frac{3}{2}\cos^2\frac{\theta}{2}$
D.Q.	$-\frac{\cos\theta}{2}$	$-\frac{1}{2}(1+\cos^2\frac{\theta}{2})$	$-\frac{1}{2}(1+\sin^2\frac{\theta}{2})$
S.Q.	$\sin\theta$	$\sin\theta$	$-\sin\theta$

$$\theta = \operatorname{atan}\left(\frac{2\omega_{1S}}{\omega_Q}\right)$$

$$\text{Z.Q.} = \frac{1}{2}\left(3\,S_z^{\,2} - S(S+1)\right)$$

$$\text{D.Q.} = \frac{1}{2}\left(S_x^{\,2} - S_y^{\,2}\right)$$

$$\text{S.Q.} = S_x$$

the mixing period), while S_z^{1-2} produces an observable coefficient of $-\sin\theta$. In the case of full overlap, S_z^{2-3} generates only S_x because θ must be nearly 90°. The remainder of the polarization in each case lies in $[\frac{3S_z^2 - S(S+1)}{2}]$ (zero quantum or quadrupolar order), and $\frac{S_x^2 - S_y^2}{2}$ (double quantum order). The proportion of double and zero quantum coherence is dependent upon the matching condition. Condition 1 leads to a preponderance of double quantum order, and condition 2 to zero quantum order; when ω_Q is much larger than ω_{1S}, condition 1 becomes a purely double quantum matching condition and condition 2 becomes purely zero quantum. Because a purely zero quantum second moment vanishes (the efficiency factor in Eq. (2.99) becomes zero), the situation of zero quantum cross-polarization will never exist. By contrast, it is possible to obtain a considerable double quantum cross-polarization; the result of which is not directly observable, but may be rendered observable, most efficiently, via a hard ($\omega_{1S} >> \omega_Q$) 90° pulse 45° out of phase with the mixing field.

2.4.7 Cross-Polarized Echoes

The cross-polarized fid, as explained in section 2.1, will generally not be observable due to instrumental dead time. The solution to this problem, once again, is to use a quadrupolar echo. In order that the observable x magnetization may be echoed, it is only necessary to apply an x pulse (or, in general, a pulse in phase with the mixing field). The frequency response of the echo will be distorted due to the finite length of the echo pulse, and a distortion function may be derived as:

$$D(\omega_1,\omega_Q) = \sin^2\theta \sin^2 \frac{\omega_e t_p}{2} \quad . \tag{2.102}$$

This function is exactly the same as that for the second pulse of a two pulse sequence (see section 2.1.1).

Of course, we will always obtain some double quantum coherence, and this if of little value unless it too may be directly observed. In terms of fictitious spin 1/2 operators, $\frac{S_x^2 - S_y^2}{2} = S_x^{1-3}$ (see appendix B), and, in the "on resonance" reference frame, this becomes S_x^{1-3}. Now, we wish to investigate the effect upon this operator of a Hamiltonian:

$$\mathcal{H} = -2\omega_1 \left(S_x^{2-3} \cos\phi + S_y^{1-2} \sin\phi\right) + \frac{2\omega_Q}{3} \left(S_z^{1-2} - S_z^{2-3}\right) , \tag{2.103}$$

where ϕ is the relative phase of the r.f. In order that this equation might become somewhat more manageable, we take note of the relation [2]:

$$e^{-2i\phi\, S_x^{1-3}}\, S_x^{2-3}\, e^{2i\phi\, S_x^{1-3}} = \cos\phi\, S_x^{2-3} + \sin\phi\, S_y^{1-2} \tag{2.104a}$$

$$e^{2i\phi\, S_x^{1-3}}\, S_y^{1-2}\, e^{-2i\phi\, S_x^{1-3}} = \cos\phi\, S_x^{2-3} + \sin\phi\, S_y^{1-2} \,. \tag{2.104b}$$

Thus, in place of Eq. (2.99), we may use:

$$\mathcal{H} = -2\omega_1 S_x^{2-3} + \frac{2\omega_Q}{3} \left(S_z^{1-2} - S_z^{2-3}\right) \tag{2.105}$$

so long as we perform the following transformation prior to evolution

$$\rho'(0) = U\,\rho(0)\,U^{+} \tag{2.106}$$

and, following evolution

$$\rho(t) = U^{+}\rho'(t)U \tag{2.107}$$

where $U = e^{2i\phi\, S_x^{1-3}}$. This allows us to consider the effect of pulses of arbitrary phase. Initially, consider the effect of a hard x pulse on the double quantum coherence:

$$e^{2i\omega_1 t S_x^{2-3}}\, S_z^{1-3}\, e^{-2i\omega_1 t S_x^{2-3}} = e^{i\beta S_x^{2-3}}\, S_z^{1-3}\, e^{-i\beta S_x^{2-3}}$$

$$= S_z^{1-3} - \sin^2\frac{\beta}{2}\, S_z^{2-3} + \frac{\sin\beta}{2}\, S_y^{2-3} \quad , \tag{2.108}$$

where this evolution must be (and, has been) calculated using the rotation matrices of Table B.II. Similarly, the effect of a hard y pulse may be calculated

$$e^{2i\omega_1 t S_y^{1-2}}\, S_z^{1-3}\, e^{-2i\omega_1 t S_y^{1-2}} =$$

$$S_z^{1-3} - \sin^2\frac{\beta}{2}\, S_z^{1-2} + \frac{\sin\beta}{2}\, S_x^{1-2} \quad . \tag{2.109}$$

In each expression (Eq. (2.108) and (2.109)), only the final operator is observable, corresponding to antiphase single quantum coherence. A maximum of 1/2 of the double quantum coherence is transferred to this operator, and this occurs when $\beta = \pi/2$, or for a 45° pulse. Application

of a second pulse, in phase with the first, leads to the formation of an antiphase quadrupolar echo (see Figure 14). As mentioned in the last section, observation of the double quantum coherence is more efficiently accomplished via a pulse of 45° phase. We apply the transformation of Eq. (2.106):

$$e^{2i\phi S_x^{1-3}} S_x^{1-3} e^{-2i\phi S_x^{1-3}} = S_z^{1-3} \cos 2\phi + S_y^{1-3} \sin^2\phi, \quad (2.110)$$

and note in passing that the phase shift ϕ takes on twice its value in the double quantum reference frame. For a $\pi/4$ phase shift, Eq. (2.110) becomes S_y^{1-3}, and we may directly apply (2.105) ($\omega_1 >> \omega_Q$):

$$e^{2i\omega_1 t S_x^{2-3}} S_y^{1-3} e^{-2i\omega_1 t S_x^{2-3}} = \cos\frac{\beta}{2} S_y^{1-3} - \sin\frac{\beta}{2} S_x^{1-2} \quad , \quad (2.111)$$

and we see that, for a 90° pulse ($\beta=\pi$), all of the double quantum coherence is transferred to antiphase single quantum coherence as S_x^{1-2}. The application of Eq. (2.106) yields

$$e^{-2i\phi S_x^{1-3}} S_x^{1-2} e^{2i\phi S_x^{1-3}} = \frac{\sqrt{2}}{2} (S_x^{1-2} - S_y^{2-3}) \quad ; \quad (2.112)$$

$\frac{\sqrt{2}}{2}$ of the double quantum coherence appears in each phase detector channel. In order that all of this coherence may be echoed, a 45° phase hard pulse should be applied; $\frac{\sqrt{2}}{2}$ of the echo will now appear in each channel. The entire echo will appear in one channel if a 45° phase mixing field is used, followed by a 90°_x-90°_y echo sequence (echo appears in y channel; see Figure 14), or a 90°_y-90°_x echo sequence (echo

Figure 14. The calculated effect of various echo pulse sequences on a density matrix which would likely result from cross-polarization. The calculation assumed a ^{14}N r.f. mixing field of 20 kHz, and an ADRF proton state ($\gamma H_L/2\pi$ = 4 kHz, gaussian correlation function, τ_c = 48 μsec).

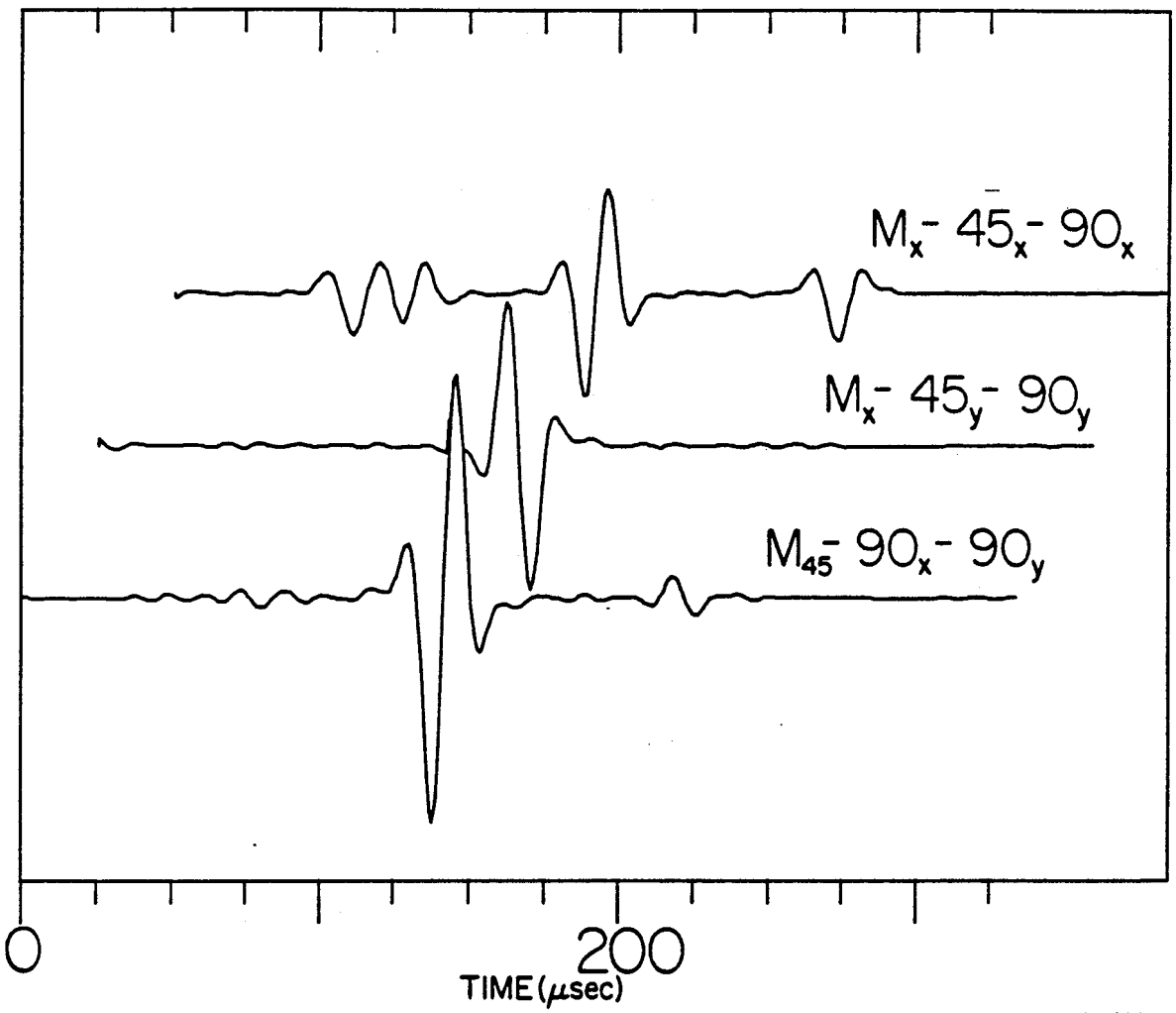

XBL 839-11500

appears in x channel). In all of my experiments I have employed a 45° phase mixing field, followed by a 90°_x-90°_y sequence. Of course, my pulses do have a finite length, so an echo sequence distortion factor must be obtained. From Eq. (2.110), we have a coefficient of S_y^{1-3} representing the double quantum coherence following the 45° mixing period. After a single pulse on such a density matrix, it is found that:

$$\rho(t) = (\cos\frac{\omega_e t}{2}\cos\frac{\omega_Q t}{2} + \cos\theta\sin\frac{\omega_e t}{2}\sin\frac{\omega_Q t}{2})S_y^{1-3}$$

$$+ (\cos\theta\sin\frac{\omega_e t}{2}\cos\frac{\omega_Q t}{2} - \cos\frac{\omega_e t}{2}\sin\frac{\omega_Q t}{2})S_x^{1-3}$$

$$- \sin\theta\sin\frac{\omega_e t}{2}\sin\frac{\omega_Q t}{2}\,S_y^{1-2}$$

$$- \sin\theta\sin\frac{\omega_e t}{2}\cos\frac{\omega_Q t}{2}\,S_x^{1-2} \quad . \qquad (2.113)$$

The operators S_y^{1-3} and S_x^{1-3} commute with the quadrupolar Hamiltonian, and their evolution will not contribute to the echo. The other two operators will contribute to the echo, and they have taken on a form analogous to that following an x pulse on an equilibrium density matrix. Therefore, the double quantum echo distortion factor is the same as that derived in section 2.1 (i.e., Eq. (2.19)):

$$D(\omega_1,\omega_Q) = \sin^3\theta\sin\frac{\omega_e t_1}{2}\sin^2\frac{\omega_e t_2}{2} \quad .$$

2.4.8 Observed Echo Signals

In order that the usefulness of the cross-polarization scheme may

be tested experimentally, ammonium sulfate was chosen as a model compound. Its room temperature crystal structure gives rise to two inequivalent nitrogen nuclear sites with the following quadrupole couplings [65]

$$\text{site I:} \quad e^2qQ/h = 154.55 \text{ kHz}, \ \eta = 0.684$$
$$\text{site II:} \quad e^2qQ/h = 115.71 \text{ kHz}, \ \eta = 0.749 \quad .$$

A standard proton decoupled quadrupolar echo spectrum is shown in Figure 15. This compound is convenient for study due to its long proton $T_{1\rho}$ (> 80 msec) and T_{1D} (> 1 sec) at room temperature. The general method of sample preparation and experimental set-up will be given in the next chapter.

Figure 16 shows the two experiments used to observe the density matrix coherences produced during the mixing period. These are merely the cross-polarized echo sequences discussed in the last section. In the single quantum experiment, a single pulse yields a single echo. This would also be the case for the double quantum experiment, if a purely double quantum density matrix were present following the mixing period. In reality, the density matrix contains double, single, and zero quantum. The simultaneous presence of double and zero quantum coherences complicates the pulse response of the system somewhat, but it may be easily shown that the effect of a 90° pulse of 45° phase is to rotate <u>only</u> double quantum into single quantum; zero quantum is partially rotated into double quantum, but will not contribute to any echoes. By contrast, a 45° pulse (along x or y) has the effect of rotating a mixture of zero and double quantum into single quantum (the

Figure 15. A room temperature proton decoupled quadrupolar echo spectrum of ammonium sulfate. This signal is the result of 3000 acquisitions using 3.7 μsec 90° pulses and an 80 μsec interpulse delay. The dotted line represents the rigid lattice spectrum calculated on the basis of the quadrupole coupling parameters given in section 2.4.8, and multiplied by the echo sequence distortion function (Eq. (2.19)).

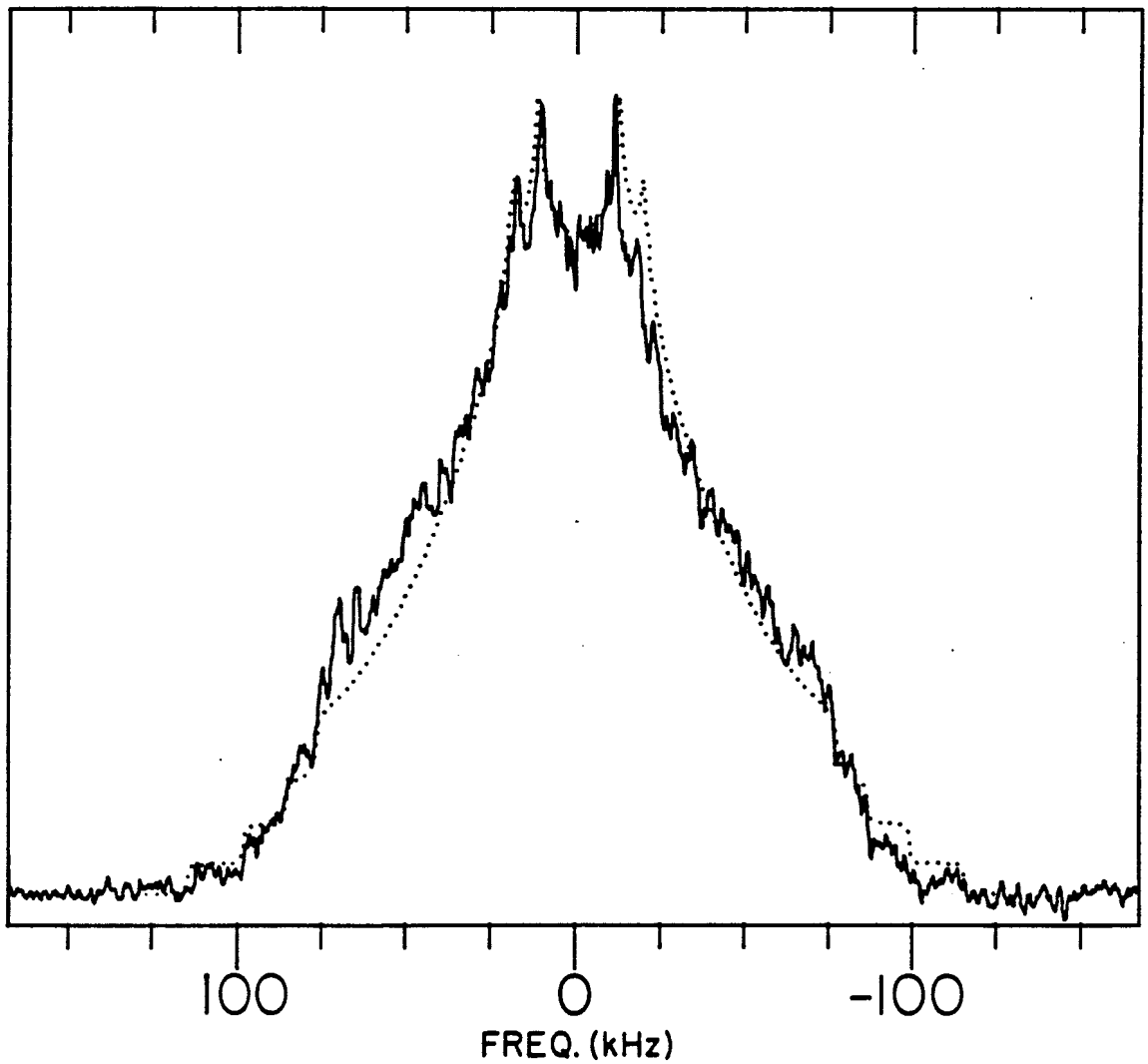

XBL 834-9391

Figure 16. A schematic representation of the cross-polarization quadrupolar echo sequences. In our experiments, all of the pulses are of 90° and ϕ in the double quantum experiment is 45°.

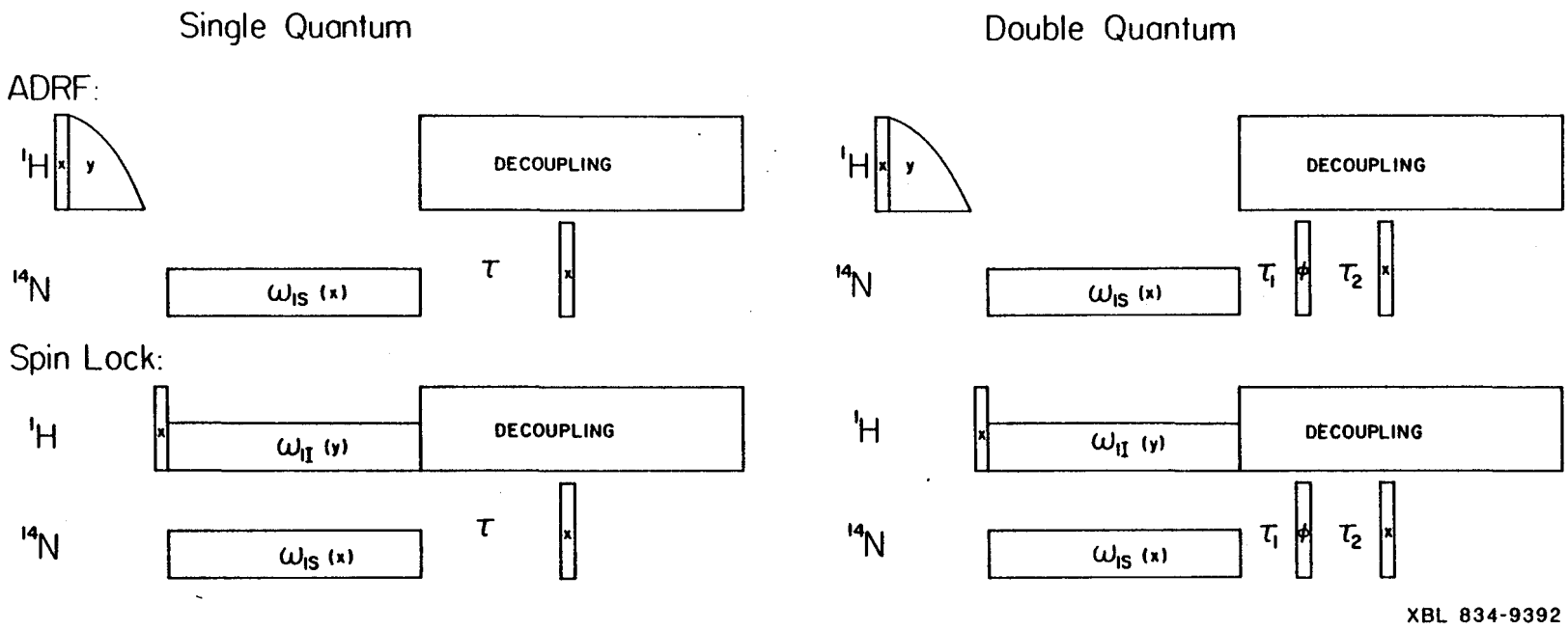
Single Quantum
Double Quantum
ADRF:
^{1}H
x
y
DECOUPLING
^{14}N
ω_{IS} (x)
τ
τ_1
ϕ
τ_2
Spin Lock:
ω_{1I} (y)
XBL 834-9392

complicated effect of this is responsible for the difference between the two 45° pulse sequences in Figure 14). With these considerations in mind, application of the double quantum echo sequence is expected to result in three echoes. The first occurs τ_1 following the second pulse and is the result of observable x magnetization being stored along z during τ_2 due to the 45° out of phase pulse at τ_1. The next echo is expected to occur at $\tau_2-\tau_1$, and is the stimulated echo of observable x magnetization (reduced by a factor of $\frac{\sqrt{2}}{2}$). The final echo occurs at τ_2 and is due to magnetization created by the pulse at τ_1: double quantum coherence. In Figure 17 we observe 3 echoes, but they occur at $\tau_2-\tau_1$, τ_2, and $\tau_2+\tau_1$. The echo predicted to occur at τ_1 has been subtracted away by the phase cycling technique used in order to minimize transient instrument response caused by the final echo pulse (i.e., the initial pulse of the sequence is alternately phase shifted by 180°, while the resulting echoes are alternately added and subtracted--see section 2.1.1). The echo at τ_2 manifests a derivative character, clearly showing it as the double quantum echo. We observe an unpredicted ("forbidden") echo at $\tau_2+\tau_1$. In order that we might be enlightened on this matter, a computer simulation was performed in which an initial density matrix is populated in accordance with Eq. (2.75a) along the two matching conditions, carried through an evolution corresponding to our experimental pulse sequence, and integrated over a weighted distribution of quadrupolar frequencies (i.e., a powder pattern) to give a time domain response signal (the simulating program, DQTP, is discussed a bit later and presented in Appendix C). The result of the calculation, in Figure 18, shows that the echo is indeed predicted theoretically. Forbidden echoes have been mentioned in previous

Figure 17. The experimental result of the double quantum SL experiment on ammonium sulfate. A 43 kHz ^{14}N r.f. field, 24 kHz ^{1}H r.f. field and 3.5 μsec 90° pulses were used to elicit this response. The first delay τ_1 was 80 μsec and the second delay τ_2 was 140 μsec. The phases were cycled as described in section 2.4.8 to eliminate the transient response of the final echo pulse.

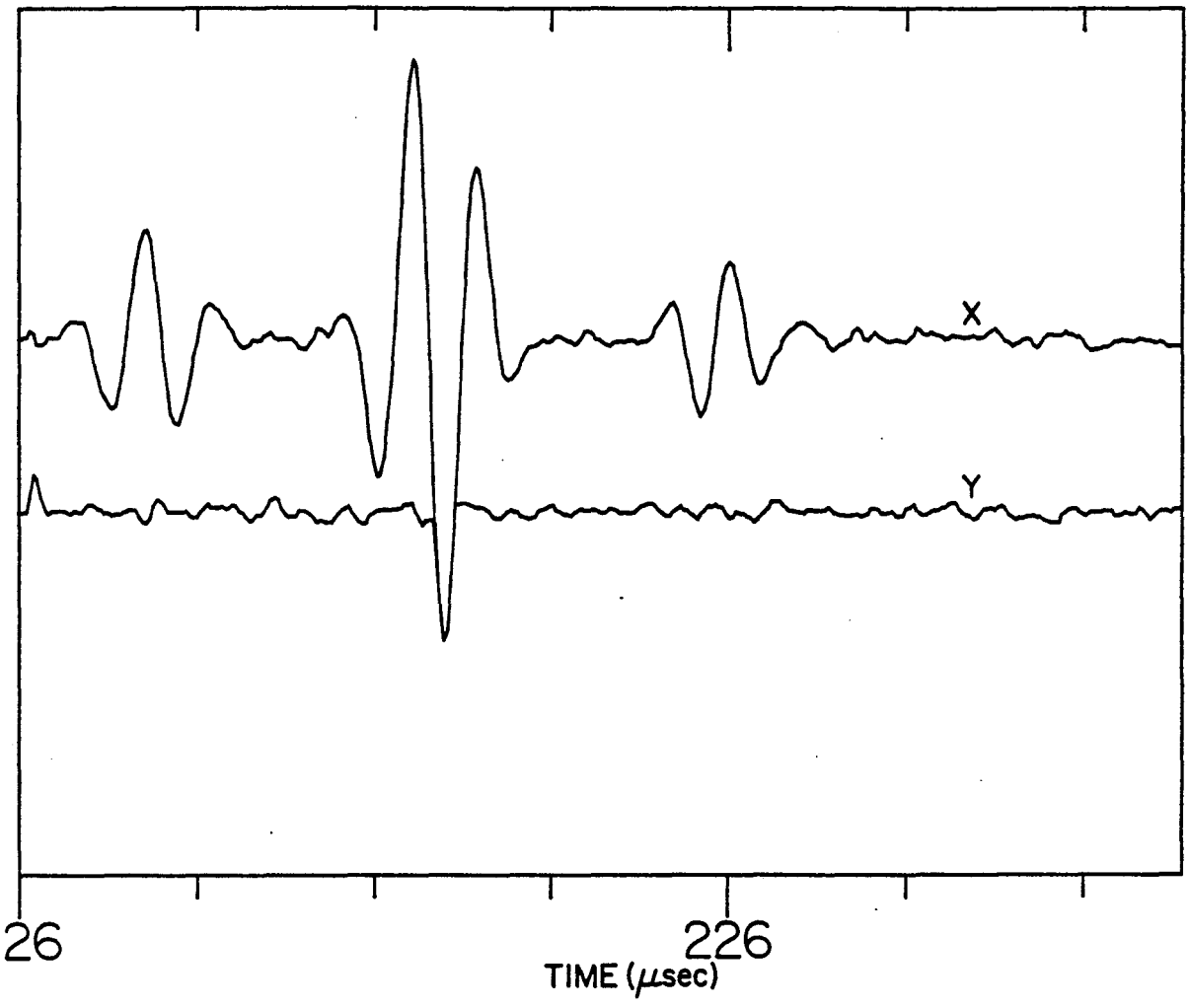

XBL 834-9385

Figure 18. Calculated response to the experimental parameters of Figure 17; a gaussian spectral density function with a correlation time of 65 μsec was used to represent the dipolar flip-flops of the protons.

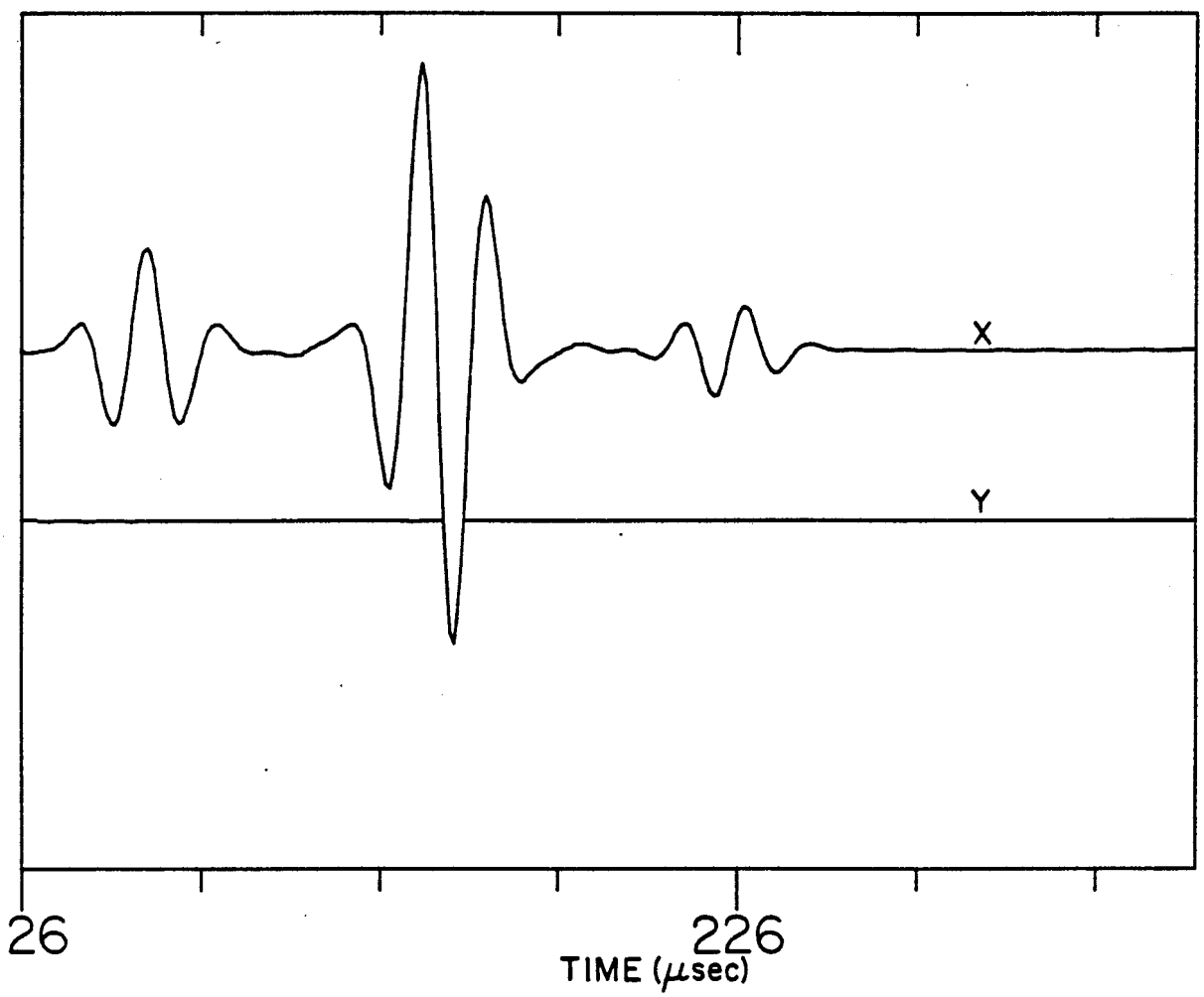

XBL 834-9384

literature [31], and are generally thought to result from pulse imperfections. Because of the time dependence of this third echo, it seemed likely to be a product of first pulse imperfections. In order to examine this hypothesis, a series of calculations were carried out (via DQTP) in which the amplitude of the first pulse was increased. The result in Figure 19 indicates that a "perfect" pulse will indeed produce no third echo. Although this echo manifests a derivative character, its time dependence indicates that it must result from single quantum evolution. This statement is further fortified by the observation that this echo and the stimulated single quantum echo bear a strong amplitude relationship to one another (for various mixing field amplitudes).

In the double quantum experiment, it is generally desirable to eliminate all but the double quantum echo. This can be satisfactorally approached in the following manner. The echo at τ_1 follows the phase of the final pulse (so long as the mixing field and first pulse phase are held constant), and is easily subtracted out as mentioned previously; this echo may easily be moved away from the double quantum echo by making τ_1 short, and so presents no problems in any case. The stimulated echo can be suppressed, and the echo at $\tau_2+\tau_1$ made to cancel by the following sequence: [(mixing field phase, first pulse phase, second pulse phase)] (45,0,90) add, (45,180,90) subtract. The stimulated echo does not occur for the same reason that two pulses of the same phase do not produce a quadrupolar echo from a system initially characterized by a Zeeman polarization. The "forbidden" echo at $\tau_1+\tau_2$ is subtracted away as it follows the phase of the mixing field. The echo at τ_1 depends upon the phase of both the mixing field and the second pulse, and so does not cancel in this sequence.

Figure 19. Calculated effect of varying the amplitude of the first 90° pulse on the size of the "forbidden" third echo in the double quantum echo experiment. The single quantum echo which preceeds the double quantum echo does not appear on this plot since it forms in the other phase detector channel.

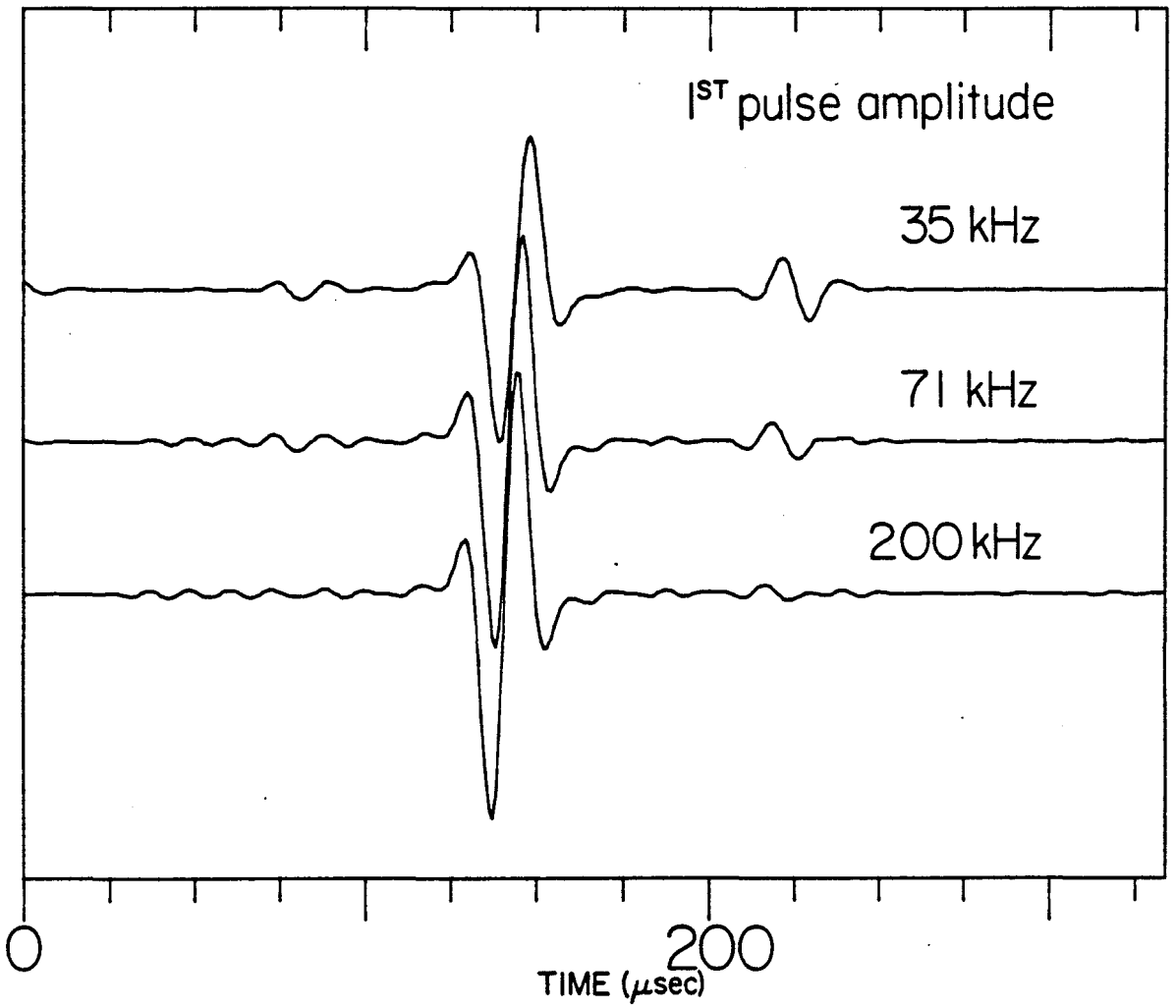

XBL 839-11501

Figure 20. The experimental result of the double quantum SL experiment using the same parameters as Figure 17, but here the phases were cycled (45,0,90) add, (45,180,90) subtract [the notation is defined: (mixing field phase, first pulse phase, second pulse phase)]

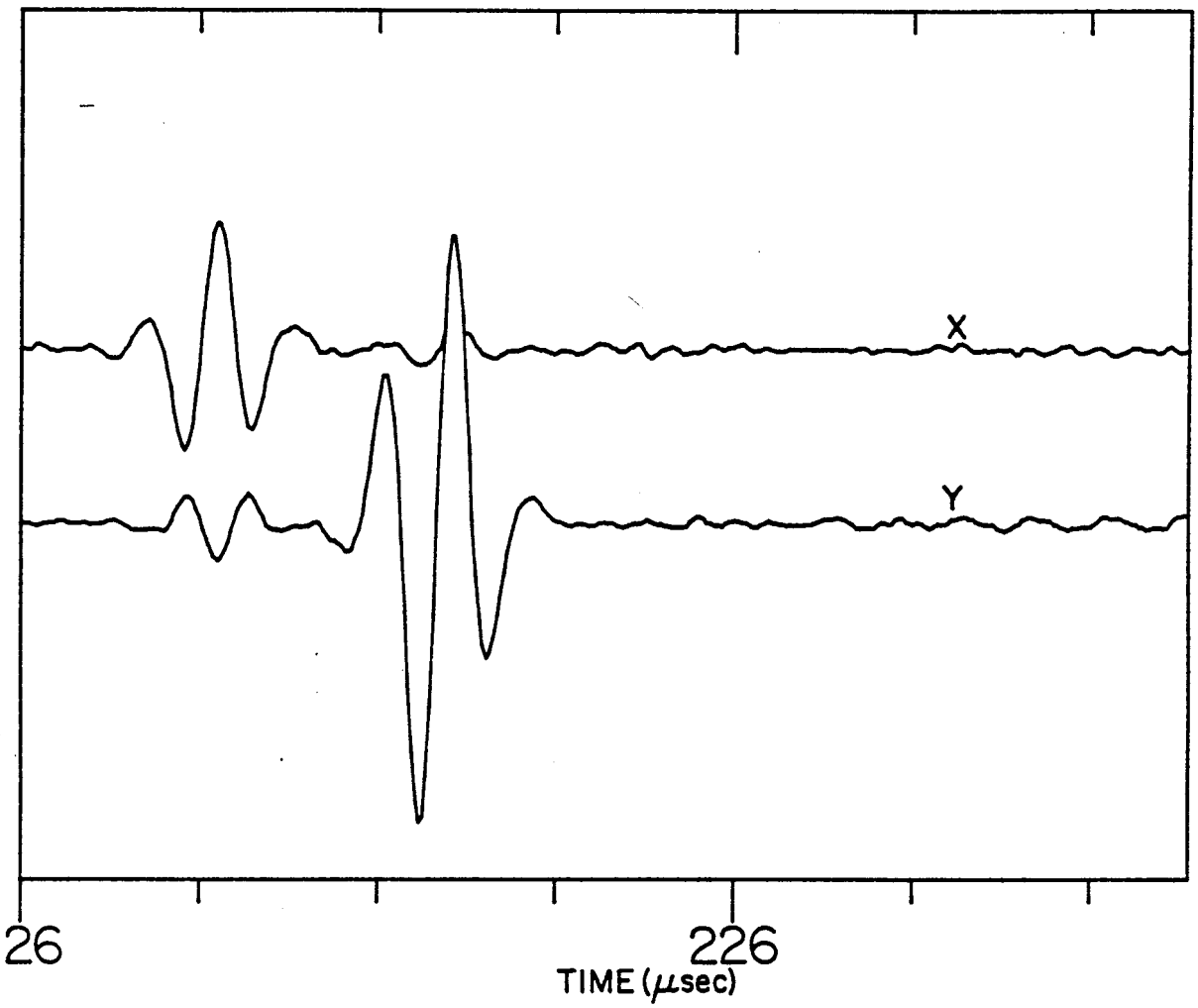

XBL 834-9386

Figure 21. Experimental single quantum (S.Q.) and double quantum (D.Q.) echoes resulting from the experimental parameters of Figure 17.

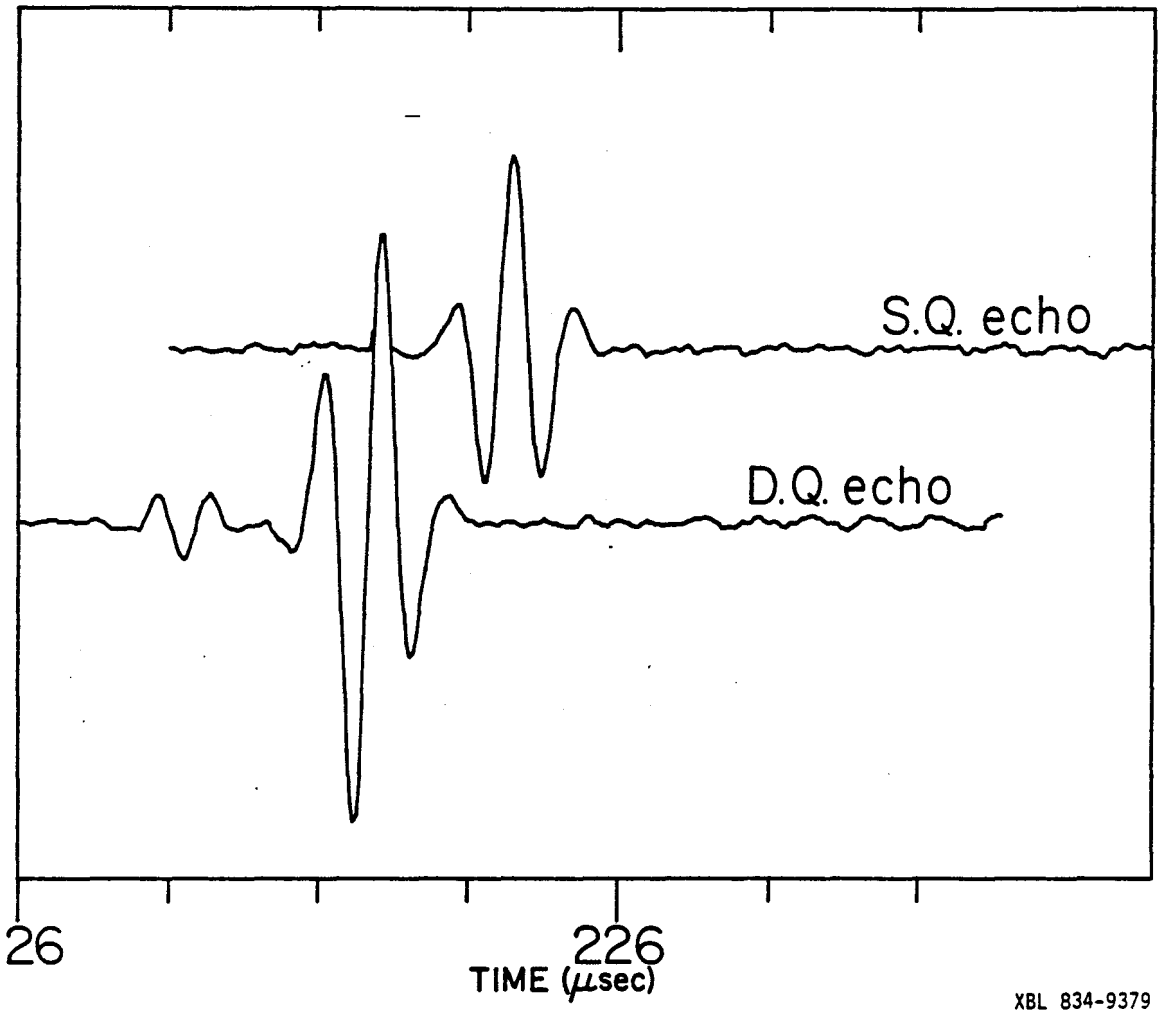

XBL 834-9379

The double quantum echo will appear entirely in the quadrature channel (as noted previously), and 100% of this polarization is echoed by this sequence (in the limit that we use ideal hard pulses). Also, all pulses and mixing periods may be cycled through 90° phase increments in order to equalize the two channels in quadrature phase operation (i.e., QPD in the Nicolet software package NTCFTB). The successful result is presented in Figure 20, and compared with the single quantum echo acquired under the same mixing conditions in Figure 21.

2.4.9 Observed Frequency Response of the Cross-Polarization

Upon fourier transformation of the second half of the aforementioned echoes, we will obtain a frequency domain spectrum which will always consist of two lobes, except for the single quantum situation $\omega_{1I} = \omega_{1S}$, where the center of the spectrum is preferentially enhanced. The width of the lobes may be dependent upon several factors: which condition is matched (or, which operator is populated in the tilted frame), the single or double quantum nature of the polarization produced, and the width of the spectral density function.

In Figure 22 is shown single quantum frequency domain spectra as a function of proton r.f. field amplitude using the spin lock experiment. Solving the matching conditions for ω_Q, we find that, for fixed ω_{1I} and ω_{1S} we should have rotating frame effective field equality (i.e, a Hartmann-Hahn match) between the I and S spins at

$$\omega_Q = (\omega_{1S}^2 - \omega_{1I}^2)/\omega_{1I} \qquad (2.114a)$$

for condition 1, and

Figure 22. Frequency domain response of the single quantum SL experiment as a function of proton r.f. field amplitude for ammonium sulfate. The sequence used a ^{14}N r.f. field amplitude of 33 kHz, 2 msec mixing time, a 3.5 μsec 90° pulse, and a τ of 100 μsec.

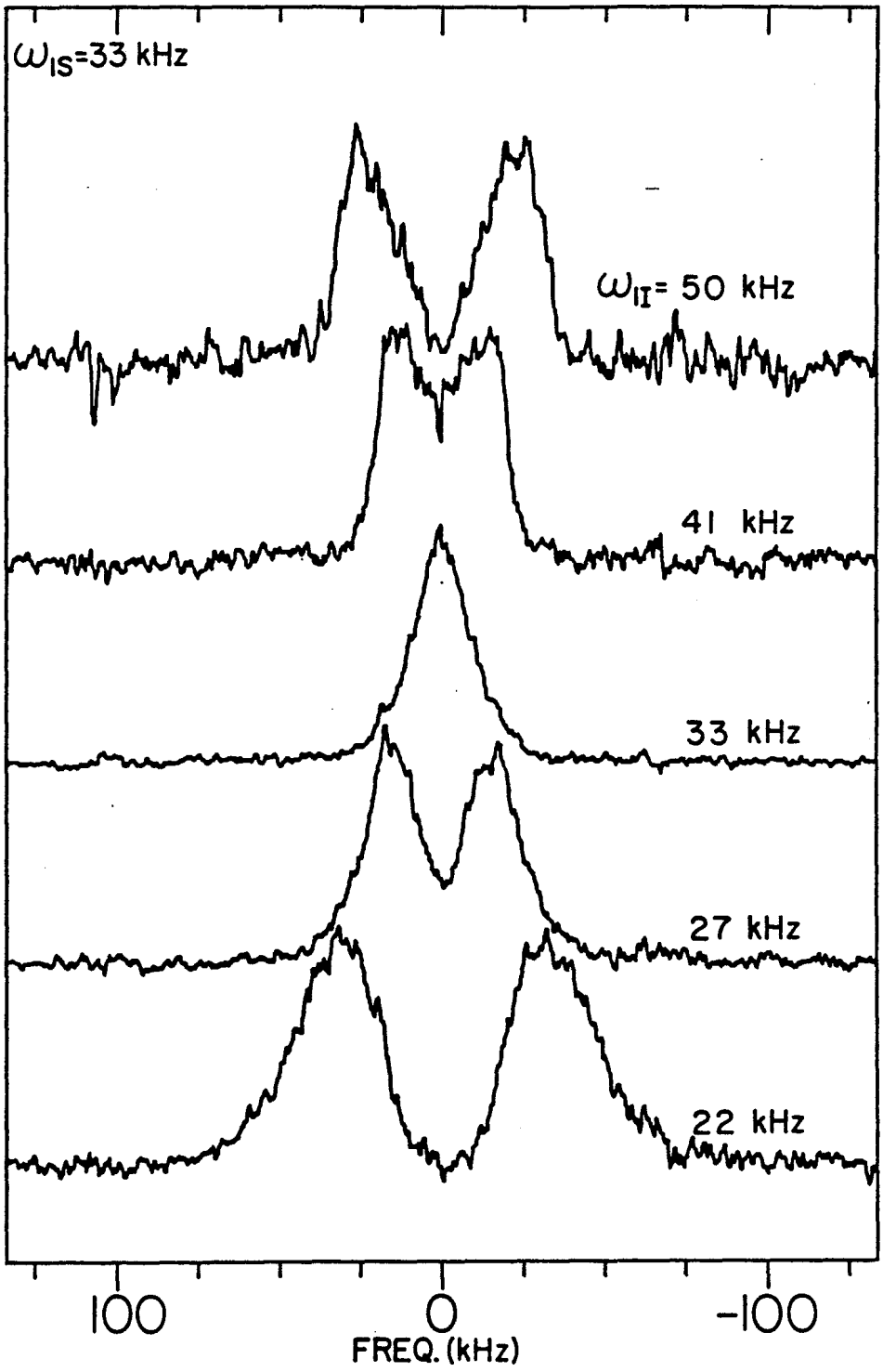
ω_{IS}=33 kHz
ω_{II}= 50 kHz
41 kHz
33 kHz
27 kHz
22 kHz
100
0
-100
FREQ. (kHz)

XBL 834-9387

$$\omega_Q = (\omega_{1I}^2 - \omega_{1S}^2)/\omega_{1I} \tag{2.114b}$$

for condition 2. It is observed that the separation of the two lobes decreases with increasing ω_{1I} in accordance with Eq. (2.114a). As ω_{1I} is increases above ω_{1S}, the lobes once more separate and follow Eq. (2.114b). The reason for the rapid S/N degradation was alluded to in section 2.4.6. The relaxation rate for this transition (Eq. (2.99)) contains a $\sin^2 \frac{\theta}{2}$ efficiency factor which decreases precipitously toward zero with increasing ω_Q. Therefore matching condition 2 is of no practical interest in the enhancement of large quadrupolar splittings.

An important difference between the two matching conditions may be readily seen in Figure 13. For large ω_Q, condition 1 has a very small negative slope (i.e., it becomes nearly independent of ω_Q), while condition 2 has a very large positive slope. This causes spectra due to relaxation according to condition 1 to tail off toward large ω_Q, and that due to condition 2 to have a sharp cutoff at large ω_Q. The best advantage may be taken of condition 1 in the ADRF experiment, where the effect is one of broadening the cross-polarization greatly (we can reduce ω_{1S} to move into a region where the slope of the matching condition is smaller). It should be mentioned that the observed difference between SL and ADRF experiments (see Figure 23) could be due to a broader spectral density for the ADRF. Indeed, in simulations of the echoes performed with DQTP, the SL experiments fit to a dipolar correlation time of about 67 μsec, while the ADRF echo seems to fit best to about 50 μsec. This is probably not a significant difference, especially in light of the simple treatment which the simulation makes of the cross-polarization

Figure 23. SL and ADRF double quantum frequency domain spectra of ammonium sulfate. In each case a 2 msec mixing period was followed by a D.Q. echo sequence using 3.5 μsec 90° pulses, a τ_1 of 80 μsec, and a τ_2 of 140 μsec. For the SL experiment the ^{14}N r.f. field amplitude was 18.5 kHz and that of the protons was 23 kHz; while for the ADRF experiment the ^{14}N r.f. field amplitude was 18.5 kHz.

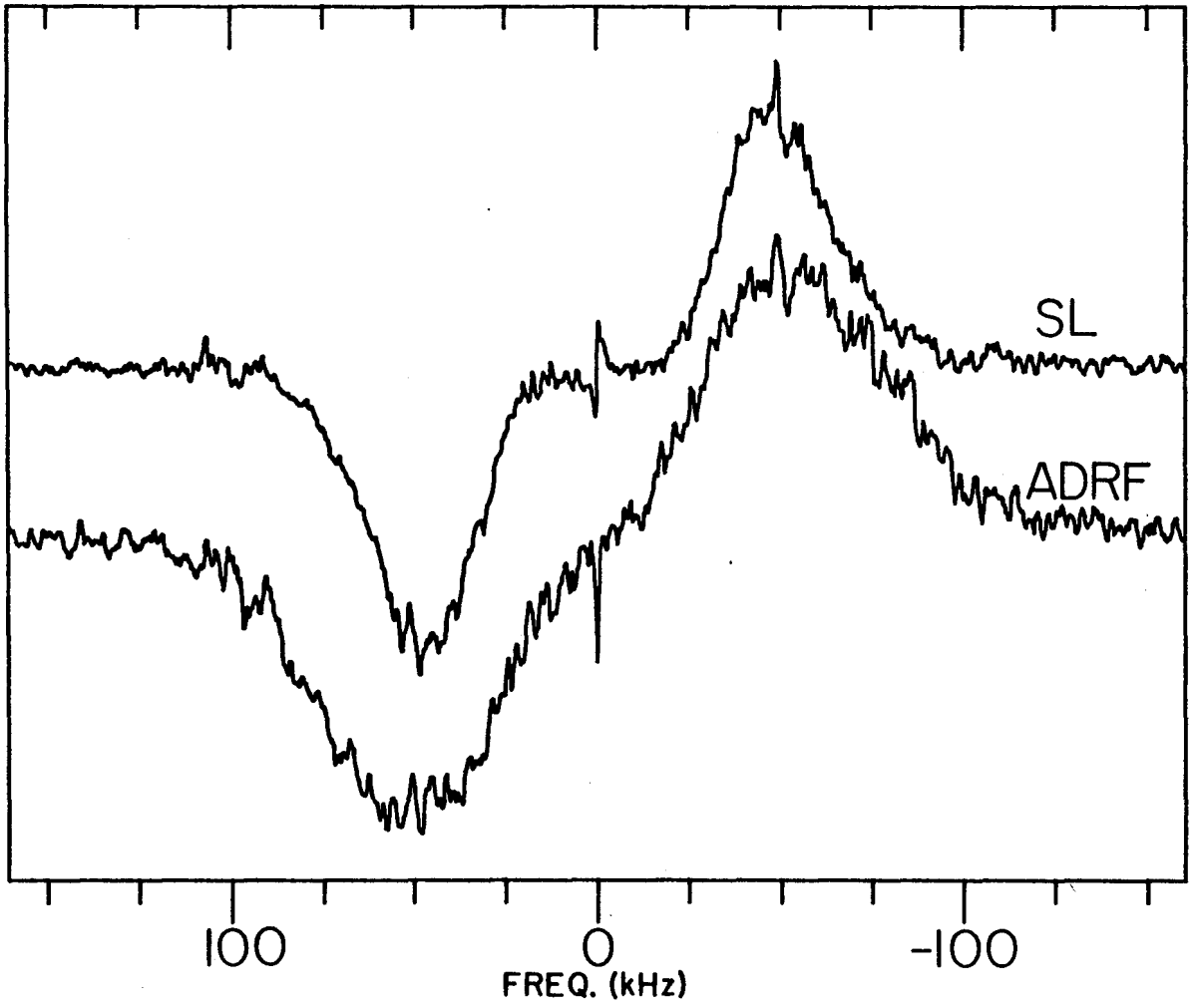

XBL 834-9405

process. In every $^{14}N-^{1}H$ cross-polarization experiment I have performed, the ADRF gives the broadest matching.

Figure 24 shows the resulting fourier transformation of single and double quantum echoes. As expected, the double quantum echo has greater S/N overall, and much greater response in the wings of the spectrum. Of course, there is also a corresondingly lesser response near the center (at frequencies less than $2\omega_{1S}$). The full width of the cross-polarization is best realized by observing the double quantum response. Of course, as I explained in section 2.4.7, the distortion factor for the double quantum echo will be smaller (i.e., more distortion) than for the single quantum echo; the former generally being the latter raised to the three halves power.

Because of the dependence of the equilibrium spin temperature on the S spin effective field (see Eqs. (2.64), (2.70), and (2.75)), the spectrum will always suffer some distortion, even for infinitely long mixing times. The result of this for matching condition 1 is that the center of the spectrum is preferentially enhanced even though T_{IS} in the wings may be shorter. This fact is demonstrated in Figure 25.

2.4.10 Some Quantitative Results from Simulations

I will now attempt to answer the question of whether anything quantitative may be said as a result of one hundred cpu hours of cross-polarized echo simulations. In Figure 26 I show a typical series of double quantum echoes along with the computer generated (DQTP) fit to each. All three echoes are reasonably well reproduced with only the ^{14}N r.f. mixing field varying from one simulation to the next (the same parameter which is experimentally varied). Assuming an

Figure 24. Frequency domain response of single (S.Q.) and double (D.Q.) quantum echoes for ammonium sulfate. Proton order was established via an ADRF. The ^{14}N r.f. field amplitude was 8 kHz, mixing time was 2 msec, and 3.5 μsec 90° pulses were used. For the S.Q. case, τ was 140 μsec, while for the D.Q. case τ_1 was 80 μsec and τ_2 was 140 μsec. The spikes near the center of these spectra represent the inner inflection points V_{xx} for sites I and II; which occur at 18.3 kHz and 10.9 kHz respectively.

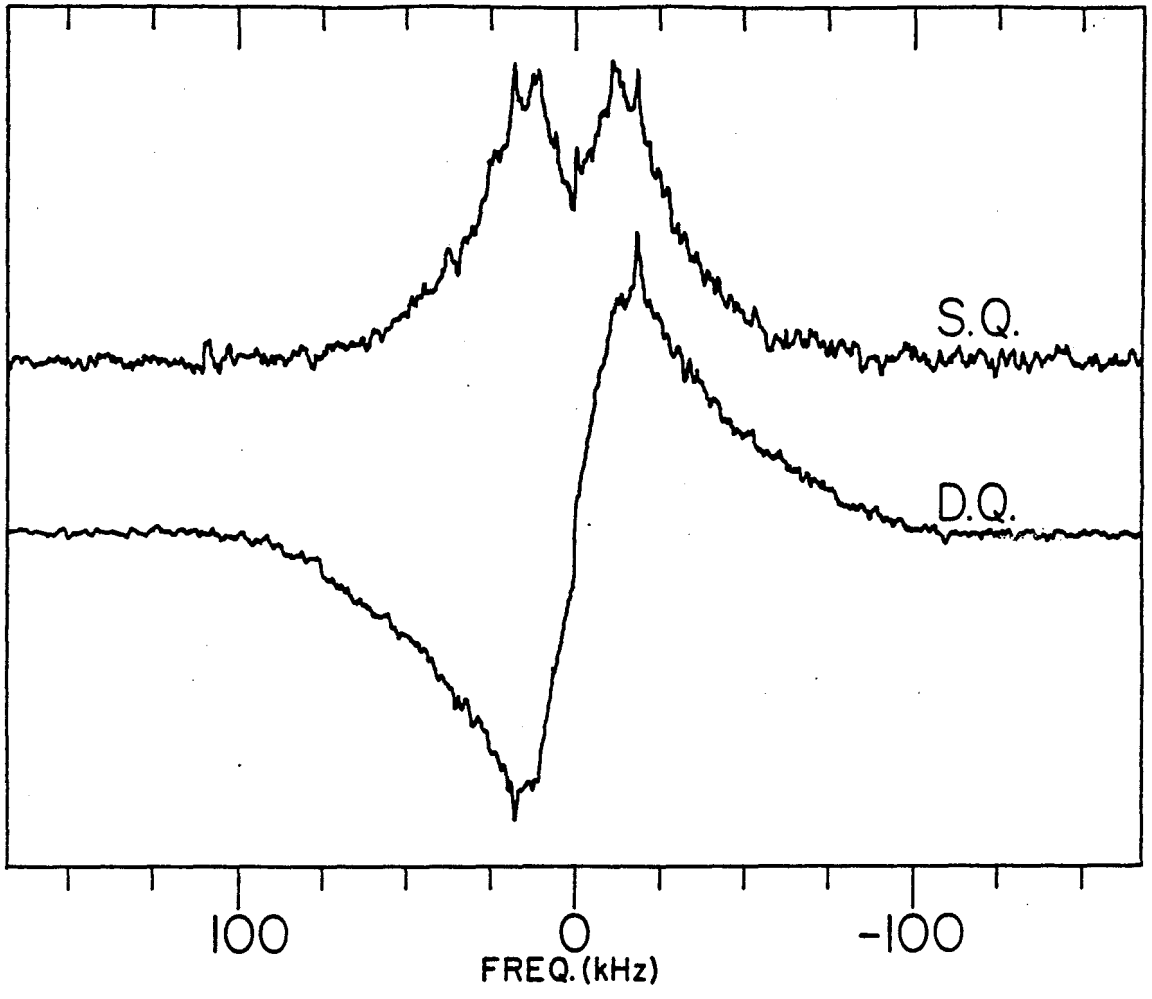

XBL 834-9388

Figure 25. The effect of the mixing time upon the double quantum frequency domain spectrum of ammonium sulfate. The double quantum ADRF experiment was used with an 8 kHz ^{14}N r.f. field amplitude, 3.5 μsec 90° pulses, a τ_1 of 80 μsec and a τ_2 of 140 μsec. The comment in the caption of Figure 24 as to the origin of the spikes near the center of the lineshape applies here also.

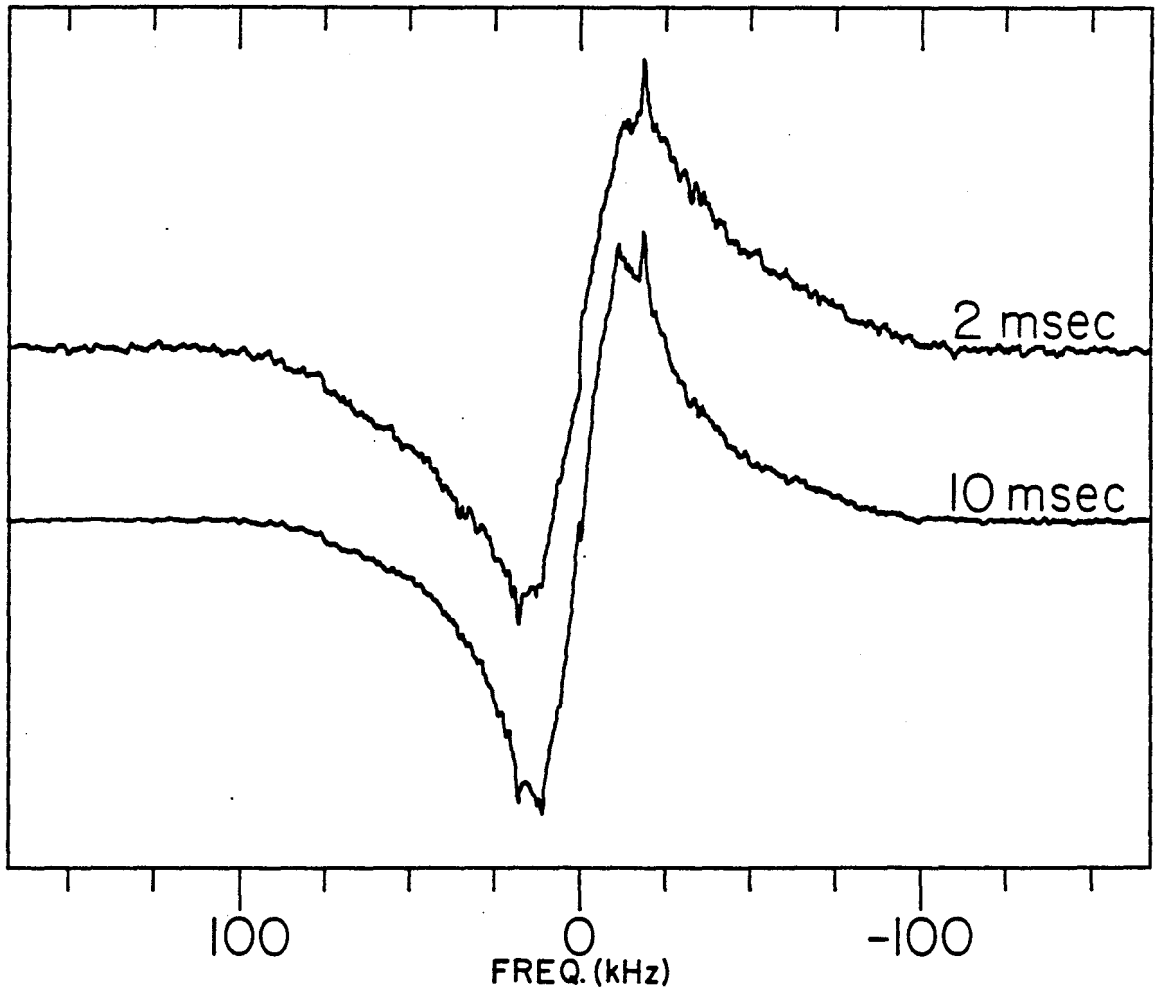

XBL 834-9389

ADRF on the protons, there are four critical parameters to be set in the calculation (see Eqs. (2.40) and (2.75)) the ^{14}N r.f. field, the local field of the protons (H_L), the dipolar correlation time (and correlation function), and the relative mixing time. As mentioned previously, I ignore spin-lattice couplings $T_{1\rho}$ and T_{1D}. Of the critical parameters, the r.f. field should be known from the experimental conditions, and the calculation is fairly sensitive to this parameter. The local field may be determined from the second moment of the proton resonance line using [50]:

$$H_L^{\ 2} = \frac{1}{3} M_{2II} \quad . \tag{2.115}$$

We may now employ Eq. (2.28) to relate the second moment to the fwhm, and derive:

$$\gamma H_L = \frac{\Delta\omega_{fwhm}}{4.09} \quad ; \tag{2.116}$$

assuming a purely gaussian lineshape. The $(NH_4)_2SO_4$ proton resonance line observed using the magic echo technique [67,70] fits fairly well to a gaussian of fwhm 18.9 kHz (using the Nicolet NTCFTB subroutine LF) at 20°C. This implies a local field $\gamma H_L/2\pi$ of 4.6 kHz. The calculation used the value 4 kHz, but the result is not extremely sensitive to this parameter (4 and 4.6 kHz calculations are indistinguishable). The dipolar spectral density is obviously a very important consideration, and I have found that the data for both SL and ADRF experiments cannot be fit using a lorentzian correlation function (an exponential spectral density) for any set of parameters. The results of the calculation seem to indicate a spectral density

Figure 26. Experimental (solid line) and calculated (dotted line) double quantum echo responses to an ADRF cross-polarization for various values of the ^{14}N r.f. mixing field. The experimental echoes were all the result of a 5 msec contact time, and this was represented in the calculation by a relative mixing time (Eq. (2,119)) of 1.5. The proton dipolar state was represented in the calculations by a local field ($\gamma H_L/2\pi$) of 4 kHz, and a gaussian correlation function of correlation time 48 μsec. The ^{14}N r.f. field amplitudes, used both experimentally and in the calculation, were: (a) 14.3 kHz, (b) 16.7 kHz, and (c) 22.7 kHz.

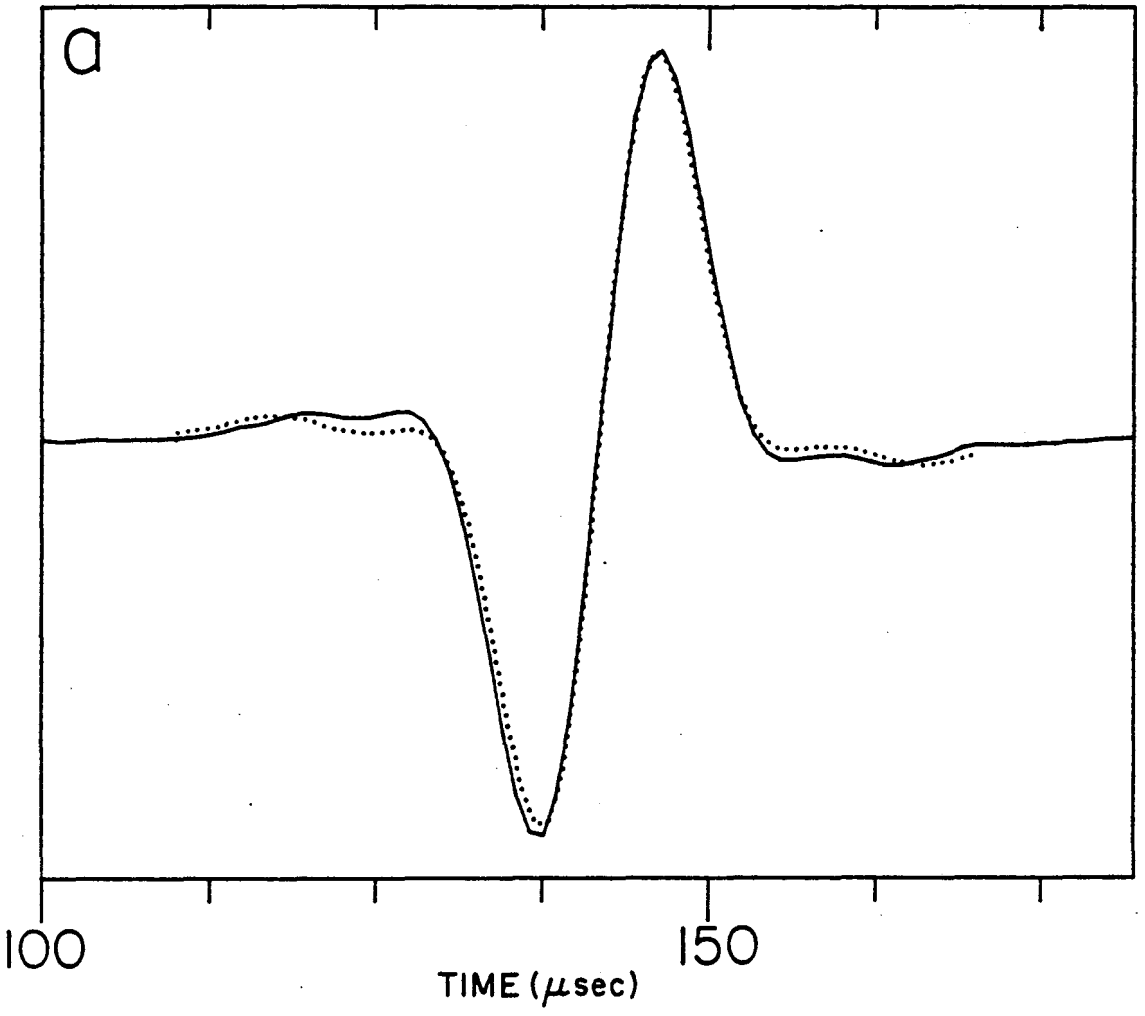

XBL 834-9377

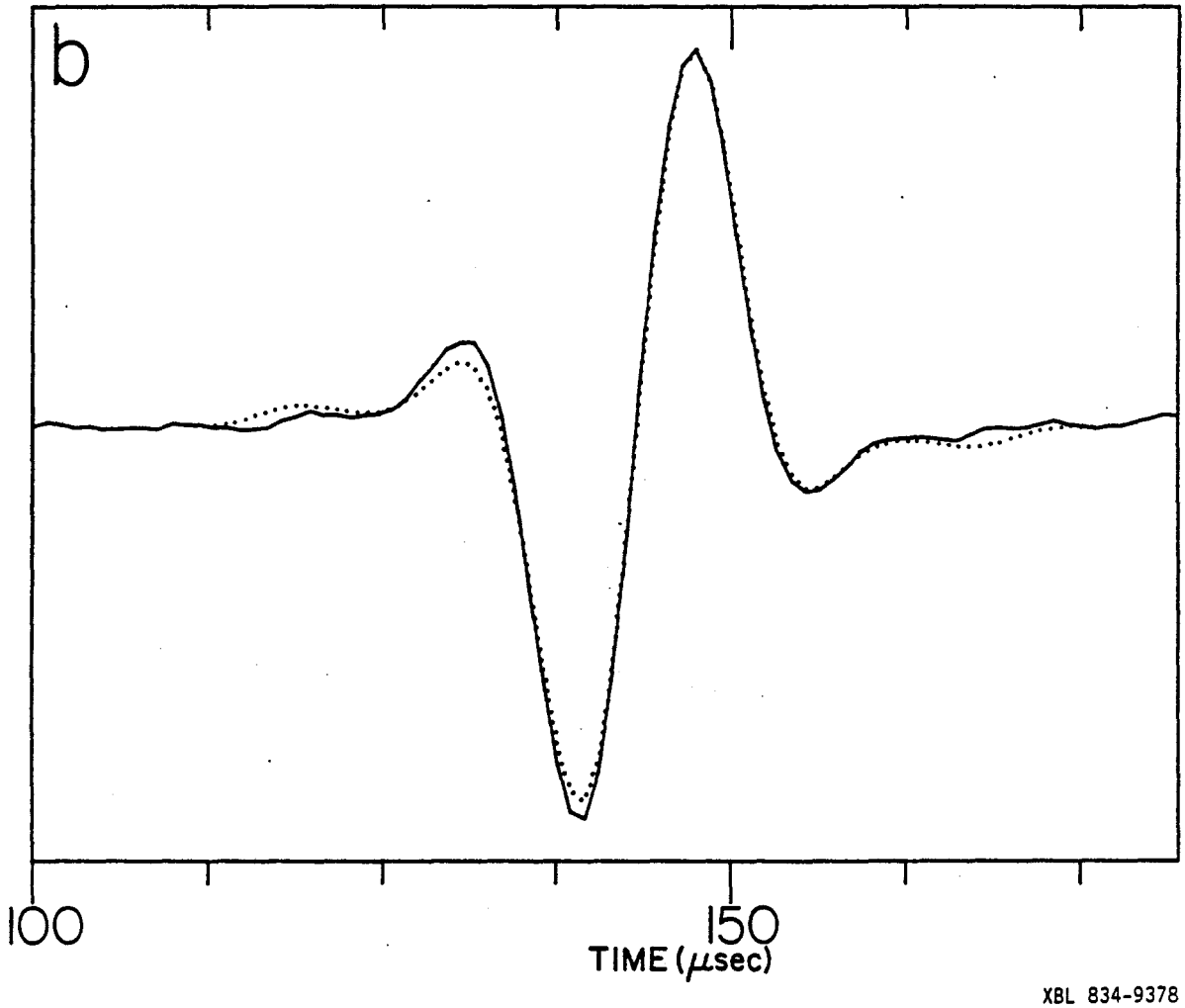

XBL 834-9378

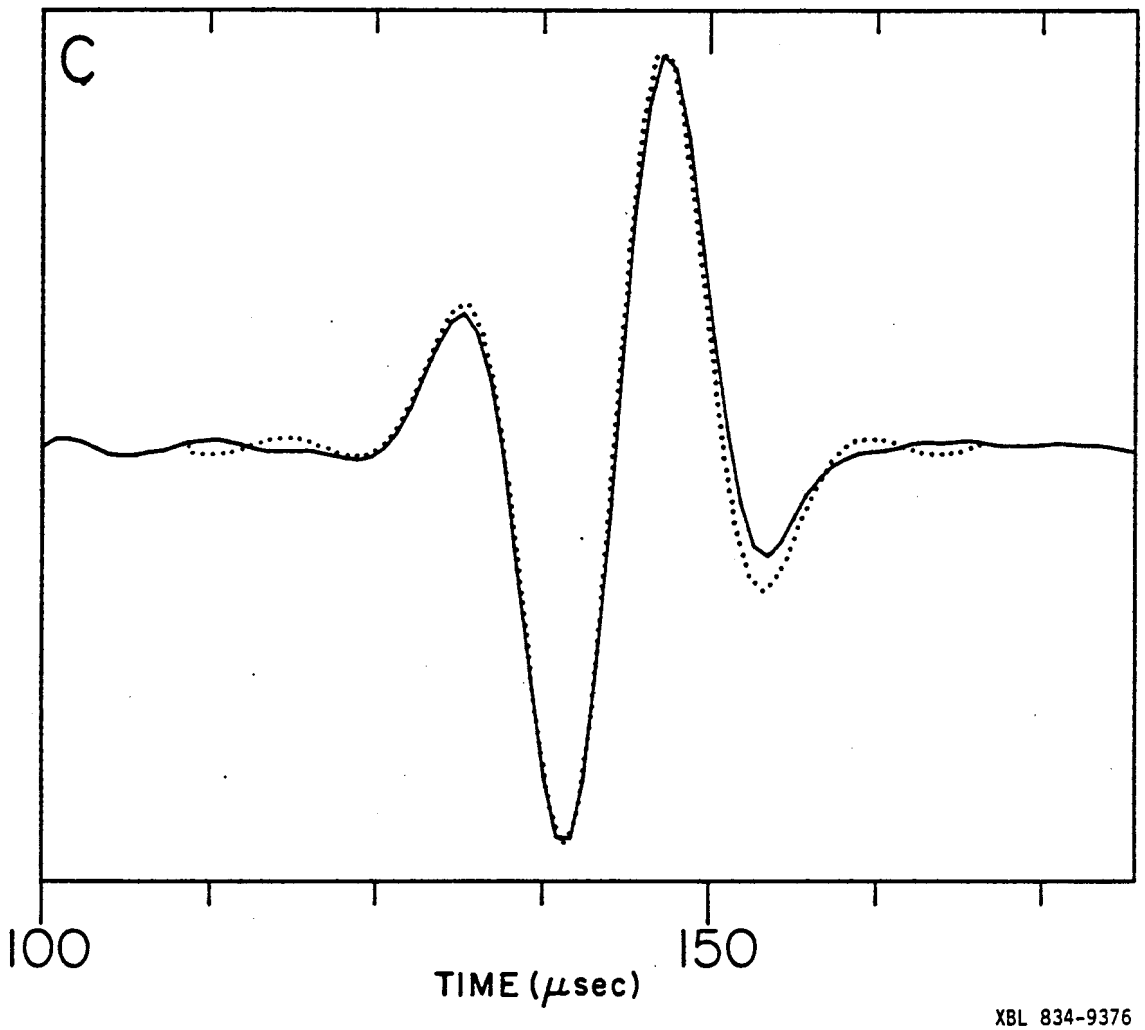

XBL 834-9376

which approaches zero much more rapidly (i.e., has a smaller fourth moment), and a gaussian function gives a reasonable result. This result is in disagreement with previous studies, which indicate a lorentzian dipolar correlation function for the ADRF state [57,58,68]. I shall not dwell upon this further, since the aforementioned studies were considerably more quantitative than this, but merely mention that this is possibly the first observation of a non-lorentzian ADRF correlation function. As for the correlation time, it may be estimated using the formula [68]:

$$\frac{1}{\tau_c^2} = \frac{M_{2II}}{9} K \tag{2.117}$$

where K is a constant depending upon the geometric arrangement of nuclei in the lattice (also, note that Eq. (2.117) was derived under the assumption of a lorentzian correlation function, but will also be valid for a gaussian since the first two terms in the Taylor expansion of each are equal). The constant K is most commonly defined in terms of lattice sums [40,58,68] as:

$$K = \frac{S_1 S_2 - S_4}{S_1 S_2} \quad . \tag{2.118}$$

Assuming K is equal to one (which is not exactly reasonable), and using the second moment derived from the proton linewidth, I obtain a correlation time of 375 μsec. The value used in the calculation is a factor of seven lower than this, implying $K \sim 0.2$. This is not an unreasonable value, but tedious lattice sums would need to be calculated in order to verify it. The relative mixing time entered into the

calculation represents a lumping together of several parameters from Eqs. (2.75a) and (2.80b):

$$t_{relative} = t_{mix}\, \tau_c\, M_{2IS} \quad , \tag{2.119}$$

where the factor of τ_c comes from the fourier transform of the gaussian correlation function:

$$C(\tau) = e^{-\tau^2/\tau_c^{\,2}} \tag{2.120a}$$

as

$$J(\omega) = \frac{\sqrt{\pi}}{2}\, \tau_c\, e^{-\omega^2 \tau_c^{\,2}/4} \quad . \tag{2.120b}$$

Using a value of M_{2IS} from Eq. (2.31) (which is applicable to $NH_4C\ell$, and a very rough estimate for $(NH_4)_2SO_4$), a value of τ_c equal to 50 μsec; and an experimental tmix of 5 msec; the relative mixing time turns out to be equal to 1.Ø. The value which has found to best represent the data is about 1.5. So, all of the parameters used in the calculated fits are more or less justified. This lends some credence to the simple treatment of rotating frame cross-relaxation laid out in the preceeding sections.

2.4.11 Large Off-Resonance Effects

In section 2.4.4 I showed that the cross-polarization situation will become extremely complicated when $\Delta\omega$ is of the order of ω_{1S} and ω_Q. The experimentally observed result of this is shown in Figure 27a. As can be seen, if we irradiate one satellite line of a quadrupolar

Figure 27. Large off resonance effects in cross-polarization. (a) Experimental result of the off resonance ($\omega_{1S} \sim \Delta\omega$) cross-polarization of a quadrupolar doublet for a particular orientation of a $(NH_4)_2HPO_4$ single crystal as a function of the ^{14}N r.f. mixing field amplitude. The ^{14}N resonances were saturated prior to the experiment, so the signal amplitude in the absence of cross-polarization would be near zero. (b) Calculated parameters corresponding to the situation in (a); ν_{eff} is the ^{14}N energy splitting in the rotating frame, and the efficiency factor is the square of the coefficient which multiplies $\mathcal{H}_{IS}$ in the diagonal reference frame (see section 2.4.11).

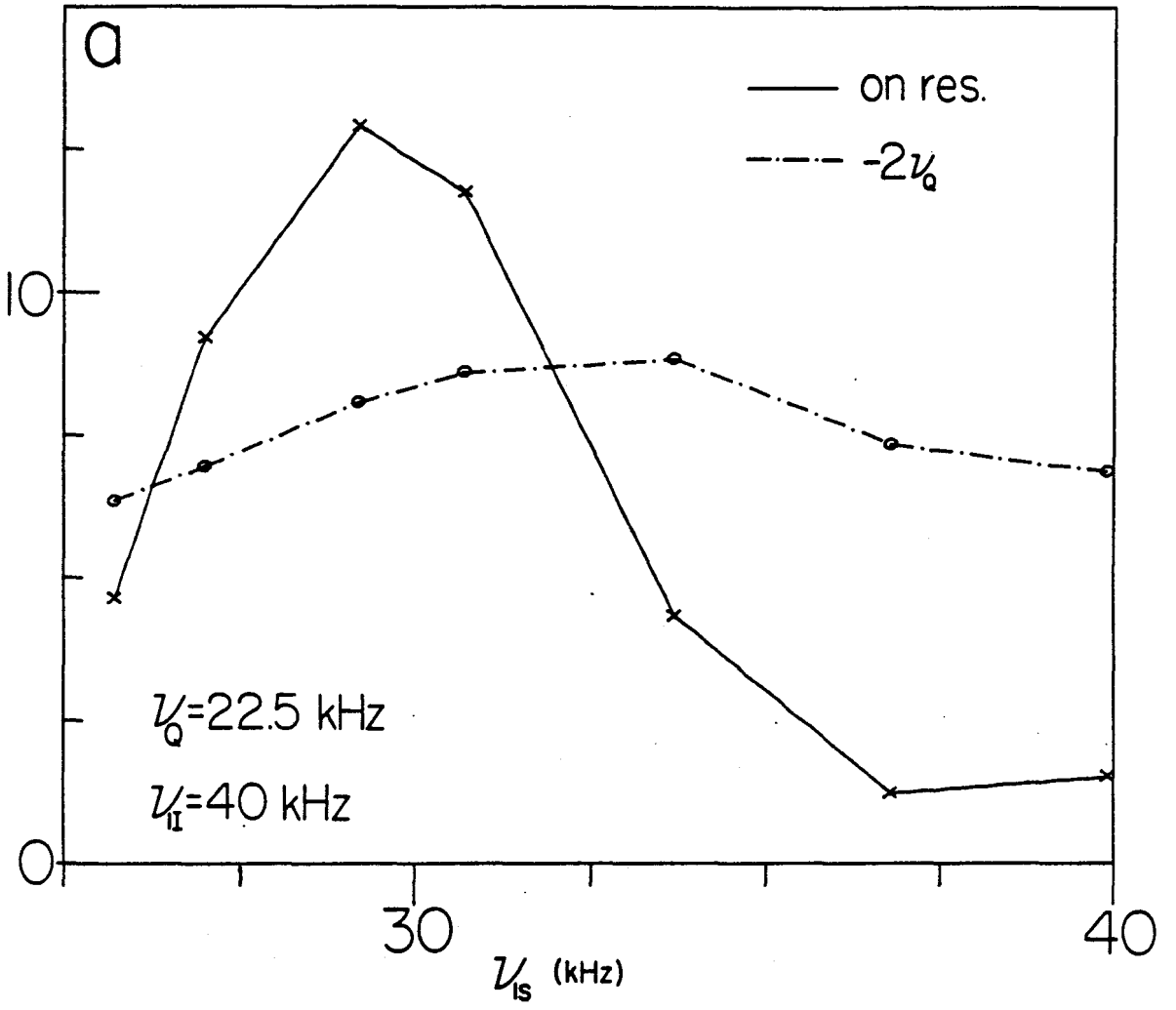

XBL 839-11502

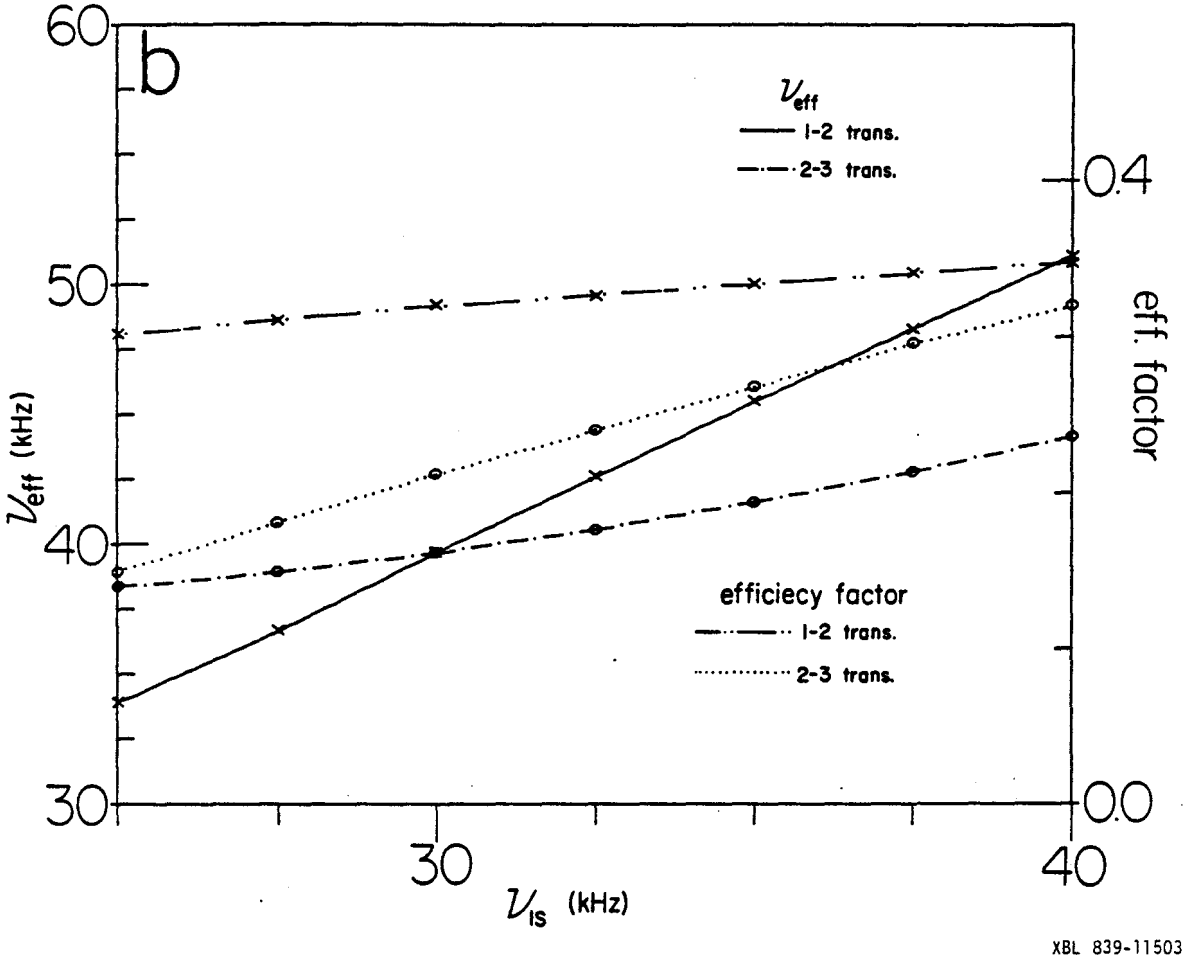

XBL 839-11503

split doublet under these conditions, its mate on the other side of the spectrum is significantly enhanced over a broad range of ^{14}N r.f. field amplitudes. Initially, this seems to violate our common sense; but, after calculating a few of the quantities involved in the cross-relaxation (Figure 27b), our senses (or, at least mine) are restored. We see that the effective field for the on resonance 1-2 transition varies rapidly with ^{14}N r.f. amplitude, while that of the off resonance 2-3 transition varies much more slowly. The efficiency factors, which result from the tilt of $\mathcal{H}_{IS}$ into the diagonal frame, indicate that both transitions will cross-relax, although the 1-2 transition is more efficient. The overall result is the observed broad but inefficient cross-polarization of the off resonance transition, and the narrow, fairly efficient cross-polarization of the on resonance transition. This situation, not commonly encountered experimentally, will be dealt with no further.

2.4.12 Practical Considerations

I have used this direct detection cross-polarization technique to great advantage in my studies of tetraalkylammonium salts. As I will discuss in the next chapter, many of these compounds exhibit exceedingly long ^{14}N T_1's, which the cross-polarization will alleviate so long as the proton T_1 is much shorter (which, I find, is usually the case). From the preceeding discussion, the relevant experimental considerations for successful cross-polarization should be obvious. When attempting to cross-polarize a fairly narrow powder pattern, it is most feasible to match $\omega_{1S}=\omega_{1I}$, with each being as large as possible. For powder patterns of any breadth, one should decrease ω_{1I} below ω_{1S}, and even use ADRF if T_{1D} allows. In the latter case, most of the signal

appears in the double quantum echo and, upon fourier transformation, yields a totally asymmetric spectrum. If necessary, this asymmetry can be overcome via a magnitude calculation, or preferably integration of the fid prior to fourier transformation. Unfortunately, T_{1D} is almost always less than $T_{1\rho}$ (because the spectral density samples lower frequencies in Eq. (2.77)), so ADRF is not always possible. In cases where both $T_{1\rho}$ and T_{1D} are sufficiently long, it is best to view the center of a broad line via a single quantum SL experiment with $\omega_{1I}=\omega_{1S}$, and the wings via a double quantum ADRF experiment.

Onward, into the fog of experimental results.

Chapter 3:

^{14}N Studies of Tetraalkylammonium Compounds

Studies of NMR couplings in solids have yielded a wealth of information regarding their chemical structure. My study of ^{14}N quadrupolar couplings is motivated by the increased use of the ^{14}N quadrupolar interaction as a probe of order in model membrane systems [74-80]. The required efg parameters may be estimated from the isotropic phase spin-lattice relaxation time T_1 using [47]:

$$\frac{1}{T_1} = \frac{3}{8} \left(\frac{e^2qQ}{\hbar}\right)^2 \left(1 + \frac{\eta^2}{3}\right)\tau_c \tag{3.1}$$

if the correlation time for molecular reorientation is known, or from the residual quadrupolar splitting in a partially ordered phase using [107]:

$$\Delta\omega = \frac{3}{4} \frac{e^2qQ}{\hbar} \cdot \{S_{22}[\cos^2\beta + \frac{\eta}{3} (1 + \sin^2\beta)] + S_{11}[\sin^2\beta + \frac{\eta}{3} (1 + \cos^2\beta)]\} \tag{3.2}$$

if the order parameters S_{11} and S_{22}, and the angle between the principle axis of the efg and the axis of reorientation β are known. Unfortunately, in order to use Eqs. (3.1) and (3.2), assumptions must be made regarding the dynamics of the system, which is not always a valid procedure (unless, of course, the dynamics are known from other types of measurements). Therefore, I have chosen to determine e^2qQ and η via the measurement of the inflection point frequencies of

a rigid powder (Eqs. (1.56)). In order to determine whether I am observing completely rigid lattice effects, the spectra are observed at a number of different temperatures, any temperature dependent effects being noted.

3.1 Experimental Procedures

All compounds were purchased from one of a variety of sources, including Eastman Kodak, Sigma and Calbiochem. Tetraethylammonium triiodide was prepared from an equimolar mixture of tetraethylammonium iodide and iodine in methanol. An elemental analysis was performed on the resulting rust colored crystals, and they were found to deviate little from their expected composition. All compounds, with the exception of phosphorylcholine chloride, were recrystallized from an appropriate solvent; either methanol/diethyl ether, or isopropanol. Ammonium compounds possess a marked propensity to attract water. Some, such as choline chloride, are observed to become completely saturated with atmospheric water in a time of the order of one minute. Therefore all compounds, regardless of their hygroscopic nature, were dried in a drying pistol in vacuo (3×10^{-5} atm) over P_2O_5 at 85°C for at least 12 hours piror to being sealed in 5 mm glass tubes in an argon dry box. Dimyristoyl phosphatidylcholine samples were prepared in a variety of ways prior to drying. The compound was either taken directly from the manufacturers (Calbiochem) bottle, precipitated from chloroform solution with diethyl ether [81], or prepared by slow evaporation of a chloroform-methanol solution [81]. The samples were all analyzed by TLC after drying and found to be of high purity. A powder x-ray diffraction pattern of the sample precipitated from chloroform showed the Bragg spacings to be similar to those which had been reported

previously [81].

All ^{14}N NMR spectra presented here were acquired at 19.507 (± Ø.007) MHz using a spectrometer whose basic design features have been described in detail [82], any modifications which I have made to the spectrometer are described in appendix D. Software control of the spectrometer is provided by the Nicolet Instrument Corp. program NTCFTB through a Nicolet 1180 computer and 293 B programmable pulser. The actual lineshapes have been obtained by fourier transformation of the second half of the quadrupolar echo, a finite amount (200-2000 Hz) of lorentzian linebroadening being applied prior to the ft. The NTCFTB routine QPD was always employed in order to minimize the effect of differing instrumental channel characteristics upon the observed spectrum. Acquisition was triggered at least 10 μsec prior to the expected echo maximum, and the data were then left shifted prior to fourier transformation. This procedure required that the echo be sampled at several times its bandwidth in order that the echo maximum not be missed. In this regard, the sampling was executed by a Nicolet Explorer IIIa digital oscilloscope with a maximum data acquisition rate of 50 nsec/point (most data was sampled every 0.5 to 2 μsec). The echo pulse amplitude was usually in the range of 60-75 kHz (with 1-1.5 kWatt of r.f. into the probe). The proton decoupling field strength was almost always 50 kHz. The cross-polarization was carried out according to the prescription of section 2.4, and favorable results were almost always obtained. The r.f. field amplitudes (for both ^{14}N and ^{1}H) were computed by measuring the time required to invert the magnetization (a 180° pulse), or by giving a train of 90° pulses and looking for a null every two pulses. This measurement was always

performed on a solid compound with a fairly narrow resonance, such as $NH_4C\ell$. The r.f. field amplitude thus obtained was correlated with an attenuator setting in the transmitter amplifier train, and this was checked for drift every few experiments. I would like to note in passing that the peak voltage amplitude entering the probe in volts was nearly always equal to the r.f. field amplitude in gauss (see also Appendix D).

Temperature dependent effects become important for some of these compounds, and so temperature control is important. In this regard, the sample temperature was measured with a copper constantan thermocouple placed directly beneath the sample. From experiments performed on samples with calorimetrically known phase transitions, it is estimated that the thermocouple and sample temperatures differed by at most 2°C (see Figure 28). The sample temperature was regulated via boiling LN_2 from dewar with a resistive heater, whose current was provided by a programmable power supply (Kepko KS36-15) controlled through the NTCFTB subroutine VT (a slight modification of VT was required, as described in Appendix D). Above 0°C, the temperature was regulated by blowing N_2 through a gas trap wrapped in heating tape. The lower temperature limit which I have been able to attain is approximately -150°C (123 K), and this would certainly be surpassed were more current passed through the resistive heater in the LN_2 dewar. The upper temperature is limited by the melting point of the wax used to seal the sample tubes; generally paraffin was used and its melting point is about 54°C (327 K). This upper temperature limit could easily be increased by using a different method to seal the sample tubes. At lower temperatures (below -90°C) I would have benefitted by the use

Figure 28. Proton decoupled ^{14}N NMR spectra of NH_4Br through its order-disorder phase transition at -38°C. The spectra acquired below -36°C employed a quadrupolar echo sequence.

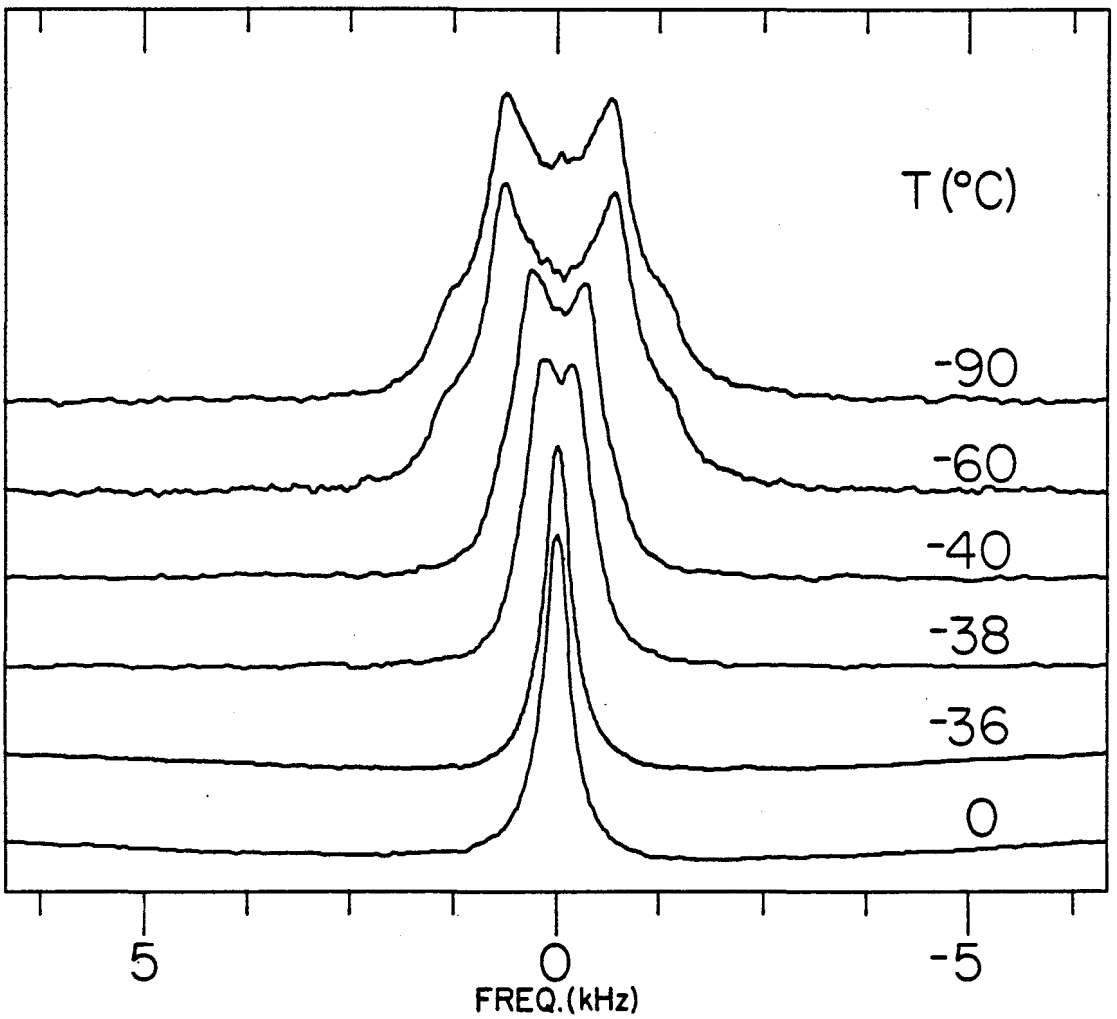

XBL 839-11497

of a different cooling gas, since nitrogen gives an NMR signal which did interfere with weak signals which were of interest.

^{14}N spin-lattice relaxation times were measured from echo amplitudes using the progressive saturation technique. Transverse echo relaxation times (T_{2e}) were similarly measured from echo amplitudes by varying the interpulse delay. It should be emphasized that the T_{2e} experiment must be performed on resonance, for otherwise the signal amplitude will decrease simply because of off resonance effects (section 2.1.1). The data were then fit to one of the following equations:

$$A_e = A_o \left(1 - e^{-t/T_1}\right) \quad , \tag{3.3a}$$

$$A_e = A_o \, e^{-2\tau/T_2} \tag{3.3b}$$

using the NTCFTB subroutine LF, except for noted occasions where the IMSL subroutine ZXSSQ was used [83]. Measuring relaxation times from echo amplitudes eliminates the possibility of observing anisotropic relaxation effects, with the exception of a non-exponential relaxation which will result in the anisotropic case from the sum of exponential terms which contribute to the echo decay (the echo maximum reflects contributions from all orientations).

Proton spectra are not a major topic of discussion here, but those which are discussed were recorded using the magic echo sequence [67,70] which was found to be far superior to the two pulse dipolar echo. Quoted proton linewidths are the result of fits to either a lorentzian or gaussian function using the NTCFTB subroutine LF. Proton T_1's were

measured by the application of a sequence of saturating pulses (usually 10 90° pulses) followed by a variable delay and an echo. The resulting echo amplitudes were then fit to Eq. (3.1a). Spin lattice relaxation in the rotating frame ($T_{1\rho}$) was measured via the technique of spin locking the magnetization for a variable period of time and measuring the fid (or echo) amplitude. The dipolar relaxation time (T_{1D}) could be measured by a variety of methods. The technique of Jeener and Broekaert [53] was always a possibility, but it is about twice as efficient to perform an ADRF followed by a variable delay τ and a 45° pulse. The height of the derivative fid was then taken as the amount of dipolar order which remained at time τ. Unfortunately, as dipolar order relaxes to Zeeman order, an fid is excited by the readout pulse which interferes with our measurement of the dipolar order. This problem may be removed by proper adjustment of the phase detector, but this was difficult in my experiments since I use the same phase detector for both ^{14}N and ^{1}H. I have chosen to eliminate the problem by destroying the Zeeman order during the delay period with a 90° pulse (i.e., the sequence: ADRF-τ-90-τ_1-45-acquisition; τ is varied). The 90° pulse has the effect of converting the dipolar order to -1/2 its previous value (see Eq. (2.81)), so this method is not as useful as adjusting the phase detector. It is always necessary to use the Jeener-Broekaert technique when $T_{1\rho}$ is too short to perform the ADRF.

The ^{14}N powder lineshapes were analyzed by successively fitting the experimental data to a rigid lattice powder lineshape convolved with a broadening function (generally the same as the linebroadening applied prior to fourier transformation) and multiplied by the echo sequence distortion function either Eq. (2.19), or Eq. (2.102). The cross-

polarized spectra showed further distortion resulting from anisotropic cross-relaxation rates and heat capacities (see section 2.4.3), but no attempt was made to correct the theoretical lineshape for these. When cross-polarization was employed, the experimental parameters were adjusted to minimize the distortion present (this is more or less an empirical process). The errors quoted in Table 3.I give the range of quadrupole coupling parameters which appear to adequately fit the data. Aside from S/N considerations, the accuracy of the data is limited by two factors: (1) the amount of distortion introduced by the cross-polarization, and (2) T_2 broadening mechanisms not accounted for by the ^{14}N-^{1}H heteronuclear dipolar interaction (e.g., slow motion, lattice defects, etc.).

3.2 Overview of Experimental Results

The data in Table 3.I reveal that the range of quadrupole coupling constants for these compounds is approximately 10-200 kHz. This implies a fairly symmetric electronic environment, as would be expected for a tetrasubstituted nitrogen. The asymmetry parameters cover the entire range from 0 to 1.0. This result is rather surprising since it would be expected that a tetraalkylammonium ion would have at least a three fold intramolecular symmetry axis. The non-zero asymmetry parameters could be explained by the presence of a rapid anisotropic jumping motion which would superpose two axial tensors of differing orientation to form a non-axial tensor [84,85,86]. By performing the measurements over a range of temperatures, we have attempted to either confirm or rule out such effects. As I will discuss in the next chapter, thermally activated motional effects will result in a characteristic variation with temperature of the observed

Table 3.I

^{14}N Quadrupole Coupling Constants (e^2qQ/h) and Asymmetry Parameters (η)

Compound	e^2qQ/h (kHz)	η	T(K)
Tetraalkylammonium Salts			
TMA Br	26.6±0.2[a]	0.00±0.02	290
TMA I	31.5±0.2[a]	0.00±0.02	293
TMA I	34.0±0.2	0.00±0.02	223
TMA I	35.7±0.2	0.00±0.02	193
TMA Cl	17.3±0.2[a]	0.00±0.02	293
TMA Cl	17.4±0.2	0.00±0.02	187
TMA Cl	17.2±0.2	0.00±0.02	185
TMA Cl	24.9±0.2	0.31±0.03	183
TMA Cl	26.4±0.8	0.36±0.04	181
TMA Cl	31.8±1.0	0.47±0.02	175
TMA Cl	37.3±1.0	0.55±0.03	163
TMA Cl	40.0±2.0	0.60±0.04	155
TEA Cl	∿ 65[d]	--	273-188
TEA Br	68.0±1.0	0.40±0.05	292
TEA Br	69.0±1.0	0.37±0.03	238
TEA Br	78.2±0.5	0.40±0.03	193
TEA I	40.5±0.2	0.00±0.01	292
TEA I	41.3±0.2	0.00±0.01	238
TEA I	42.3±0.2	0.00±0.01	173
TEA I_3	49.0±1.0	0.66±0.02	292
TEA I_3	52.0±2.0	0.61±0.02	248
TEA I_3	63.0±1.0	0.45±0.02	213

Table 3.I continued

TEA I_3	65.0±1.0	0.42±0.02	198
TEA I_3	68.0±1.0	0.44±0.03	178
TPrABr	47.0±0.5	0.00±0.02	293
TPrABr	49.2±0.3	0.00±0.03	238
TPrABr	51.0±0.3	0.00±0.03	198
TPrAI	99.0±1.0	0.54±0.02	198
TPrAI	102.0±2.0	0.55±0.02	183
TBA Br	26.4±0.2	0.44±0.02	293
TBA Br	24.4±0.2	0.55±0.01	213
TBA Br	22.5±0.3	0.65±0.01	175
TBA Br	21.8±0.3	0.68±0.01	164
TBA I	11.8±0.2	0.70±0.02	293
TBA I	11.4±0.2	0.60±0.02	273
TBA I	11.4±0.2	0.50±0.02	239
TBA I	12.1±0.2	0.36±0.02	188
TPnABr	40.0±1.0	0.79±0.03	292
TPnABr	39.0±1.0	0.85±0.03	233
TPnABr	37.0±0.4	0.92±0.03	193
TPnABr	36.1±0.6	0.95±0.04	177
Choline Halides			
choline Cl	40.0±0.5[b]	0.31±0.02	321
choline Cl	40.0±0.5[b]	0.33±0.03	291
choline Cl	48.0±1.0[b]	0.34±0.06	213
choline Cl	51.0±2.0	0.24±0.02	175

Table 3.I continued

choline Cl	50.0±2.0	0.22±0.04	155
choline Br	156.0±1.0	0.31±0.02	290
choline Br	172.0±1.0	0.48±0.02	223
choline Br	179.0±2.0	0.52±0.02	193
choline I	46.3±0.3	0.04±0.01	313
choline I	46.7±0.4	0.08±0.02	290
choline I	48.0±0.4	0.12±0.02	273
choline I	47.8±0.4[b]	0.17±0.02	253
choline I	48.3±0.4[b]	0.22±0.02	233
choline I	48.5±0.4[b]	0.27±0.02	214
choline I	48.5±0.6[c]	0.29±0.02	203
PCC	∿ 120[d]	--	190-158
Amphiphiles			
DTAB	116.0±1.0	0.85±0.02	293
DTAB	106.0±1.0	0.98±0.02	223
DTAB	101.0±1.0	1.00±0.02	193
DTAB	104.0±2.0	1.00±0.02	175
HTAB	98.0±1.0	0.90±0.02	293
HTAB	95.0±1.0	1.00±0.02	223
DDAB	190.0±3.0	0.73±0.03	293
DDAB	177.0±4.0	0.64±0.04	178
DML	∿ 90[d]	--	190-158

Table 3.I continued

TMA = tetramethylammonium

TEA = tetraethylammonium

TPrA = tetrapropylammonium

TBA = tetrabutylammonium

TPnA = tetrapentylammonium

DTAB = decyltrimethylammonium bromide

HTAB = hexadecyltrimethylammonium bromide

DDAB = didodecyldimethylammonium bromide

PCC = phosphorylcholine chloride

DML = dimyristoylphosphatidylcholine

[a]These values have been reported previously in reference 79.

[b]The spectral lineshapes appear to have some motional contribution.

[c]The spectral lineshapes appear to be dominated by motion.

[d]The spectra are completely washed out and featureless.

spectrum. While we do indeed observe such variations for some compounds (see Figure 29), for most of these substances no thermally activated motional effects were observed.

A small nearly linear temperature dependence of the efg parameters is observed for most of the compounds studied (see Table 3.I and Figure 30). This phenomenon is clearly not due to large amplitude motions, and probably originates in thermally activated field gradient averaging mechanisms involving small amplitude torsional motions [87], or variation of the crystalline field due to expansion or contraction of the unit cell with temperature [88,89]. That these small variations are not the result of large amplitude motions of the efg is supported by the observation of T_{2e} which are not strongly temperature dependent for these compounds. For example, choline bromide, which exhibits no obvious motional contribution to its lineshape, exhibits the following T_{2e}: 0°C = 2.4 msec, -20°C = 2.2 msec, -40°C = 2.0 msec, -60°C = 2.0 msec, and -80°C = 1.2 msec. Over this same temperature range the choline bromide quadrupole coupling constant increases by 10%, and the asymmetry parameter registers a 40% increase.

Under the assumption that we are observing rigid molecules, we must consider two factors responsible for the observed quadrupole coupling parameters: (1) the deviation from tetrahedral symmetry of the nitrogen electronic distribution due to intramolecular effects, and (2) the contribution of the lattice or extramolecular crystalline field to the field gradient at nitrogen. The former effect is expected to dominate over the latter simply because of the much closer proximity of the perturbation. In ionic compounds such as these, antishielding effects will increase the extramolecular contribution greatly [90].

Figure 29. Proton decoupled quadrupolar echo spectra of choline iodide as a function of temperature. The echo sequence in all spectra used 3.7 μsec 90° pulses and 80 μsec interpulse delays. The recycle time was 2 sec in all spectra; T_1 was found to be much less than 2 sec at all temperatures.

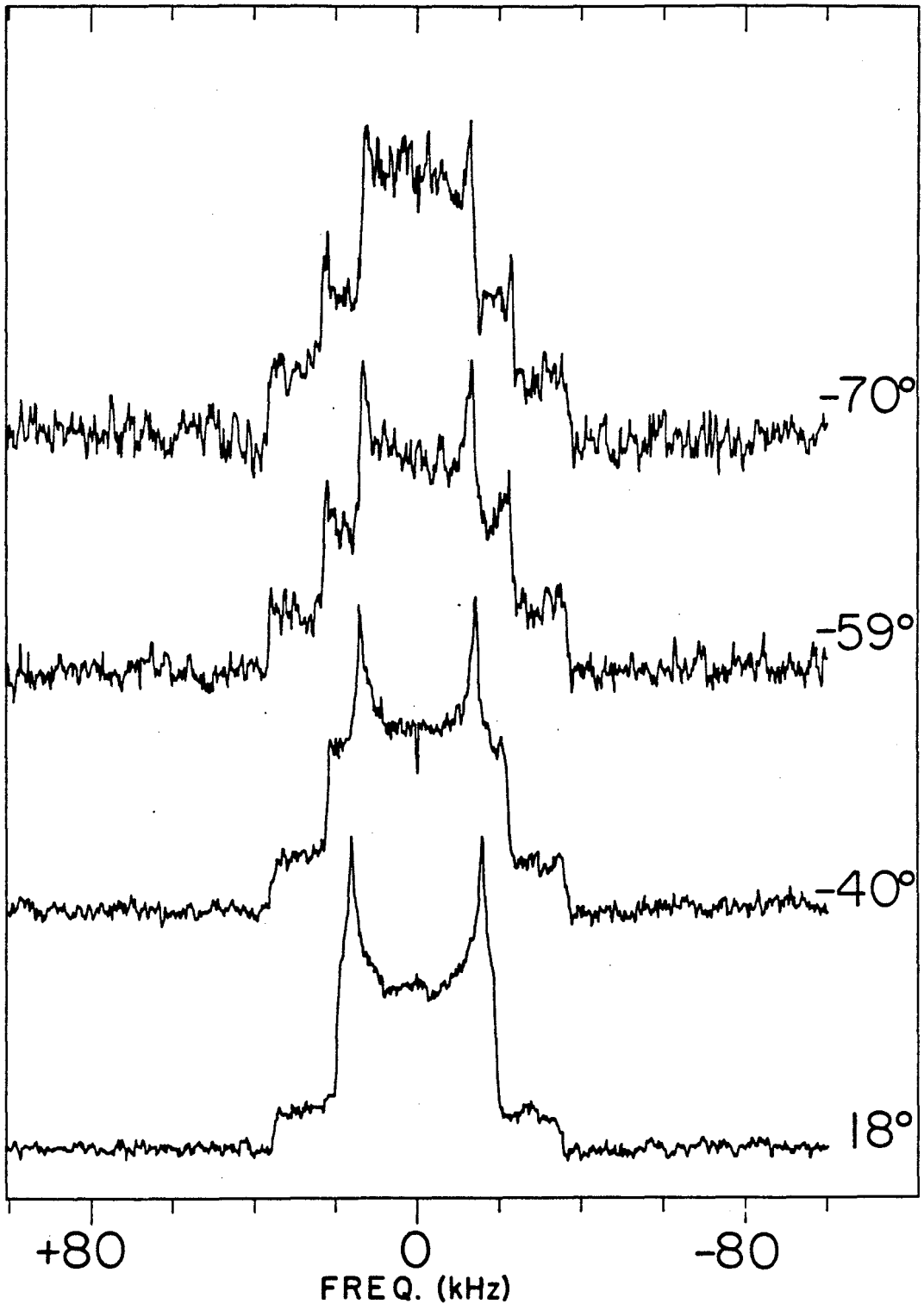

XBL 831-7627

Figure 30. The observed variation of the asymmetry parameter with temperature for several tetraalkylammonium salts.

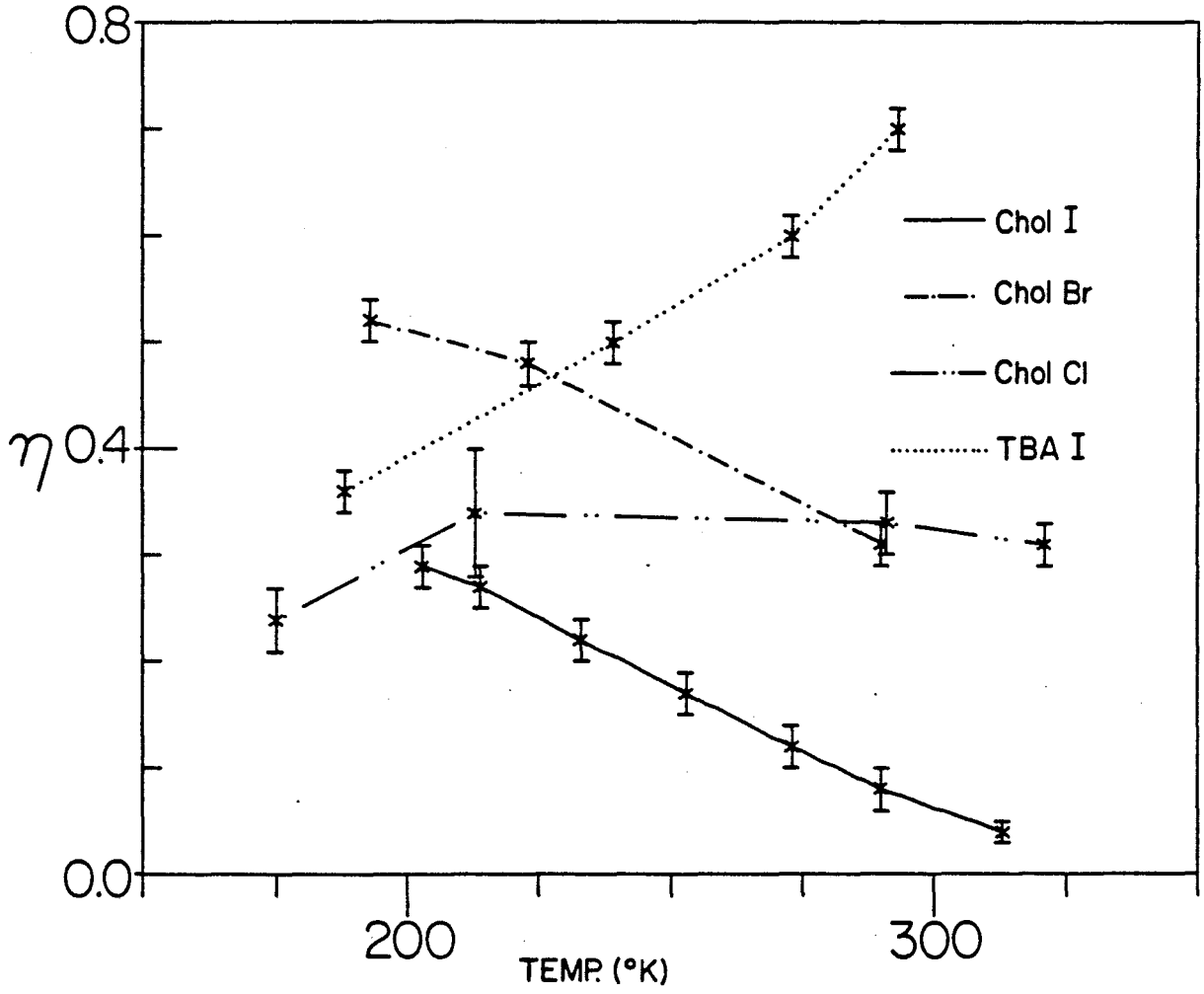

XBL 839-11512

Edmonds, et al., were able to rationalize the quadrupole coupling parameters of some tetrahedral ammonium salts by considering only the bonds existing within the ion itself [91] (i.e., this is a completely intramolecular argument). Their argument will not suffice to explain the results presented here, particularly those of the tetramethylammonium halides, as I will discuss in the next section.

3.3 Discussion of Specific Compounds

Of the compounds listed in Table 3.I, complete structural information is available for tetramethylammonium (TMA) chloride, bromide, and iodide [9]], tetraethylammonium (TEA) iodide [93], tetraethylammonium triiodide [94], tetrapropylammonium (TPrA) bromide [95], choline chloride [96], and choline iodide [97]. In addition, partial structural information is available for choline bromide [98] and hexadecyltrimethylammonium bromide (HTAB) [99]. A discussion in some detail is warranted for these compounds.

3.3.1 Tetraalkylammonium Salts and Choline Halides

For the TMA compounds in particular, the explanation of the observed quadrupole coupling parameters seems rather clear-cut. The available room temperature structural data indicate that the intramolecular nitrogen symmetry in these compounds is strictly tetrahedral, implying that the intramolecular field gradient vanishes. Proton NMR studies have shown that the TMA halides undergo isotropic reorientation at room temperature (isotropic here presumably means a motion in which all of the methyls are able to exchange positions), and that this motion persists to a temperature between 250 and 200 K, depending upon the halide [100,101]. This motion would tend to greatly reduce, or average to zero any intramolecular effects present. The temperature

dependence of the quadrupole coupling parameters for these compounds (see Table 3.I) indicates that this motion has no effect upon the observed parameters. For example, TMA iodide exhibits a small linear temperature dependence of 43 Hz/K for its quadrupole coupling constant over the temperature range investigated. This is not the type of behavior we expect to see over a temperature regime in which a field gradient averaging mechanism is quenched, and is much easier to explain in terms of a variation of the unit cell dimensions (and hence the crystalline field) with temperature [88]. More revealing are the data for TMA chloride which are plotted in Figure 31. Here we see that the efg parameters are static down to the λ point at 184.9 K [102]. In this regime the efg is axially symmetric and of small magnitude while the lattice is tetragonal. Below the λ point both the coupling constant and asymmetry parameter increase rapidly indicating that the electronic symmetry at nitrogen decreases with further lowering of the temperature. At the λ point the symmetry of the lattice will change abruptly, while the displacement of the ions begins a continuous change which extends over a large temperature range. The symmetry of the lattice in the low temperature phase is nearly always lower than that of the high temperature phase, although Landau [103] does give the counter example of Rochelle salt (potassium sodium tartrate), so it is not unreasonable to assume that the symmetry of TMA Cl below 184.9 K is lower than tetragonal. It is not possible from our data to determine whether the low temperature phase is orthorhombic or monoclinic since the efg tensor will always possess three twofold symmetry axes, while orthorhombic is the lowest symmetry lattice to possess these properties. The observation (see Figure 31)

Figure 31. ^{14}N NMR observation of the second order phase transition in TMA Cl.

(a) The efg parameters e^2qQ/h and η as a function of temperature. The solid line through the upper points follows the equation $\eta = 0.93[(T_c-T)/T_c]^{0.24}$ below the phase transition, while that through the lower follows $e^2qQ/h = 17.3 + 47.66\ [(T_c-T)/T_c]^{0.41}$. T_c is the temperature at the γ point; 184.9 K.

(b) From top to bottom: the field gradient components V_{zz}, V_{xx}, and V_{yy} as a function of temperature; the algebraic signs are arbitrary. The solid line through the upper points follows the equation $V_{zz} = 12.98 + 36.23\ [(T_c-T)/T_c]^{0.41}$ below the phase transition, while that through the lower points follows $V_{yy} = -6.49 - 36.30\ [(T_c-T)/T_c]^{0.41}$. V_{xx} is invariant within experimental error at -6.49 kHz.

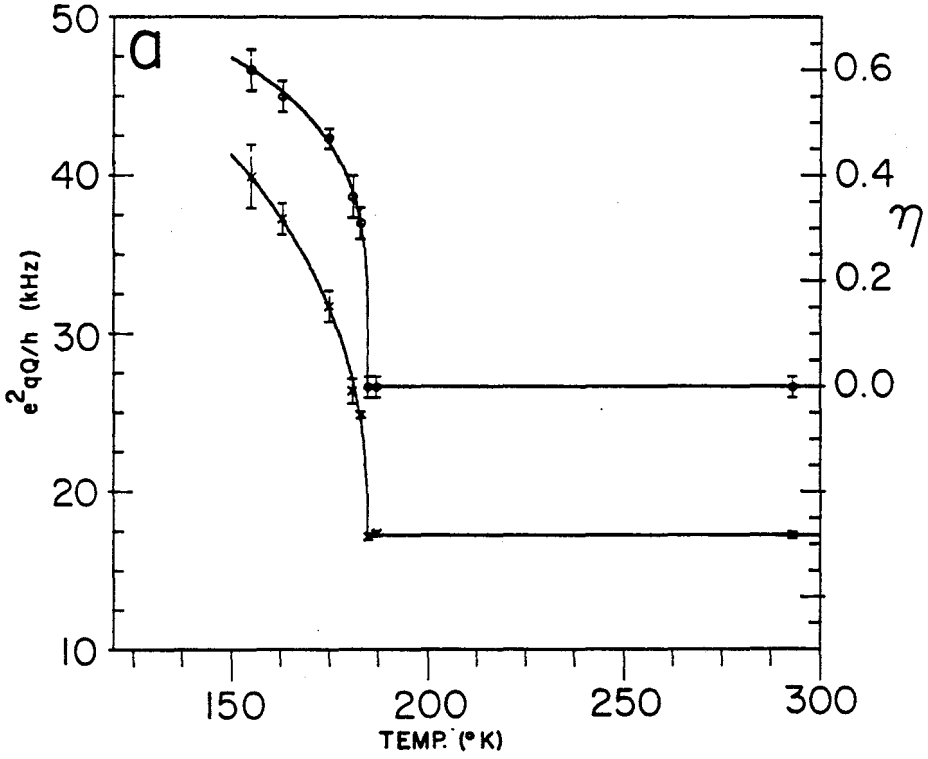

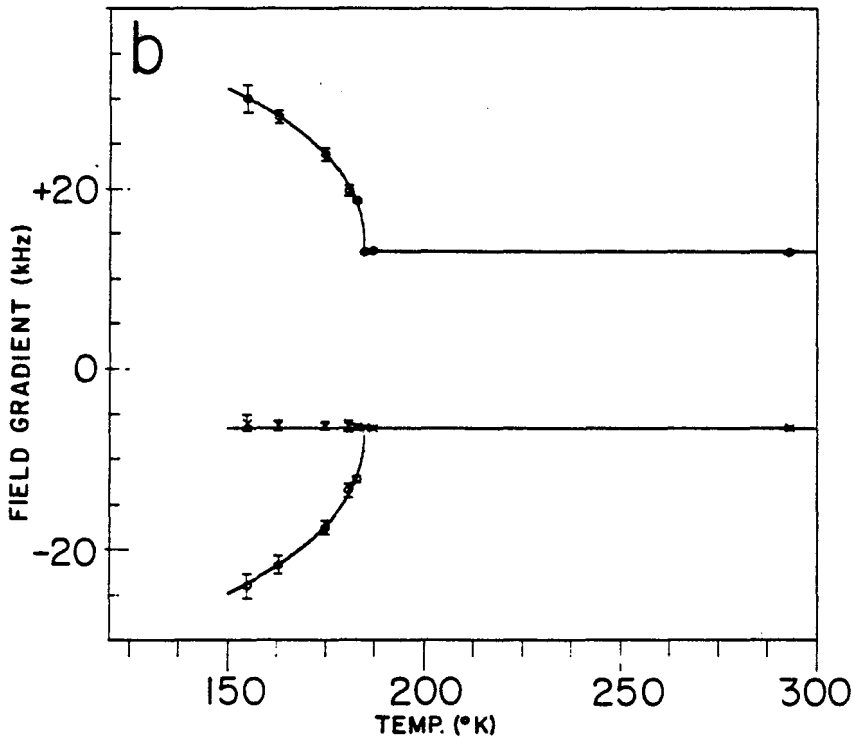

XBL 831-7633A

that one field gradient component is static (within experimental error) through the phase transition invites the incorrect conclusion that, below the λ point, the lattice is displaced in two dimensions while the third remains fixed. This conclusion cannot be drawn from our data because the Laplace equation requires all three principle values to change in such a transformation (assuming, of course, that the efg is crystalline in origin). An interesting contrast between TMA Cl and TMA I is given by their respective temperature behaviors. From the temperature dependence of the efg parameters it appears that the TMA I lattice remains tetragonal while the unit cell dimensions vary (no phase transitions are reported for this compound in the temperature range investigated [102]). Concurrently, the efg parameters of TMA Cl indicate that its' lattice remains static until it becomes unstable at the λ point. An analysis similar to that given for TMA Cl may also be applied to ammonium bromide (Figure 28) where no quadrupole coupling is observed in the cubic β phase, while a small axial coupling is observed in the tetragonal γ phase [104,105].

TPrA bromide and TEA iodide (Figure 32) show axially symmetric efgs at all temperatures investigated. Proton NMR studies indicate that it is unlikely that longer chain tetraalkylammonium compounds such as these undergo isotropic reorientation in the temperature range studied [106], but the high degree of intramolecular symmetry present in these two compounds leads us to believe that here too the efgs may be ascribed to the tetragonal lattices both compounds possess.

TEA triiodide and choline chloride show definite deviation of the intramolecular environment from that of tetrahedral symmetry;

Figure 32. Proton decoupled quadrupolar echo spectrum at TEA iodide at -90°C. The signal is the result of 280 acquisitions using an ADRF cross-polarization technique. The mixing time was 10 msec, the echo delay was 80 μsec, and a 3.5 μsec 90° echo pulse was used. The dotted line represents a rigid lattice powder spectrum with e^2qQ/h = 42.3 kHz and η = 0.0; this has been convolved with 300 Hz of lorentzian line broadening and multiplied by Eq. (2.102) to account for the finite duration of the single echo pulse.

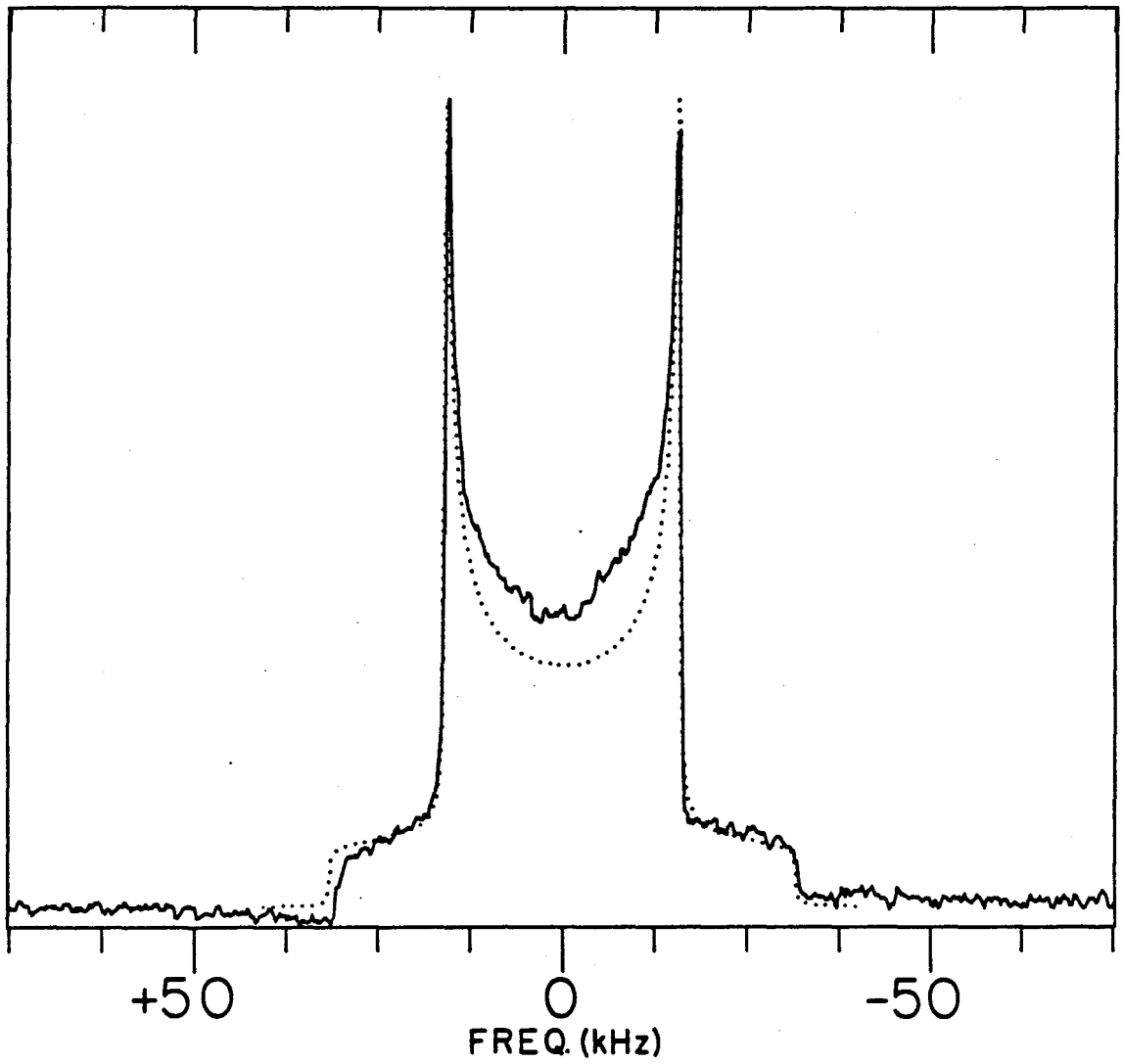

XBL 831-7631

these compounds also possess orthorhombic lattices. Whether the efg parameters are dominated by intramolecular or crystalline field effects is unknown, but it is likely that the crystalline field has some effect. In TEA triiodide, an interesting discontinuity of the efg parameters occurs between 248 and 213 K. Perhaps a differential scanning calorimetry or x-ray study would confirm the existence of a phase transition in this temperature region. In choline chloride, we have the added complication of motion at room temperature, which I will discuss in detail in the next chapter. At the lowest temperature investigated the spectrum appeared to arise from rigid molecules, although the S/N at this temperature is low owing to a rather long ^{14}N T_1 of several minutes (both the proton $T_{1\rho}$ and T_{1D} are too short at this temperature to permit an effective cross-polarization).

For choline iodide the x-ray structural data are insufficient to describe accurately the intramolecular nitrogen environment. The situation here is very similar to that of choline chloride; the efg parameters are such that they could be determined entirely by crystalline field effects (the lattice here is monoclinic), but there may also be some intramolecular contribution. Here again there are complications arising from the presence of motion which apparently is rapid at room temperature, but slows as the temperature is lowered (see Figure 29). This motion will be analyzed in detail in the next chapter, but I wish to point out that the variation of the quadrupole coupling parameters (in particular, the asymmetry parameter) with temperature (see Figure 31) appears to occur independent of the motion, presumably through the temperature variation of the unit cell dimensions.

Figure 33. Proton decoupled quadrupolar echo spectrum of choline bromide at -80°C. This signal is the result of 4196 acquisitions using 3.7 μsec 90° pulses and an 80 μsec interpulse delay. The dotted line represents a rigid lattice powder spectrum with e^2qQ/h = 178.9 kHz and η = 0.52; this has been convolved with 1000 Hz of lorentzian linebroadening and multiplied by Eq. (2.19) to account for the finite duration of the pulses employed.

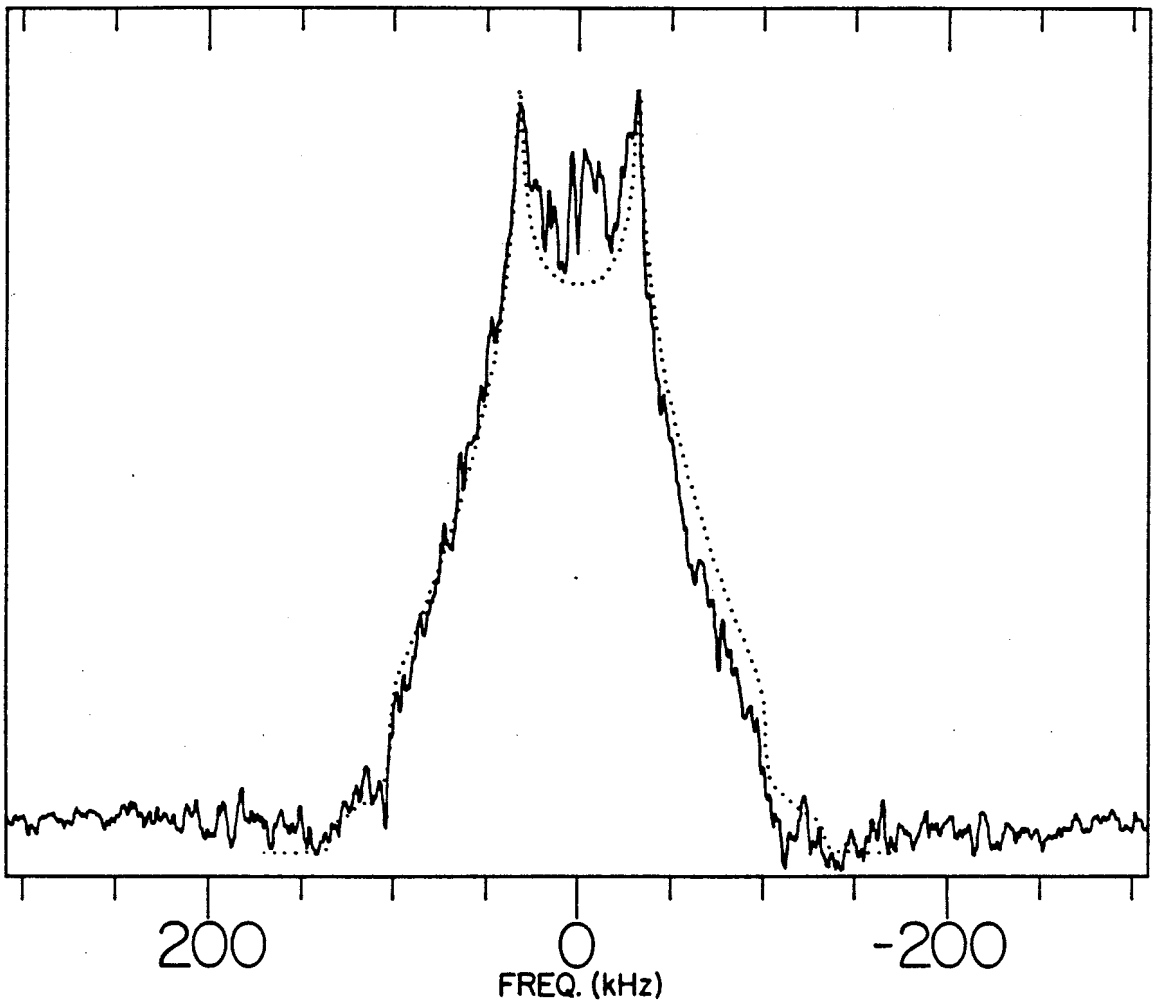

XBL 839-11490

The quadrupole coupling of choline bromide differs substantially from that of the other two halides (see Figure 33). It is unfortunate that no detailed structure is available for this compound; the dimensions of its orthorhombic unit cell differ considerably from those of choline chloride (both compounds have four molecules per unit cell), and this may have some effect upon the crystalline field. In contrast to the other two halides, choline bromide shows no noticeable temperature dependent motional effect upon the ^{14}N NMR spectrum over the temperature range investigated; although it is possible for motions similar to those present in the other two halides to be present here, but to have no noticeable effect because of the range of quadrupolar couplings involved (this will become clear in the next chapter).

3.3.2 Amphiphiles

The long chain amphiphilic molecules studied (HTAB, decylrimethylammonium bromide [DTAB], didodecyldimethylammonium bromide [DDAB]) exhibit very large asymmetry parameters (see Figures 34a, 35), with DDAB having the largest quadrupole coupling constant of those we have studied. The observed asymmetry parameters may be the result of a flip-flop motion of low activation energy, but I was not able to observe any temperature dependent effects over the temperature range studied. It is also possible to disperse DDAB in water (0.5 gm/ml) to form a lyotropic lamellar mesophase in which a residual quadrupolar splitting of 8.85 kHz is observed (see Figure 34b). This splitting is of the same order as that observed for dimyristoyl phosphatidylcholine (DML) dispersions at room temperature [77,79]. It should be emphasized that, in the presence of a nonzero rigid lattice asymmetry parameter,

Figure 34. Solid and dispersion spectra of didodecyldimethylammonium bromide (DDAB). (a) Proton decoupled quadrupolar echo spectrum of the solid powder at 20°C. This signal is the result of 54,000 acquisitions using 3.7 μsec 90° pulses and a 70 μsec interpulse delay. The dotted line represents a rigid lattice powder spectrum with e^2qQ/h = 190 kHz and η = 0.73; this has been convolved with 2000 Hz of lorentzian linebroadening and multiplied by Eq. (2.19) to account for the finite duration of the pulses employed. (b) Proton decoupled quadrupolar echo sepctrum of a DDAB dispersion (500 mg/ml) at 20°c. The dotted line represents e^2qQ/h = 11.8 kHz, η = 0.0 convolved with 300 Hz of lorentzian linebroadening.

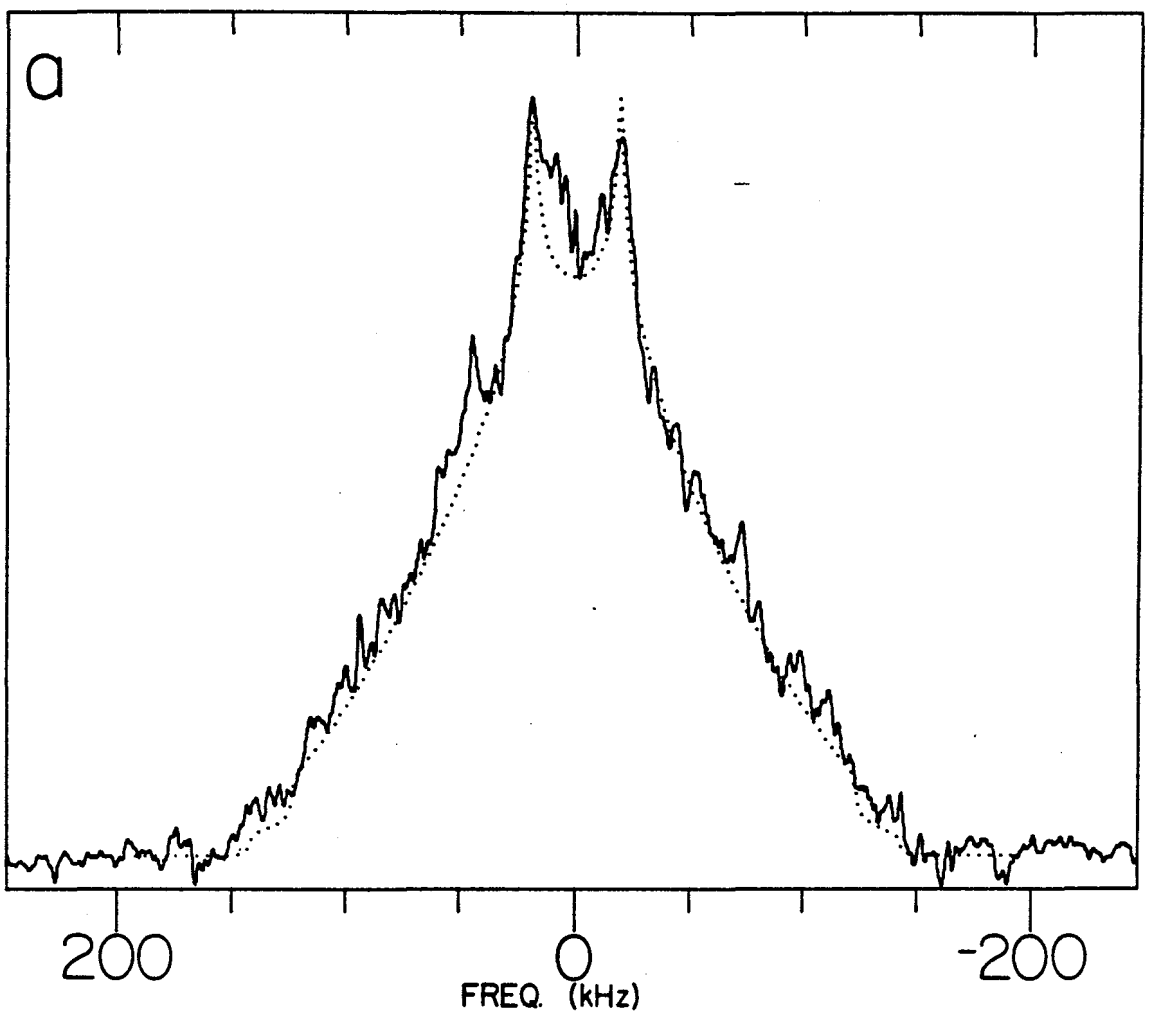

XBL 839-11513

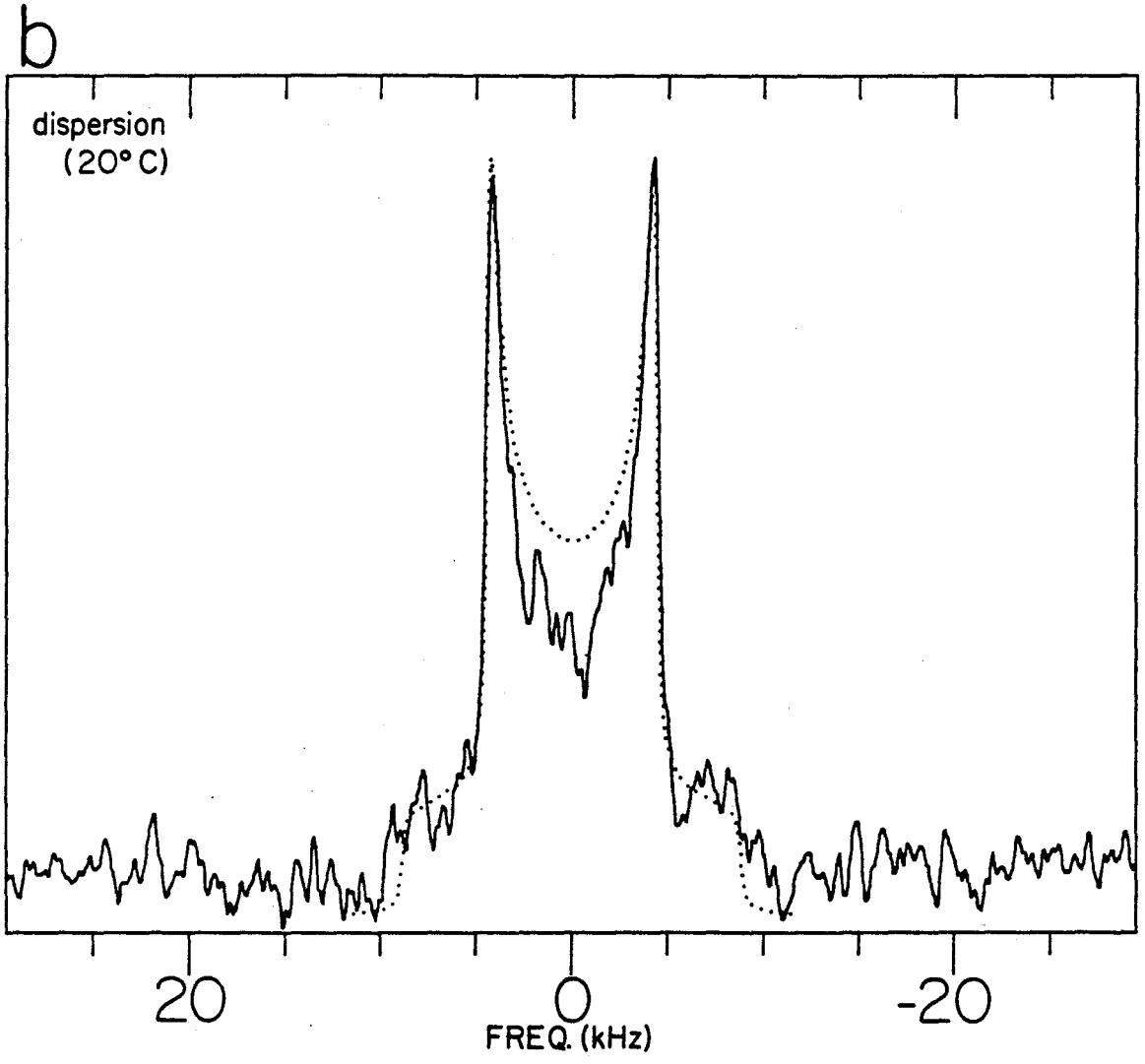

XBL 839-11489

Figure 35. Proton decoupled quadrupolar echo spectrum of decyltrimethylammonium bromide (DTAB) at -50°C. This signal is the result of 12000 acquisitions using 3.7 μsec 90° pulses and a 60 μsec interpulse delay. The dotted line represents a rigid lattice powder spectrum with e^2qQ/h = 106 kHz and η = 0.98; this has been convolved with 800 Hz of lorentzian line broadening and multplied by Eq. (2.19) to account for the finite duration of the pulses employed.

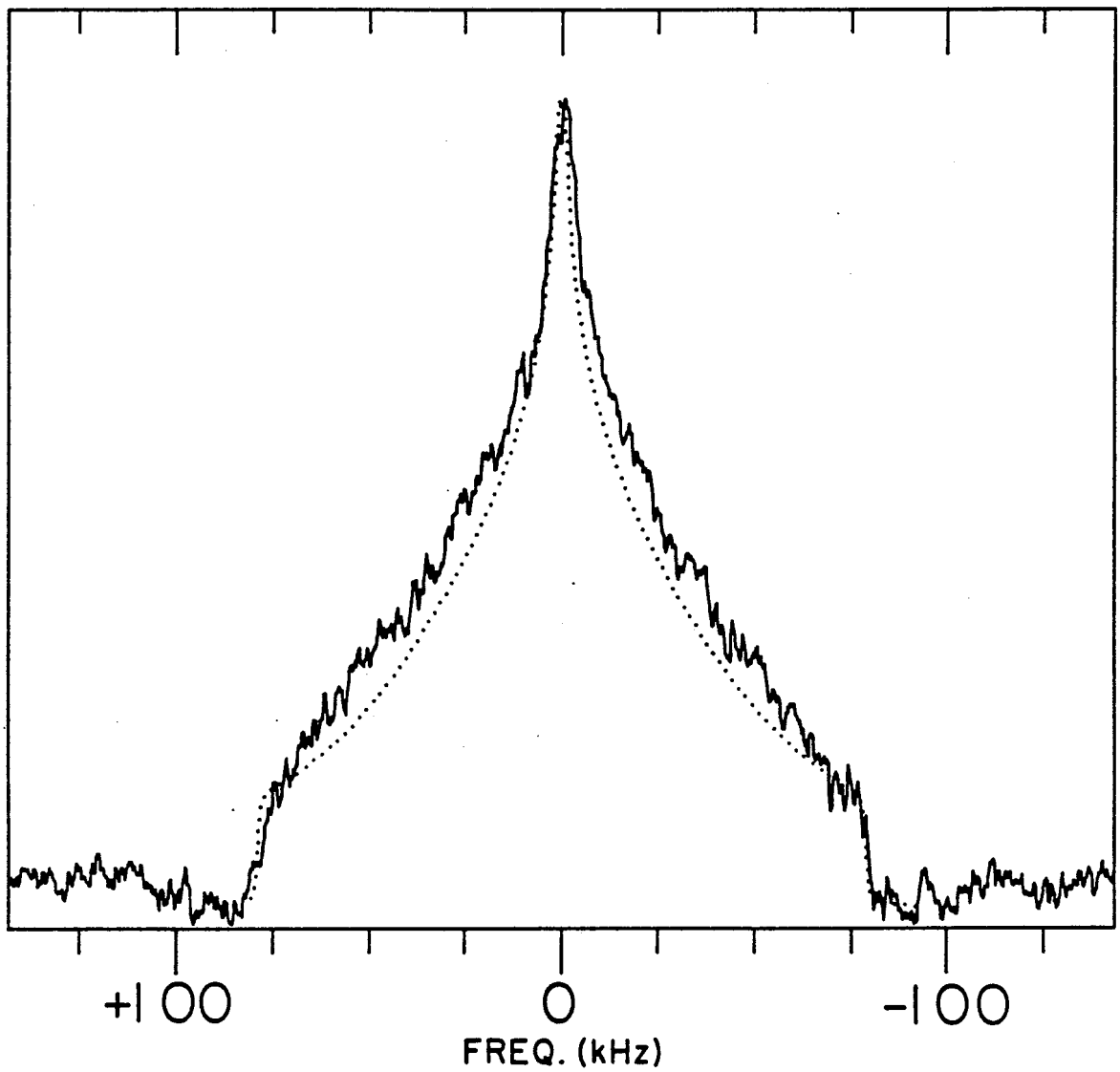

XBL 831-7630

the oreitnational order of the system is not uniquely described by the residual quadrupolar splitting and at least one other independent measurement is required [107].

The efg parameters in HTAB could be due entirely to the crystalline field (the lattice is monoclinic), but this material is known to give rise to quadrupolar relaxation in isotropic phases. This relaxation leads to a linebroadening which may be analyzed by calculating the spin-spin relaxation time in the rapid motion limit ($\tau_c^{-1} >> \nu_o$, $T_2 = T_1$, and $\Delta\omega_{fwhm} = \frac{2}{T_2}$) via Eq. (3.1). This type of analysis leads to a quadrupolar coupling not inconsistent with our measurements in the solid [74]. Thus we know that there must be some contribution to the efg from intramolecular effects. It is interesting to note that in the related compound hexadecyltrimethylammonium dichloroiodide the crystal structure reveals [108], within experimental error, no deviation from tetrahedral symmetry at nitrogen.

The experiments on DML and phosphorylcholine chloride (PCC) yielded disappointing results. Each compound gave what could more or less be described as a gaussian curve (see Figure 36) upon fourier transformation of its echo (note that a similar type of spectrum is also observed for HTAC). For DML, the lineshape was independent of the method of sample preparation. For PCC, and some preparations of DML, the room temperature S/N was nearly 60 times lower than at 158 K (based upon echo amplitudes), while for other preparations of DML just the opposite was true (i.e., the room temperature S/N was much greater than at low temperature). Since this observation is independent of recycle delay it must be a T_2 rather than a T_1 effect. Unfortunately, a systematic measurement of T_{2e} as a function of temperature was not carried out, although T_{1D} was found to be fairly

Figure 36. Proton decoupled quadrupolar echo spectrum of dimyristoyl phosphatidylcholine (DML) at -80°C. This signal is the result of 87,960 acquisitions using 3.7 μsec 90° pulses separated by a 60 μsec interpulse delay.

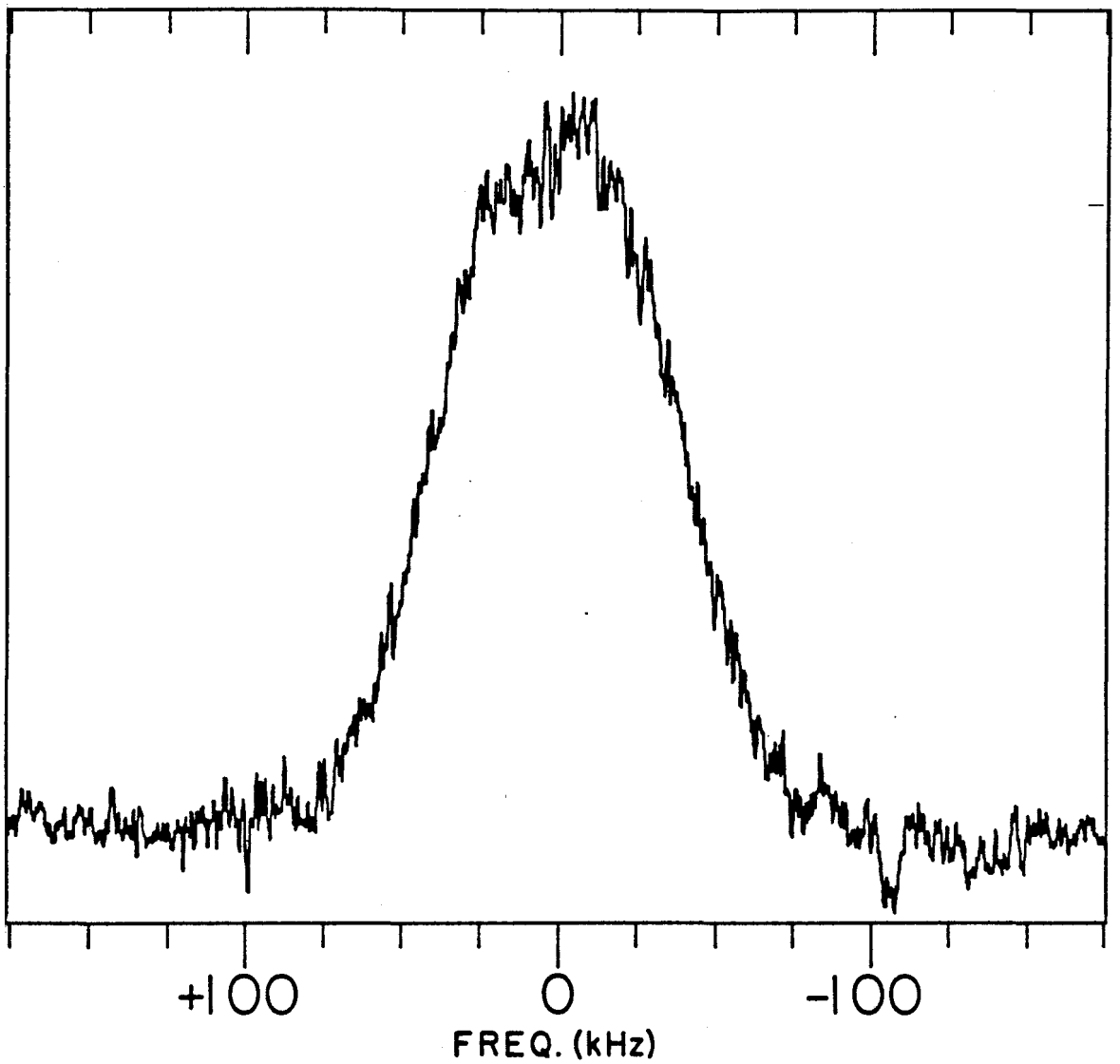

XBL 831-7629

short (under 30 msec) at all temperatures investigated for both compounds. Because it is likely that the protons on each molecule do not form a single thermodynamic reservoir (differing motions on different portions of the molecule likely decouple them from one another) any proton measurements are difficult to interpret and I choose not to present them here. The observed lineshapes can also be explained by motional arguments, but there is probably also a contribution from a disordered crystalline field as the powder x-ray diffraction pattern of DML shows fairly diffuse lines indicating a lack of long range order, a distribution of efgs (assuming the efg is highly dependent on local order), and hence a featureless spectrum. I tend to favor this latter explanation since the T_{2e}'s which I did measure were much longer than I would expect for such a washed out spectrum (e.g., the ^{14}N T_{2e} for the sample whose spectrum is shown in Figure 36 was 440 μsec, indicating a homogeneous line-width of 4.5 kHz).

Insufficient data are available to warrant detailed discussion of the other compounds listed in Table 3.I. I would, however, like to point out some observations with respect to TEA chloride. This compound was prepared four times (the first three were not recrystallized, while the fourth was recrystallized from acetone) and a distinctly different ^{14}N NMR spectrum was observed for each preparation. The first three were probably hydrated to varying degrees (TEA Cl is extremely hygroscopic) for they were not subjected to the rigorous drying treatment of the final sample. The first three samples gave rigid lattice lineshapes indicative of an axially asymmetric efg, but the efg parameters differed considerably between samples. The

Figure 37. Result of single and double quantum ADRF cross-polarized echo sequences on tetrapropylammonium iodide (TPrAI) at -90°C. In both cases the dotted line represents a rigid lattice powder pattern with e^2qQ/h = 102 kHz and η = 0.55, convolved with 800 Hz of lorentzian line broadening and multiplied by Eq. (2.102) (single quantum) or Eq. (2.19) (double quantum) to account for the finite duration of the pulse(s). (a) Single quantum frequency domain spectrum resulting from a 5 msec, 29 kHz mixing period followed by an 80 μsec delay and a 3.5 μsec 90° pulse. This signal is the result of 400 acquisitions. (b) Double quantum frequency domain spectrum resulting from a 5 msec, 30 kHz mixing period followed by an echo sequence consisting of 3.5 μsec 90° pulses, a first delay of 80 μsec and a second delay of 200 μsec. This signal is the result of 280 acquisitions. Two theoretical spectra are plotted (dotted lines), each being scaled to a different point in the experimental spectrum.

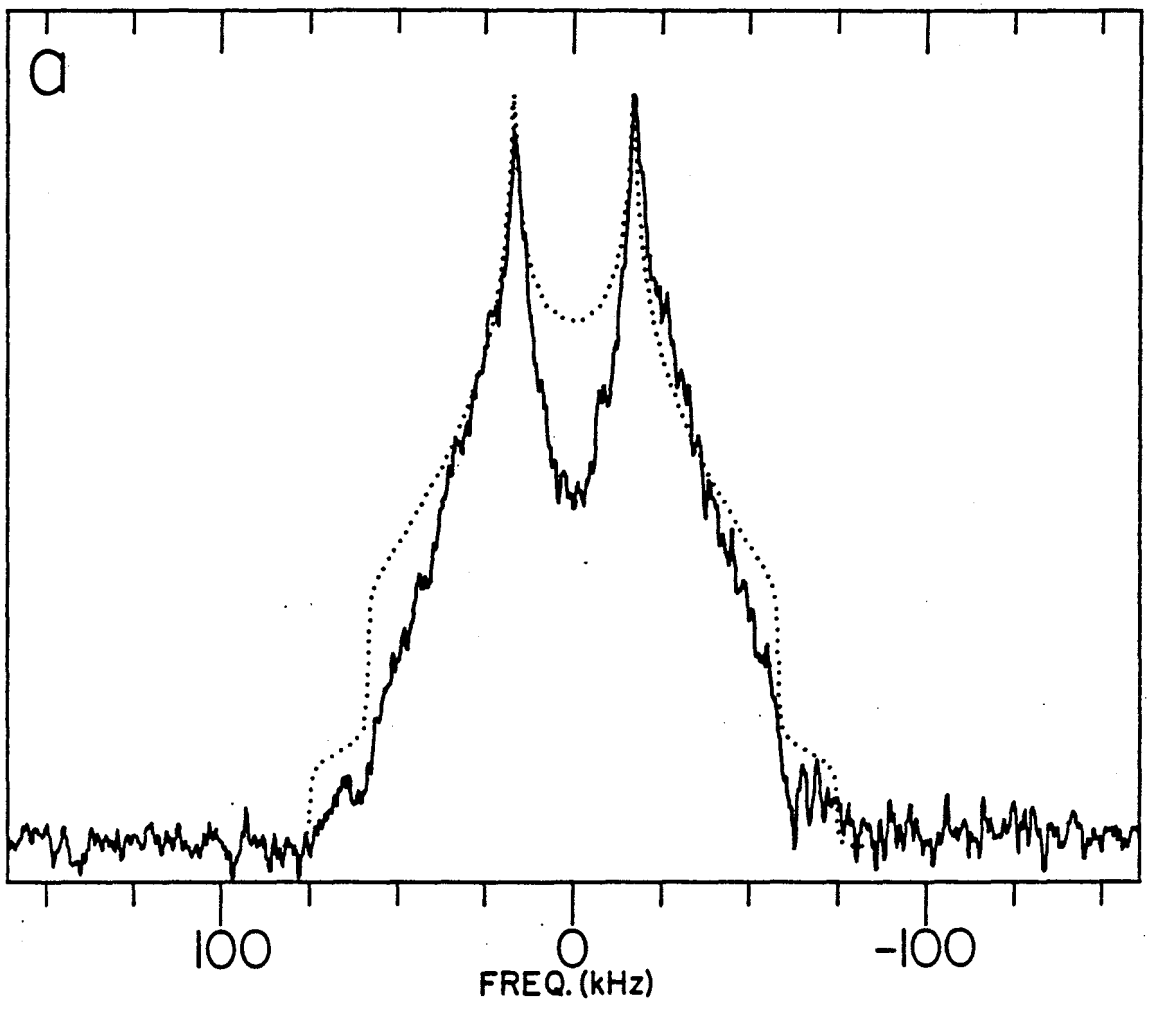

XBL 834-9390

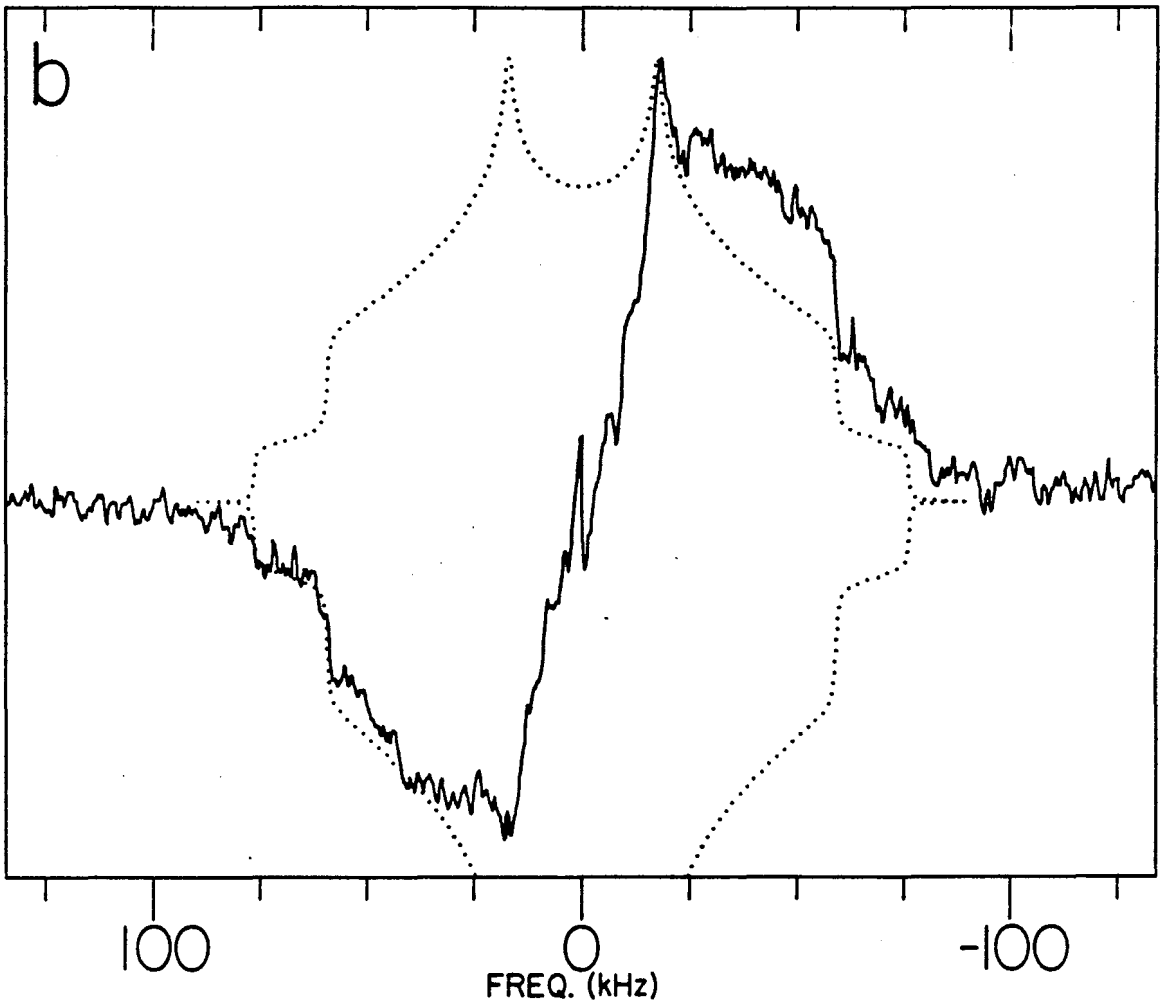

XBL 839-11488

Figure 38. Single quantum SL cross-polarized echo spectrum of tetrabutylammonium bromide (TBABr) at -60°C. This signal is the result of 280 acquisitions employing a 2 msec contact time, during which the ^{14}N and ^{1}H r.f. fields were matched at 50 kHz, followed by a 90 μsec delay and a 5 μsec 90° pulse. The dotted line represents a powder pattern with $e^2qQ/h = 24.4$ kHz and $\eta = 0.55$, convolved with 200 Hz of lorentzian linebroadening and multiplied by Eq. (2.102) to account for the finite duration of the single echo pulse.

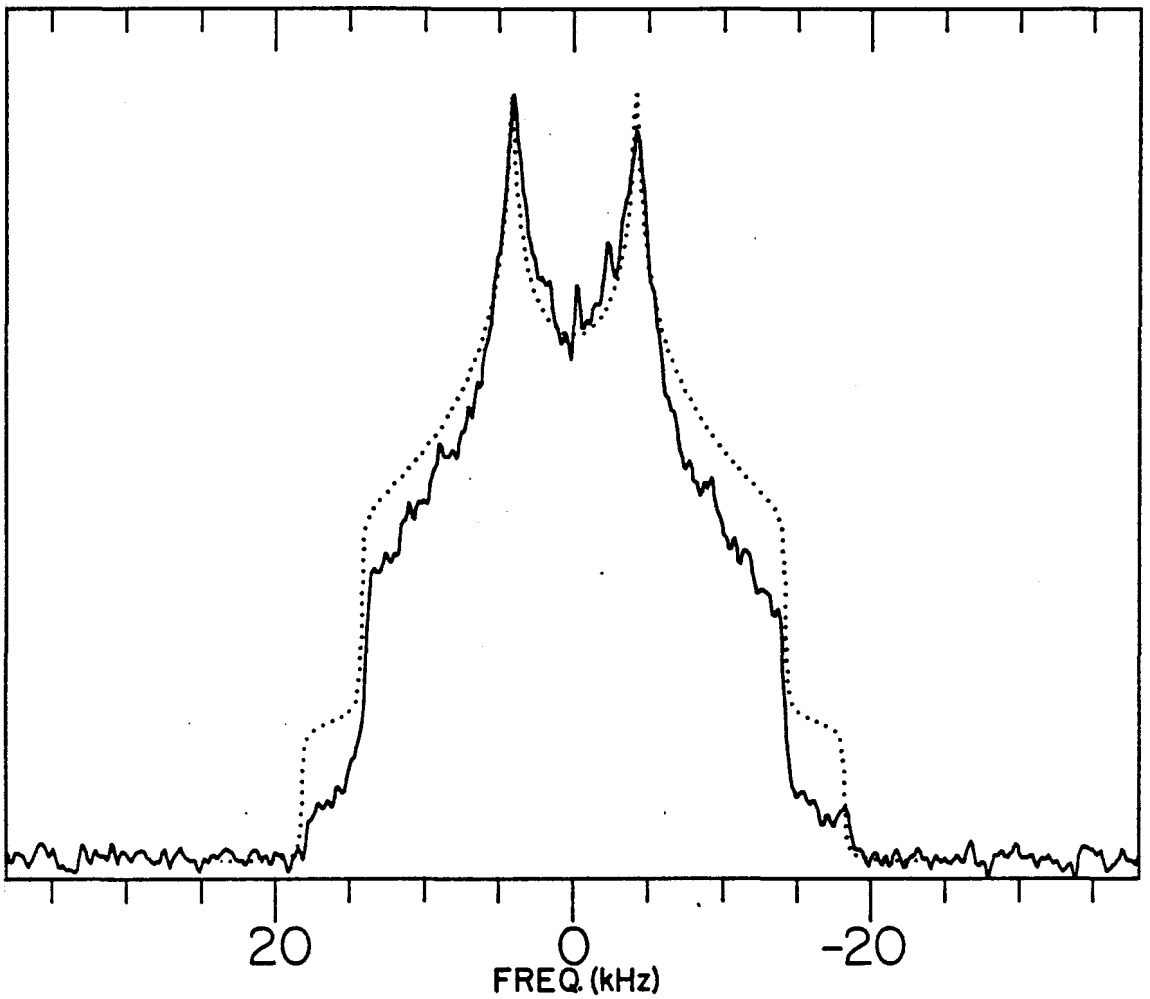

XBL 834-9381

final sample gave a featureless spectrum (very similar to that of DML) from which we can only estimate the range of quadrupolar coupling. Interestingly, I was able to cross-polarize this final sample using both ADRF and SL methods, while neither DML nor HTAC (which also exhibit washed out lineshapes) showed significant cross-polarization. Additionally, by varying the matching condition, it was possible for the spectrum to take on virtually any shape (as though it were made of silly putty). I believe this final observation to be indicative of a large amount of static disorder in the crystal lattice; emphasizing, once again, the importance of extramolecular effects in this study.

3.4 Concluding Remarks on EFGs

The origin of the observed efg parameters can only be stated with certainty for the TMA halides, TEA iodide, and TPrA bromide. For these compounds a small axial quadrupolar coupling is associated with a tetragonal crystal lattice. I find it extremely satisfying that the asymmetry parameter always shows some relation to the symmetry of the unit cell (where this is known). For a purely ionic field gradient this should be the case [109]. The other compounds which have been discussed exhibit efgs which probably originate from some combination of intra- and extra-molecular effects. It is not unreasonable that the intramolecular structure may dictate the extra-molecular structure (and vice-versa) so the two effects may not be strictly separable. In this regard, it would be interesting to investigate the NQR of the halide counterions since this should be sensitive only to the extra-molecular crystalline field.

Finally, it should be pointed out that the crystalline field effect arguments presented here have been used in the past to rationalize efg parameters in ammonium hydrogen oxalate [110], ammonium dihyrodgen phosphate [111], and ammonium aluminum alum [112]. For these compounds, the averaging of the intramolecular efg would no doubt be complete due to ammonium ion reorientation, and the agreement between the observed efg symmetry and the crystalline field symmetry is good.

3.5 A Few Remarks on the ^{14}N T_1

I have alluded several times to the observation of long ^{14}N T_1's for the tetraalkylammonium compounds. In an attempt to elucidate a spin-lattice relaxation mechanism for these compounds, I performed a measurement of the TMA Cl ^{14}N T_1 between 160 and 300 K (see Figure 39). All of my previous evidence indicates that the field gradient in this salt is of ionic origin, therefore a likely relaxation mechanism would be quadrupolar coupling through optical and acoustic phonon modes [113]. This relaxation mechanism is expected to follow a T^{-2} dependence above the Debye temperature which my data clearly do not exhibit (this region is well above the Debye temperature, as may be seen from the data presented in ref. [102]). Instead, the high temperature region of the $\log(T_1)$ vs. 1000/T plot is nearly linear (linear least squares fit slope = 1.05, correlation coefficient = .998) indicating that a thermally activated reorientational mechanism is responsible. Rotational reorientation of the TMA ion would not lead to relaxation in an ionic field gradient through a quadrupolar mechanism, so it appears that ^{14}N relaxes through a dipolar mechanism.

Figure 39. Semilog plot of the TMA Cl ^{14}N T_1 as a function of the inverse temperature. The T_1 values were determined from echo amplitudes using the progressive saturation technique. The error bars were estimated from the errors in the best exponential fits to the data.

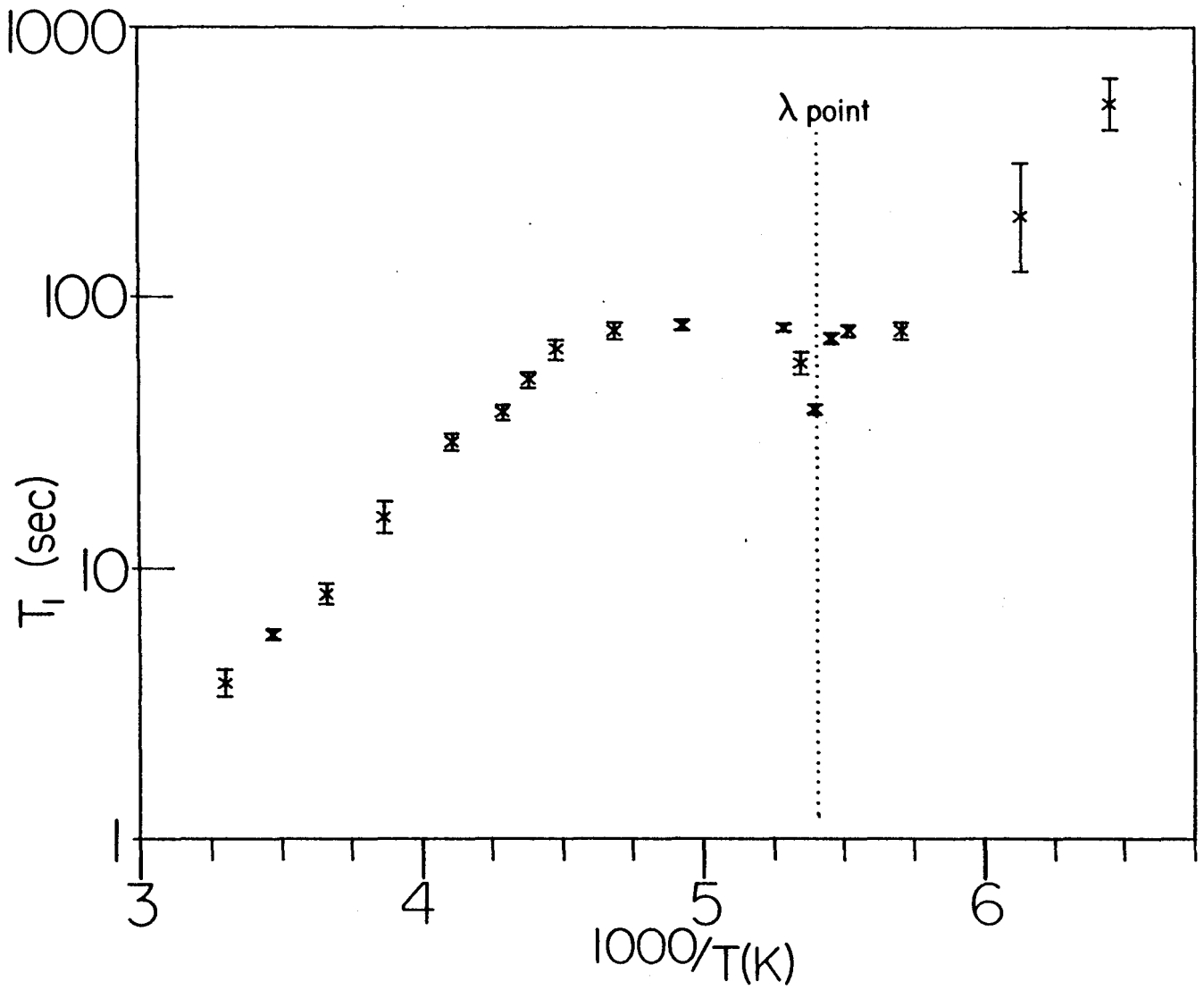

XBL 8310-12061

This contention is supported by the observation of TMA Cl proton T_1's which are between 2 (high temperatures) and 10 (low temperatures) times shorter than those for ^{14}N (simple mindedly, protons should relax more rapidly via a dipolar mechanism because of their larger gyromagnetic ratio). The activation energy determined from the slope of the straight line proton of Figure 39 is 4.8 kcal. This low activation energy probably corresponds to methyl group rotation, although it is about 25% lower than that obtained from proton second moment [100] and relaxation time [115] studies of TMA Cl.

The plateau region (175-213 K) around the λ point and the cusp at the λ point are apparently the result of cooperative effects near the phase transition and corresponding features have been observed in other second order phase transitions [114]. Proton relaxation studies of TMA Cl [115] indicate that the second order phase transition has no effect on the reorientational motion of the TMA ion, so it would appear that the plateau region and cusp are due to quadrupolar relaxation from low frequency critical fluctuations of the lattice [116].

Although these data are difficult to generalize, I do in most cases observe a ^{14}N T_1 which is much longer than the corresponding proton T_1. This is most easily rationalized by invoking a dipolar relaxation mechanism. Those tetraalkylammonium compounds in which one or more of the alkyl groups is a methyl are observed to have much shorter ^{14}N T_1's than the corresponding unmethylated tetraalkylammoniums. This rather indirect evidence would seem to indicate that methyl group rotation is an important relaxation mechanism for ^{14}N. Additionally, the observation of small NOE's for many of these compounds indicates that spin-lattice relaxation, to a small extent,

occurs through the protons.

Chapter 4

Effects of Motion in the Choline Halides

4.0 Previous Work

The choline salts are extremely unusual in their sensitivity to ionizing radiation [117]. Upon irradiation choline chloride rapidly decomposes exhibiting G values as high as 5.5×10^4 (the G value is defined as the number of molecules destroyed per 100 eV absorbed), whereas G values for most compounds are in the range of 0.1 to 10 [118]. Choline bromide also exhibits radiation sensitivity, although only to half the extent of the chloride, and choline iodide appears completely normal with respect to ionizing radiation. The temperature dependence of the radiation sensitive behavior shows that it begins at about 0°C and climbs in a sigmoidal manner until it reaches a maximum just below the order-disorder phase transition (transition temperatures: chloride 351 K, bromide 363 K, and iodide 367 K; the low temperature phase is referred to as the α phase, and the high temperature phase as the β phase) [117,119]. Thereafter, the enhanced radiation sensitivity falls off rapidly, being non-existent in the high temperature disordered phase.

The major radiolysis products are trimethylamide hydrochloride and acetaldehyde. This observation has lead to the proposed mechanism of C-N bond cleavage through a free radical chain reaction involving ethylol and hydrogen radicals [117]. Attempts to rationalize this through x-ray studies [96,98,120] have yielded only the observation of a somewhat longer C-N bond in the α phase of choline chloride than

normally encountered (1.56 Å vs. 1.50 Å), and the presence of a large amount of disorder in the high temperature β phase of choline chloride. Additionally, an x-ray study of the radiation normal choline iodide shows that a certain anisotropic disorder is present at room temperature [97] which apparently results from a flip-flop motion about an axis passing through the nitrogen and oxygen atoms (see Figure 46). Unfortunately, a detailed structure is not available for choline bromide. The association of dynamic disorder with the absence of radiation sensitivity in choline iodide and the β phase of choline chloride indicates that NMR may be useful for investigating the dynamic properties of the solid. To this end, a number of studies have been accomplished. A proton second moment study of all three salts from 77 K to 400 K [121] showed that three types of motions occur (in order of appearnace from low temperature): methyl group rotation (∿ 140 K), reorientation about the $C-N^{+}(Me)_3$ bond (∿ 250 K), and isotropic reorientation of the choline ion (∿ 360 K). The presence of isotropic reorientation in the radiation stable high temperature phase of the bromide and chloride was confirmed, but nothing could be said as to the difference in radiation sensitivity between the three salts (no tremendous differences are observed between the second moments of the three compounds). Proton spin-lattice relaxation time measurements (T_1,$T_{1\rho}$) in the three salts [122,123] show, in addition to the previously mentioned motions, a slow reorientational motion with low activation energy occuring between room temperature and the phase transition temperature. Recent solid state ^{13}C NMR spectra [97] indicate further the presence of this motion and lend credence to the idea that the rapid decrease in radiation sensitivity just below

the phase transition is associated with the onset of motion.

In the previous chapter, I alluded to the observation of motionally distorted solid state ^{14}N NMR spectra for choline chloride and iodide. These spectra clearly show anisotropic distortion which must be the result of anisotropic motion. The motion affects the NMR spectrum by making the quadrupolar frequency time dependent. I will attempt to analyze the distorted spectra by assuming that the efg undergoes thermally activated random rotational jumps about a fixed axis. This is a reasonable model only if the efg is of intramolecular origin; a point to which I will return later.

4.1 Anisotropic Motion and Anisotropic Interactions in NMR

In liquids it is reasonably assumed that any ordering due to intermolecular interactions is weak and the potential seen by the molecule is isotropic. This leads to isotropic Brownian motion which averages the anisotropic spectral features of the quadrupolar interaction but retains its relaxation properties through rapid random modulation. In crystalline solids the ordering potential is anisotropic and isotropic Brownian motion is highly unlikely. Instead the molecule jumps between discrete orientations in the lattice at a rate (κ) such that the time between jumps ($1/\kappa$) is much shorter than the residence time at each orientation. In the rapid motion limit ($\kappa \gg e^2qQ/h$) the observed efg is the partially averaged result of the static efg; the observed tensor depending in detail upon the manner in which the static tensor was modulated (see Figure 50). When the motion slows to the intermediate exchange region ($\kappa \sim e^2qQ/h$), interesting effects occur which have been previously discussed [124,125, 126,127], and it is these upon which I will concentrate. The additional

distortion caused by the use of the quadrupolar echo sequence has been discussed by Spiess and Sillescu [127], but it is appropriate to go over this one more time.

To begin, it is most reasonable to assume that the motional process is of a stationary Markov nature. In other words, the molecular orientation Ω at time t is dependent only upon its value at a previous time t' and upon the time difference $\Delta t = t-t'$. Because of this, the occupation probability of orientation Ω, $P(\Omega,t)$, will satisfy:

$$\frac{\delta}{\delta t} P(\Omega,t) = \Gamma_\Omega P(\Omega,t) \quad , \tag{4.1}$$

where Γ_Ω is now referred to as a time independent Markov operator (the symbol Γ is usually used to describe diffusion, while Λ is used to describe jumping, but I will not make this distinction here). The time evolution of the density matrix (Eq. (2.41)), upon which all of our observable reality is based, may now be written [128]:

$$\frac{\delta\rho}{\delta t} = -\frac{i}{\hbar}[\mathcal{H}(\Omega),\rho] - \frac{\rho_{diag}-\rho_0}{T_1} - \frac{\rho_{off}}{T_2} + \Gamma_\Omega\rho \quad , \tag{4.2}$$

where it is assumed that the phenomenological relaxation times T_1 and T_2 are due to perturbations other than those described by Γ_Ω, and are orientation independent. The solution of Eq. (4.2) is in general a formidable problem, but may be simplified as follows: (1) neglect T_1, (2) assume no motion occurs during the periods in which r.f. fields are applied, and (3) assume the molecule performs planar jumps of fixed

angle. The fid:

$$g(t) = \mathrm{Tr}[I_+\rho(t)] \tag{4.3}$$

may now be expressed in matrix form as [129]

$$g(\Omega,t) = \underset{\sim}{G}(0)\cdot(\exp(i\underset{\approx}{\omega} - \frac{1}{T_2}\cdot\underset{\approx}{I} + \underset{\approx}{\pi})t)\cdot\underset{\sim}{1} \tag{4.4}$$

where $\underset{\sim}{G}(0)$ is a row vector containing the <u>a priori</u> occupation probabilities of the sites (orientations) which are in exchange, $\underset{\approx}{\omega}$ is a diagonal matrix whose elements are the frequencies of the sites which exchange, $\underset{\approx}{I}$ is the identity matrix, $\underset{\approx}{\pi}$ is the matrix form of the Markov operator, and $\underset{\sim}{1}$ is a column vector whose elements equal one. Fourier transformation of the fid described by Eq. (4.4) followed by integration over all angular space, will yield the powder spectrum:

$$I(\omega) = \int_\Omega \underset{\sim}{G}(0) \int_0^\infty \exp\{(i(\underset{\approx}{\omega}-\omega\underset{\approx}{I}) - \frac{1}{T_2}\underset{\approx}{I} + \underset{\approx}{\pi})t\}dt\ d\Omega$$

$$= \int_\Omega \underset{\sim}{G}(0)\cdot\underset{\approx}{A}^{-1}\cdot\underset{\sim}{1}\ d\Omega \quad , \tag{4.5}$$

where

$$A = [i\ (\underset{\approx}{\omega}-\omega\underset{\approx}{I}) - \frac{1}{T_2}\underset{\approx}{I} + \underset{\approx}{\pi}]^{-1} \tag{4.6}$$

In order that the fid resulting from the quadrupolar echo sequence may be cauculated, I will initially assume that the pulses perform

90° rotations in an infinitesimal period of time (i.e., ideal pulses), and so the effect of the echo pulse at time τ is to cause those spins possessing frequency $\omega(\Omega)$ at time $t < \tau$ to have frequency $-\omega(\Omega)$ at time $t > \tau$. Now, Eq. (4.4) becomes

$$g(\Omega,t) = \underset{\sim}{G}(0)\cdot(\exp(i\underset{\approx}{\omega} - \frac{1}{T_2} I + \underset{\approx}{\pi})\tau)\cdot$$

$$\exp(-i\underset{\approx}{\omega} - \frac{1}{T_2} \underset{\approx}{I} + \underset{\approx}{\pi})(t+\tau))\cdot\underset{\sim}{1} \quad , \tag{4.7}$$

which may be fourier transformed, starting from the echo maximum at $t=0$, to yield

$$I(\omega) = \int_{\Omega} \underset{\sim}{G}(0)\ \underset{\approx}{E}(\tau)\ \underset{\approx}{A}^{-1}\ \underset{\approx}{1}\ d\Omega \quad , \tag{4.8}$$

where

$$\underset{\approx}{E}(\tau) = \exp(i\underset{\approx}{\omega} - \frac{1}{T_2} \underset{\approx}{I} + \underset{\approx}{\pi})\tau\cdot$$

$$\exp(-i\underset{\approx}{\omega} - \frac{1}{T_2} \underset{\approx}{I} + \underset{\approx}{\pi})\tau \quad , \tag{4.9}$$

and

$$\underset{\approx}{A}^{-1} = [-i(\underset{\approx}{\omega} + \omega\underset{\approx}{I}) - \frac{1}{T_2} \underset{\approx}{I} + \underset{\approx}{\pi}]\tau \quad . \tag{4.10}$$

As a first approximation to the effect of finite duration pulses, we may alter $\underset{\approx}{G}(0)$ such that

$$G_i(0) = W_i \cdot D(\omega_1, \omega_i) \quad , \tag{4.11}$$

where W_i is the <u>a priori</u> probability of site i, ω_i is the quadrupolar frequency of site i, and $D(\omega_1,\omega)$ is given by Eq. (2.19). The spectra I am considering here are sufficiently narrow that I may safely neglect this type of spectral distortion (discussed in detail in section 2.1.1). The solution of Eq. (4.8) is best accomplished by utilizing the following procedure [129], which in general must be carried out numerically (i.e., on a digital computer). First, the matrix describing the time evolution is diagonalized to determine its eigenvalues and eigenvectors. The matrix of eigenvectors is then inverted to yield the following expression:

$$\underset{\approx}{S}^{-1} \cdot [i\underset{\approx}{\omega} - \frac{1}{T_2} \underset{\approx}{I} + \underset{\approx}{\pi}] \cdot \underset{\approx}{S} = \underset{\approx}{\lambda} \quad , \tag{4.12}$$

where $\underset{\approx}{S}$ is the matrix of eigenvectors corresponding to the eigenvalues $\underset{\approx}{\lambda}$. This step need only be performed once at each orientation. Now, Eq. (4.7) becomes

$$\begin{aligned} g(\Omega,t) = \underset{\sim}{G}(0) \cdot \underset{\approx}{S} \cdot \exp(\underset{\approx}{\lambda}\tau) \underset{\approx}{S}^{-1} \cdot \\ \underset{\approx}{S}^{*} \cdot \exp(\underset{\approx}{\lambda}^{*}\tau) \underset{\approx}{S}^{*-1} \cdot \\ \underset{\approx}{S}^{*} \cdot \exp(\underset{\approx}{\lambda}^{*}t) \underset{\approx}{S}^{*-1} \cdot \underset{\sim}{1} \quad , \end{aligned} \tag{4.13}$$

where the superscript * should be taken to denote the complex

conjugate. Fourier transformation of Eq. (4.13), followed by integration over angular space, yields:

$$I(\omega) = \int_{\Omega} \underset{\sim}{G}(0)\cdot\underset{\approx}{E}(\tau)\cdot\underset{\approx}{S}^{*}[\underset{\approx}{\lambda}-i\omega\underset{\approx}{I}]^{-1}\ \underset{\approx}{S}^{*-1}\cdot\underset{\sim}{1}\ d\Omega \tag{4.14}$$

where $\underset{\approx}{E}(\tau)$ is the same as Eq. (4.9), but may also be expressed as

$$\underset{\approx}{E}(\tau) = \underset{\approx}{S}\cdot\exp(\underset{\approx}{\lambda}\tau)\underset{\approx}{S}^{-1}\cdot$$

$$\underset{\approx}{S}^{*}\cdot\exp(\underset{\approx}{\lambda}^{*}\tau)\underset{\approx}{S}^{*-1} \quad . \tag{4.15}$$

Note that inversion of the diagonal matrix $\underset{\approx}{\lambda}-i\omega\underset{\approx}{I}$ trivially reduces to inversion of each of its elements. The problem with using Eq. (4.14) is that there is no guarantee that all of ω space is represented by $\underset{\approx}{\lambda}$. This results in the appearance of false spikes in the lineshape if $I(\omega)$ is evaluated at improper points. It has therefore been suggested that the fid (Eq. (4.13)) be integrated over angular space prior to performing a numerical fourier transform [130]. This procedure is always stable, and I have found it to be the more useful of the two methods. The numerical transform takes almost no time, but the integration of the fid will take more time than the evaluation of Eq. (4.14) because more points need to be calculated in the fid to prevent its truncation (and corresponding wiggles in the transform), and also because the amount of cpu time required to evaluate the complex exponential is much greater than that required to invert a complex number.

In order to evaluate Eq. (4.13), it is necessary to determine

the frequencies which are exchanging due to the jump process ($\omega_i = \omega(\Omega_i)$), and the jump probability matrix $\underset{\approx}{\pi}$. The frequency $\omega(\Omega_i)$ may be deduced from the relationship between the quadrupolar frequency and the angular rotation about the flipping axis at a particular orientation with respect to the static field. This relationship is obtained by transforming the secular part of the quadrupole interaction (A_{20} in Appendix A) to the molecular flipping frame, rotating by an angle δ (the flip angle) about the z axis in this frame, and then transforming to the laboratory frame (i.e., with respect to H_0). This transformation is easily accomplished using the rotation properties of spherical tensors. Fortunately Mehring [130] has already given us the result in the case of a chemical shift interaction, and this result may be applied to quadrupolar coupling with only the change of a few constants. The resulting expression is:

$$\begin{aligned}\omega(\Omega_i,\delta) = \frac{3}{4}\frac{e^2qQ}{\hbar}\{&[P_2(\cos\beta)P_2(\cos\theta) - \\ &\frac{3}{4}(\sin^2\beta\,\sin 2\theta\,\cos(\gamma+\phi+\delta) - \sin^2\beta\,\sin^2\theta\,\cos 2(\gamma+\phi+\delta))] \\ &+ \frac{\eta}{2}[P_2(\cos\theta)\sin^2\beta\,\cos 2\alpha + \sin\beta\,\sin 2\theta\cdot \\ &\cdot(\cos\beta\,\cos 2\alpha\,\cos(\gamma+\phi+\delta) - \sin 2\alpha\,\sin(\gamma+\phi+\delta)) \\ &+ \sin^2\theta(\tfrac{1}{2}(1+\cos^2\beta)\cos 2\alpha\,\cos 2\,(\gamma+\phi+\delta) \\ &- \cos\beta\,\sin 2\alpha\,\sin 2(\gamma+\phi+\delta))]\} \qquad , \end{aligned} \tag{4.16}$$

where (α,β,γ) are the polar angles which relate the PAS of the efg to the molecular flipping frame (see Figure 40), δ is the angle of

Figure 40. The relationship between the principle axes of the electric field gradient tensor (defined by V_{xx}, V_{yy}, and V_{zz}) and the molecular flipping frame (defined by x", y", and z"). Rotational jumps occur about the z" axis. The angle γ has not been included since it is of no importance when a powder average is calculated.

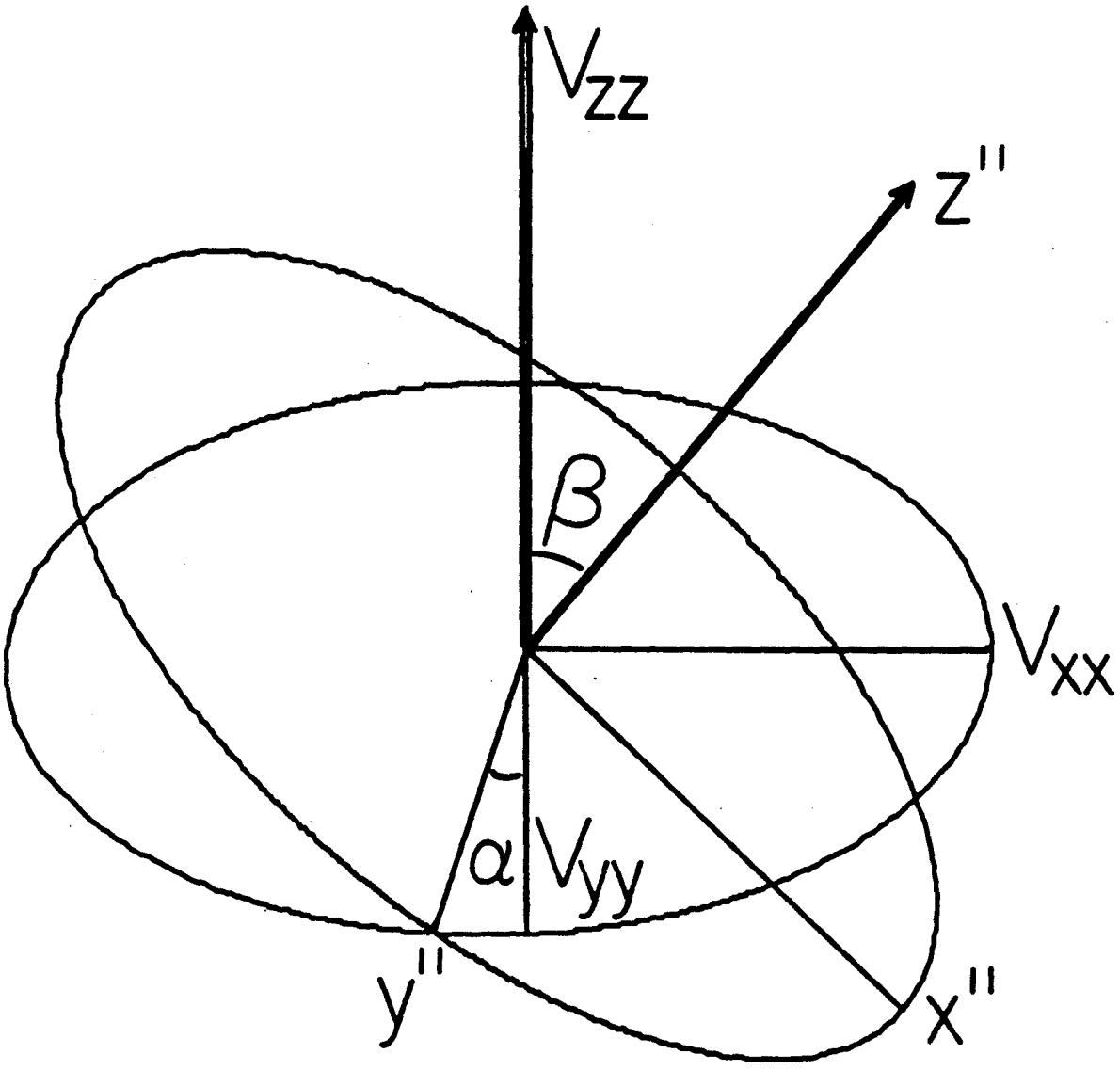

XBL 8310-12170

the flip about z" (Figure 40), and (θ,ϕ) relate the flipping frame to H_0. Note that the angle γ in Eq. (4.16) will drop out of the calculation (i.e., become unimportant) when we average over ϕ in the angular integration.

The matrix $\underset{\approx}{\pi}$ is constructed as follows: the off diagonal elements (π_{ij}, $i \neq j$) equal the probability per unit time that site i jumps to site j, and the diagonal elements are chosen to satisfy the relation

$$\sum_j \pi_{ij} = 0 \quad , \tag{4.17}$$

which must be true in any equilibrium situation. We may construct $\underset{\approx}{\pi}$ in any way we wish so long as Eq. (4.17) is satisfied, but two limiting cases are of interest. In the so called "hard collision" limit all sites are equally accessible from any other site, and so all of the off diagonal elements are identically equal to the jump probability κ, while the diagonal elements equal $-(n-1)\kappa$ (where n is the number of sites sampled by the process). In the "soft collision" limit only neighboring sites are accessible, so the off diagonal elements equal κ if $|i-j| = 1$, equal 2κ if $|i-j| = 1$ and i or j equal n, and the diagonal elements equal -2κ (all other elements are zero). Of course, other models are also possible in which various sites have various probabilities of occupation, but I will not consider these here. Utilizing this approach we can calculate the spectra which would result from many simple types of motion, but other methods are probably better for more complex diffuse type motions [125,131,132,133,134].

4.2 Experimental Results

The experiments were performed in accordance with the general description of section 3.1. An attempt was made to acquire spectra at several echo delay (τ) values for each value of the temperature. As pointed out by Spiess and Sillescu [127], the lineshape should change in a characteristic way as we vary τ in the intermediate exchange "slow motional" region ($\kappa \sim e^2qQ/h$). Unfortunately, in some temperature regions the echo completely disappears because T_{2e} (the characteristic echo amplitude decay time) is drastically shortened as a result of the motion. This effect may be calculated by integrating Eq. (4.13) over Ω for each τ value at t=0 and I have performed such calculations to see if my proposed motional models could be responsible for the observed T_{2e}. Additionally, the ^{14}N T_1 for these compounds seems to increase greatly at low temperature. For example, at -98°C the choline chloride T_1 is about 30 seconds, while at -120°C it is estimated to be in the neighborhood of 5 minutes. Long T_1's equal low S/N per unit time, so that the lineshapes obtained in the low temperature region are nothing short of pitiful (see Figure 42). It should be noted that lineshape distortions may also be caused by anisotropic T_1 effects, but the experiments I present here were run at several recycle delays, and significant differences in the results were not observed (also, anisotropic T_1 will not cause anisotropic lineshape distortion as τ is varied).

In Figure 41 I present T_{2e} data for all three salts. I would like to emphasize that these data are only presented to indicate general trends. In many cases, especially when T_{2e} is less than 100 μsec, the S/N was low enough to give the data a large error

Figure 41. ^{14}N quadrupolar echo decay times (T_{2e}) as a function of the inverse temperature for the three choline salts. In each case the data were fit to Eq. (3.3b).

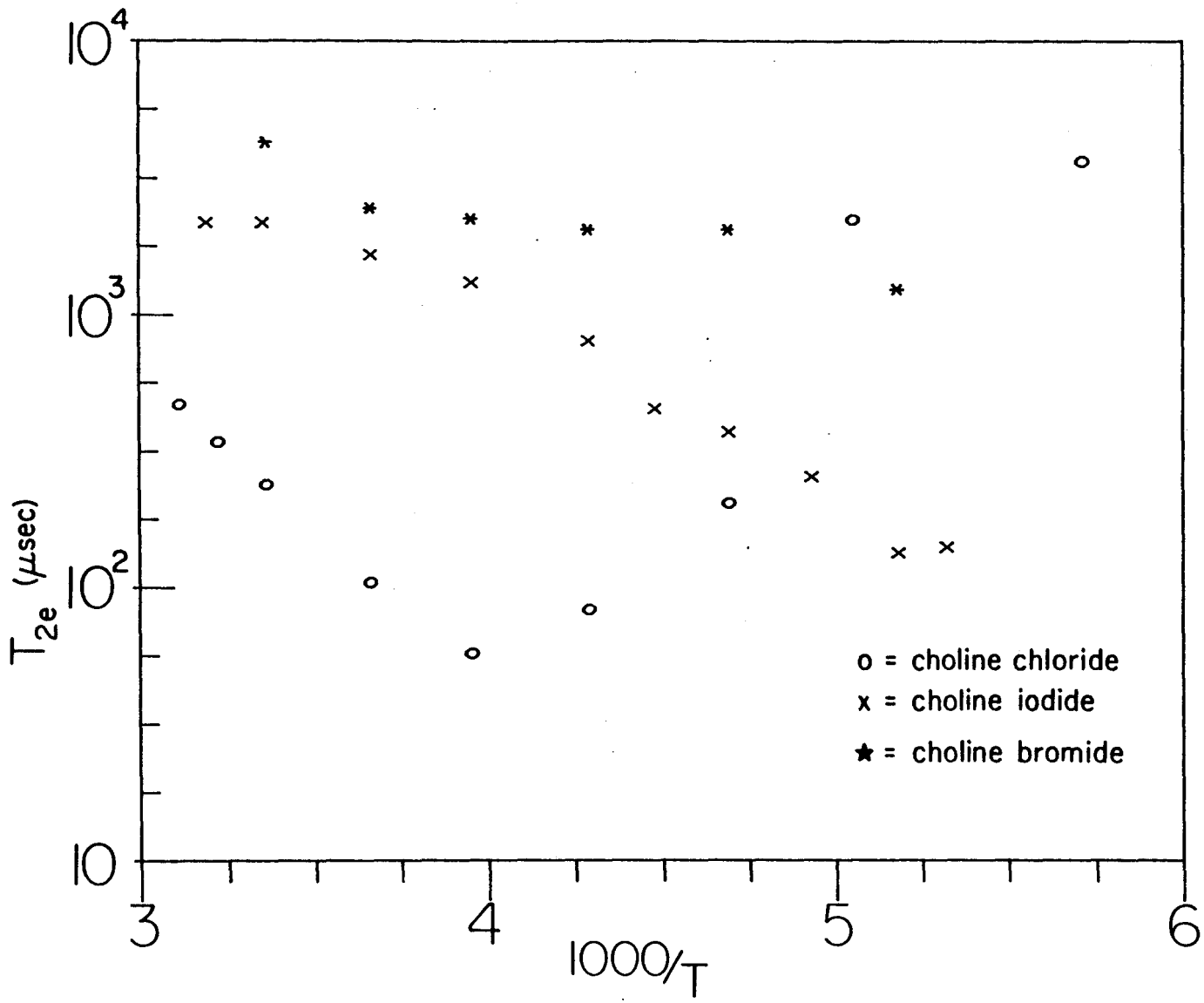

XBL 8310-12062

(I have made no attempt to fit error bars). Also, the echo amplitude decay was, in many cases, observed to be non-exponential (as we would expect), but the T_{2e} given is the best fit to a single exponenential.

4.2.1 Assumptions Made in the Analysis

Unfortunately, many assumptions had to be made prior to embarking upon the analysis of the lineshapes. These assumptions reflect an ignorance of the system under study, and I feel that they should be presented and discussed at this time.

The absence of effects relating to C_3 reorientation about the $C\text{-}N^+(Me)_3$ bond in these salts is very puzzling. This type of motion, which is clearly indicated by proton NMR studies [121,122], would result in an axial intramolecular efg in the rapid motion limit. If the jump site are not quite related by C_3 symmetry the resulting efg may be slightly nonaxial. The proton second moment data in particular indicate that at room temperature the rate of C_3 reorientation is on the order of 50 kHz to 500 kHz and this is supported by the proton $T_{1\rho}$ data. Therefore we should either observe an axial efg, or a motionally distorted spectrum, depending upon the magnitude of the static efg parameters. At 200 K the proton second moment study indicates that this motion has essentially ceased and we should observe a rigid lattice efg. The choline bromide efg parameters in particular clearly show no effect from this motion, even though I was able to reproduce the proton linewidth of reference [121] (so the motion was apparently occurring in my samples.) The most reasonable rationalization for this observation is that which was invoked in the last chapter: the efg is of

intermolecular (crystalline) origin. For the chloride and iodide salts this explanation is not completely consistent with the observed ^{14}N spectra since they clearly show the effects of efg motion (see Figures 42-51). Most likely, the efg's for all three compounds possess contributions from both inter- and intramolecular effects. On this basis, the only proper method to analyze the motional effects would be to separate the inter- and intramolecular field gradient components; applying the motion to only the intramolecular efg. Such a procedure would increase the number of independent variables greatly for we must now consider the relative magnitude, asymmetry, and orientation of the two tensors. There is no justification for embarking upon such an analysis when all of my experimental observations derive from powder patterns, and the analysis appears to have no precedent in the literature which I have surveyed. A single crystal study of the orientation dependence of the efg to determine the relationship between the observed efg and the molecular reference frame, coupled with a point charge model calculation [109] to determine the approximate magnitude and orientation of the crystalline efg, may shed some light upon the present perplexing situation. Since this laborious procedure has not been accomplished, I will here assume the efg's of the chloride and iodide salts to be entirely of intramolecular origin. This assumption further requires me to ignore the effects of C_3 reorientation about the $C\text{-}N^+(Me)_3$ bond, since such motion is not consistent with the spectra I observe.

4.2.2 Choline Bromide

As Figure 41 indicates, this compound shows no large T_{2e} deviations over the temperature range studied. The lineshapes which

I have obtained at each temperature show no obvious motional distortion, although the S/N is low enough to mask small distortions (see Figure 33). It is possible that any motion present is either too slow ($\kappa >> e^2qQ/h$) or too rapid ($\kappa >> e^2qQ/h$) to noticeably affect the lineshape. In this regard it may prove useful, at some time in the future, to monitor the decay of the quadrupolar order (T_{1Q}) [135] so that the presence of extremely slow motion may be checked. This experiment has not been performed and I will discuss this compound no further.

4.2.3 Choline Chloride

In Figure 41 we see that the T_{2e} for this salt passes through a minimum at about 250 K, below which it increases rapidly to what appears to be a rigid lattice value at about 175 K. On the high temperature side of the minimum T_{2e} increases, but does not reach a rapid motion ($\kappa >> e^2qQ/h$) value at the highest temperature investigated (321 K). Not much weight should be given to the linearity of the T_{2e} data between 250 and 321 K since the T_{2e} values in many cases result from exponential fits to non-exponential data (I do not believe that there are sufficient data to justify a multiexponential fit).

In Figure 42 we observe the effects of anisotropic motion on the powder patterns at various temperatures. This is further reinforced in Figure 43, where the variation of the lineshape with τ is illustrated. At high temperatures the center of the lineshape (between the points $\pm V_{yy} = (1+\eta)\frac{3}{8}\frac{e^2qQ}{h}$) appears to collapse (see Figure 44), while at low temperatures the wings of the spectrum (near $\pm V_{zz} = \frac{3}{4}\frac{e^2qQ}{h}$) seem to be washed out. Unfortunately the

Figure 42. Proton decoupled quadrupolar echo spectra of choline chloride as a function of temperature. 3.5 μsec 90° echo pulses were employed in each case; the number of acquisitions were: 48° = 2400, 38° = 2400, 25° = 8000, 20° = 5400, -69° = 2000, -80° = 1300.

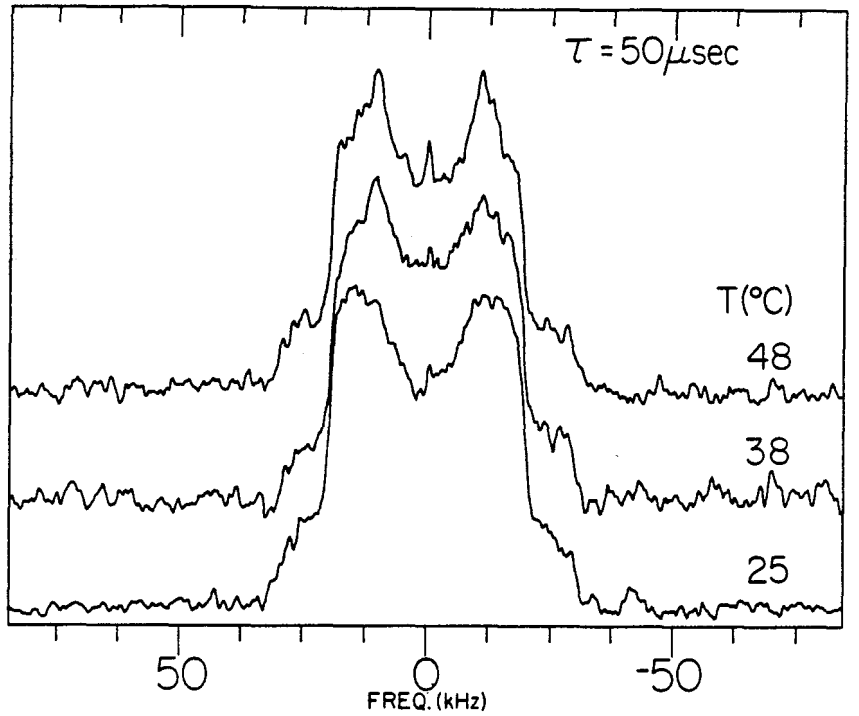

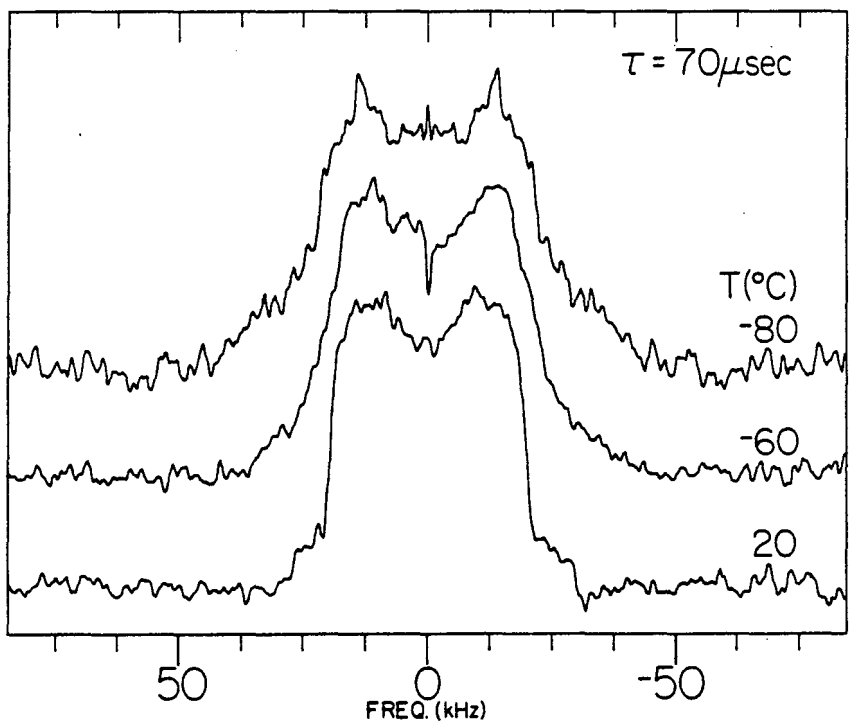

XBL 8310-12071

Figure 43. Proton decoupled quadrupolar echo spectra of choline chloride as a function of the interpulse delay τ. (a) At a temperature of 25°C, each spectrum results from 8000 acquisitions. (b) At a temperature of 48°C, number of acquisitions as follows: τ = 50, 2400 acq.; τ = 200, 9600 acq.; τ = 300, 7840 acq.

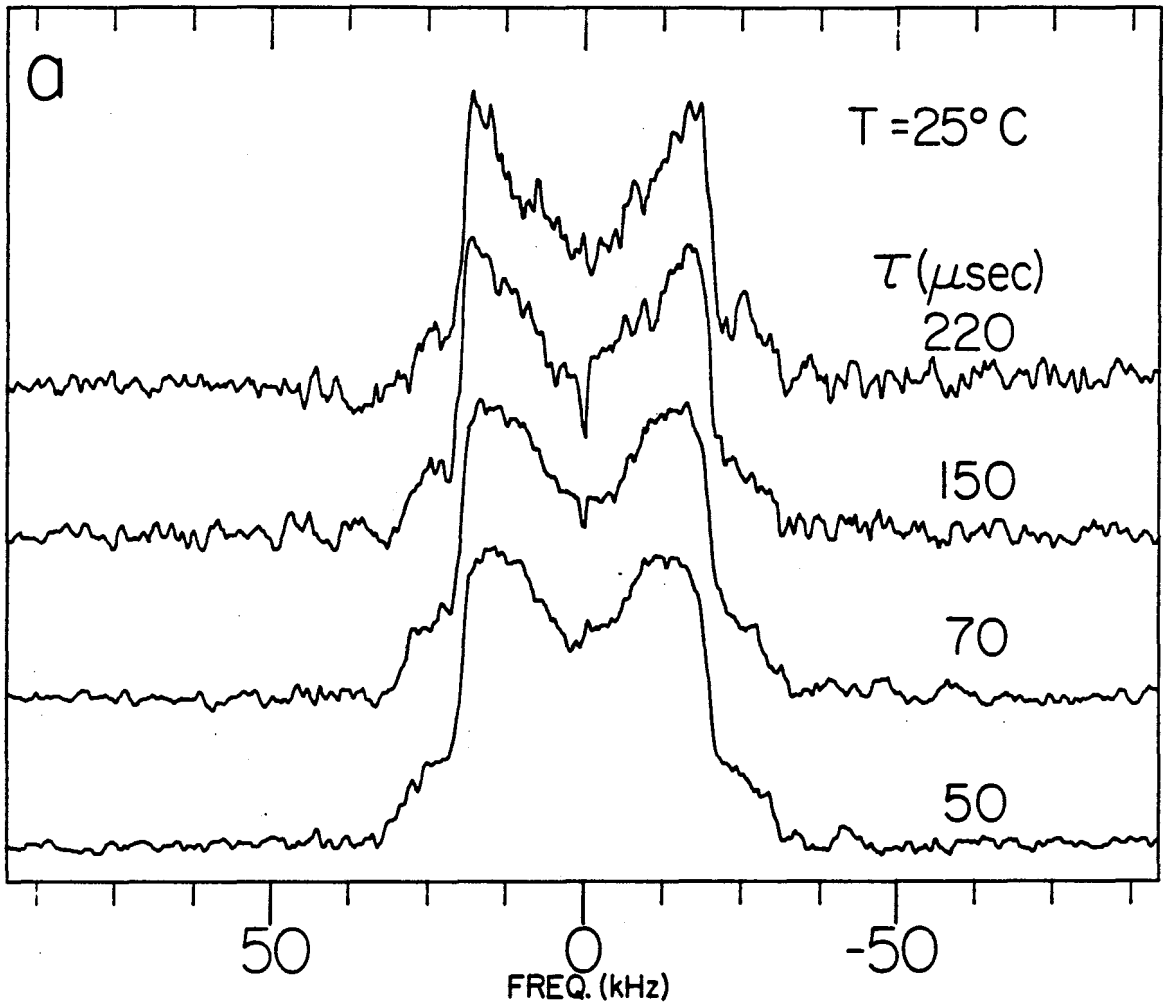

XBL 839-11498

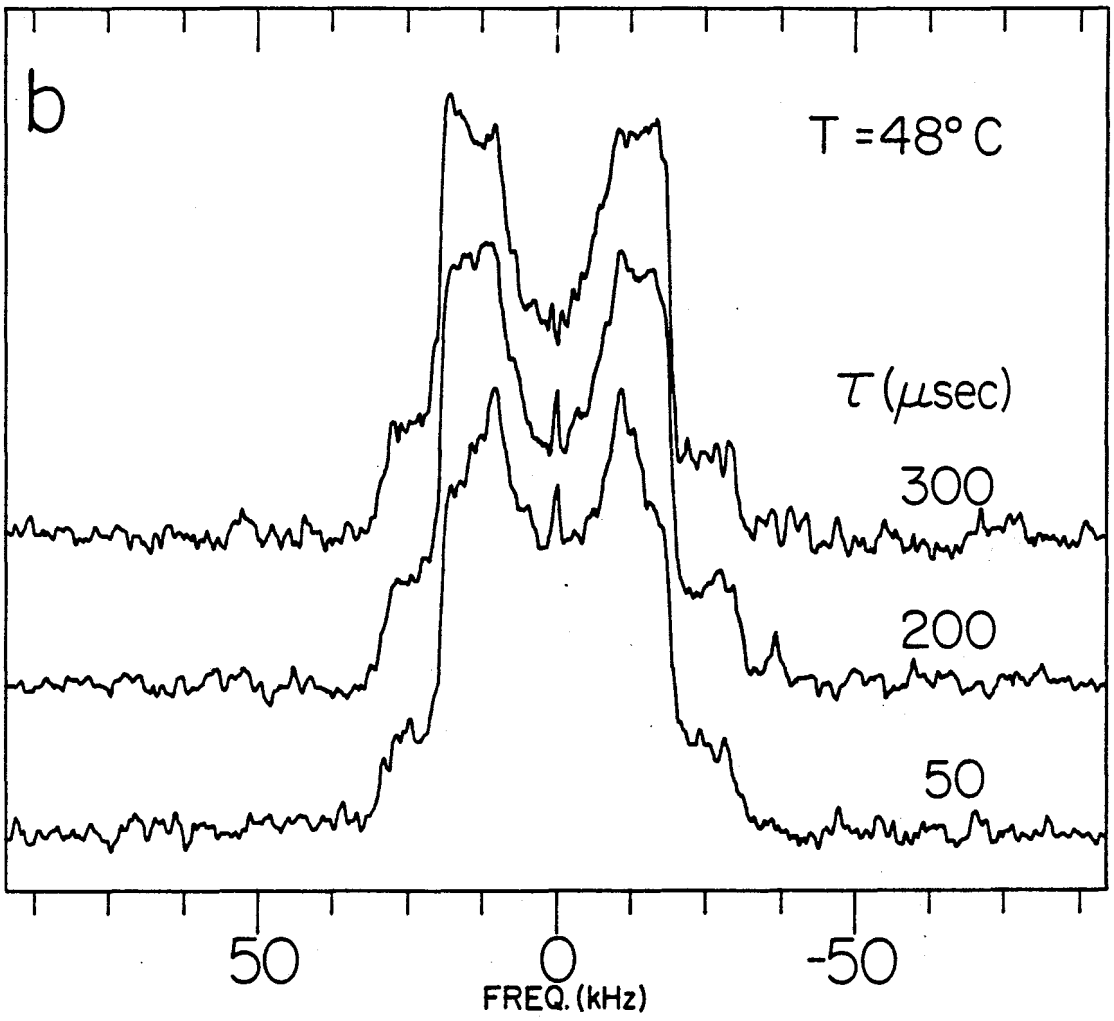

XBL 839-11496

Figure 44. The τ = 300 μsec spectrum from Figure 43b with a rigid lattice powder spectrum (e^2qQ/h = 40 kHz, η = 0.31) superimposed. It appears as if the infection points at $\pm V_{yy} = \frac{3}{8}\frac{e^2qQ}{h}(1+\eta)$ have grown in magnitude relative to the rest of the spectrum. This is an illusion caused by the relative scaling of the experimental and calculated spectra. Actually, the inflection points at $\pm V_{xx} = \frac{3}{8}\frac{e^2qQ}{h}(1-\eta)$ have collapsed relative to those at $\pm V_{yy}$.

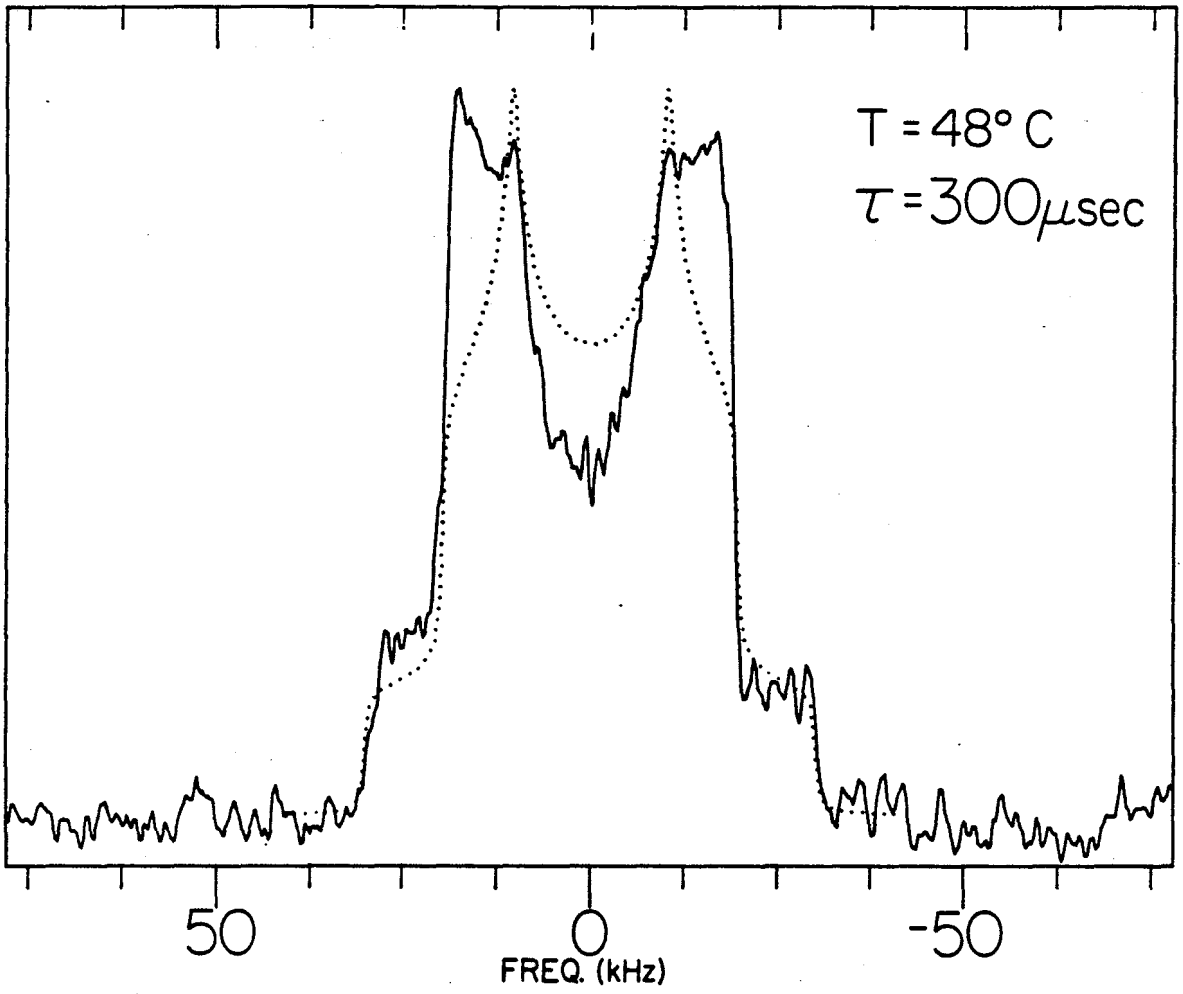

XBL 839-11487

S/N at low temperature is too low to make a definite statement regarding this last observation. The experimental data seem to immediately indicate that either the motion occurs about an axis near V_{zz}, or is of low amplitude, for otherwise the lineshape would be expected to vary to a much greater degree over this temperature range. The least distorted region of the powder pattern occurs near the inflection point corresponding to V_{yy}, indicating that the axis about which the motion occurs is probably near V_{yy}. This motion apparently occurs to a significant extent at room temperature, and should show up in room temperature crystal structure data unless it occurs by a mechanism in which the molecule flips between indistinguishable (symmetry related) positions. The crystal structure data [96,98] show very little symmetry in the molecule; even the axis passing through the $C-N^{+}(Me)_3$ moiety is not truly a C_3 axis. The crystallographic symmetry of the unit cell allows for a two fold rotation coupled with a translation (a 2_1 screw axis), but an actual molecular motion corresponding to this is very unlikely. Taking this information into account, it is nearly impossible to conceive of the molecule flipping between symmetry related positions. It has therefore been suggested that the motion is "hidden" in the anisotropic thermal parameters [136]. Fortunately Hjortas and Sorum [96] determined the anisotropic thermal parameters for all non-hydrogen atoms in their detailed crystallographic analysis of choline chloride. The motion may be inferred from such data by examination of the anisotropic thermal ellipsoids, but is more straightforwardly extracted by performing a rigid body analysis on the crystallographic data [137,138]. Such an analysis was

performed on the data of Hjortas and Sorum using the computer program THMV-1 [138]. One major axis of rotational libration with a rms amplitude of 10° (i.e., peak to peak amplitude 28°) was found passing close to the nitrogen and oxygen atoms (see Figure 45). Another smaller rotational motion of rms amplitude 3° was found approximately along the $C\text{-}N^{+}(Me)_3$ axis. This latter motion is probably associated with "C_3" rotation and I will consider it no further. Not much weight should be given to the exact orientation of the axis in Figure 45, since the program which determined it treated the entire molecule as a rigid body, when this may not be a totally adequate description. However, this axis does nearly coincide with the 180° flipping axis of choline iodide (see Figure 46). It therefore seemed reasonable to perform the lineshape calculation based upon a motion of total magnitude 30° along an axis nearly coincident with V_{yy}. Later it was found that moving slightly off V_{yy} (i.e., decreasing α in Figure 40) would account for the apparent increase in e^2qQ and decrease in η as the temperature is lowered, and also give computer simulations which are in somewhat better agreement with experiment. Initially a simple two site flip-flop model was chosen, although this certainly isn't a realistic model. The result of this calculation for various overall flip-flop rates is presented in Figure 47. There are similarities between the observed and calculated spectra, but there are also differences. The major difference is the overall more washed out appearance of the observed spectra, where the sharp spikes of the calculated spectra are not observed. This is not surprising on the basis of the unrealistic model assumed for the

Figure 45. ORTEP plots of the thermal ellipsoids of all non-hydrogen atoms in choline chloride. The methyl groups are represented by C_1, C_2, and C_3, and the chain by C_4, C_5, and O (formula: $(CH_3)_3{}^+NCH_2CH_2OH \cdot Cl$). The axis passing close to the nitrogen and oxygen atoms is that which was determined by performing a rigid body motion analysis ad described in section 4.2.3.

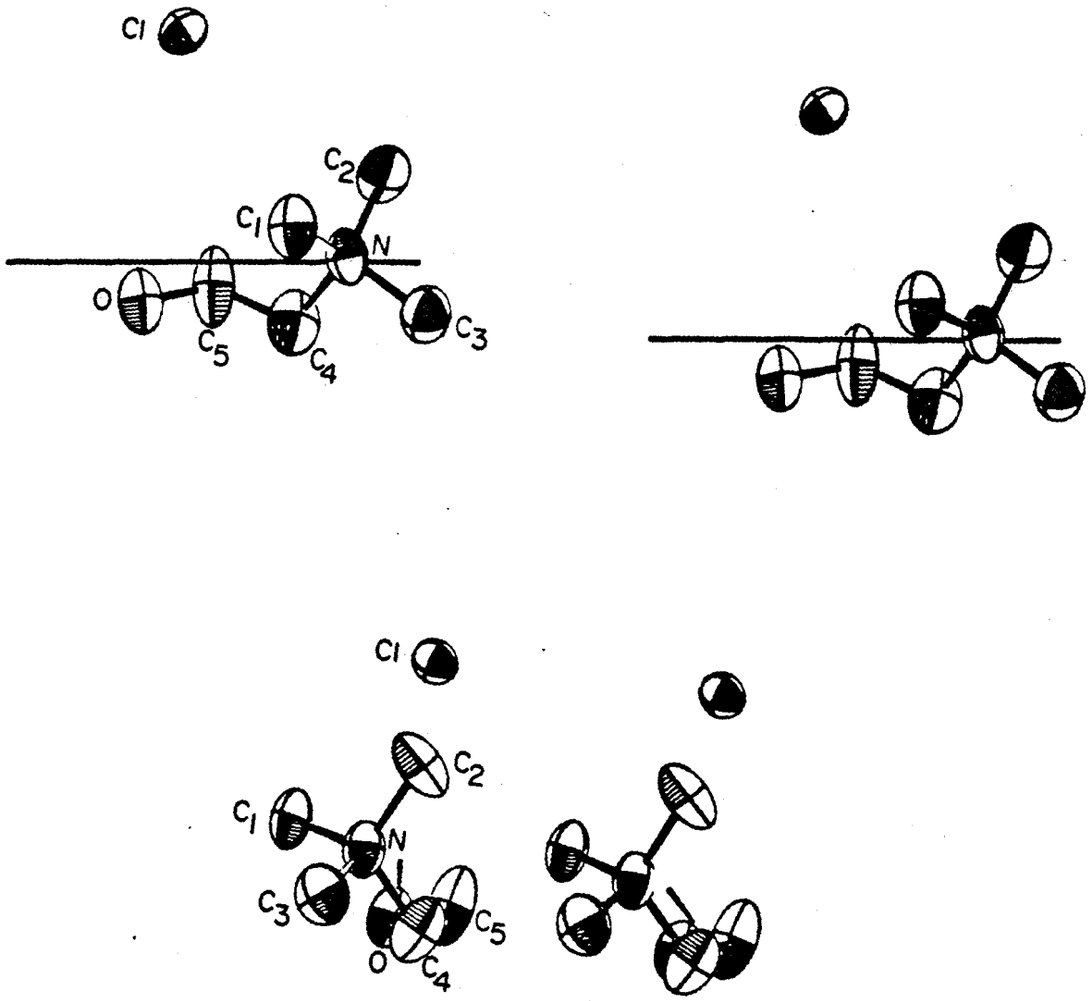

XBL 8310-12060

Figure 46. The axis of the 180° flip-flop motion in choline iodide as determined by Wemmer, *et al.* [97]. The atoms are defined as in Figure 45.

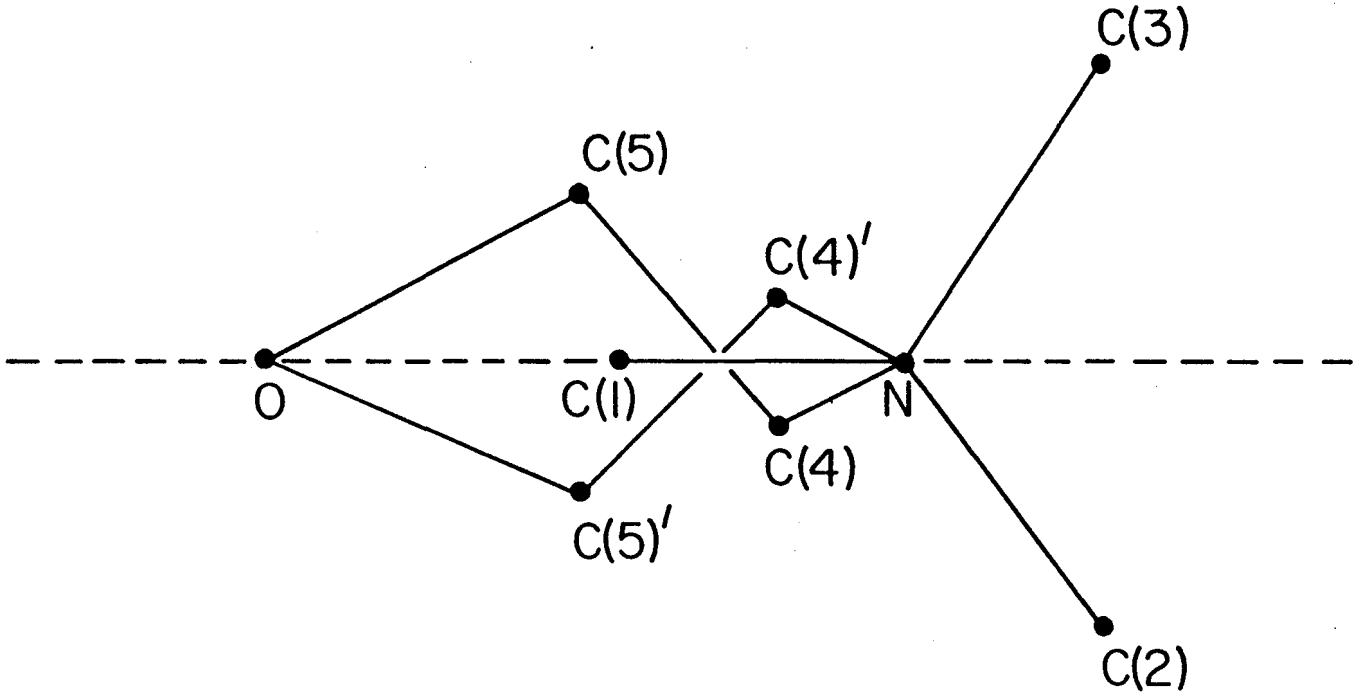

XBL 808-4306

motion. Since the molecule is probably reorienting in a potential well, a more realistic model would be one in which a large number of angular jumps were accessible to the molecule with the probability of the jump decreasing as its angular amplitude increased. This type of model is not easily calculated using the method presented in section 4.1, and a much better approach would be the asymptotic expansion method [133,134]. Nevertheless, I can try to approximate it with the method of section 4.1 by breaking the 30° jump angle into many equally spaced increments and calculating the spectrum in the hard collision limit (this is referred to by Wemmer [139] as the rotational random jump model). As the number of angular divisions increases, this model begins to approximate rotational diffusion in a square potential well. Figure 48 would seem to indicate that this model does not approximate the observed data any better; in fact it is worse. The agreement between experiment and this model would be better if the total jump angle were increased from 30°, but this diverges from the crystallographic data. If the potential well were smoothed out such that it extended well beyond 30°, but with low probability, this would probably simulate the experimental data better and would not necessarily disagree with the crystallographic data. Such a calculation, as I pointed out previously, is best done utilizing the asymptotic expansion method [132,133,134]. I should also mention that the T_{2e}'s calculated by integrating Eq. (4.13) for various τ values using the two site 30° jump model are of the same order as those observed experimentally, so that this model appears to adequately account for the variation of T_{2e} with temperature.

Figure 47. Simulations of a 30° restricted flip-flop motion in choline chloride using the parameters: e^2qQ/h = 48 kHz, η = 0.3, α = 60° and β = 90°. (a) Spectra as a function of the jump rate κ. (b) Spectra as a function of the interpulse delay τ; note that in the absence of an echo (τ=0) the spectrum appears almost as it would in the rapid motion limit.

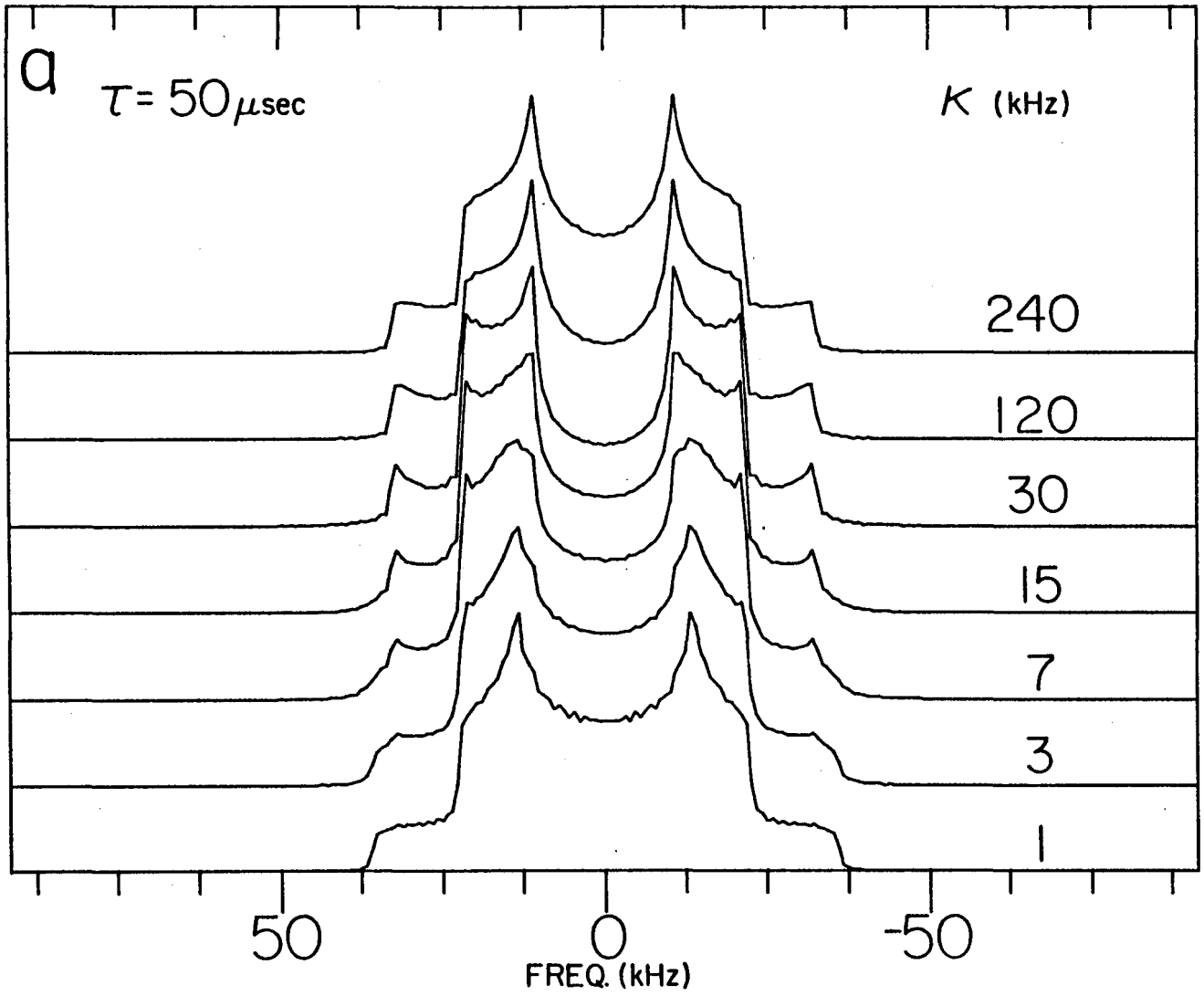

XBL 8310-12063

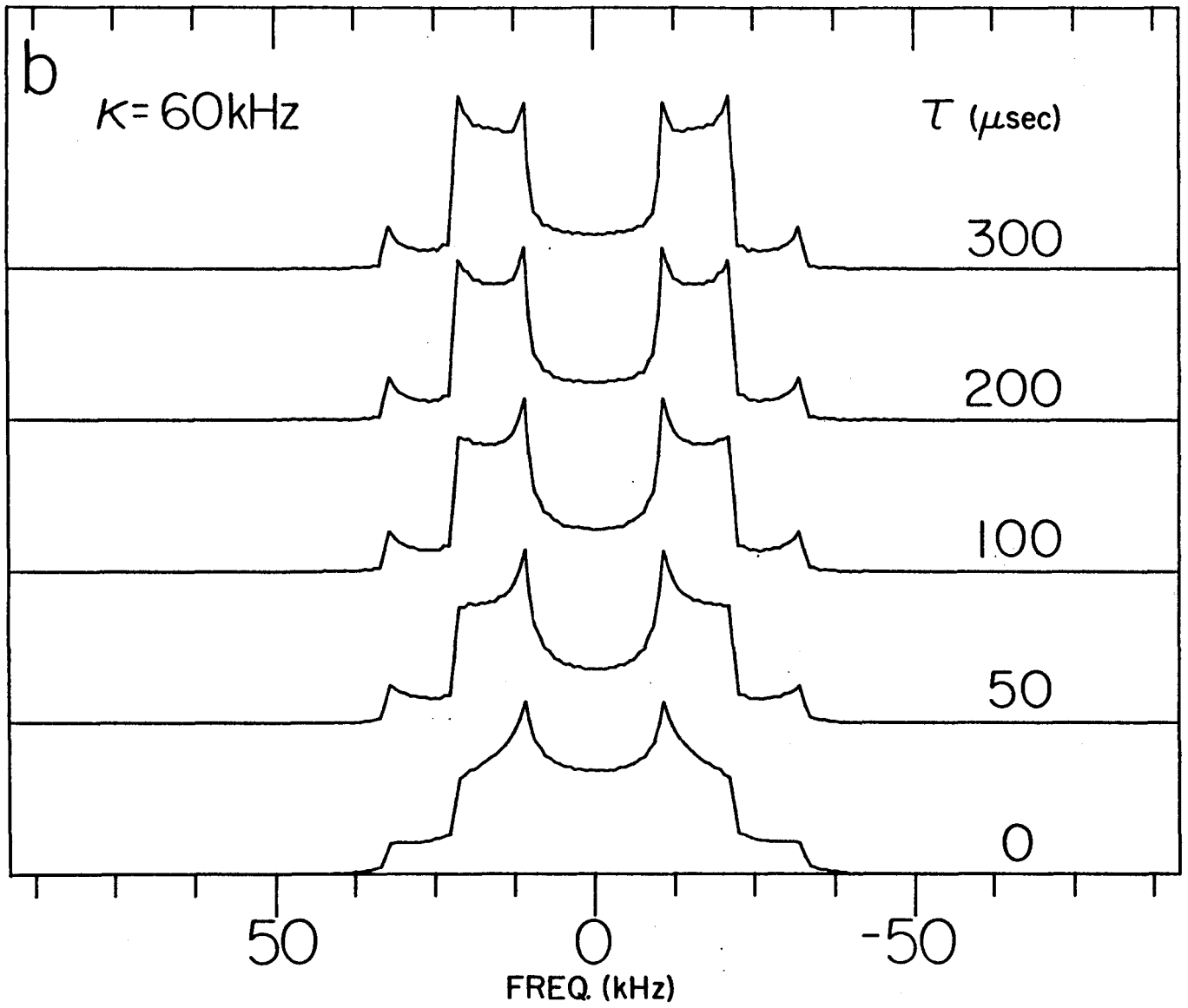

XBL 8310-12064

Figure 48. Simulations of a 30° restricted flip-flop motion in choline chloride using the same parameters as Figure 46, but the 30° were divided into 5 equal intervals and the molecule was assumed to jump between the 6 sites in the hard collision limit.

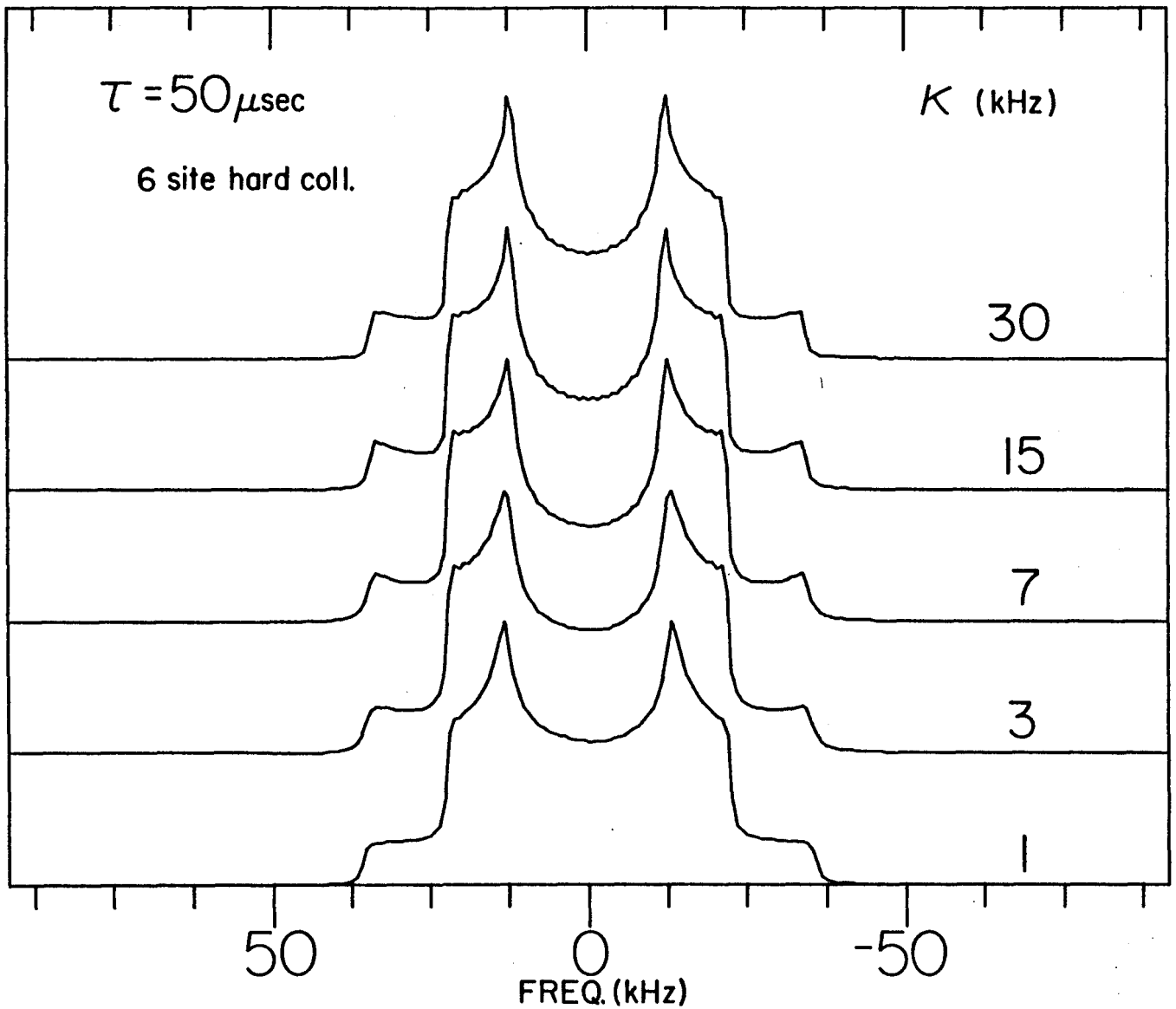

XBL 8310-12065

4.2.4 Choline Iodide

As Figure 41 indicates, the T_{2e} of choline iodide steadily decreases as the temperature drops, until at about -90°C (183 K), the echo signal disappears completely. Prior to the disappearance of the signal a broad component appears to grow in at the center of the spectrum (see Figures 29 and 49). Presumably, the signal disappears due to the presence of slow motions, and should reappear upon lowering the temperature sufficiently. At about -116°C (157 K) the signal reappeared, but the ^{14}N T_1 had increased to about 30 seconds (from 600 msec at -85°C), the T_{2e} was still very short, and a spectrum with good S/N could not be obtained. The spectrum which was obtained at this temperature appeared as a "blob" of about 100 kHz breadth. This indicates that e^2qQ/h has increased by about 50%, but we are still in an intermediate motion region (short T_{2e}, distorted spectrum.) As the temperature was lowered further, it was increasingly difficult to obtain reasonable S/N, presumably because T_1 was increasing rapidly. At -148°C (125 K) it was impossible to obtain a reasonable signal, even with recycle delays of 5 minutes. Note also that at this temperature the proton spectrum appeared as the characteristic triplet of a rigid methyl group. Unfortunately, both $T_{1\rho}$ and T_{1D} of the protons appeared to be very short ($\sim$ 100 μsec), and a cross polarization experiment would have been useless. I cannot completely disregard the possibility that this behavior has some connection with a phase transition, but I certainly would be surprised if this were the case since this behavior diverges greatly from that observed in NH_4Br and TMA Cl (see section 3.3.1). From proton resonance studies the only known

Figure 49. Proton decoupled quadrupolar echo spectra of choline iodide. (a) at various temperatures for a fixed τ; 2400 transients were acquired at each temperature. (b) at various τ's for a fixed temperature. All spectra result from 2400 acquisitions.

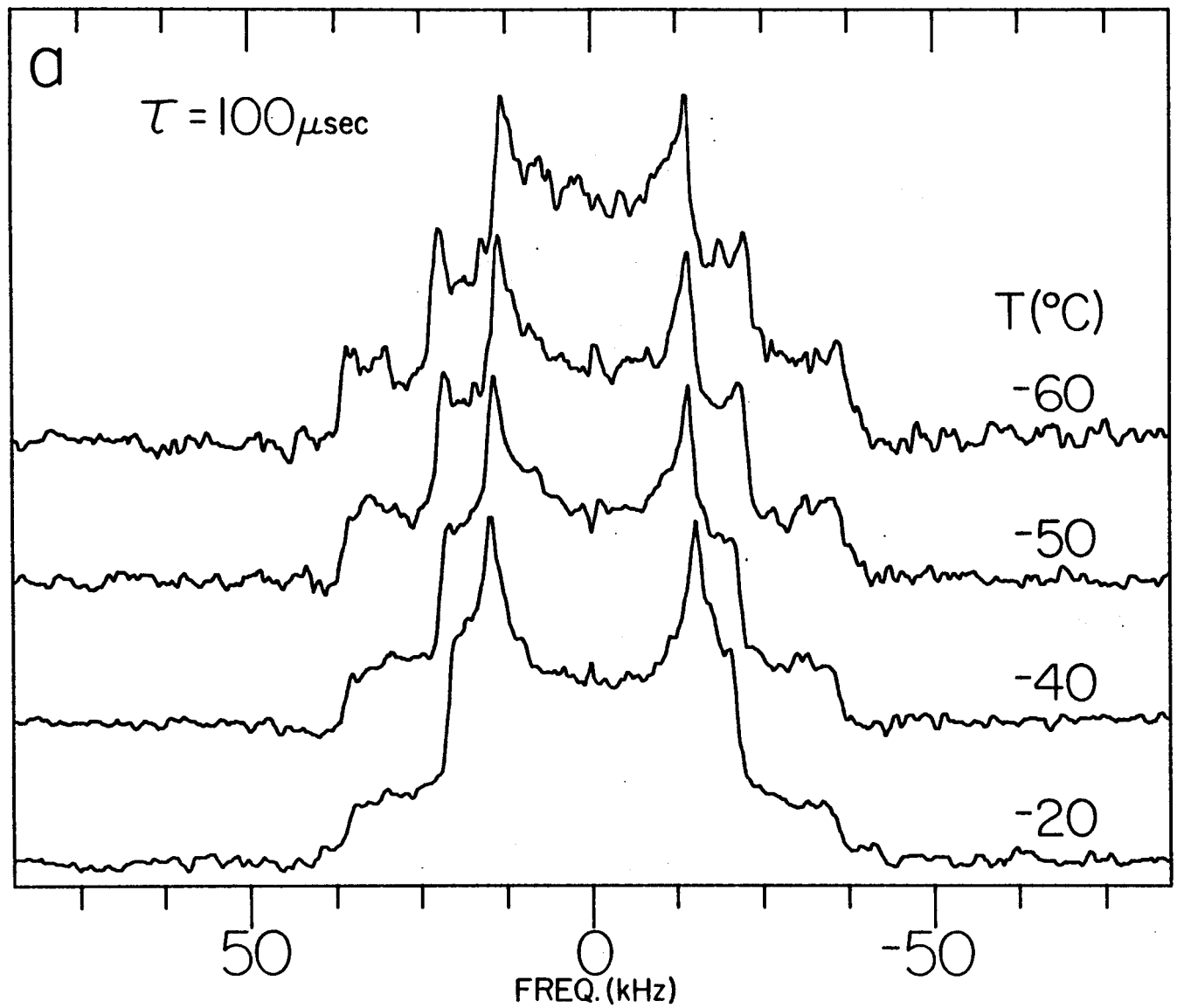

XBL 8310-12066

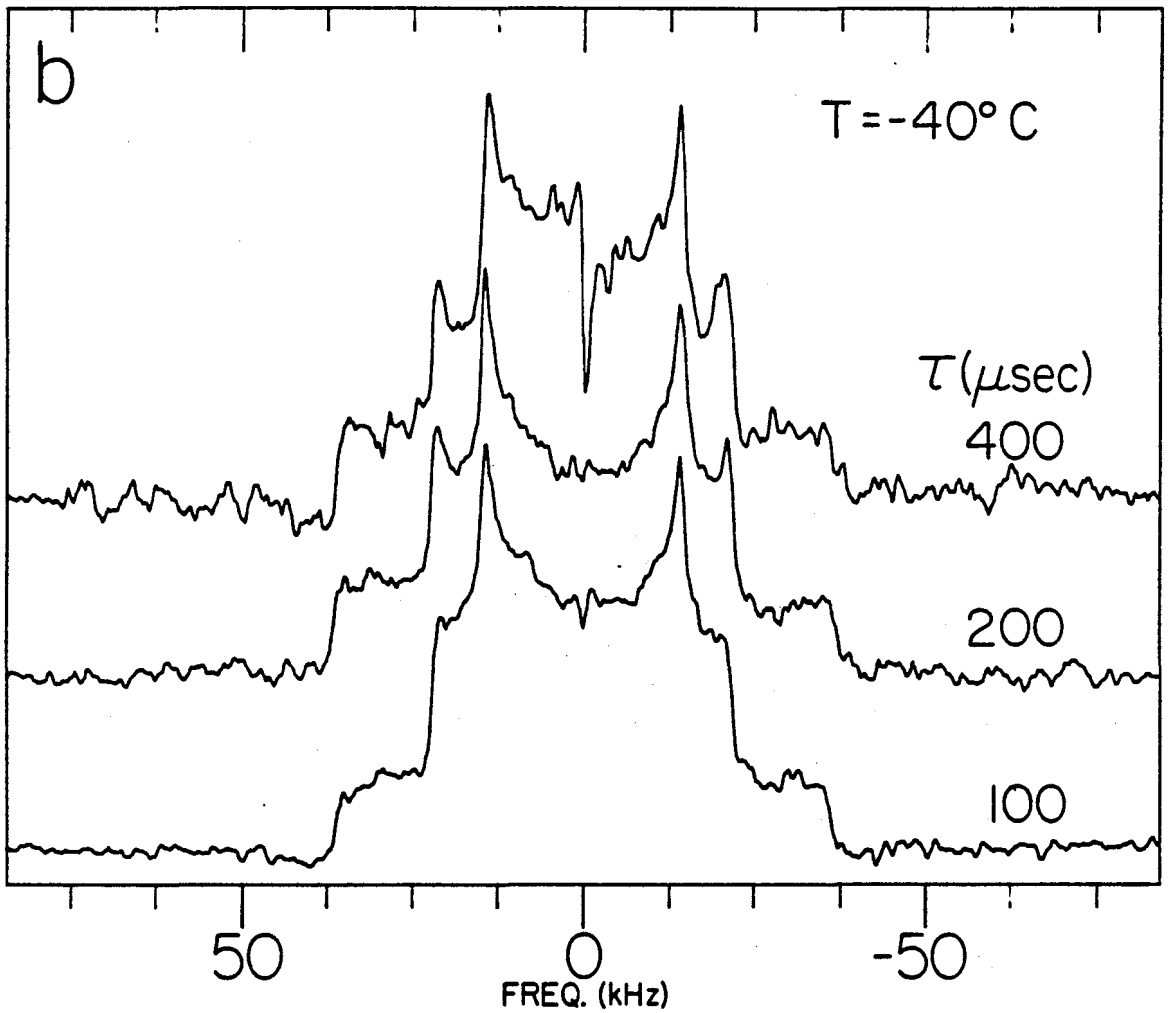

XBL 839-11493

motion which could be quenched in this low temperature region is methyl group rotation, and it is difficult to imagine how this might have such a large effect on the ^{14}N efg, especially when it does not seem to have much effect in choline chloride (other than increasing the ^{14}N T_1). The 180° flip-flop motion inferred from the x-ray crystallographic study [97] is therefore assumed to be the cause. If we assume the static efg to be axially symmetric and of 50% larger magnitude than that observed in the rapid motion limit, it becomes possible to calculate the orientation of the molecular flipping axis relative to the principle axis of the static efg (see Figure 50). It was found that the observed spectra (Figure 51) could not be simulated by assuming an axially symmetric efg. The flipping of an axially symmetric efg always leads to a collapse of the center of the lineshape in the quadrupolar echo spectra (see, for example, references [86] and [127]) while the observed spectra show sharp spikes at V_{xx}, V_{yy}, and V_{zz}. It was found that this type of distortion is easily simulated if the static efg is assumed to be axially asymmetric, and if the flipping axis is situated near the V_{xx} direction, or if the flipping axis is nearly 90° relative to V_{xx} (i.e., nearly along V_{yy}). Since V_{xx}, V_{yy}, and V_{zz} are two-fold axes, flipping about any of these will not alter the spectrum. Therefore, the angles α and β (see Figure 40) must be chosen such that α is nearly 90° and β is between 0° and 90°. If the static value of V_{zz} is assumed to be 50% larger than the motionally averaged V_{zz}, then the required angle β may be determined and also the value of the static asymmetry parameter. The required static efg is given by e^2qQ/h = 67 kHz, η = 0.5, where α = 90° and β = 25°. The results of

Figure 50. Calculated variation of the quadrupole coupling constant and asymmetry parameter (as observed in the rapid motion limit) as a function of the angle between the principle axis of the efg and the axis of 180° flip-flop (see Figure 40). The static asymmetry parameter is assumed to be zero, so this plot would be of more use in ^2H NMR. Values for $\beta > 45°$ are a reflection of the data for $\beta < 45°$. The angle α (Figure 40) has no meaning here since $V_{xx} = V_{yy}$ in the static efg.

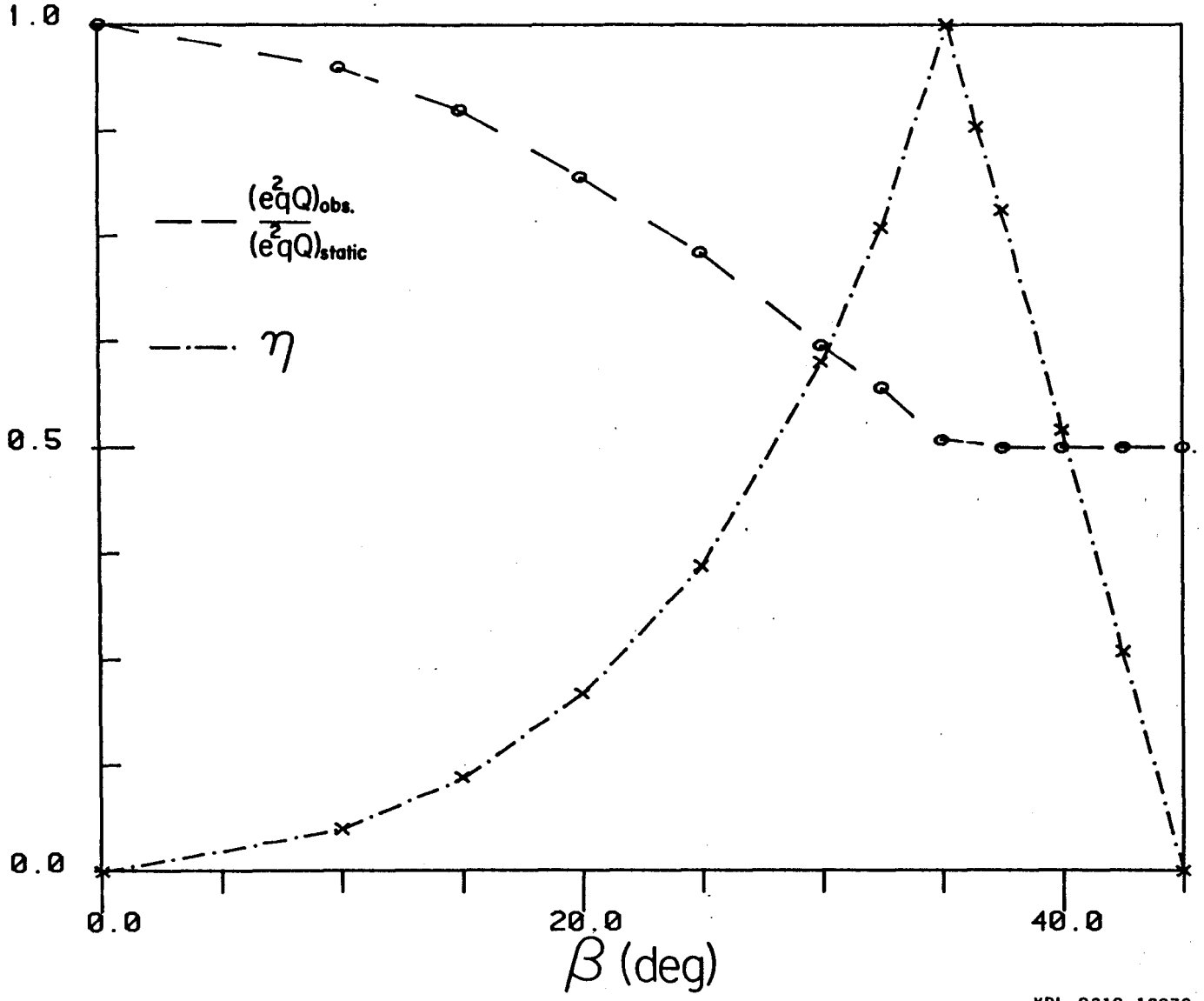

XBL 8310-12070

Figure 51. Proton decoupled quadrupolar echo spectrum of choline iodide at -50°C with a rigid lattice powder spectrum (e^2qQ/h = 48 kHz, η = 0.24) superimposed. Note how the infection points V_{yy} and V_{zz} appear as spikes.

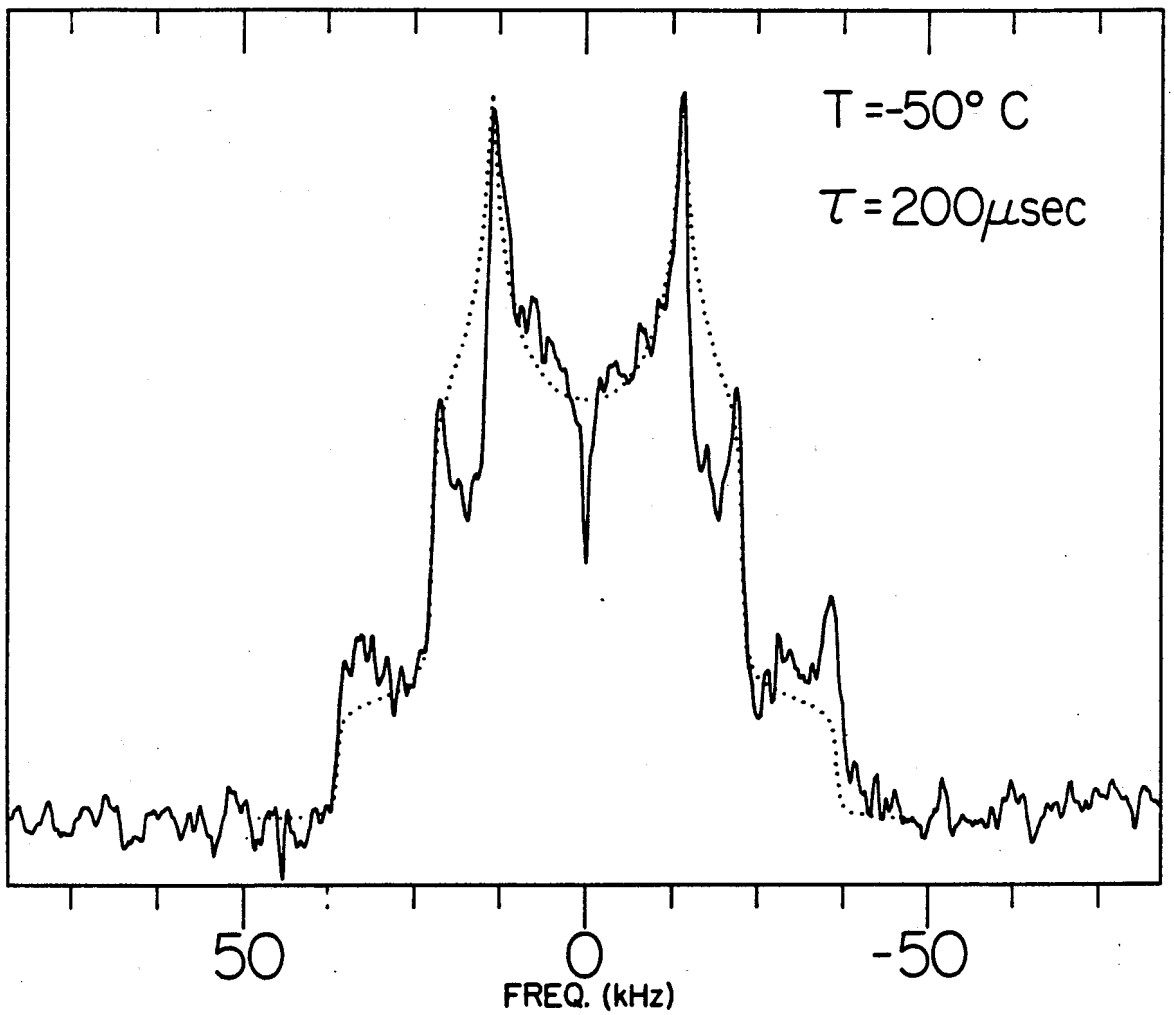

XBL 839-11486

a 180° flip-flop calculation using these parameters are shown in Figure 52. The spikes at the inflection points are reproduced, but there are differences between the observed and calculated spectra. The intensity between the V_{xx} points decreases in the calculated spectra in a way which is not observed experimentally. Instead, the center of the observed spectra seems to fill in; and, as I mentioned before, the lineshape eventually becomes entirely washed out. This behavior cannot be simulated by any type of 180° flip-flop motion; the echo spectra resulting from such a mechanism will always have a "hole" near the center because T_2 here is very short (frequencies near the center result from exchange between widely separated parts of the spectrum). The easiest way to simulate this behavior with a jump model is if the jumps occur about V_{zz} (3 fold jumps about this axis seem best). This immediately brings to mind 3 fold jumps about the $C\text{-}N^{+}(Me)_3$ axis, but the proton NMR studies show that this motion is completely quenched by -40°C [121]. An additional discrepancy is the observation that the shoulders of the calculated spectra wash out as the frequency drops, while this is not observed in the experimental lineshape prior to its disappearance at -90°C. It is easily understood why the shoulders of the calculated spectra wash out: as the flip-flop frequency decreases the static V_{zz} is ineffectively averaged and begins to reappear, thus washing out the higher frequency parts of the powder pattern. Decreasing the value of the static efg will cause this washing out effect to become less important, and this observation led me to assume that the efg being averaged by the flip-flops is nearly the same as that observed

Figure 52. The calculated effect of 180° flip-flops in choline iodide. The static efg was assumed to be given by e^2qQ/h = 67 kHz and η = 0.5, and relationship between the flipping axis and the efg was given by α = 90° and β = 25°. The calculation was run at low frequency resolution to save cpu time; in a higher resolution calculation the spikes at V_{yy} and V_{zz} would be more prominent.

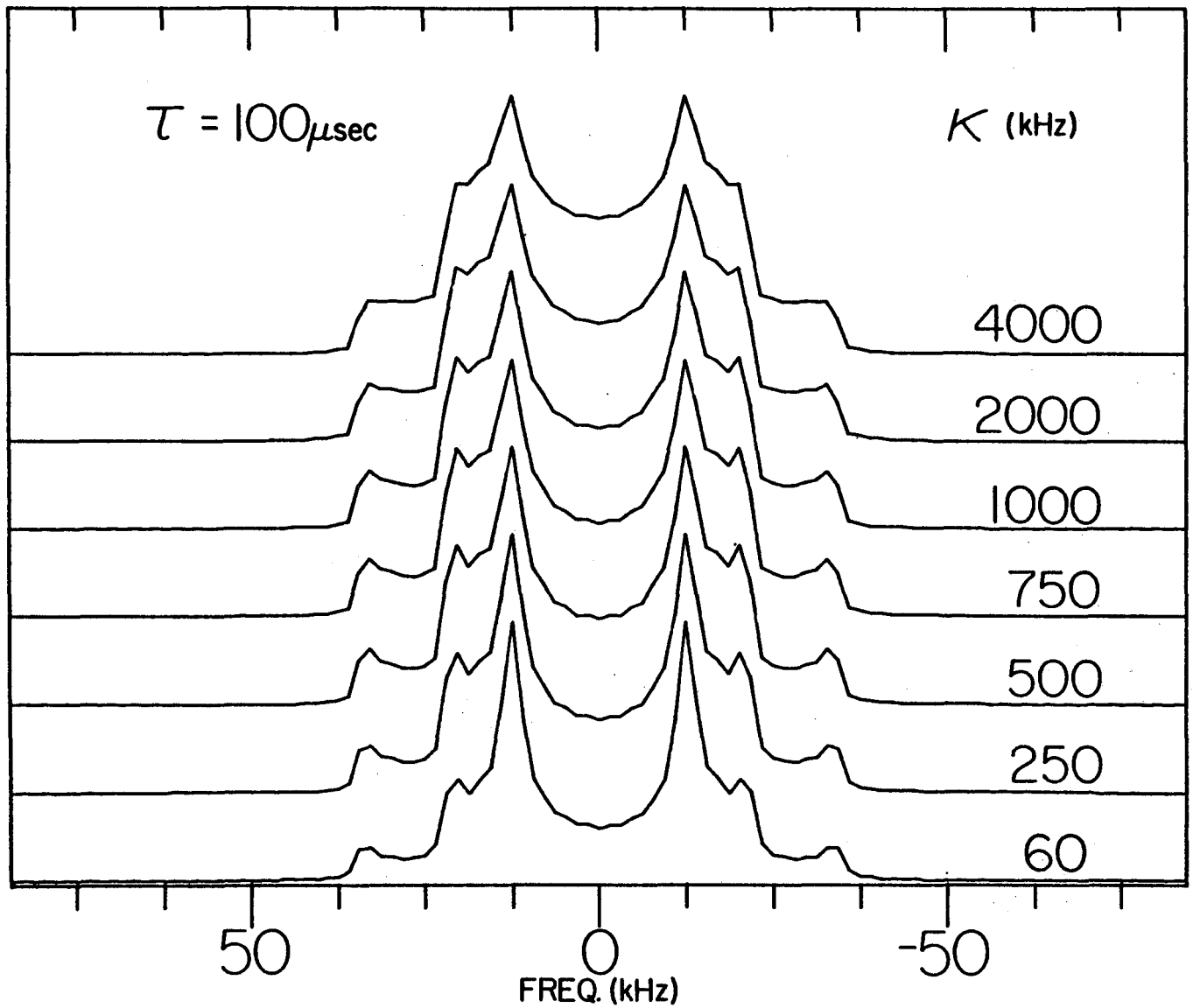

XBL 8310-12069

at higher temperatures. Making such an assumption leads to the simulations of Figure 53, which seem to approximate the observed data somewhat more closely. The axis about which this flip-flop motion occurs has very nearly the same relationship to the efg as does the axis which I determined for choline chloride. Since the crystallographic evidence indicates that the relationship of the two axes in the reference frame of the choline ion is nearly coincident (see Figures 45 and 46), this observation makes some sense. The T_{2e}'s which were calculated based upon this model, by integrating Eq. (4.13) for various τ values, were found to approximate those observed experimentally, but this model does not predict that T_{2e} will become so short as to cause a disappearance of the echo signal. Additionally, the rate of the motion in Figure 52 is too slow to be an effective ^{14}N spin-lattice relaxation mechanism, while the very short ^{14}N T_1's observed indicate that a very effective relaxation mechanism is active above -90°C. For this reason I must assume that two motions are present, a relatively slow 180° flip-flop motion and a much more rapid motion of undefined nature which acts as an effective T_1 mechanism and also causes a filling in of the center of the echo spectra. This is yet another enigma upon which some light may be shed by a single crystal study (the single crystal lines could probably be observed throughout the temperature range since a quadrupolar echo would be unnecessary).

4.3 Conclusions

Unfortunately, I have been required to make so many assumptions here that the validity of any conclusions is difficult to assess. Nevertheless, I do believe that a few strong statements can be

Figure 53. The calculated effect of 180° flip-flops in choline iodide. The static efg was assumed to be given by e^2qQ/h = 48 kHz and η = 0.3, and the relationship between the flipping axis and the efg was given by α = 90° and β = 85°. Note that an identical result is obtained for α = 90° and β = 5° since a plane of reflection exists with respect to this calculation at β = 45°.

(a) Spectra at various flip-flop rates (K) for a fixed τ = 100 μsec.

(b) Spectra at various τ's for a fixed K = 60 kHz (compare this with Figure 49b). The calculation here was done at lower resolution than (a) in order that cpu time might be saved.

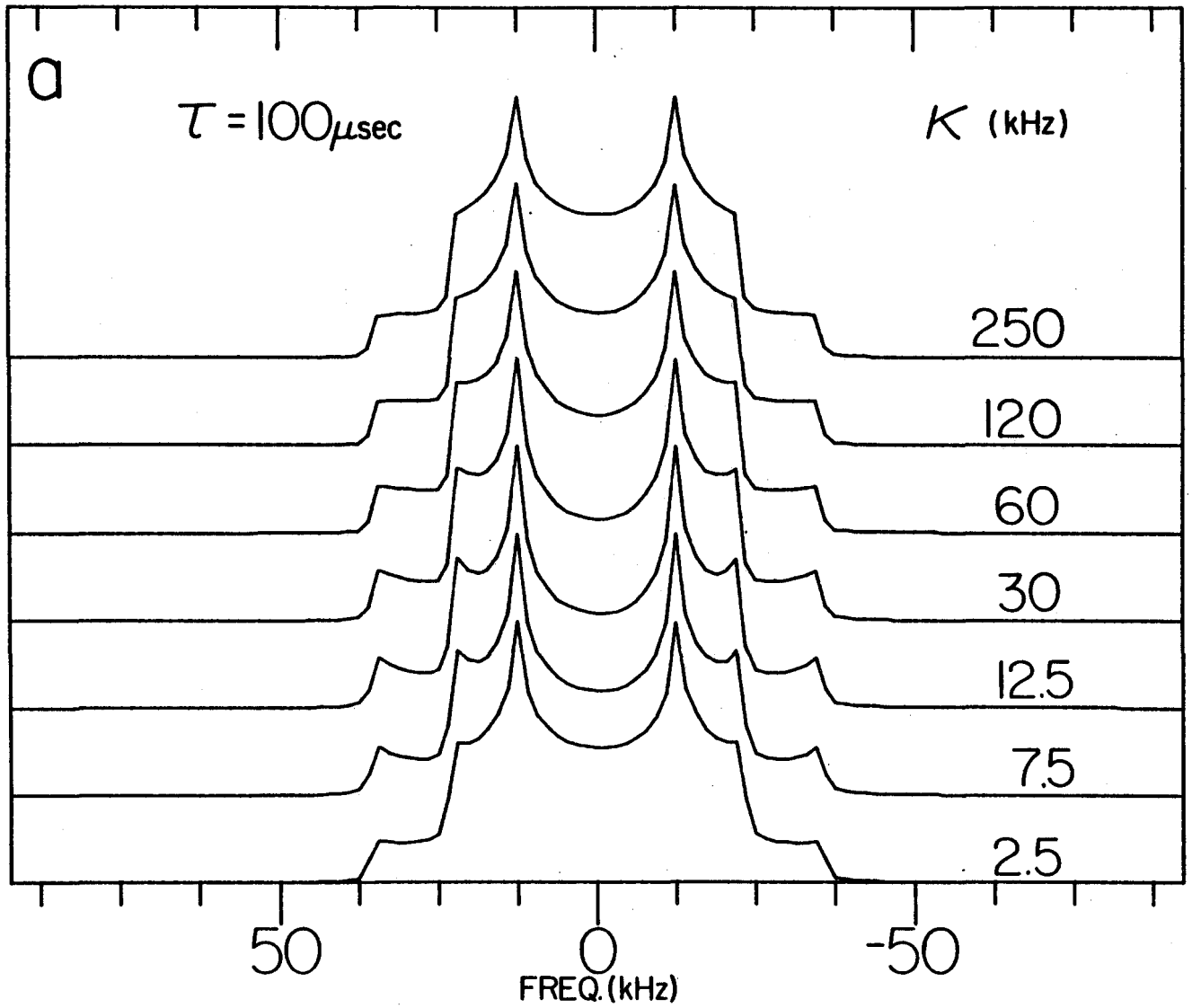

XBL 8310-12067

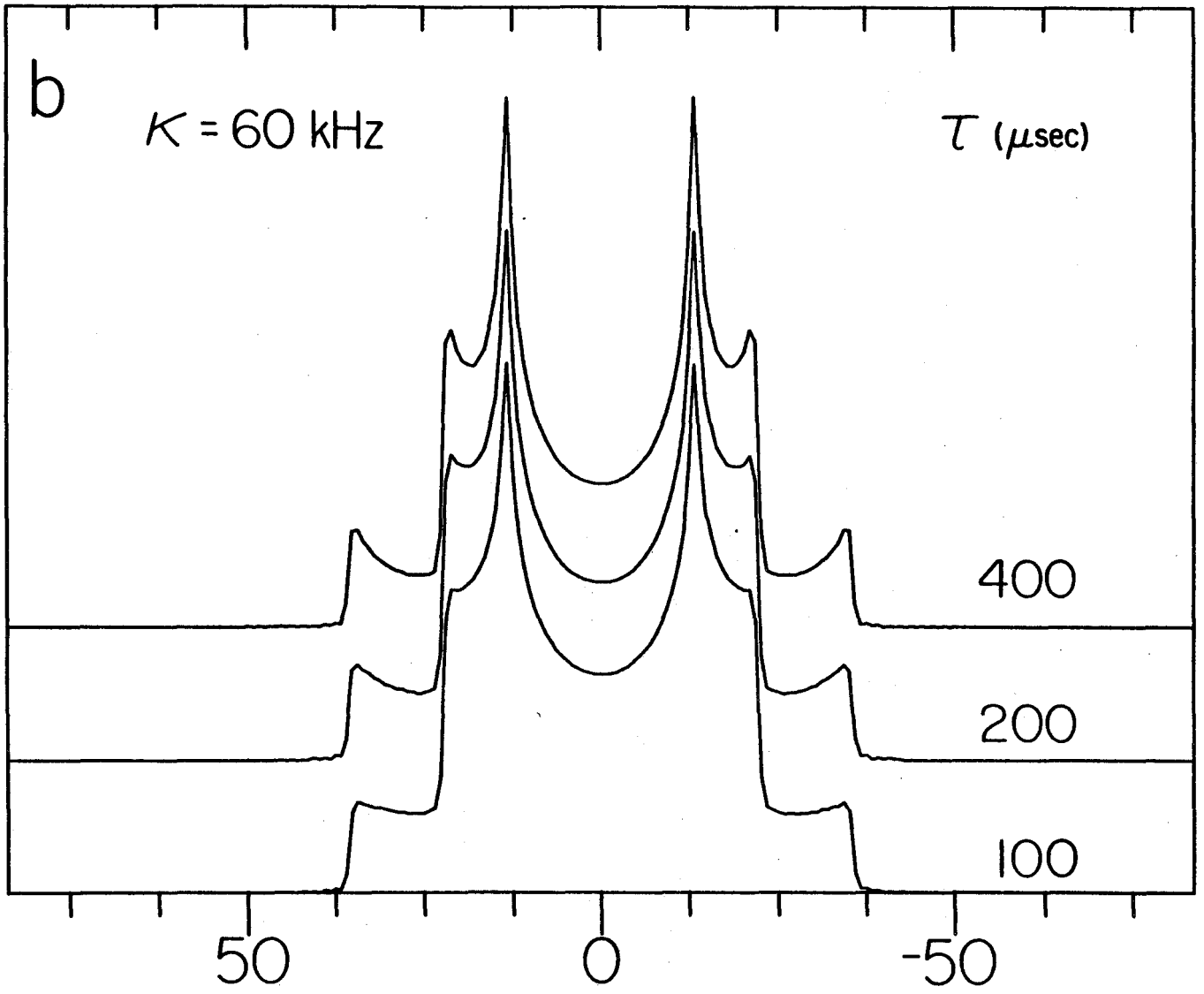

XBL 8310-12068

made.

The assumption of a substantially, or entirely intramolecular efg seems justified, although a truly rigorous approach to this problem may lead to a different conclusion. Invoking this assumption leads to the conclusion that the observed choline chloride spectra can be approximated by assuming a restricted motion about a fixed axis of total approximate amplitude 30°. The agreement between experimental and theoretical spectra would no doubt be helped by the assumption of a distribution of jump angles with a total width of about 30°.

There appear to be a number of ways in which the observed choline iodide spectra could come about, and these should be narrowed prior to making any definite statements. Still, the appearance of spikes in the lineshape near V_{xx}, V_{yy}, and V_{zz} indicate that 180° flip-flop motions are occurring on a tensor which would be axially asymmetric were it not flipping. The mounding of the lineshape and its disappearance at low temperature must, for the present, be classified as due to unknown processes.

In a global context, it appears that both choline chloride and iodide have a tendency to flip, but the potential barrier is too high in the chloride, permitting only torsional oscillations in its potential well. In this context, an x-ray crystallographic study is clearly indicated for choline bromide to determine whether it too has a tendency to flip; as well as to seek the origins of its vastly different quadrupolar coupling parameters. The rapid flip-flop motions present in choline iodide (whose rate must exceed 500 kHz at room temperature) may explain the radiation insensitivity

of this salt by preventing chain propogation steps necessary for radiolysis from occurring. If this is true, then any such motions present in choline bromide must be restricted, as they are in the chloride.

I have several times mentioned that a single crystal ^{14}N NMR study is in order for these salts. As far as elucidating the molecular dynamics of the ion are concerned, a much easier procedure would be to perform deuterium NMR on a series of deuterated analogues. Wemmer et al. [97] have performed ^{2}H NMR on these compounds substituted at the hydroxyl position (which are easily prepared by exchange with D_2O), and it is not surprising that few interesting observations are made. The most useful position to locate ^{2}H in order to investigate the motions which have been proposed, would be C(4) (see Figure 45). By employing ^{2}H NMR one would not have to deal with the difficult interpretation of the ^{14}N efg in these ionic salts (the ^{2}H efg in aliphatic compounds is almost always axial, has $e^2qQ/h \sim 170$ kHz, and is almost entirely intramolecualr). Additionally, it has been shown [118] that choline chloride deuterated at this position has nearly the same degree of radiation sensitivity as the non-deuterated salt.

Appendix A

Spherical Tensors

It is generally assumed that all nuclear spin interactions in solids can be represented by second rank Cartesian tensors as [41]

$$\mathcal{H} = \underset{\sim}{I} \cdot \underset{\approx}{A} \cdot \underset{\sim}{S}$$

$$= (I_x, I_y, I_z) \cdot \begin{bmatrix} A_{xx} & A_{xy} & A_{xz} \\ A_{yx} & A_{yy} & A_{yz} \\ A_{zx} & A_{zy} & A_{zz} \end{bmatrix} \cdot \begin{bmatrix} S_x \\ S_y \\ S_z \end{bmatrix} \quad , \qquad (A.1)$$

where $\underset{\sim}{I}$ and $\underset{\sim}{S}$ are tensors of the first rank and $\underset{\approx}{A}$ is a tensor of the second rank. $\underset{\approx}{A}$ will relate to the dipolar, quadrupolar, or chemical shift coupling of the molecule, and will contain all of the geometrical information relating the principle axis system (PAS) of the tensor to the outside world. (The PAS defines the reference frame in which the tensor is diagonal). It is most convenient to derive a relation between the tensor and the static field H_0, with respect to which the interaction is generally truncated. This relation may be obtained by construction of a spherical tensor $\underset{\approx}{T}_k$ from $\underset{\approx}{A}$, and rotation of that tensor about the Euler angles (α,β,γ) as [42]:

$$T'_{kq} = R(\alpha,\beta,\gamma)\ T_{kq} R^{-1}(\alpha,\beta,\gamma) = \sum_{p=-k}^{k} T_{kp} D^{k}_{pq}(\alpha,\beta,\gamma) \quad , \qquad (A.2)$$

where $D^k_{pq}(\alpha,\beta,\gamma)$ represent Wigner rotation matrix elements. The spherical tensor $\underset{\approx}{T}_k$ may be constructed from $\underset{\approx}{A}$ via the product rule for two irreducible tensor operators [42]:

$$T_{kq}(x,y) = \sum_{m_1 m_2} \langle k_1 m_1 k_2 m_2 | k, m_1+m_2 \rangle T_{k_1 m_1}(x) T_{k_2 m_2}(y) \qquad (A.3)$$

where $T_{k_1 m_1}(x)$ and $T_{k_2 m_2}(y)$ represent first rank irreducible tensors and $\langle k_1 m_1 k_2 m_2 | k, m_1+m_2 \rangle$ is a Clebsch-Gordan coefficient. The components T_{kq} of the spherical tensor derived from a Cartesian tensor $\underset{\approx}{A}$ will be

$$T_{00} = -\frac{1}{3}(A_{xx}+A_{yy}+A_{zz}) \qquad (A.4a)$$

$$T_{10} = -\frac{i}{2}(A_{xy}-A_{yx}) \qquad (A.4b)$$

$$T_{1\pm1} = -\frac{1}{2}(A_{zx}-A_{xz} \pm i(A_{yz}+A_{zy})) \qquad (A.4c)$$

$$T_{20} = \frac{1}{\sqrt{6}}(3\,A_{zz}-(A_{xx}+A_{yy}+A_{zz})) \qquad (A.4d)$$

$$T_{2\pm1} = \pm\frac{1}{2}(A_{xz}+A_{zx} \pm i(A_{yz}+A_{zy})) \qquad (A.4e)$$

$$T_{2\pm2} = \frac{1}{2}(A_{xx}-A_{yy} \pm i(A_{xy}+A_{yx})) \quad . \qquad (A.4f)$$

Equation (A.1) may be expressed as

$$\mathcal{H} = A_{xx}I_xS_x + A_{yx}I_yS_x + A_{zx}I_zS_x$$

$$+ A_{xy}I_xS_y + A_{yy}I_yS_y + A_{zy}I_zS_y$$

$$+ A_{xz}I_xS_z + A_{yz}I_yS_z + A_{zz}I_zS_z$$

$$= \sum_{i,j=x,y,z} A_{ij}I_iS_j \quad , \tag{A.5}$$

which, in terms of spherical tensors, becomes

$$\mathcal{H} = \sum_{k=0}^{2} \sum_{q=-k}^{k} (-1)^q \, A_{kq}T_{kq} \quad . \tag{A.6}$$

Here, A_{kq} are the spherical tensor elements derived from the Cartesian tensor $\underset{\approx}{A}$, and T_{kq} are derived from the product of two first rank tensors I S. Under geometrical rotation, the A_{kq} only are rotated; T_{kq} will be rotated in "spin space".

To see how this works, consider the all important quadrupole coupling interaction:

$$\mathcal{H}_Q = \frac{eQ}{2I(2I-1)\hbar} \; \underset{\sim}{I} \cdot \underset{\approx}{V} \cdot \underset{\sim}{I} \quad . \tag{A.7}$$

Here, $\underset{\approx}{V}$ refers to the Cartesian electric field gradient (efg) tensor, which is diagonal in its own PAS. There are, therefore, only two irreducible spherical tensor elements which are non-zero

$$A_{20} = \frac{3}{\sqrt{6}} V_{zz} \quad , \quad \text{and}$$

$$A_{2\pm2} = \frac{1}{2} (V_{xx}-V_{yy}) \quad .$$

From (A.6) it is apparent that the only irreducible spin tensor elements needed are

$$T_{20} = \frac{1}{\sqrt{6}} (3\ I_z^{\ 2} - (I_x^{\ 2}+I_y^{\ 2}+I_z^{\ 2}))$$

$$= \frac{1}{\sqrt{6}} (3\ I_z^{\ 2} - I(I+1)), \quad \text{and}$$

$$T_{2\pm2} = \frac{1}{2} (I_x^{\ 2}-I_y^{\ 2}\pm i(I_xI_y+I_yI_x)) \quad ,$$

to yield

$$\mathcal{H}_Q = \frac{eQ}{4I(2I-1)\hbar} (V_{zz}(3\ I_z^{\ 2}-I(I+1)) + (V_{xx}-V_{yy})(I_x^{\ 2}-I_y^{\ 2})) \tag{A.8}$$

$$= \frac{e^2qQ}{4I(2I-1)\hbar} (3\ I_z^{\ 2}-I(I+1) + \eta(I_x^{\ 2}-I_y^{\ 2})) \quad , \tag{A.9}$$

where $\eta = \frac{V_{xx}-V_{yy}}{V_{zz}}$ and $eq = V_{zz}$. For our application to high field, the term $I_x^{\ 2}-I_y^{\ 2}$ will mix the Zeeman eigenstates $|+1\rangle$ and $|-1\rangle$ (i.e., it is non-secular)and needs to be lopped off, giving the truncated Hamiltonian:

$$\mathcal{H}_Q = \frac{eQ}{4I(2I-1)\hbar} V_{zz}(3\ I_z^{\ 2}-I(I+1)) \quad . \tag{A.10}$$

To obtain the orientation dependence of $\mathcal{H}_Q$ with respect to H_0, we need only rotate $V_{zz} = \frac{\sqrt{6}}{3} A_{20}$ about the Euler angles (α,β,γ) using Equation (A.2):

$$V'_{zz} = \frac{\sqrt{6}}{3} \left(\frac{3}{\sqrt{6}} D^2_{00} V_{zz} + \frac{(D^2_{20}-D^2_{-20})}{2} (V_{xx}-V_{yy})\right) \quad . \tag{A.11}$$

The $D^k_{pq}(\alpha\beta\gamma)$ may be determined using the relation [42]:

$$D^k_{pq}(\alpha\beta\gamma) = e^{-i\alpha p}\, d^k_{pq}(\beta)\, e^{-i\gamma q} \tag{A.12}$$

and any standard table of d^k_{pq} to yield:

$$\mathcal{H}_Q = \frac{eQ}{4I(2I-1)\hbar} (3\, I_z{}^2 - I(I+1)) \cdot$$

$$\left(\frac{3\cos^2\beta-1}{2}\right) V_{zz} + \frac{\sin^2\beta\, \cos 2\alpha}{2} (V_{xx}-V_{yy}) \tag{A.13}$$

$$= \frac{e^2 qQ}{4I(2I-1)\hbar} (3\, I_z{}^2 - I(I+1)) \left(\frac{1}{2}(3\cos^2\beta-1) + \frac{\eta}{2} \sin^2\beta\, \cos 2\alpha\right) \tag{A.14}$$

This expression is introduced in chapter 1, and used extensively throughout this work.

Appendix B

Fictitious Spin 1/2 Operators

The dynamics of a spin 1/2 particle may be completely described by the three angular momentum operators I_x, I_y and I_z; while, for a spin one particle, eight orthogonal operators are required. We may choose these to be the three angular momentum operators, plus linearly independent quadratic combinations of them. On this basis it is possible to construct the fictitious spin 1/2 operators. Our purpose in constructing them is to have three pseudo-two level angular momentum operators in each of three pseudo-Cartesian reference frames. The name "fictitious spin 1/2" derives from the supposition that a perturbation at resonance on one transition of a multilevel system will allow us to ignore all other transitions and consider a fictitious spin 1/2 system [3].

The double quantum operators [23] $I_{p,i}$ ($p = x,y,z$; $i=1,2,3$) have been constructed solely for the purpose of describing the dynamics of spin 1 nuclei, while the single transition operators [21] I_p^{i-j} ($p = x,y,z$; $i,j=1,2,3$) have been constructed for use on any multi-level spin system. With regard to spin one nuclei, the $I_{p,i}$ operators will lead to more efficient computation when the system is very near to Larmor resonance, but the I_p^{i-j} operators are somewhat easier to visualize in terms of the spin 1/2 operators and I will present them here.

In the Zeeman basis $|+1\rangle$, $|0\rangle$, $|-1\rangle$ we can construct nine operators which span the space of a spin one nucleus as [22]:

$$I_x^{1-2} = \frac{1}{2}\begin{pmatrix} 0 & 1 & 0 \\ 1 & 0 & 0 \\ 0 & 0 & 0 \end{pmatrix}, \quad I_y^{1-2} = -\frac{i}{2}\begin{pmatrix} 0 & 1 & 0 \\ -1 & 0 & 0 \\ 0 & 0 & 0 \end{pmatrix}, \quad I_z^{1-2} = \frac{1}{2}\begin{pmatrix} 1 & 0 & 0 \\ 0 & -1 & 0 \\ 0 & 0 & 0 \end{pmatrix}$$

$$I_x^{2-3} = \frac{1}{2}\begin{pmatrix} 0 & 0 & 0 \\ 0 & 0 & 1 \\ 0 & 1 & 0 \end{pmatrix}, \quad I_y^{2-3} = -\frac{i}{2}\begin{pmatrix} 0 & 0 & 0 \\ 0 & 0 & 1 \\ 0 & -1 & 0 \end{pmatrix}, \quad I_z^{2-3} = \frac{1}{2}\begin{pmatrix} 0 & 0 & 0 \\ 0 & 1 & 0 \\ 0 & 0 & -1 \end{pmatrix}$$

$$I_x^{1-3} = \frac{1}{2}\begin{pmatrix} 0 & 0 & 1 \\ 0 & 0 & 0 \\ 1 & 0 & 0 \end{pmatrix}, \quad I_y^{1-3} = -\frac{i}{2}\begin{pmatrix} 0 & 0 & 1 \\ 0 & 0 & 0 \\ -1 & 0 & 0 \end{pmatrix}, \quad I_z^{1-3} = \frac{1}{2}\begin{pmatrix} 1 & 0 & 0 \\ 0 & 0 & 0 \\ 0 & 0 & -1 \end{pmatrix}$$

where the I_z^{i-j} operators are linearly dependent through

$$I_z^{1-3} = I_z^{1-2} + I_z^{2-3} \quad . \tag{B.1}$$

Obviously, these operators are meant to perform as Cartesian angular momentum operators I_x, I_y and I_z for the $|+1\rangle-|0\rangle$, $|0\rangle-|-1\rangle$ and $|+1\rangle-|-1\rangle$ transitions. Their relationship to the spin 1 angular momentum operators

$$I_x = \frac{1}{\sqrt{2}}\begin{pmatrix} 0 & 1 & 0 \\ 1 & 0 & 1 \\ 0 & 1 & 0 \end{pmatrix}, \quad I_y = -\frac{i}{\sqrt{2}}\begin{pmatrix} 0 & 1 & 0 \\ -1 & 0 & 1 \\ 0 & -1 & 0 \end{pmatrix}, \quad I_z = \begin{pmatrix} 1 & 0 & 0 \\ 0 & 0 & 0 \\ 0 & 0 & -1 \end{pmatrix}$$

is

$$I_x = \sqrt{2}\,(I_x^{1-2} + I_x^{2-3}) \quad , \tag{B.2a}$$

$$I_y = \sqrt{2}\,(I_y^{1-2} + I_y^{2-3}) \quad , \text{ and} \tag{B.2b}$$

$$I_z = 2\, I_z^{1-3} \quad . \tag{B.2c}$$

Additionally, the double quantum 1-3 operators are given by

$$I_x^{1-3} = \frac{1}{2}\,(I_x^{\,2} - I_y^{\,2}) \quad , \quad \text{and} \tag{B.2d}$$

$$I_y^{1-3} = \frac{1}{2}\, I_x I_y + I_y I_x) \quad . \tag{B.2e}$$

The operators I_+^{i-j} and I_-^{i-j} are formed in complete analogy with the spin 1/2 case.

In the case of Cartesian angular momentum operators we know that

$$e^{-i\theta I_p}\, I_q\, e^{i\theta I_p} = I_q \cos\theta + i[I_q, I_p]\sin\theta \quad , \tag{B.6}$$

Thus, knowledge of the cyclic commutators [21]:

$$[I_x^{i-j}, I_y^{i-j}] = i\, I_z^{i-j} \quad , \tag{B.7a}$$

$$[I_x^{i-j}, I_x^{j-k}] = \frac{i}{2}\, I_y^{i-k} \quad , \tag{B.7b}$$

$$[I_y^{i-j}, I_y^{j-k}] = -\frac{i}{2}\, I_y^{j-k} \quad , \tag{B.7c}$$

$$[I_x^{i-j}, I_y^{j-k}] = -\frac{i}{2}\, I_x^{i-k} \quad , \tag{B.7d}$$

and the non-cyclic ones (see Table B.I) allow one to determine the evolution of any operator due to any other, and thus the evolution of any density matrix expanded in terms of these operators. In the case of the I_z^{i-j} operators, their linear dependence (Equation (B.1))

precludes the use of Eq. (B.6) and the rotation matrices of Table B.II must be used

$$e^{-i\theta I_p} I_q e^{i\theta I_p} = U I_q U^{\dagger} \quad . \tag{B.8}$$

When considering a system on resonance, it is desirable to condense the I_p^{i-j} operators to the form of the $I_{p,i}$ operators via a rotation about I_y^{1-3} of $\pi/2$. The correspondence between the two sets of operators in this frame becomes:

$$I_{x,1} = I_x^{2-3} \tag{B.9a}$$

$$I_{y,1} = I_y^{1-2} \tag{B.9b}$$

$$I_{z,1} = I_x^{1-3} \tag{B.9c}$$

$$I_{x,2} = - I_y^{2-3} \tag{B.9d}$$

$$I_{y,2} = I_x^{1-2} \tag{B.9e}$$

$$I_{z,2} = I_y^{1-3} \tag{B.9f}$$

$$I_{x,3} = - I_z^{2-3} \tag{B.9g}$$

$$I_{y,3} = - I_z^{1-2} \tag{B.9h}$$

$$I_{z,3} = I_z^{1-3} \quad . \tag{B.9i}$$

These relations allow us the possibility of using the large volume of work already present regarding the $I_{p,i}$ operators [2,23,40] for calculations involving the I_p^{i-j} operators.

Table B.I
$[A,B] = x$

A \ B	S_x^{1-2}	S_x^{2-3}	S_x^{1-3}	S_y^{1-2}	S_y^{2-3}	S_y^{1-3}	S_z^{1-2}	S_z^{2-3}	S_z^{1-3}
S_x^{1-2}	0	$\frac{i}{2} S_y^{1-3}$	$\frac{i}{2} S^{2-3}$	$i\, S_z^{1-2}$	$-\frac{i}{2} S_x^{1-3}$	$-\frac{i}{2} S_x^{2-3}$	$-i\, S_y^{1-2}$	$\frac{i}{2} S_y^{1-2}$	$-\frac{i}{2} S_y^{1-2}$
S_x^{2-3}	$-\frac{i}{2} S_y^{1-3}$	0	$-\frac{i}{2} S_y^{1-2}$	$\frac{i}{2} S_x^{1-3}$	$i\, S_z^{2-3}$	$\frac{i}{2} S_x^{1-2}$	$\frac{i}{2} S_y^{2-3}$	$-i\, S_y^{2-3}$	$-\frac{i}{2} S_y^{2-3}$
S_x^{1-3}	$-\frac{i}{2} S_y^{2-3}$	$\frac{i}{2} S_y^{1-2}$	0	$-\frac{i}{2} S_x^{2-3}$	$\frac{i}{2} S_x^{1-2}$	$i\, S_z^{1-3}$	$-\frac{i}{2} S_y^{1-3}$	$-\frac{i}{2} S_y^{1-3}$	$-i\, S_y^{1-3}$
S_y^{1-2}	$-i\, S_z^{1-2}$	$-\frac{i}{2} S_x^{1-3}$	$\frac{i}{2} S_x^{2-3}$	0	$-\frac{i}{2} S_y^{1-3}$	$\frac{i}{2} S_y^{2-3}$	$i\, S_x^{1-2}$	$-\frac{i}{2} S_x^{1-2}$	$\frac{i}{2} S_x^{1-2}$
S_y^{2-3}	$\frac{i}{2} S_x^{1-3}$	$-i\, S_z^{2-3}$	$-\frac{i}{2} S_x^{1-2}$	$\frac{i}{2} S_y^{1-3}$	0	$-\frac{i}{2} S_y^{1-2}$	$-\frac{i}{2} S_x^{2-3}$	$i\, S_x^{2-3}$	$\frac{i}{2} S_x^{2-3}$
S_y^{1-3}	$\frac{i}{2} S_x^{2-3}$	$-\frac{i}{2} S_x^{1-2}$	$-i\, S_y^{1-3}$	$\frac{i}{2} S_y^{2-3}$	$\frac{i}{2} S_y^{1-2}$	0	$\frac{i}{2} S_x^{1-3}$	$\frac{i}{2} S_x^{1-3}$	$i\, S_x^{1-3}$
S_z^{1-2}	$i\, S_y^{1-2}$	$-\frac{i}{2} S_y^{2-3}$ *	$\frac{i}{2} S_y^{1-3}$ *	$-i\, S_x^{1-2}$	$-\frac{i}{2} S_x^{2-3}$ *	$-\frac{i}{2} S_x^{1-3}$ *	0	0	0
S_z^{2-3}	$-\frac{i}{2} S_y^{1-2}$ *	$i\, S_y^{2-3}$	$\frac{i}{2} S_y^{1-3}$ *	$\frac{i}{2} S_x^{1-2}$ *	$-i\, S_x^{2-3}$	$-\frac{i}{2} S_x^{1\ 3}$ *	0	0	0
S_z^{1-3}	$\frac{i}{2} S_y^{1-2}$ *	$\frac{i}{2} S_y^{2-3}$ *	$i\, S_y^{1-3}$	$-\frac{i}{2} S_x^{1-2}$ *	$-\frac{i}{2} S_x^{2-3}$ *	$-i\, S_x^{1-3}$	0	0	0

*because of the linear dependence of the S_z^{i-j} operators, this commutator cannot be used to perform rotations.

Table B.II

$$U_p^{i-j}(\theta) = \exp(-i\theta I_p^{i-j})$$

$$U_x^{1-2}(\theta) = \begin{bmatrix} \cos\frac{\theta}{2} & -i\sin\frac{\theta}{2} & 0 \\ -i\sin\frac{\theta}{2} & \cos\frac{\theta}{2} & 0 \\ 0 & 0 & 1 \end{bmatrix}, \qquad U_y^{1-2}(\theta) = \begin{bmatrix} \cos\frac{\theta}{2} & -\sin\frac{\theta}{2} & 0 \\ \sin\frac{\theta}{2} & \cos\frac{\theta}{2} & 0 \\ 0 & 0 & 1 \end{bmatrix}$$

$$U_x^{2-3}(\theta) = \begin{bmatrix} 1 & 0 & 0 \\ 0 & \cos\frac{\theta}{2} & -i\sin\frac{\theta}{2} \\ 0 & -i\sin\frac{\theta}{2} & \cos\frac{\theta}{2} \end{bmatrix}, \qquad U_y^{2-3}(\theta) = \begin{bmatrix} 1 & 0 & 0 \\ 0 & \cos\frac{\theta}{2} & -\sin\frac{\theta}{2} \\ 0 & \sin\frac{\theta}{2} & \cos\frac{\theta}{2} \end{bmatrix}$$

$$U_x^{1-3}(\theta) = \begin{bmatrix} \cos\frac{\theta}{2} & 0 & -i\sin\frac{\theta}{2} \\ 0 & 1 & 0 \\ -i\sin\frac{\theta}{2} & 0 & \cos\frac{\theta}{2} \end{bmatrix}, \qquad U_y^{1-3}(\theta) = \begin{bmatrix} \cos\frac{\theta}{2} & 0 & -\sin\frac{\theta}{2} \\ 0 & 1 & 0 \\ \sin\frac{\theta}{2} & 0 & \cos\frac{\theta}{2} \end{bmatrix}$$

$$U_z^{1-2}(\theta) = \begin{bmatrix} e^{-\frac{i\theta}{2}} & 0 & 0 \\ 0 & e^{\frac{i\theta}{2}} & 0 \\ 0 & 0 & 1 \end{bmatrix}, \qquad U_z^{2-3}(\theta) = \begin{bmatrix} 1 & 0 & 0 \\ 0 & e^{-\frac{i\theta}{2}} & 0 \\ 0 & 0 & e^{\frac{i\theta}{2}} \end{bmatrix}$$

Table B.II continued

$$U_z^{1-3}(\theta) = \begin{bmatrix} e^{-\frac{i\theta}{2}} & 0 & 0 \\ 0 & 1 & 0 \\ 0 & 0 & e^{\frac{i\theta}{2}} \end{bmatrix}$$

Appendix C

Computer Programs

Several times I present computer simulations which are intended to link my ideas with the observable world. It is probably not inappropriate here to present two of the programs which were used for simulating purposes on the Laboratory of Chemical Biodynamics VAX 11/780.

The program DQTP is a derivative of Jim Murdoch's DQC [2]. DQTP performs a number of useful calculations pertaining to isolated spin one nuclei. Time domain signals may be generated for arbitrary pulse sequences by integrating over ideal powder lineshapes (which must be supplied externally). Additionally, the simple cross-polarization theory outlined in section 2.4 is employed to calculate cross-polarized echo signals such as those which are presented in Figures 18, 19 and 26. The time domain signals which are generated are easily Fourier transformed using the IMSL routine FFT2C [83].

The program RJUMP integrates Eq. (4.13) over all orientations to produce a time domain echo signal which begins at the echo maximum. This signal is then numerically transformed using the IMSL routine FFT2C [83]. If the imaginary part of the time domain signal is retained in the transform, then a chemical shift type of powder pattern will result, while if this channel is zeroed then a spin one quadrupolar powder pattern is produced. Two other programs were often used which are simple extentions of this program. T2JUMP was used to calculate echo decays (T_{2e}) caused by jumping motions via integration of Eq. (4.13) for various τ values at t=0 . FTJUMP was used to calculate frequency domain spectra by integrating Eq. (4.14) over orientations.

```
 program dqtp
c
c calculates evolution in a spin 1 system
c
 dimension yy(2048,4),xx(2048,4),sumyy(2048,4),ixx(4),iyy(4),
 1wt(2048,2)
 character*1 joff,yyy,ans,ans2,hans,ansq,ansr,ansp,ansn,typps
 1,ansswp,dmflag,typcp
 data yyy/121/
 data sumyy,wt/8192*0.0,4096*0.0/
 integer rlim
 complex dm
 common n,woff,wq,v1(20),ph(20),t(20),as(3,3),dm(3,3),
     1  idm/ksfx/ivar,nvar,nvinc,vinc/test/hans,yyy,typps,dmflag,typcp
 1/bdpar/wt/MIXDM/NOP,IDMM(9),COEFX(9)/cppar/omegh,bdeff,tmix,epsln
c
 isumwq=0
 nsum=1
 wqnot=0.0
 noff=1
 woffinc=0.0
 wqinc=0.0
c
 type 500
500 format(t2,'Evolution of an initial density matrix is calculated'/
 1t2,'possible IDM s:'/t10,'x1=1,x2=2,x3=3'/t10,'y1=4,y2=5,y3=6'/
 1t10,'z1=7,z2=8,z3=9'/t10,'mixture=10,cp dm=11'/)
 type 489
489 format(t2,'do you want to use the x,y,z(y) ',
 1',or the +1,0,-1(m) basis?',$)
 read(5,10)hans
 if(hans.ne.yyy)then
 type 490
490 format(t2,'-in this basis we start with Z, 3(z**2)-s(s+1) (=9)',
 1'or cp dm')
 end if
 type 501
501 format(/,' what is the initial density matrix ? ',$)
 accept *,idm
 if(idm.eq.10)call mixset
 if(idm.eq.11)call predm(ncpstp,pdmf)
 type 502
502 format(' how many steps in your pulse sequence ? ',$)
 accept *,nsteps
c
 type 460
460 format(t2,'do you wish to at some point swap/zero dm elements',
 1'(y/n)?',$)
 read(5,10)ansswp
 if(ansswp.eq.yyy)call swapp
 type 450
450 format(/t2,'do you wish to average a parameter over many quadrup',
 1'ole frequencies(y/n)?',$)
 read(5,10)ansq
```

```
 if(ansq.eq.yyy)then
 wqnot=0.0
 end if
c
 type 470
470 format(t2,'do you wish to read the intensities out of a pporg4',
 1' file(y/n)?',$)
 read(5,10)ansn
 if(ansn.eq.yyy)then
 call ppread(wqc,mpts,llim)
 wqc=wqc*1.0e-03
 go to 475
 end if
c
 type 508
508 format(' what is the limiting quadrupole frequency',
     1 ' in kHz ? ',$)
 accept *,wqc
475 type 509
509 format(' how many different quadrupole frequencies do you ',
     1  'want ? ',$)
 accept *,nwq
c
 if(nwq .eq. 1) go to 160
 type 505
505 format(t2,'do you want +/- Omega-q(y), or just one side(n)?',$)
 read(5,10)ans
 type 511
511 format(' does voff vary with vq ? (y/n) ',$)
 read(5,10)joff
10 format(a1)
 if(joff.ne.yyy) go to 160
 type 512
512 format(/,' voff = a * vq  +  b  (b in kHz)'/t10,' enter a:'$)
 accept *,a
 type 506
506 format(t10,'enter b:',$)
 accept *,b
 go to 170
c
160 type 513
513 format(/,' what is the fixed or initial voff in kHz ? ',$)
 accept *,woff
 woff0=woff
 if(nwq .gt. 1) go to 170
 type 514
514 format(' how many voff values do you want ? ',$)
 accept *,noff
 if(noff.eq.1)go to 170
 type 515
515 format(' what is the increment in kHz ? ',$)
 accept *,woffinc
c
170 do 525 i=1,nsteps
```

```
 type 516,i
516 format(/,' Enter the pulse magnitude for step',1x,i2,'(khz):',$)
 accept *,v1(i)
 if(v1(i).eq.0.0)go to 524
 type 517
517 format(t10,' pulse phase (in degrees) ',$)
 accept *,ph(i)
524 type 518
518 format(t10,' time interval (in usec) ',$)
525 accept *,t(i)
 type 400
400 format(t2,'do you wish to vary a pulse sequence parameter(y/n)?'$)
 read(5,10)ans2
 if(ans2.eq.yyy)call vpsp
c
 if(hans.eq.yyy)then
 type 519
519 format(t2,'possible output parameters:'/t10,'x1=1,x2=2,x3=3'/
 1t10,'y1=4,y2=5,y3=6'/t10,'z1=7,z2=8,z3=9'/t10,'omega q=10,'
 1'omega off=11'/t10,'rf field=12,phase=13,time=14'/t10,
 1'x2+y1=15, x1+y2=16, wq+woff=17')
 else
 type 521
521 format(t2,'possible output parameters:'/t10,'x=1,x2=2'/
 1t10,'y=4,y2=5'/t10,'z=7,3(z**2)-s(s+1)=9'/t10,'omega q=10,'
 1'omega off=11'/t10,'rf field=12,phase=13,time=14'/t10,
 1'wq+woff=17')
 end if
 type 530
530 format(t2,'how many parameters do you want to save?'$)
 accept *,npsv
 do 550 i=1,npsv
 type 520,i
520 format(t2,'x output in file ',i2,'??',$)
 accept *,ixx(i)
 type 522,i
522 format(t2,'y output in file',i2,'??',$)
 accept *,iyy(i)
550 continue
c
c
 if(idm.eq.11)then
 type 300
300 format(/t2,'is this an ADRF(a) or SL(s) experiment?',$)
 read(5,10)typcp
 type 301
301 format(t2,'what is the I spin mixing field(khz)?',$)
 accept *,omegh
 type 302
302 format(t2,'is the power spectrum of the lattice lorentzian(l),'/
 1t3,'gaussian(g), or exponential(e)?',$)
 read(5,10)typps
 type 303
303 format(t2,',what is the correlation time(usec)',
```

```
 1' of the dipolar state?'$)
 accept *,bdeff
 bdeff=bdeff*1.0e-03
 type 307
307 format(t2,',and what is the relative mixing time',
 1'                          ?',$)
 accept *,tmix
 type 310
310 format(t2,'ratio of S spin to I spin energy states',
 1'(epsilon)?',$)
 accept *,epsln
 type 305
305 format(t2,'a look at the dms(y/n)?',$)
 read(5,10)dmflag
 end if
c
c
 if(nwq .gt. 1)isumwq=1
 if(ans2.ne.yyy)then
 nmx=max0(noff,nwq)
 else
 nmx=nvinc
 end if
c
c
 do 201 i=1,np
 do 201 j=1,npsv
 yy(i,j)=0.0
201 xx(i,j)=0.0
c
 if(nwq .eq. 1) go to 202
c
c set up wqinc parameters, fppf=ratio of pporg4 points to desired points
 qnwq=nwq-1
 wqinc=abs(wqc-wqnot)/ qnwq
 if(ansn.eq.yyy)fppf=float(mpts-1)/qnwq
 if(ans.eq.yyy)then
 nwqd=nwq
 wq=-wqc
 if(ansq.eq.yyy)fppf=fppf*0.50
 wqinc=2.0*wqinc
 else
 wq=0.0
 end if
c
 if(ansn.eq.yyy)wqinc=wqinc*sign(1.0,wqc)
c
 if(ansq.eq.yyy)then
 type 554
554 format(/t2,'you can see how fast the calcns progress...',
 1/t3'...only if you want(y/n)?'$)
 read(5,10)ansr
 end if
 go to 203
```

```
c
202 wq=wqc
c
c
203 wqs=wq
 nsfw=llim
 np=nmx
c
 do 280 iq=1,nmx
c
 if(ansq.eq.yyy)then
 wq=wqs
 nsum=1
 nsf=llim
 end if
c
206 if(joff.eq.yyy) woff=a * wq  +  b
 sex=1.0
 l=iq
210 n=0
c
 if(idm.eq.11.and.iq.ne.1)then
 n=n+ncpstp-1
 istrt=ncpstp
 else
 istrt=1
 end if
c
c step through the pulse sequence
 do 215 in=istrt,nsteps
 n=n+1
 if(ans2.eq.yyy.and.in.eq.nvar.and.iq.ne.1.and.nsum.eq.1)then
 go to(401,402,403),ivar
401 v1(n)=v1(n)+vinc
 go to 405
402 ph(n)=ph(n)+vinc
 go to 405
403 t(n)=t(n)+vinc
 else if(ans2.eq.yyy.and.iq.eq.1.and.in.eq.nvar)then
c save the density matrix from the period prior to the variation, so
c not to waste time calculating it many times over
 call savdm(nsum,1)
 end if
405 if(ansq.eq.yyy.or.ans2.eq.yyy)then
  if(iq.gt.1.and.in.lt.nvar)then
   go to 215
  else if(iq.gt.1.and.in.eq.nvar)then
   call savdm(nsum,2)
   call igor(iq,nsum,ansswp,ncpstp,pdmf)
  else
   call igor(iq,nsum,ansswp,ncpstp,pdmf)
  end if
 else
  call igor(n,nsum,ansswp,ncpstp,pdmf)
```

```
 end if
 if(n .ne. nsteps) go to 215
 do 214 k=1,npsv
 call specify(yy(1,k),iyy(k))
 if(ansn.eq.yyy.and.ansq.ne.yyy)yy(1,k)=yy(1,k)*wt(nsfw,2)
 if(ansq.eq.yyy.and.nsum.lt.nwq)then
 if(ansn.eq.yyy)then
 sumyy(1,k)=sumyy(1,k)+wt(nsf,2)*yy(1,k)
 else
 sumyy(1,k)=sumyy(1,k)+yy(1,k)
 end if
 go to 214
 end if
 call specify(xx(1,k),ixx(k))
214 continue
215 continue
c
 if(ansq.eq.yyy)then
 nsum=nsum+1
c
 if(nsum.le.nwq)then
  if(ans.eq.yyy)then
   if(mod(float(nsum),2.0).eq.0.0.and.nsum.ne.1)then
   wq=-wq
   sex=-sex
   else if(nsum.ne.1)then
   wq=wq+wqinc*sex
   if(ansn.eq.yyy)nsf=nint(float(llim)+float(nsum-1)*fppf)
   end if
  else
  if(ansn.eq.yyy)nsf=nint(float(llim)+float(nsum)*fppf)
  wq=wq+wqinc
  end if
 go to 210
 else
 if(ansr.eq.yyy)type 220,l
220 format(t5,'calculation',1x,i3,1x,'done!')
 do 440 kn=1,npsv
440 yy(1,kn)=sumyy(1,kn)/float(nsum)
 end if
 end if
c
 if(noff .gt. 1) woff=woff + woffinc
 if(nwq .gt. 1.and.ansq.ne.yyy)then
 wq=wq + wqinc
 nsfw=nint(float(llim)+float(iq)*fppf)
 end if
280 continue
c
c
 if(idm.eq.10)idm=18
 if(idm.eq.11)idm=19
 do 602 k=1,npsv
 open(unit=1,name='DQC.DAT',type='new')
```

```
 write(1,580)nsteps,np,ixx(k),iyy(k),idm,ivar,nvar
580 format(7(i4,1x))
 if(idm.eq.18)write(1,585)nop,(idmm(i),coefx(i),i=1,nop)
585 format(t2,i2,1x,6(i2,1x,f7.5,1x))
 if(idm.eq.19)write(1,590)omegh,bdeff,typps,tmix,typcp
590 format(t2,f10.5,1x,f10.5,1x,a1,1x,f10.5,1x,a1)
 write(1,560)woff0,a,b,wqc,hans,ansq,nwq,wqnot
560 format(t2,4e13.6,1x,a1,1x,a1,1x,i3,1x,e13.6)
 do 599 j=1,nsteps,2
599 write(1,600)(v1(i),ph(i),t(i), i=j,j+1)
600 format(t2,6e13.6)
 do 601 j=1,np,3
601 write(1,600)(xx(i,k),yy(i,k), i=j,j+2)
602 close(unit=1)
 stop 'Thats all folks'
 end
c
c
c
c
c
 subroutine specify(aa,m)
 complex dm(3,3)
 common n,woff,wq,v1(20),ph(20),t(20),as(3,3),dm,idm
 1/ksfx/ivar,nvar,nvinc,vinc
c
 aa=0.0
c
 if(m .ge. 10) go to 50
 mm=m-1
 ii=mm/3 + 1
 jj=mod(mm,3) + 1
 aa=as(ii,jj)
 return
c
50 if(m .eq. 10) aa=wq
 if(m .eq. 11) aa=woff
 if(m.eq.12)aa=v1(nvar)
 if(m.eq.13)aa=ph(nvar)
 if(m.eq.14)aa=t(nvar)
 if(m.eq.15)then
 aa=as(1,2)+as(2,1)
 else if(m.eq.16) then
 aa=as(1,1)+as(2,2)
 end if
 if(m.eq.17)aa=wq+woff
 return
 end
c
c
c
c
c
 subroutine igor(iq,nsum,ansswp,ncpstp,pdmf)
```

```
c
c does the dirty work for DQTP
c
 parameter pi=3.14159265, rooto=.70710678
 dimension heg(3),isdm(10),fsdm(10)
 complex h(3,3),u(3,3),dm(3,3),s2,r(3)
 character*1 hans,yyy,typps,ansswp,dmflag,nnn,typcp
 data nnn/110/
 common n,woff,wq,v1(20),ph(20),t(20),as(3,3),dm,idm
 1/test/hans,yyy,typps,dmflag,typcp/cppar/omegh,bdeff,tmix,epsln
 1/swap/isdm,fsdm,nsswp
c
 wq3=wq/3.0
 twopi=2.0*pi
 cst=0.001 * twopi
 rad57=360.0 / twopi
c
 w1=v1(n)
 phr=ph(n) / rad57
 w1x=w1 * cos(phr)
 w1y=w1 * sin(phr)
c
 if(hans.eq.yyy)then
c H in the x,y,z basis
 h(1,1)=wq3
 h(1,2)=cmplx(0.0,-woff)
 h(1,3)=-w1y
 h(2,1)=-h(1,2)
 h(2,2)=h(1,1)
 h(2,3)=-w1x
 h(3,1)=h(1,3)
 h(3,2)=h(2,3)
 h(3,3)=-2.0 * h(1,1)
 else
c H in the +1,0,-1 basis
 h(1,1)=-woff+wq3
 h(1,2)=rooto*cmplx(-w1x,w1y)
 h(1,3)=0.0
 h(2,2)=-2.0*wq3
 h(2,3)=rooto*cmplx(-w1x,w1y)
 h(3,3)=woff+wq3
 h(3,1)=0.0
 h(3,2)=conjg(h(2,3))
 h(2,1)=conjg(h(1,2))
 end if
c
c diagonalize H
 call heigen(h,u,3)
c
 do 20 i=1,3
 do 20 j=1,3
 if(i .eq. j) go to 15
 h(i,j)=0.0
 go to 20
```

```
15 heg(i)=real(h(i,i))
 h(i,i)=cexp(cmplx(0.0,(-cst * t(n) * heg(i))))
20 continue
c
c
c transform H back to prev rep
 call umua(u,h,3,r)
c
c set up cp dm
 if(idm.eq.11.and.n.eq.ncpstp)then
 call mixfld(heg,u,nsum,iq,typps,typcp,dmflag,hans,ncpstp)
 if(ansswp.eq.yyy.and.n.eq.nsswp)call swapdm
 return
 else if(idm.eq.11.and.n.lt.ncpstp)then
  if(n.eq.1)then
  call matzoo(dm,3,0)
  s1=0.5
  s2=cmplx(0.0,s1)
  dm(1,2)=s2*pdmf
  dm(2,1)=-s2*pdmf
  end if
 go to 30
 end if
 if(n .gt. 1) go to 30
c
c set up initial density matrix
c
c
 s1=0.5
 s2=cmplx(0.0,s1)
 call matzoo(dm,3,0)
c
 if(hans.eq.yyy)then
c dm in the x,y,z basis
 go to(1,2,3,4,5,6,7,8,9,10),idm
1 dm(2,3)=s1
 go to 25
2 dm(2,3)=-s2
 go to 25
3 dm(2,2)=s1
 dm(3,3)=-s1
 go to 25
4 dm(1,3)=s1
 go to 25
5 dm(1,3)=s2
 go to 25
6 dm(1,1)=-s1
 dm(3,3)=s1
 go to 25
7 dm(1,2)=s2
 go to 25
8 dm(1,2)=s1
 go to 25
9 dm(1,1)=s1
```

```
 dm(2,2)=-s1
 go to 25
10 call mdm
25 dm(2,1)=conjg(dm(1,2))
 dm(3,1)=conjg(dm(1,3))
 dm(3,2)=conjg(dm(2,3))
 else
c only z, or 3(z**2)-s(s+1) possible in this basis for now
 if(idm.eq.7)then
  dm(1,1)=s1
  dm(3,3)=-s1
 else if(idm.eq.9)then
  dm(1,1)=s1
  dm(2,2)=-2.0*s1
  dm(3,3)=s1
 end if
 end if
c
c
c transform density matrix in accordance with H
30 call umua(h,dm,3,r)
c
 if(ansswp.eq.yyy.and.n.eq.nsswp)call swapdm(isdm)
c calculate expectation values of operators
 if(hans.eq.yyy)then
 as(1,1)=2 * real(dm(2,3))
 as(1,2)=-2 * aimag(dm(2,3))
 as(1,3)=real(dm(2,2) - dm(3,3))
 as(2,1)=2 * real(dm(1,3))
 as(2,2)=2 * aimag(dm(1,3))
 as(2,3)=real(dm(3,3) - dm(1,1))
 as(3,1)=2 * aimag(dm(1,2))
 as(3,2)=2 * real(dm(1,2))
 as(3,3)=real(dm(1,1) - dm(2,2))
 else
c in the +1,0,-1 basis
 as(1,1)=rooto*(real(dm(2,1)+dm(1,2)+dm(3,2)+dm(2,3)))
 as(1,2)=rooto*(aimag(dm(2,1)+dm(2,3)-dm(1,2)-dm(3,2)))
 as(2,1)=-rooto*(aimag(dm(1,2)-dm(2,1)-dm(3,2)+dm(2,3)))
 as(2,2)=rooto*(real(dm(1,2)+dm(2,1)-dm(2,3)-dm(3,2)))
 as(3,1)=real(dm(1,1)-dm(3,3))
 as(3,3)=real(dm(1,1)+dm(3,3)-2.0*dm(2,2))
 end if
c
 return
 end
c
c
c
c
c
 subroutine heigen(h,u,nm)
c
c this subroutine diagonalizes an nm by nm hermitian matrix h by
```

```
c the Jacobi method and outputs h and the unitary transformation
c matrix u.  the procedure is adapted from subroutine "eigen"
c in the IBM system/360 scientific subroutine package.
c
 complex h(nm,nm),u(nm,nm),ull,ulm,uml,umm,th,tu
 nmm=nm-1
 qn=nm
 range=5.0e-7
 do 20 i=1,nm
 do 10 j=1,nm
10 u(i,j)=0.0
20 u(i,i)=1.0
c
 anorm=0.0
 do 30 i=1,nmm
 ii=i+1
 do 30 j=ii,nm
30 anorm=anorm + real(h(i,j)*conjg(h(i,j)))
 if(anorm .le. range) return
 anorm=sqrt(2.0 * anorm)
 anormx=anorm * range / qn
 ind=0
 thr=anorm
c
40 thr=thr/qn
c
50 do 80 l=1,nmm
 ll=l+1
 do 80 m=ll,nm
 if( cabs(h(l,m)) .lt. thr ) go to 80
c
 ind=1
 diff=real( h(m,m) - h(l,l) )
 if(diff .eq. 0.0) diff=1.0e-15
 ar=0.5 * atan( 2.0 * real(h(l,m)) / diff )
 ai=0.5 * atan( 2.0 * aimag(h(l,m)) / diff )
 sini=sin(ai)
 cosi=cos(ai)
 sinr=sin(ar)
 cosr=cos(ar)
 ull=cmplx( cosr*cosi, sinr*sini )
 ulm=cmplx(-sinr*cosi,-cosr*sini )
 uml=cmplx( sinr*cosi,-cosr*sini )
 umm=cmplx( cosr*cosi,-sinr*sini )
c
 do 60 j=1,nm
 th=    ull*h(l,j) + ulm*h(m,j)
 h(m,j)=uml*h(l,j) + umm*h(m,j)
 h(l,j)=th
60 continue
c
 do 70  i=1,nm
 th=     umm*h(i,l) - uml*h(i,m)
 h(i,m)=-ulm*h(i,l) + ull*h(i,m)
```

```
 h(i,l)=th
 tu=     umm*u(i,l) - uml*u(i,m)
 u(i,m)=-ulm*u(i,l) + ull*u(i,m)
 u(i,l)=tu
70 continue
c
80 continue
c
 if(ind .eq. 0) go to 100
 ind=0
 go to 50
c
100 if(thr .gt. anormx) go to 40
 return
 end
c
c
c
c
c
        subroutine mateq(a,b,n)
c
c       this subroutine sets the nxn complex matrix b equal to a
c
        complex a(n,n),b(n,n)
        do 10 i=1,n
        do 10 j=1,n
10      b(i,j)=a(i,j)
        return
        end
c
c
c
c
c
        subroutine matzoo(a,n,k)
c
c       this subroutine sets all elements of an nxn complex matrix equal
c       zero, or creates an nxn identity matrix, depending on the value
c
        complex a(n,n)
        do 20 i=1,n
        do 10 j=1,n
10      a(i,j)=0.0
20      if(k .ne. 0) a(i,i)=1.0
        return
        end
c
c
c
c
c
 subroutine umua(u,b,n,v)
c
```

```
c performs unitary transformations:     b = u * b * u-adjoint
c
 complex u(n,n),b(n,n),v(n)
c
 call matrml(u,b,n,v)
 call mataml(b,u,n,v)
 return
 end
c
c
c
c
c
 subroutine mataml(a,b,n,rv)
c
c a matrix multiplier:     a = a * b-adjoint
c
 complex a(n,n),b(n,n),rv(n),s
 do 14 i=1,n
 do 12 j=1,n
 s=0.0
 do 11 k=1,n
11 s=s + a(i,k)*conjg(b(j,k))
12 rv(j)=s
 do 13 j=1,n
13 a(i,j)=rv(j)
14 continue
 return
 end
c
c
c
c
c
 subroutine matrml(a,b,n,cv)
c
c a matrix multiplier:     b = a * b
c
 complex a(n,n),b(n,n),cv(n),s
 do 14 j=1,n
 do 12 i=1,n
 s=0.0
 do 11 k=1,n
11 s=s + a(i,k)*b(k,j)
12 cv(i)=s
 do 13 i=1,n
13 b(i,j)=cv(i)
14 continue
 return
 end
c
c
 subroutine vpsp
 common/ksfx/ ivar,nvar,nvinc,vinc
```

```
 type 10
10 format(t2,'which parameter do you want varied:'/t10,
 1'1=rf field,2=phase,3=time?',$)
 accept *,ivar
 type 20
20 format(t2,'at which step do you wish this varied?',$)
 accept *,nvar
 type 30
30 format(t2,'how many increments do you wish to generate?',$)
 accept *,nvinc
 type 40
40 format(t2,'and what is the increment (in khz,deg,or usec)?',$)
 accept *, vinc
 return
 end
c
c
 subroutine mixset
 common/mixdm/nop,idmm(9),coefx(9)
 type 10
10 format(t2,'density matrix is to consist of how many operators',
 1'?',$)
 accept *,nop
 type 15
15 format(t2,'enter number corresponding to operator(previously'
 1,' defined)'/t2,'and fractional composition:')
 do 100 i=1,nop
 type 20
20 format(t5,'operator?',$)
 accept *,idmm(i)
 type 25
25 format(t5,'fraction:',$)
100 accept *,coefx(i)
 return
 end
c
c
 subroutine mdm
 complex dm(3,3),s2
 common n,woff,wq,vl(20),ph(20),t(20),as(3,3),dm,idm
 1/mixdm/ndme,idmm(9),coefx(9)
 s1=0.5
 s2=cmplx(0.0,s1)
 call matzoo(dm,3,0)
 do 25 i=1,ndme
 px=sqrt(coefx(i))
 call dmas(px,idmm(i))
25 continue
 return
 end
c
c
c
 subroutine mixfld(eigenv,u,ndm,iq,typmf,typcp,dmflag,hans,ncpstp)
```

```
 complex dm(3,3),u(3,3),tdm(8096),r(3),cdm(3,3)
 dimension eigenv(3)
 character*1 typmf,dmflag,yyy,hans,nnn,mmm,typcp
 data yyy,nnn,mmm/121,110,109/
 common n,woff,wq,v1(20),ph(20),t(20),as(3,3),dm,idm
 1/cppar/wheff,ewidth,tmix,epsln
 incdm=(ndm-1)*9
 ndmt=incdm+1
 if(iq.gt.1)go to 50
 call matzoo(cdm,3,0)
c
c populate the dm in accordance with the matching conditions;
c once we have rotated ourself into the proper interaction representatio
c two operators get populated in this simple two effective field
c treatment, there is the possibility that a third may also
c
c in the +1,0,-1 basis
 if(hans.eq.mmm)then
 wneff1=eigenv(3)-eigenv(1) !            (we-wq)/2
 wneff2=eigenv(2)-eigenv(1) !               we
 wneff3=eigenv(3)-eigenv(2) !            (we+wq)/2
 omegf=abs(wneff2)
 wneff=wneff1
 coefdm=dmc(13,wq,omegf,wneff,wheff,ewidth,epsln,tmix,typmf,typcp)
 dm1=sign(1.0,wneff1)*coefdm
c we coeff of Sz(2-3) is ineffective in cross relaxation
 dm2=0.0
 wneff=wneff3
 coefdm=dmc(12,wq,omegf,wneff,wheff,ewidth,epsln,tmix,typmf,typcp)
 dm3=sign(1.0,wneff3)*coefdm
c
c populate Sz(1-3)
 cdm(1,1)=-dm1*0.50
 cdm(3,3)=dm1*0.50
c populate Sz(1-2)
 cdm(2,2)=-dm3*0.50
 cdm(3,3)=cdm(3,3)-cdm(2,2)
c populate Sz(2-3)
 cdm(2,2)=cdm(2,2)+dm2*0.50
 cdm(1,1)=cdm(1,1)-dm2*0.50
 go to 10
 end if
c
c x,y,z effective fields
 wneff1=eigenv(1)-eigenv(2)  !            z,3
 wneff2=eigenv(2)-eigenv(3)  !            x,3
 wneff3=eigenv(3)-eigenv(1)  !            y,3
c
c for xyz, check for irradiation along x or y
c
 ru1=real(u(1,1))
 ru2=real(u(2,2))
c in the x,y,z basis
 if(max(ru1,ru2).eq.ru1.and.hans.eq.yyy)then
```

```
c irradiation along x
 omegf=abs(wneff2)
 wneff=wneff1 !                          (we-wq)/2
 coefdm=dmc(13,wq,omegf,wneff,wheff,ewidth,epsln,tmix,typmf,typcp)
 dm1=sign(1.0,wneff1)*coefdm
c we coeff of x,3 is ineffective in cross relaxation
 dm2=0.0
 wneff=wneff3 !                          (we+wq)/2
 coefdm=dmc(12,wq,omegf,wneff,wheff,ewidth,epsln,tmix,typmf,typcp)
 dm3=sign(1.0,wneff3)*coefdm
c populate y,3 then x,3 for x irradiation
 cdm(3,3)=(dm3-dm2)*0.50
 cdm(1,1)=-dm3*0.50
 cdm(2,2)=dm2*0.50
c irradiation along y, or at 45 degrees
 else
 omegf=abs(wneff3)
 wneff=wneff1 !                          (we-wq)/2
 coefdm=dmc(13,wq,omegf,wneff,wheff,ewidth,epsln,tmix,typmf,typcp)
 dm1=sign(1.0,wneff1)*coefdm
 wneff=wneff2 !                          (we+wq)/2
 coefdm=dmc(12,wq,omegf,wneff,wheff,ewidth,epsln,tmix,typmf,typcp)
 dm2=sign(1.0,wneff2)*coefdm
c we coeff of y,3 is ineffective in cross relaxation
 dm3=0.0
c populate x,3 then y,3 in this frame
 cdm(3,3)=(dm3-dm2)*0.50
 cdm(2,2)=dm2*0.50
 cdm(1,1)=-dm3*0.50
 end if
c
c populate S(z,3)
 cdm(1,1)=cdm(1,1)+dm1*0.50
 cdm(2,2)=cdm(2,2)-dm1*0.50
c
10 if(dmflag.eq.yyy)type 999,wq,eigenv(1),eigenv(2),eigenv(3),
 1wneff1,dm1,wneff2,dm2,wneff3,dm3
999 format(t2,'wq=',e11.4,1x,'e1=',e11.3,'e2=',e11.3,'e3=',e11.3/
 1t4,'w1e=',e11.3,'dm1=',e11.3,1x,'w2e=',
 1e11.3,'dm2=',e11.3/t4,'w3e=',e11.3,'dm3=',e11.3)
c
c transform density matrix back to previous representation
c
 call umua(u,cdm,3,r)
c
c add on the previous evolution period, if it exists
 do 15 i=1,3
 do 15 j=1,3
 if(ncpstp.ne.1)then
 dm(i,j)=dm(i,j)+cdm(i,j)
 else
 dm(i,j)=cdm(i,j)
 end if
15 continue
```

```
c
 if(dmflag.eq.yyy)then
 do 900 i=1,3
900 type 998,(dm(i,j),j=1,3)
998 format(t5,3(e11.3,1x,e11.3,3x))
 end if
 do 20 i=ndmt,ndmt+8
 mm=i-incdm-1
 ii=mm/3+1
 jj=mod(mm,3)+1
20 tdm(i)=dm(ii,jj)
 return
50 do 60 i=ndmt,ndmt+8
 mm=i-incdm-1
 ii=mm/3+1
 jj=mod(mm,3)+1
60 dm(ii,jj)=tdm(i)
 return
 end
c
c
c
 function fcnm(fuv,fcnz,hh,bd,typcp)
 character*1 bd,111,eee,aaa,typcp
 data 111,eee,aaa/108,101,97/
 parameter pi=3.141592654
c calculates lorentzian, gaussian, or exponential function values
c for random inputs
 fua=abs(fuv)
 if(typcp.ne.aaa)then
 afuv=2.0*pi*abs(fua-fcnz)
 else
 afuv=2.0*pi*fua
 end if
 if(bd.eq.eee)go to 200
 if(bd.eq.111)go to 100
c this is fully converted to the correlation time format
c gaussian........
 fu=afuv*hh
 arg=-fu**2/4.0
 if(arg.le.-30.0)then
 fcnm=0.0
 return
 end if
c fcnm=qz*exp(arg)
 fcnm=exp(arg)
 return
100 fu=afuv*hh
c lorentzian.......
 arg=1.0+fu**2
 if(arg.gt.1.0e+09)then
 fcnm=0.0
 return
 end if
```

```
c fcnm=qz*(1.0/arg)
 fcnm=1.0/arg
 return
c exponential for....whatever you want to use it for
200 fu=afuv
 arg=-fu*hh
 if(arg.le.-30.0)then
 fcnm=0.0
 return
 end if
 fcnm=exp(arg)
 return
 end
c
c
c
 subroutine predm(ncp,pdmf)
 character*1 ans,yyy
 data yyy/121/
 complex dm(3,3)
 common n,woff,wq,vl(20),ph(20),t(20),as(3,3),dm,idm
c gets data for pre cp period/sets up idm for this period
 type 10
10 format(t2,'do you wish a pre-cross polarization evolution(y/n)?',$)
 read(5,12)ans
12 format(a1)
 if(ans.ne.yyy)then
 ncp=1
 return
 end if
 type 20
20 format(t2,'how many steps in the pre-cp period?',$)
 accept *,nsteps
 type 30
30 format(t2,'by what factor do you wish the pre-cp dm elements ',
 1'multiplied?',$)
 accept *,pdmf
 ncp=nsteps+1
 return
 end
c
c
c
 function fexp(sd,epsln,wes,wei,tmix)
c calculates amplitude due to exponential relaxation for dm elements
c assuming Tld and Tlrho are infinite
c includes thermodynamically limiting polarization as alpha
c tau=1.0/sd
c arg=tmix/tau
 eta=abs(wes/wei)
 alpha=1.0+epsln*eta**2
 arg=tmix*sd*alpha
 if(arg.le.0.01)then
 fexp=arg*eta/alpha
```

```
 else if(arg.ge.10.0)then
 fexp=eta/alpha
 else
 fexp=eta*(1.0-exp(-arg))/alpha
 end if
 return
 end
c
c
c
c
 subroutine savdm(nsum,iflag)
 complex tdm(1024,3,3),dm(3,3)
 common n,woff,wq,vl(20),ph(20),t(20),as(3,3),dm,idm
 save tdm
c either saves the dm elements for a particular value of wq, or retrieve
c them from tdm; depending upon the value of iflag
 if(iflag.eq.1)then
 do 10 ii=1,3
 do 10 jj=1,3
10 tdm(nsum,ii,jj)=dm(ii,jj)
 else
 do 20 ii=1,3
 do 20 jj=1,3
20 dm(ii,jj)=tdm(nsum,ii,jj)
 end if
 return
 end
c
c
c
 function dmc(itrans,wq,omegf,wneff,wheff,ewidth,epsln,tmix,
 1typmf,typcp)
 character*1 typmf,typcp
 ct=abs(wq)/omegf
c determine which transition we are polarizing and figure the appropriat
c reduction factor for tis due to the tilting of His
 if(itrans.eq.13)then
 dmfact=(1.0+ct)*0.50
 else if(itrans.eq.12)then
 dmfact=(1.0-ct)*0.50
 else
 dmfact=1.0
 end if
c of course, this assumes we are damn near on resonance......
c now calculate 1.0/tis
 tisinv=fcnm(wneff,wheff,ewidth,typmf,typcp)
 tisinv=tisinv*dmfact
 dmc=fexp(tisinv,epsln,wneff,wheff,tmix)
 return
 end
```

```
 program rjump
c
c exchange matrix formalism calculation of a jumping quadrupole
c
 complex z1(32,32),z2(32,32),omeg(32,32),pii(32,32),p1(32,32),
 1p2(32,32),p1i(32,32),p2i(32,32),g(1024),r(32),w1(32),w2(32),summel
 real omegj(32),work(4096),kappa,kappa2
 real nu,nual,inot,nnot,iw1,iw2
 character*1 ansdg,yyy,anscp,ansrs,rrr,anslp,ansln,aaa,bbb,anscol,
 1sss,hhh
 common/jangle/alpha,beta,gamma,alpha2,beta2,delta/qcpar/eqqs,eta,eqqr
 data yyy,rrr,aaa,bbb,sss/121,114,97,98,115/
 parameter pi=3.141592654,rad57=1.7453293e-02,twopi=6.283185308
 type 10
10 format(t2,'Calculates effect of rotational jumping upon the spectrum'
 1,' of a spin-1 nucleus'//t5,'enter eqQ/h(kHz), eta:',$)
 accept *,eqq,eta
 type 11
11 format(t5,'fraction of tensor which is static(ionic/intra)?',$)
 accept *,pcts
c static and varying Vzz
 eqqs=pcts*0.750*eqq
 eqqr=(1.0-pcts)*eqq*0.750
 type 12
12 format(t3,'rotational hop (r), or restricted flip-flop(f)?',$)
 read(5,60)ansrs
 if(ansrs.eq.rrr)then
 type 20
20 format(t5,'number of steps in the rotational hop?',$)
 accept *,nhop
 delta=twopi/nhop
 else
 type 22
22 format(t5,'number of steps in the flip-flop?',$)
 accept *,nhop
 type 23
23 format(t5,'angle (degrees) between flops?',$)
 accept *,delta
 delta=delta*rad57
 end if
 type 24
24 format(t3,'hard(h) or soft(s) collision model?',$)
 read(5,60)anscol
 type 25
25 format(t5,'enter Euler angles relaing tensor and motional axis'/
 1t5,'(alpha[z], beta[y-prime], gamma[z-double prime]:',$)
 accept *, alpha, beta, gamma
 alpha=alpha*rad57
 beta=beta*rad57
 gamma=gamma*rad57
 alpha2=alpha*2.0
 beta2=beta*2.0
 type 30
30 format(t2,'A quadrupolar echo sequence is assumed'/
```

```
 lt5,'what is the delay between pulses (usec)?',$)
 accept *,tau
 type 35
35 format(t5,'jumping rate (kHz)?',$)
 accept *,kappa
 type 38
38 format(t5,'isotropic T2 (msec)?',$)
 accept *,t2
 t2i=1.0/t2
c
 if(anscol.ne.sss)then
c set up jump probability matrix pi, assume any jump orientation is
c equally probable
 kappa2=kappa*nhop
 do 40 i=1,nhop
 do 40 j=1,nhop
 pii(i,j)=kappa
 if(i.eq.j)pii(i,j)=pii(i,j)-kappa2-t2i
40 continue
 else
c soft collision assumes only neigboring positions are accessible
c to the jump
 kappa2=kappa*2.0
 do 41 i=1,nhop
 do 41 j=1,nhop
 if(i.eq.j)then
 pii(i,j)=-kappa2-t2i
 else
 srel=abs(float(i-j))
 if(srel.gt.1.0)srel=0.0
 pii(i,j)=srel*kappa
 end if
41 continue
c include endpoints of motion
 if(ansrs.eq.rrr)then
 pii(1,nhop)=kappa
 pii(nhop,1)=kappa
 else
 pii(1,2)=2.0*kappa
 pii(nhop,nhop-1)=2.0*kappa
 end if
 end if
c
c loop over phi for each nu
 type 42
42 format(t2,'enter integration limits for phi(x), nu(y)'/
 lt5'[phi limit=2*pi/x, nu limit=2*pi/y] ??',$)
 accept *,x,y
 phial=twopi/x
 nual=twopi/y
 type 45
45 format(t2,'How many points(time domain)do you wish to calculate?',$)
 accept *,nptst
 type 50
```

```
50 format(t5,'at what time resolution(usec)?',$)
 accept *,deltim
c put all time variables in millisec
 deltim=deltim*1.0e-03
 tau=tau*1.0e-03
 hzp=1.0/(deltim*nptst)
c approximate no. of integration steps required
c this is a fairly bogus method of estimating integration steps
c and is really best done away with
 nptnu=nint(1.125*eqq*nual/hzp)
 nptphi=nint(0.375*eqq*eta*phial/hzp)
c
c if we allow for flopping, we need to integrate over phi
 if(nptphi.eq.0.and.(gamma.ne.0.0.or.beta.ne.0.0))nptphi=1
c
 type 55,nptnu,nptphi
55 format(t2,'you need at least',1x,i4,1x,'nus and',1x,i4,1x,'phis'/
 1t3,'enter multiplicative factor for more(less) nus, phis:',$)
 accept *,pnu,pphi
 nptnu=pnu*nptnu
 nptphi=pphi*nptphi
 delnn=nual/nptnu
 if(nptphi.ne.0)then
 delpn=phial/nptphi
 dtp=delpn*delnn
 else
 dtp=2.0*pi*delnn
 end if
 nu=delnn*0.50
 type 56
56 format(t2,'do you wish to see calcn progress??',$)
 read(5,60)anscp
 type 58
58 format(t2,'do you wish to see diag. info.?',$)
 read(5,60)ansdg
60 format(a1)
c
c loop over nu
 itp=0
 do 200 while (nu.le.nual)
 if(anscp.eq.yyy)type 899,nu
899 format(t2,'nu=',e13.6)
 phi=delpn*0.50
 asn=abs(sin(nu))
 inot=asn*dtp
c loop over phi
 do 100 while(phi.le.phial)
 call jumpf(nhop,omegj,nu,phi)
 if(ansdg.eq.yyy)then
 type 900,phi
900 format(/t2,'phi=',e13.6)
 do 901 jjk=1,nhop
901 type 902,omegj(jjk)
902 format(t2,'jump orientation=',e13.6)
```

```
 end if
c create complex jump matrix for forward and reverse evolution periods,
c store in z1 and z2, I assume z2 is the conjugate of z1
 do 75 i=1,nhop
 do 75 j=1,nhop
 z1(i,j)=pii(i,j)
 if(i.eq.j)then
 z1(i,j)=z1(i,j)+cmplx(0.0,(omegj(i)*twopi))
 end if
75 continue
c find eigenvalues and eigenvectors of z1 and z2
 nnh=2*(nhop*nhop+nhop)
 call eigen(z1,p1,p2,w1,w2,work,nhop,nnh,ansdg)
c calculate component of fid due to this orientation
c invert matrix of eigenvalues p1 once for each orientation, use its
c conjugate for p2-inverse since all jump orientations are a priori
c equally probable
c
 call invert(p1,p1i,nhop,work)
 do 76 i=1,nhop
 do 76 j=1,nhop
  if(i.eq.j.and.tau.eq.0.0)then
  z1(i,j)=1.0
  else if(i.eq.j)then
  z1(i,j)=cexp(w1(j)*tau)
  else
  z1(i,j)=0.0
  end if
76 p2i(i,j)=conjg(p1i(i,j))
c
c the following calculations are done prior to the time loop:
c z1=p1 * z1 * p1-inverse * p2
c
 if(tau.ne.0.0)then
 call umui(p1,z1,p1i,nhop,r)
 else
 call matzoo(z1,nhop,1)
 end if
 call mtraml(z1,p2,nhop,r)
c
 t=0.0
 call matzoo(z2,nhop,0)
 do 85 j=1,nptst
c z2 is zeroed at the end of this loop by subr nsum
 tau2=t+tau
 do 80 k=1,nhop
80 z2(k,k)=cexp(w2(k)*tau2)
c
 call mdraml(z2,p2i,nhop,r)
c sum all matrix elements in z1 * z2 to find this component of fid
c [assuming all orientations are equally probable]
 call nsum(z1,z2,nhop,summel)
 g(j)=inot*summel+g(j)
85 t=t+deltim
```

```
c continue angular integration b   s
100 phi=phi+delpn
200 nu=nu+delnn
 open(unit=1,type='new',form='formatted',name='sfid.dat')
 write(1,225)eqq,eta,tau,deltim,t2,anscol,nhop,nptst,ansrs,
 1alpha,beta,gamma,kappa,delta
225 format(t2,3(f10.5,1x),e13.6,1x,f10.5,1x,a1/t2,2(i4,1x),a1,1x,'t'
 1/t2,5(e13.6,1x))
 write(1,250)(g(kk),kk=1,nptst)
250 format(t2,6e13.6)
 stop'Thats all folks'
 end
c
c
c
 subroutine nsum(a,b,n,s)
 complex a(32,*),b(32,*),s
c sums all of the elements of a complex matrix: a * b ,
c then zeroes the matrix b
 s=0.0
 do 14 j=1,n
 do 12 i=1,n
 do 12 k=1,n
12 s=s+a(i,k)*b(k,j)
 do 13 i=1,n
13 b(i,j)=0.0
14 continue
 return
 end
c
c
c
 subroutine matzoo(a,n,k)
 complex a(32,*)
c zeroes a complex matrix, or creates an identity matrix;
c depending upon the value of k
 do 20 i=1,n
 do 20 j=1,n
 a(i,j)=0.0
 if(k.ne.0.and.i.eq.j)then
 a(i,j)=1.0
 end if
20 continue
 return
 end
c
c
c
 subroutine mtraml(a,b,n,cv)
 complex a(32,*),b(32,*),cv(32),s
c a matrix multiplier:    a = a * b
 do 14 i=1,n
 do 12 j=1,n
 s=0.0
```

```
 do 11 k=1,n
11 s=s+a(i,k)*b(k,j)
12 cv(j)=s
 do 13 j=1,n
13 a(i,j)=cv(j)
14 continue
 return
 end
c
c
c
 subroutine mdraml(a,b,n,cv)
 complex a(32,*),b(32,*),cv(32),s
c a matrix multiplier: a = a * b
c where a is diagonal
 do 14 i=1,n
 do 12 j=1,n
 s=0.0
12 cv(j)=a(i,i)*b(i,j)
 do 13 j=1,n
13 a(i,j)=cv(j)
14 continue
 return
 end
c
c
c
 subroutine matrml(a,b,n,cv)
 complex a(32,*),b(32,*),cv(32),s
c a matrix multiplier:    b = a * b
 do 14 j=1,n
 do 12 i=1,n
 s=0.0
 do 11 k=1,n
11 s=s+a(i,k)*b(k,j)
12 cv(i)=s
 do 13 i=1,n
13 b(i,j)=cv(i)
14 continue
 return
 end
c
c
c
 subroutine madrml(a,b,n,cv)
 complex a(32,*),b(32,*),cv(32),s
c a matrix multiplier : b = a * b
c where b is diagonal
 do 14 j=1,n
 do 12 i=1,n
 s=0.0
12 cv(i)=a(i,i)*b(i,j)
 do 13 i=1,n
13 b(i,j)=cv(i)
```

```
14 continue
 return
 end
c
c
c
 subroutine jumpf(n,omega,nu,phi)
 real nu,nu2,omega(32)
 common/jangle/alpha,beta,gamma,alpha2,beta2,delta/qcpar/eqqs,eta,eqqr
 parameter pi=3.141592654,rad57=1.7453293e-02
c
c loads array omega with frequencies which exchange due to jumping
c
 deltn=0.0
 nu2=nu*2.0
c
c if a static part of the tensor exists, calculate it and add it to
c the rotationally time dependent part
c the formula assumes that the two tensors are aligned and have the same
c symmetry
 omegas=eqqs*(p2(nu)+0.50*eta*sin(nu)**2*cos(2.0*phi))
c
 do 90 i=1,n
 angl3=gamma+phi+deltn
 angl32=angl3*2.0
c calculate symmetric part (formula from Mehring p 37)
 omegal=eqqr*(p2(beta)*p2(nu)-0.75*(sin(beta2)*sin(nu2)*cos(angl3)
 1                          -(sin(beta)*sin(nu))**2*cos(angl32)))
c calculate asymmetric part
 if(eta.eq.0.0)then
 omega2=0.0
 else
 omega2=0.5*eqqr*eta*(p2(nu)*sin(beta)**2*cos(alpha2)+sin(beta)*sin(nu2)
 1*(cos(beta)*cos(alpha2)*cos(angl3)-sin(alpha2)*sin(angl3))
 1+sin(nu)**2*(0.50*(1.0+cos(beta)**2)*cos(alpha2)*cos(angl32)
 1-cos(beta)*sin(alpha2)*sin(angl32)))
 end if
 omega(i)=omegal+omega2+omegas
90 deltn=deltn+delta
 return
 end
c
c
c
 function p2(theta)
c calculates P2(cos(theta))
 ct=cos(theta)
 p2=(3.0*ct**2-1.0)*0.5
 return
 end
c
c
c
 subroutine eigen(a,c,d,el,e2,work,n,nn,ansdg)
```

```
 complex a(32,*),c(32,*),d(32,*),e1(32),e2(32)
 real work(nn)
 character*1 ansdg,yyy
 data yyy/121/
c calculate eigenvalues and eigenvectors, use eigenvectors for
c transformation matrix.....
c general laziness dictates the use of IMSL routines
 ijob=2
 call eigcc(a,n,32,ijob,e1,c,32,work,ierr)
 if(ansdg.eq.yyy)then
 do 902 jjk=1,n
902 type 901,jjk,e1(jjk)
901 format(t2,'eigenvalue 1',1x,i2,1x,'=',e13.6,1x,e13.6)
 type 903,work(1)
903 format(t3,'I was this good==>',e13.6)
 end if
c
c since the jump matrix is symmetric, then
c the eigenvalues and eigenvectors for the period following the echo
c pulse are merely conjugates of those preceeding it, elsewise the
c following call statement is necessary:
c call eigcc(b,n,32,ijob,e2,d,32,work,ierr); b has been removed from the
c subroutine and needs to be replaced
c
 do 50 j=1,n
50 e2(j)=conjg(e1(j))
c
c normalize eigenvectors
 do 100 j=1,n
 sumz1=0.0
 do 90 i=1,n
90 sumz1=sumz1+real(c(i,j)*conjg(c(i,j)))
 sumz1=sqrt(sumz1)
 do 100 i=1,n
 c(i,j)=c(i,j)/sumz1
100 d(i,j)=conjg(c(i,j))
c
 return
 end
c
c
c
 subroutine invert(a,ai,n,work)
 complex a(32,*),ai(32,*),da(32,32),r(32)
 real work(n)
c inverts a general complex matrix using an IMSL routine
 ijob=0
 call matzoo(ai,n,1)
c input matrix a is destroyed, set up dummy matrix da
 do 10 i=1,n
 do 10 j=1,n
10 da(i,j)=a(i,j)
c
 call leqt1c(da,n,32,ai,n,32,ijob,work,ierr)
```

```
c
 return
 end
c
c
c
 subroutine umui(u,a,ui,n,cv)
 complex a(32,*),u(32,*),ui(32,*),cv(32)
c performs complex transformations:   a = u * a * u-inverse
c when the inverse matrix is supplied externally
c a is assumed to initially be diagonal
c
 call mdraml(a,ui,n,cv)
 call matrml(u,a,n,cv)
 return
 end
```

Appendix D

Spectrometer Modifications

The design details of the spectrometer which was employed to perform the experiments I describe here have been discussed profusely in reference [82]. For the first several years of it's life, this machine performed only high resolution NMR in liquids, but it's extremely versatile design allows it to perform many other experiments. Several modifications have been made, which almost entirely involve the addition of peripheral equipment, and these are presented here for the interested reader.

D.1 Pulse Programmer

The addition of a Nicolet Instrument Corporation 293B programmable pulser has added new dimensions to the experiments which can be performed. With this device, pulse programs of up to 256 steps may be executed (this is currently software limited to 128 steps), and each interval in the sequence may gate as many as twenty different devices simultaneously. The outputs of this instrument require a certain amount of decoding, and their current carrying capability must also be increased to enable them to drive the gates present on various pieces of peripheral equipment. The Nicolet 293B Auxiliary Logic box ('Joe') has been constructed for this purpose, and is described in detail in LBL print number 26X140. The following special features have been built into this interface: (1) an interlock to the power supply of the 293B to prevent indeterminant output states from gating high power amplifiers and destroying sensitive equipment, (2) phase indicator LEDS which flash for approximately 30 msec when a particular phase is gated, and (3) a time out on the H1 gate which

limits the longest high power pulse to 24 msec (just in case an inexperienced user enters a pulse length of several seconds instead of several μsec).

D.2 Amplifiers

The amplifiers present on the spectrometer during the time of Willy Shih [82] were, unfortunately, insufficient to provide enough H_1 to rapidly rotate low γ nuclei such as ^{14}N. Several solutions to this problem were attempted, but the best by far has been the addition of a high power Bruker pulse amplifier between the single sideband generator and the existing power amplifier (LBL print number 10X229). This one-two punch provides about 270 volts into 50Ω at 19.5 MHz, and this translated into nearly 260 gauss in the rotating frame using the probe described in Figure 54. The extreme non linearity of the Bruker amplifier necessitates the use of extreme care when attempting to vary the output by attentuation of the input (the input is best attenuated in 0.1 db steps).

The amplifiers used for ^{1}H irradiation are exactly as described in reference [82], except for the replacement of the final stage of the 270 MHz driver amplifier (LBL print number 10X225) with one employing a higher frequency Motorola MRF326 transistor. The total proton power amplifier combination generally yielded about 100 volts peak at 270 MHz (this has now been exceeded by Sun Un).

D.3 Probe

Not surprisingly, the probe turned out to be the most critical part of the entire spectrometer system, and considerable time has been spent playing with various designs. The final design is based upon a simple single coil double tuned design [140] in which high frequency

Figure 54. ^{14}N - ^{1}H double resonance NMR probe

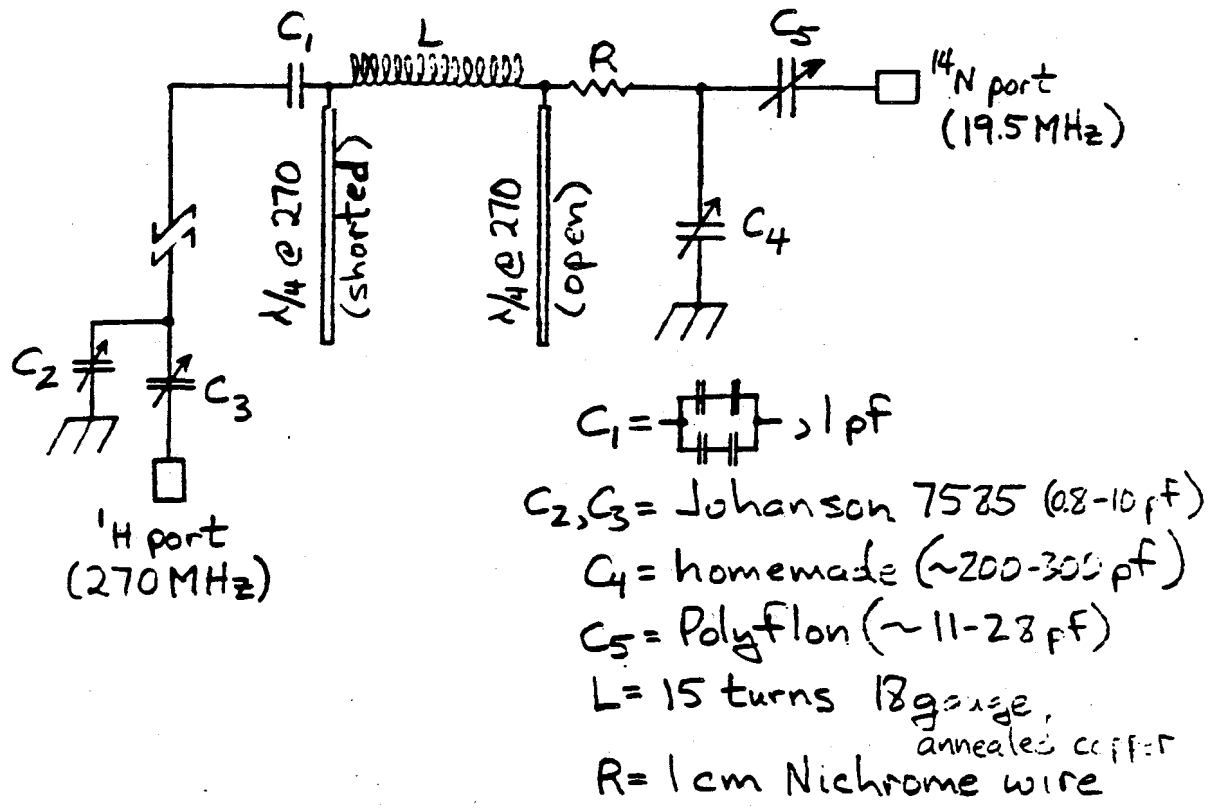

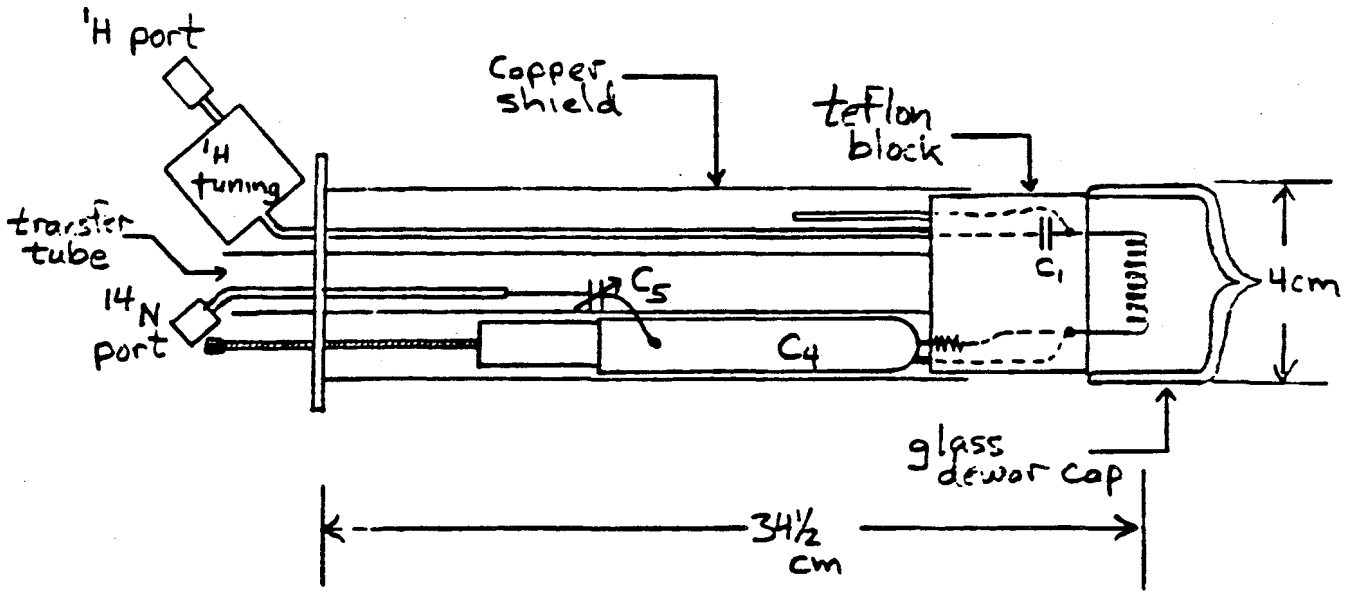

$\lambda/4$ lines are used for isolation purposes, and the tuning for the high frequency (^{1}H) side is performed outside of the probe body (see Figure 53). The optimum coil design was found to be a 15 turn coil of 5 mm diameter and 25 mm length set in epoxy. The high frequency Q is rather low ($\sim$ 75) because of lead lengths and the proximity of the turns, but the low frequency Q had to be reduced from about 110 to 60 with a short piece of nichrome wire so that the broad ^{14}N powder line-shapes could be more easily observed.

One rather severe problem which is encountered when operating at low frequency is that of magneto-acoustic ringing [33], and I am not the recipient of any special immunity to this spurious disturbance. The solutions given in references [33b] and [33c] were tried, but neither worked. I found that the only solution to the problem is to keep metal objects as far from the coil as possible (as is suggested in [33b]). This necessitated removal of the shield from the outside of the probe to a distance approximately 2 inches below the center of the coil. In this way, and employing the alternating 180° echo phase shifts of section 2.1.1, the total dead time was found to be less than 40 μsec for most samples at room temperature, and had a tendency to increase as the temperature was lowered.

D.4 Preamplifiers

Next to the probe, the preamp is the second most important piece of equipment in determining the S/N of the spectrometer system. On the low frequency ^{14}N side, low noise, high gain, and rapid recovery are all very important. The preamp design which was finally settled on is described in Figure 55. The presence of the many PIN diode switches (described in Figure 56) is necessary in order to prevent the very high

Figure 55. ^{14}N preamplifier

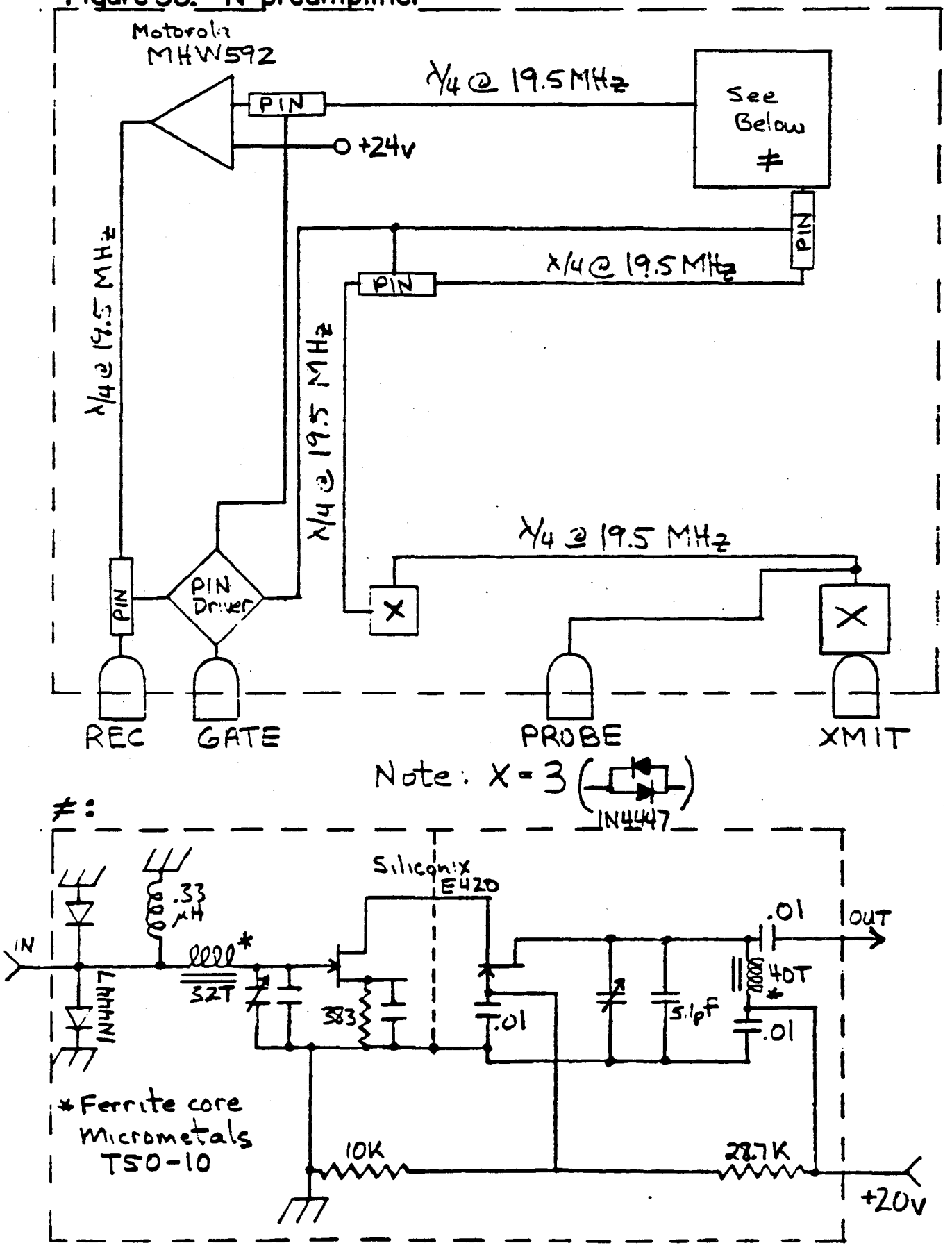

voltage present at the XMIT port from overloading the preamp and downconverter. The first stage of the preamp is merely a retuning of a design previously used by Willy Shih (LBL print number 16X903) for observation of ^{15}N at 27 MHz. It was found that this amplifier, in combination with a Motorola MHW592 wideband module, formed an extremely stable high gain (∿ 50 db) pair with a reasonable noise figure of about 2 db. The recovery time of the preamp is about 10 μsec, and due almost entirely to the recovery time of the PIN diode switches. The S/N of this combination has been measured repeatedly using a sample of powdered NH_4Cl, and employing the NTCFTB subroutine SN to perform the calculation, and is usually in the neighborhood of 150 for 16 pulses.

The high frequency observation employed the same preamp described in [82] (LBL print number 16X955); with the addition of two λ/4-PIN switches (the PIN switch design is similar to Figure 56, but the PIN diode used is a HP5082-3040, and the values of the capacitors are obviously much smaller). This preamp, even with the PIN switches, which cut the pulse breakthrough to less than 500 mv, has a severe saturation recovery problem and apparently is not a good design for high power NMR in solids.

Many simple peripheral devices were added to the spectrometer to enable it to perform experiments involving ADRF, bilevel pulses, 45° phase shifts, etc. The implementation of these functions was performed by switching in an appropriate element (such as an attenuator, or λ/8 line) while simultaneously switching out the other path available to the r.f. (an ANZAC HV-50, or Minicircuits ZFSC-2-1 power combiner was used to split the input signal). A complimentary pair of LM311 comparators were used to drive either a Relcom S1 switch or a HP mixer

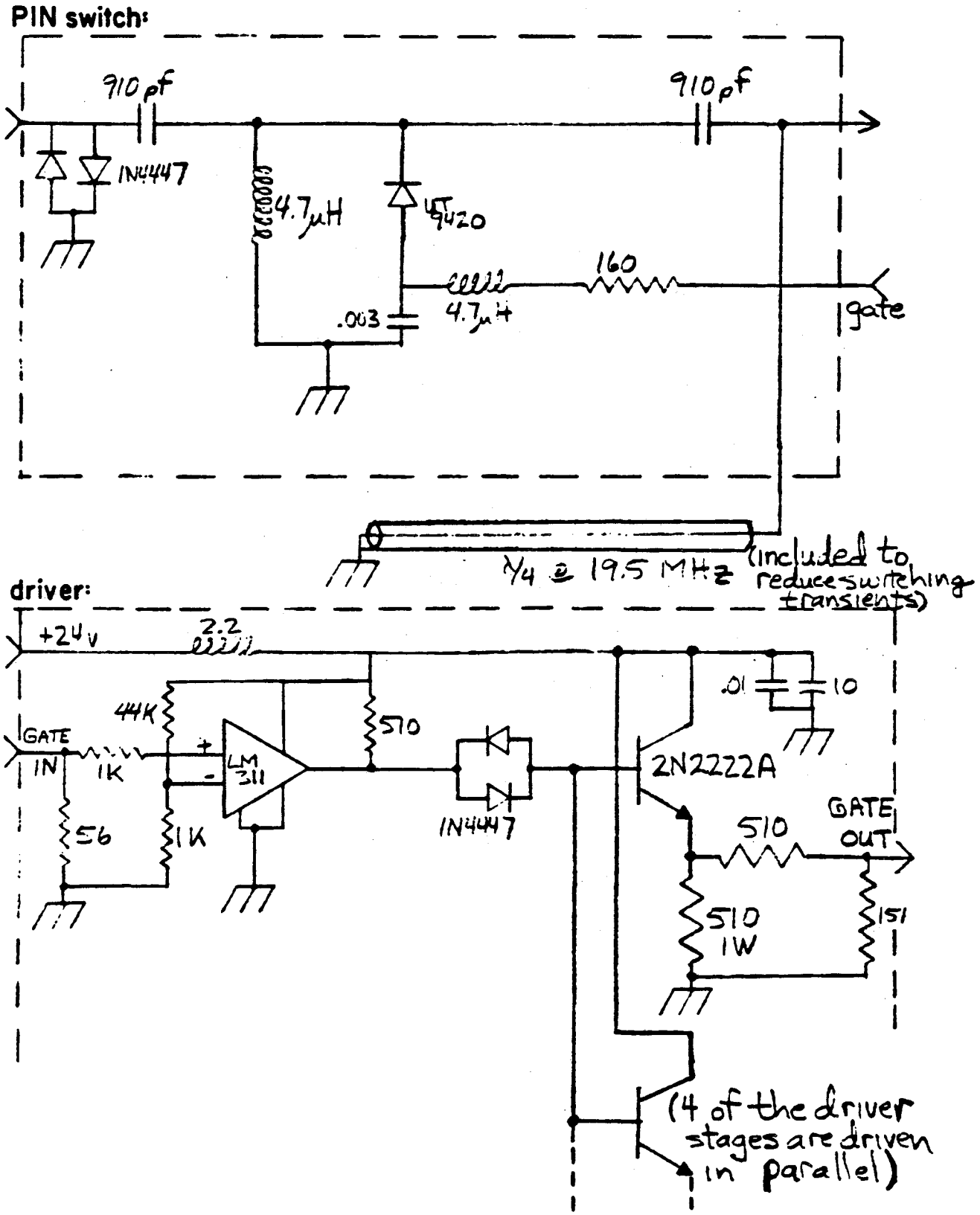

Figure 56. PIN diode switch and driver

(used as a switch). This circuit is so straight-forward that I choose not to present it here.

It was found that a surprisingly simple ADRF switch is sufficient for my experiments (see Figure 57). In this circuit, a decaying RC transient is summed with a constant (but variable) voltage (to account for non linear amplifier cutoff) and used to drive the X port of a mixer (HP10514A). With proper adjustment, good ADRF's could be obtained even for the most non linear of amplifiers. The only problem with the circuit is its farily long recovery time (since the RC circuit must be given time to charge), but this has seldom been annoying.

D.6 Additions to NTCFTB

The only unusual modification made to NTCFTB is that shown on the next page to operate the Temperature Control device (LBL print number 16X950). This modification of the VT subroutine increases the DAC voltage output as the temperature increases (i.e., is meant to boil LN_2 from a dewar), and statement 4650 should be changed to 4661 from 123000 for normal heater operation (when 4650 → 4661, 4651 → 0).

Modified NTCFTB USR overlay (VT)

```
 4571/ 0603111
4572/ 0643114
4573/ 0643112
4574/ 0735322
4575/ 0670400
4576/ 1503060
4577/ 1473060
4600/ 0262002
4601/ 0044611
4602/ 0111654
4603/ 1436605
4604/ 0216207
4605/ 2000206
4606/ 0004603
4607/ 0722622
4610/ 0002666
4611/ 0216003
4612/ 1413061
4613/ 1603050
4614/ 0722602
4615/ 0701003
4616/ 1221050
4617/ 1421050
4620/ 0722604
4621/ 0262017
4622/ 1621050
4623/ 1535061
4624/ 0004615
4625/ 1117060
4626/ 1433050
4627/ 1217054
4630/ 1413060
4631/ 0216003
4632/ 1413061
4633/ 1217050
4634/ 3657060
4635/ 1535061
4636/ 0004634
4637/ 1735053
4640/ 0062666
4641/ 1217055
4642/ 1223056
4643/ 0701002
4644/ 1221055
4645/ 0701001
4646/ 1223057
4647/ 1225047
4650/ 1230000
4651/ 0004661
```

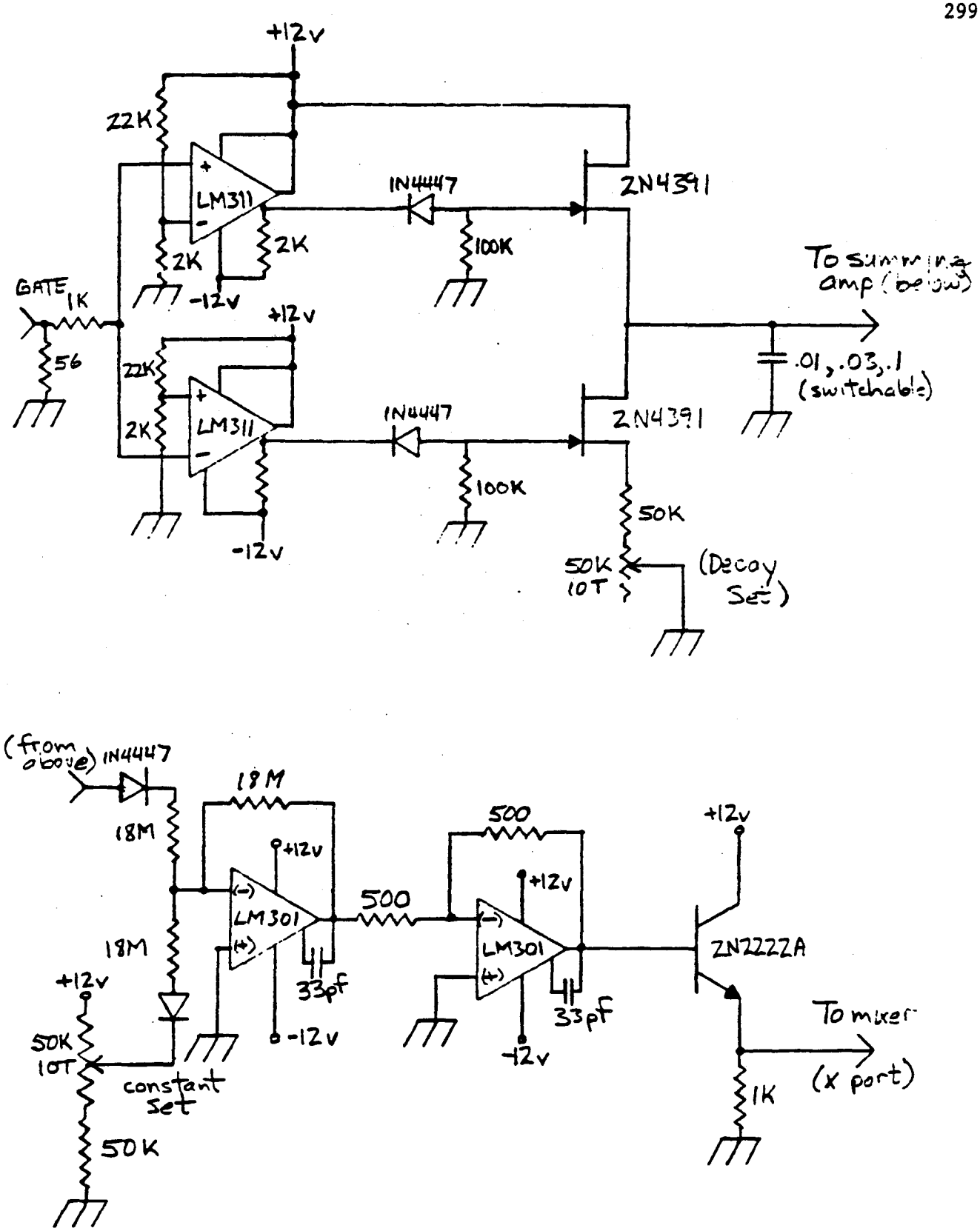

Figure 57. ADRF switch (circuit to drive mixer)

References

1. U. Fano, Rev. of Mod. Phys. 29, 74 (1957).
2. J. B. Murdoch, Ph.D. Thesis, University of California, Berkeley, 1982, L.B.L. Report #15254.
3. A. Abragam, The Principles of Nuclear Magnetism (Oxford University Press, London, 1961).
4. N. F. Ramsey, Phys. Rev. 103, 20 (1954).
5. C. P. Schlichter, Principles of Magnetic Resonance (Springer-Verlag, New York, 1978).
6. P. Kusch, S. Millman, and I. I. Rabi, Phys. Rev. 55, 1176 (1939).
7. B. T. Feld and W. E. Lamb, Phys. Rev. 67, 15 (1945).
8. M. H. Cohen and F. Reif, Solid State Physics Vol. 5, pg. 322, F. Seitz and D. Turnbull editors, (Academic Press, New York, 1957).
9. N. F. Ramsey, Nuclear Moments, Appendix B, (John Wiley and Sons, New York, 1953).
10. Reference 3, chapter 7.
11. (a) S. Vega and Y. Naor, J. Chem. Phys. 75, 75 (1981); (b) Y. Zur and S. Vega, Chem. Phys. Lett. 80, 381 (1981).
12. Reference 3, chapter 3.
13. G. W. Leppelmeir and E. L. Hahn, Phys. Rev. 141, 724 (1966).
14. R. W. G. Wyckoff, Crystal Structures, Vol. I. Chapt. III, pg. 42a (Interscience, New York, 1960).
15. M. Mehring, Principles of High Resolution NMR in Solids, appendix H, (Springer-Verlag, New York, 1983).
16. M. Witanowski and G. A. Webb, Nitrogen NMR (Plenum Press, New

York, 1983).

17. L. M. Ishol and T. A. Scott, J. Magn. Reson. 27, 23 (1977). L. M. Ishol, Ph.D. Thesis, University of Florida, 1976.

18. G. Harbison, J. Herzfeld, and R. G. Griffin, J. Am. Chem. Soc. 103, 4753 (1981). D. T. Edwards and P. A. Speight, Phys. Lett. 34A, 325 (1971).

19. N. Bloembergen and T. J. Rowland, Acta. Metallurgica 1, 731 (1953).

20. M. Abramowitz and I. A. Steegun, Handbook of Mathematical Functions. (U.S. Dept. of Commerce, NBS).

21. (a) S. Vega, J. Chem. Phys. 68, 5518 (1978); (b) A. Wokaun and R. R. Ernst, J. Chem. Phys. 67, 1752 (1977).

22. M. Mehring, E. K. Wolff and M. E. Stoll, J. Magn. Reson. 37, 475 (1980).

23. S. Vega and A. Pines, J. Chem. Phys. 68, 5624 (1977).

24. R. Kubo and K. Tomita, J. Phys. Soc. of Japan 9, 880 (1954).

25. I. J. Lowe and R. E. Norberg, Phys. Rev. 107, 46 (1957).

26. R. R. Ernst and W. A. Anderson, Rev. Sci. Inst. 37, 93 (1966).

27. D. I. Hoult and R. E. Richards, J. Magn. Reson. 24, 71 (1976).

28. D. I. Hoult, Rev. Sci. Instrum. 53, 193 (1979).

29. I. J. Lowe and M. Englesberg, Rev. Sci. Instrum. 45, 631 (1974).

30. E. L. Hahn, Phys. Rev. 80, 580 (1950).

31. I. Solomon, Phys. Rev. 110, 61 (1958).

32. J. H. Davis, K. R. Jeffrey, M. Bloom, and M. I. Valic, Chem. Phys. Lett. 42, 390 (1976).

33. (a) W. G. Clark, Rev. Sci. Instrum. 35, 316 (1964); (b) P. A. Speight, K. R. Jeffrey, and J. A. Courtney, J. Phys.

E. 7, 801 (1974); (c) E. Fukushima and S. B. W. Roeder, J. Magn. Reson. 33, 199 (1979).

34. M. Bloom, J. H. Davis and K. R. Jeffrey, Can. J. Phys. 58, 1510 (1980).

35. J. D. Ellett, M. G. Gibby, U. Haeberlen, L. M. Huber, M. Mehring, A. Pines, and J. S. Waugh, "Spectrometers for Multiple-Pulse NMR", Advances in Magnetic Resonance, Vol. 5 (Academic, New York, 1971).

36. M. Mehring and J. S. Waugh, Rev. Sci. Instrum. 43, 649 (1972).

37. Reference 3, chapter 4.

38. M. Goldman, Spin Temperature and Nuclear Magnetic Resonance in Solids, Appendix B, (Oxford Press, London, 1970).

39. (a) N. Boden and Y. K. Levine, J. Mag. Reson. 30, 327 (1978); (b) J. McLean and M. A. B. Whitaker, J. Phys. C 12, 1761 (1979).

40. T. W. Shattuck, Ph.D. Thesis, University of California, Berkeley 1976, LBL Report #5458.

41. Reference 15, appendix A.

42. M. E. Rose, Elementary Theory of Angular Momentum (John Wiley and Sons, New York, 1983).

43. U. Haeberlen and J. S. Waugh, Phys. Rev. 175, 453 (1968).

44. A. Pines, S. Vega and M. Mehring, Phys. Rev. B 18, 112 (1978).

45. F. Bloch, Phys. Rev. 70, 460 (1946).

46. N. Bloembergen, E. M. Purcell, and R. V. Pound, Phys. Rev. 73, 67 (1948).

47. Reference 3, chapter 8.

48. M. G. Gibby, Ph.D. Thesis, Massachusetts Institute of Technology, 1972 .

49. A. G. Redfield, Phys. Rev. 98, 1787 (1955).

50. Reference 38, chapter 2.

51. C. P. Slichter and W. C. Holton, Phys. Rev. 122, 1701 (1961).

52. S. R. Hartmann and E. L. Hahn, Phys. Rev. 128, 2042 (1962).

53. J. Jeener and P. Broaekaert, Phys. Rev. 157, 232 (1967).

54. A. Pines, M. G. Gibby, and J. S. Waugh, J. Chem. Phys. 69, 569 (1973).

55. H. E. Bleich and A. G. Redfield, J. Chem. Phys. 67, 5040 (1977).

56. R. T. Schumacher, Phys. Rev. 112, 837 (1958).

57. D. A. McArthur, R. E. Walstedt, and E. L. Hahn, Phys. Rev. 128, 609 (1969).

58. D. E. Demco, J. Tegenfeldt, and J. S. Waugh, Phys. Rev. B 11, 4133 (1975).

59. S. Vega, T. W. Shattuck, and A. Pines, Phys. Rev. A 22, 638 (1980).

60. (a) P. Brunner, M. Reinhold, and R. R. Ernst, J. Chem. Phys. 73, 1088 (1980); (b) M. Reinhold, P. Brunner, and R. R. Ernst, J. Chem. Phys. 74, 184 (1981).

61. J. Seliger, R. Blinc, M. Mali, R. Osredkar, and A. Prelesnik, Phys. Rev. B 11, 27 (1975).

62. T. K. Pratum and M. P. Klein, J. Magn. Reson., in press, 1983.

63. S. Vega, Phys. Rev. A 23, 3152 (1981).

64. F. Bloch and A. Siegert, Phys. Rev. 57, 522 (1940).

65. L. S. Batchelder and J. L. Ragle, J. Magn. Reson. 37, 469 (1980).

66. D. C. Ailion, "NMR and Ultraslow Motions", reference 35, page 177.

67. R. C. Bowman and W. K. Rhim, J. Magn. Reson. 49, 93 (1982).

68. H. T. Stokes and D. C. Ailion, Phys. Rev. B 15, 1271 (1977).

69. D. C. Look and I. J. Lowe, J. Chem. Phys. 44, 2995 (1966).

70. W. K. Rhim. A. Pines, and J. S. Waugh, Phys. Rev. B 3, 684 (1971).

71. R. Freeman, S. P. Kempsell, and M. H. Levitt, J. Magn. Reson. 38, 453 (1980).

72. (a) E. Schneider and R. Tyco, personal communication; (b) R. Tyco, Phys. Rev. Lett. 51, 775 (1983).

73. T. K. Pratum and M. P. Klein, J. Magn. Reson. 53, 473 (1983).

74. U. Henriksson, L. Odberg, J. C. Eriksson, and L. Westman, J. Phys. Chem. 81, 76 (1977).

75. Y. Kanazawa and K. Koga, Biochem. Biophys. Res. Commun. 95, 269 (1980).

76. K. Koga and Y. Kanazawa, Biochemistry 19, 2779 (1980).

77. D. J. Siminovich, M. Rance and K. R. Jeffrey, FEBS Lett. 112, 79 (1980).

78. D. J. Siminovich and K. R. Jeffrey, Biochem. Biophys. Acta. 645, 270 (1981).

79. T. M. Rothgeb and E. Oldfield, J. Biol. Chem. 256, 6004 (1981).

80. P. Ericksson, A. Khan, and G. Lindblom, J. Phys. Chem. 66, 387 (1982).

81. D. Chapman, R. M. Williams and B. D. Ladbrooke, Chem. Phys. Lipids 1, 445 (1967).

82. W. C. Shih, Ph.D. Thesis, University of California, Berkeley, 1979, LBL report #10097.

83. IMSL Users Manual (IMSL Inc., Houston, 1982).

84. T. Chiba, J. Chem. Phys. 39, 947 (1963).

85. G. Soda and T. Chiba, J. Chem. Phys. 50, 439 (1969).

86. D. M. Rice, R. J. Wittebort, R. G. Griffin, E. Meirovitch, E. R. Stimson, Y. C. Meinwald, J. H. Freed and H. A. Scheraga,

J. Am. Chem. Soc. 103, 7707 (1981).

87. H. Bayer, Z. Phys. 30, 222 (1951).

88. T. Kushida, G. B. Benedek, and N. Bloembergen, Phys. Rev. 104, 1364 (1956).

89. H. S. Gutowsky and G. A. Williams, Phys. Rev. 105, 464 (1957).

90. H. M. Foley and R. M. Sternheimer, Phys. Rev. 93, 734 (1957).

91. D. T. Edmonds, M. J. Hunt and A. L. Mackay, J. Magn. Reson. 9, 66 (1973).

92. R. W. G. Wyckoff, Crystal Structures, Vol. I, pg. 107 (Interscience, New York, 1963).

93. E. Wait and H. M. Powell, J. Chem. Soc. 872 (1958).

94. T. Migchelson and A. Vos, Acta. Cryst. 23, 796 (1967).

95. A. Zalkin, Acta. Crystallogr. 10, 557 (1956).

96. J. Hjortas and H. Sorum, Acta. Crystallogr. Sect. B. 27, 1320 (1971).

97. D. Wemmer, V. Petrouleas, N. Pantagiotopoulos, S. E. Filippakis, and R. M. Lemmon, J. Phys. Chem. 87, 999 (1983).

98. M. E. Senko and D. H. Templeton, Acta. Crystallogr. 13, 281 (1960).

99. J. Chonjacki, J. Grochowski, E. Hoffman-Zaborowska, M. Kruszek, and T. Wojtasik, Rocz. Chem. 45, 1997 (1971).

100. J. DuFourcq and B. Lemanceau, J. Chem. Phys. 67, 9 (1970).

101. E. R. Andrew and P. C. Canepa, J. Magn. Reson. 7, 429 (1972).

102. S. Chang and E. Westrum, J. Chem. Phys. 16, 2420 (1962).

103. L. D. Landau and E. M. Lifshitz, Statistical Physics, chapt. 14 (Pergamon Press, New York, 1969).

104. M. Stammler, J. Inorg. Nucl. Chem. 29, 2203 (1967).

105. R. Blinc, M. Burgar and U. Rutar, Solid State Commun, 27, 1021 (1978).

106. (a) R. Goc, Z. Pajak and B. Szafranska, Proc. of 18th Cong. AMPERE, 1974, p. 405; (b) F. Koksal, Z. Naturforsch. 34, 11, 1296 (1979); (c) B. Safranska and Z. Pajak, J. Mol. Struct. 99, 147 (1983).

107. R. Y. Dong, Can. J. Phys. 56, 678 (1978).

108. G. Bandoli, D. A. Clement, and M. Nicolini, J. Cryst. Mol. Struct. 8, 279 (1978).

109. G. G. Belford, R. A. Bernheim and H. S. Gutowsky, J. Chem. Phys. 35, 1032 (1961).

110. E. K. Wolff, R. G. Griffin and C. Watson, J. Chem. Phys. 66, 5433 (1977).

111. T. Chiba, Bull. Chem. Soc. Japan 38, 490 (1964).

112. W. C. Bailey and H. S. Story, J. Chem. Phys. 60, 1952 (1974).

113. J. Van Kranendouk, Physica 20, 781 (1954).

114. A. Avogadro, G. Bonera, and A. Rigamoni, J. Magn. Reson. 20, 399 (1975).

115. S. Albert, H. S. Gutowsky, and J. A. Ripmeester, J. Chem. Phys. 56, 3672 (1972).

116. F. Borsa and A. Rigamonti, "NMR and NQR in Fluids, Paramagnets and Crystals", Magnetic Resonance of Phase Transitions, F. J. Owens, C. P. Poole and H. A. Farach, editors (Academic Press, New York, 1979).

117. V. Petrouleas, A. Nath and R. M. Lemmon, Radiat. Phys. Chem. 16, 113 (1980).

118. R. O. Lindblom, Ph.D. Thesis, University of California, Berkeley, 1959, published as LBL report #8910.

119. V. Petrouleas and R. M. Lemmon, J. Chem. Phys. 69, 1315 (1978).

120. V. Petrouleas, R. M. Lemmon, and A. Christensen, J. Chem. Phys. 68, 2243 (1978).

121. J. D. Graham and R. H. Hannon, J. Chem. Phys. 64, 1204 (1976).

122. C. A. McDowell, P. Raghunathan, and D. S. Williams, J. Chem. Phys. 66, 3240 (1977).

123. L. J. Burnett, R. M. Knowles and J. D. Graham, J. Chem. Phys. 68, 2514 (1978).

124. H. Sillescu, J. Chem. Phys. 54, 2110 (1974).

125. J. H. Freed, G. V. Bruno, and C. F. Polnazek, J. Phys. Chem. 75, 3385 (1971).

126. H. W. Spiess, Chem. Phys. 6, 217 (1974).

127. H. W. Spiess and H. Sillescu, J. Magn. Reson. 42, 381 (1981).

128. R. Kubo, J. Phys. Soc. Japan Supplement to Vol. 26, pg. 1 (1969).

129. H. W. Spiess, "Rotation of Molecules and Nuclear Spin Relaxation", NMR Basic Principles and Progress, P. Diehl, E. Fluck, and R. Kosfeld editors (Springer-Verlag, New York, 1978).

130. Reference 15, chapter 2.

131. S. Alexander, A. Baram, and Z. Luz, Mol. Phys. 27, 441 (1974).

132. A. Baram, Z. Luz, and S. Alexander, J. Chem. Phys. 64, 4321 (1976).

133. S. Alexander, Z. Luz, Y. Naor, and R. Poupko, Mol. Phys. 33, 1119 (1977).

134. A. Baram, Mol. Phys. 41, 823 (1980).

135. H. W. Spiess, J. Chem. Phys. 72, 6755 (1980).

136. T. S. Young, personal communication.

137. S. R. Holbrook, personal communication.

138. V. Schomaker and K. N. Trueblood, Acta. Cryst. Sect. B, 24, 63 (1968).

139. D. E. Wemmer, Ph.D. Thesis, University of California, Berkeley, 1978, LBL report #8042.

140. V. R. Cross, R. K. Hester, and J. S. Waugh, Rev. Sci. Inst. 47, 1486 (1976).